

Cristiano
Loss



UNIVERSITÀ DEGLI STUDI
DI TRENTO

Doctoral School in
Engineering of Civil and
Mechanical Structural Systems

Cristiano Loss

DISPLACEMENT-BASED SEISMIC DESIGN OF TIMBER STRUCTURES

DISPLACEMENT-BASED SEISMIC
DESIGN OF TIMBER STRUCTURES

March, 2011



University of Trento
University of Brescia
University of Padova
University of Trieste
University of Udine
University IUAV of Venezia

Cristiano Loss (Ph. D. Student)

DISPLACEMENT-BASED SEISMIC DESIGN OF TIMBER STRUCTURES

Dr. Daniele Zonta

Prof. Maurizio Piazza

March, 2011

All the material in this document is protected by copyright.
Any use of the work other than as authorized under copyright law is prohibited.

UNIVERSITY OF TRENTO

Doctoral School in Engineering of Civil and Mechanical Structural Systems

Cycle: XXIII

Head of the Doctoral School: Prof. Davide Bigoni

Displacement-Based Seismic Design of Timber Structures

Cristiano Loss

Department of Mechanical and Structural Engineering

Via Mesiano 77 - 38123

University of Trento - ITALY

Phone number: +39 0461 282556

Fax number: +39 0461 882599

E-mail: cristiano.loss@ing.unitn.it

Final Examination 7 April 2011

Board of Examiners

Prof. Piazza Maurizio (University of Trento, Italy)

Prof. Marotti De Sciarra Francesco (University of Naples "Federico II", Italy)

Prof. Joan Ramon Casas (University of Barcelona "Politecnica de Catalunya", Spain)

SUMMARY

The research is aimed at developing seismic methods for the design and evaluation of the seismic vulnerability of wooden structures, using a displacement-based approach. After a brief introduction on the seismic behaviour of timber structures, the general Direct Displacement-Based Design (Direct-DBD) procedure and the state-of-the-art are presented, with clear reference to the application of the Direct-DBD method to wooden buildings. The strength of the Direct-DBD method is its ability to design structures in a manner consistent with the level of damage expected, by directly relating the response and the expected performance of the structure. The research begins with a description of the procedural aspects of the Direct-DBD method and the parameters required for its application.

The research presented focuses on the formulation of a displacement-based seismic design procedure, applicable to one-storey wooden structures made with a portal system. This typology is very common in Europe and particularly in Italy. A series of analytical expressions have been developed to calculate design parameters. The required analytical Direct-DBD parameters are implemented based on the mechanical behaviour of the connections, made with metal dowel-type fasteners. The calibration and subsequent validation of design parameters use a Monte Carlo numerical simulation and outcomes obtained by tests in full-scale.

After the description of the Displacement-Based method for one-storey wooden structures, a series of guidelines to extend the Direct-DBD methodology to other types and categories of timber systems are proposed. The thesis presents the case of a multi-storey wood frame construction, which is a simple extension of the glulam portal frame system.

Part of this work has been done within the **RELUIS** Project, (**RE**te dei **L**aboratori **U**niversitari di **I**ngegneria **S**ismica), Research Line IV, which in the years between 2005 and 2008 involved several Italian universities and Italian institutes of research in the development of new seismic design methods. The Project produced the first draft of model code for the seismic design of structures based on displacement (Direct-DBD). This thesis is the background to the section of the model code developed for timber structures.

SOMMARIO

La ricerca è finalizzata allo sviluppo di un approccio agli spostamenti per il progetto e la valutazione della vulnerabilità sismica delle strutture in legno. Dopo una breve introduzione sulle problematiche che caratterizzano il comportamento delle strutture lignee in zona sismica, si presenta la procedura del Direct Displacement-Based Design (Direct-DBD) e il relativo stato dell'arte, con chiaro riferimento alla sua applicazione su edifici in legno. Le potenzialità dell'approccio Direct-DBD si possono ascrivere alla capacità di progettare la struttura in modo coerente con lo stato di danneggiamento previsto. Nella fase iniziale della ricerca sono descritti gli aspetti procedurali e i parametri richiesti per l'applicabilità del metodo Direct-DBD.

La parte innovativa del lavoro presentato si incentra sulla formulazione di una procedura basata sul protocollo agli spostamenti applicata alla struttura lignea a portale monopiano. Questa tipologia costruttiva è molto diffusa in Europa e in particolare in Italia. Nel corso del lavoro di ricerca sono state sviluppate relazioni analitiche per il calcolo dei parametri di progetto. La formulazione analitica dei parametri si basa sul modello meccanico implementato per descrivere il comportamento locale delle connessioni che utilizzano connettori a gambo cilindrico. La calibrazione e la successiva validazione dei parametri di progetto si avvale di una simulazione numerica Monte Carlo (MC) e dei risultati ottenuti da prove sperimentali.

A valle della formulazione sono proposte linee guida mediante le quali estendere la metodologia proposta ad altre tipologie e categorie di edifici in legno. Per questo, nella tesi, è studiata la tipologia di edificio residenziale multipiano in legno, quale semplice estensione del sistema intelaiato.

Il lavoro di studio è stato svolto all'interno della Linea di Ricerca No. 4 del progetto **RELUIS (REte dei Laboratori Universitari di Ingegneria Sismica)** che nel triennio 2005-2008 ha visto impegnate numerose università ed enti di ricerca italiani nello studio di nuovi approcci alla progettazione sismica. Il progetto si è concluso con la stesura di una prima versione di codice modello per la progettazione di strutture secondo il Direct-DBD, per il quale il lavoro rappresenta il background della parte dedicata alle strutture lignee.

To my family and my girlfriend

ACKNOWLEDGEMENTS

La conclusione di questo lavoro segna un passaggio importante della mia vita, un percorso partito molti anni fa in una fredda mattinata di dicembre, dove le alte cime dolomitiche riparano un ambiente semplice e discreto. Da allora ne è passato di tempo e molti sono stati gli ostacoli da superare, le fatiche, ma soprattutto i sacrifici fatti.

Molte sono le persone che meritano un “Grazie” e un caloroso abbraccio. È stata anche la loro presenza e i loro consigli che mi hanno permesso di raggiungere questo traguardo.

Un doveroso ringraziamento va al Dr. Daniele Zonta per l’incoraggiamento e la fiducia concessami e al Prof. Maurizio Piazza per la sua pazienza e cordialità. Desidero ricordare le persone più care con cui ho dialogato in questi ultimi tre anni. Molto importante è stato l’appoggio e lo stimolo del team di ricerca che si occupa delle strutture lignee, coordinato dal Prof. M. Piazza e composto in ordine da Acler Ermanno, Andreolli Mauro, Polastri Andrea, Sartori Tiziano e Tomasi Roberto.

Sono grato a tutte le persone che lavorano presso il Dipartimento di Ingegneria Meccanica e Strutturale dell’Università di Trento (DIMS), in particolare Rosanna Verones, Cesarina Zeni, Elena Staltari e Michela Litterini, che mi hanno seguito nel lungo percorso amministrativo della scuola di dottorato.

Una dedica particolare spetta ai miei genitori, ai miei nipotini e ai miei fratelli per tutto il loro affetto e alla mia ragazza Ilaria, che mi ha irraggiato di gioia e amore in questi ultimi tre anni.

Molte altre persone inconsapevolmente mi hanno aiutato e accompagnato in questo percorso tortuoso e lungo – a tutti voi un sentito grazie di cuore! –

Imér, Marzo 2011

Cristiano Loss



CONTENTS

ACKNOWLEDGEMENTS

CONTENTS I

LIST OF FIGURES V

LIST OF TABLES XII

NOMENCLATURE XV

1 INTRODUCTION 1

1.1 General 1

1.2 Objectives and scope 4

1.3 Dissertation overview 5

2 EARTHQUAKES AND WOOD STRUCTURES 7

2.1 Performance of wood in earthquake conditions 7

2.2 Suitable wood construction systems in seismic zones 8

2.3 Timber frame systems with moment-resisting connections 16

2.4 Timber frame panel systems 19

2.5 Massive wood panel system 24

2.6 Conclusions 28

3	DIRECT DISPLACEMENT-BASED DESIGN METHODOLOGY	29
3.1	Introduction	29
3.2	Overview of the Direct-DBD procedure for MDOF System	30
3.3	State of development in timber systems	33
3.4	Conclusions	40
4	PROPOSED DIRECT-DBD METHOD FOR TIMBER SYSTEMS	41
4.1	General	41
4.2	Structure description	41
4.3	Load-slip monotonic curve for fasteners	45
4.4	Design displacement formulation	57
4.5	Ductility	66
4.6	Equivalent viscous damping	67
4.6.1	Cyclic behaviour of dowel type fastener connections	68
4.6.2	Formulation of the equivalent viscous damping analytical model	79
4.7	Conclusions	88
5	VALIDATION OF THE PROPOSED DIRECT-DBD METHOD	89
5.1	Dynamic behaviour of timber structures	89
5.2	Numerical model for non-linear static analysis	91
5.2.1	General aspects	91
5.2.2	Pushover analysis and results	93
5.3	Numerical model for non-linear dynamic analysis	95
5.3.1	General	95
5.3.2	Analytical evaluation of the moment-rotation curve for joint connections	96
5.3.3	Time-history analysis	104
5.4	EXPERIMENTAL RESULTS	104
5.5	VALIDATION OF DESIGN DISPLACEMENT	119
5.5.1	Analysis results	123

5.5.2	Numerical calibration of design displacement	127
5.6	Validation of Equivalent Viscous Damping	129
5.7	Conclusions	142
6	EXTENSION OF DIRECT-DBD METHOD TO OTHER TIMBER BUILDINGS	143
6.1	General	143
6.2	Moment-resisting joint for general dowel configuration	143
6.3	Wood light-frame system	148
6.3.1	General	148
6.3.2	Direct-DBD: formulation of design displacement	150
6.3.3	Direct-DBD: formulation of the equivalent viscous damping	158
6.3.4	Non-linear model for wood shear walls buildings	162
6.4	Comparison of results for the proposed analytical model	168
6.5	Conclusions	175
7	SUMMARY, CONCLUSIONS AND RECOMMENDATIONS	177
7.1	Summary and conclusions	177
7.2	Future work	179
	BIBLIOGRAPHY	181
	APPENDIX A	193
7.3	Pre-processing	195
7.4	Solving	197
7.5	Post-processing	198
	APPENDIX B	199
	GLULAM PORTAL FRAME SYSTEM	200
	APPENDIX C	213

LIST OF FIGURES

- Figure 1.1. Overview of building damage after recent two earthquakes: Northridge 1994 with Magnitude of 6.7 and Kobe (Hanshin-Awaji) 1995 with Magnitude of 7.2 (Richter scale) 2
- Figure 1.2 Typical performance curve for a structure with relation between displacement/force and damage (modified from Calvi 2003) 3
- Figure 2.1 (A) Typical stress-strain curves for clear coniferous wood (Piazza et al. 2005); (B) Experimental load-slip curves for joints in tension parallel to the grain (Racher 1995a) 9
- Figure 2.2 Selection of ductile timber structures; (a) Moment-resisting (MR) timber frame system; (b) Timber shear panel system; (c) Cross-laminated timber panel system; (modified from Priestley et al. 2007) 10
- Figure 2.3 Post-tensioned timber frame system (modified from Priestley et al. 2007) 10
- Figure 2.4 (a) MR joint built with flanged elements (from Piazza et al. 2005); (b) MR joint built with glued elements (from Racher 1995c); (c) MR joint built with epoxy steel rods (from Piazza et al. 2005) 11
- Figure 2.5 (a) Platform frame system (Common in 1940s in the USA): details of structure and construction sequence, from 1 to 4; (b) Balloon frame system: details of structure and construction sequence from 1 to 4 (modified from American Forest and Paper Association 2001) 13
- Figure 2.6 Prestressed System; (a) North-east perspective view of the University of Canterbury Biological Science building (modified from Fernandez 2008); (b) South-west perspective view of the University of Canterbury building (modified from Fernandez 2008) 14
- Figure 2.7 Hybrid systems, suitable for tall timber buildings up to 25 storeys; (a) Three-dimensional view of the whole resisting system in configuration No 1 (modified from Sakamoto et al. 2004); (b) Three-dimensional view of

	the whole resisting system in configuration No 2 (modified from Sakamoto et al. 2004); (c) Phase of realization of the flooring (from Fragiacommo 2009); (d) Phase of erection of post and beam gravity load resisting element (from Fragiacommo 2009)	15
Figure 2.8	3D View (I) and exploded view of the scheme of assembly (II); (a) Dowelled cross-lapped joint; (b) Internal metal plates connected with fasteners; (c) Nailed plywood gussets or metal plate with fasteners	17
Figure 2.9	Drawing of the common bracing systems between timber frames (Gojkovic and Stojic 1996)	18
Figure 2.10	Commercial “Kerto” portal frame solution for light industrial, warehouse, agricultural or equestrian buildings; Three dimensional view of prefabricated elements (modified from Finnforest 2009)	19
Figure 2.11	(a) Three-dimensional view of the Timber Portal frame system with dowelled cross-lapped joints (so-called “heavy timber structure”); (b) Details of an industrial warehouse built in Trentino (Italy)	20
Figure 2.12	Details of wall-to-floor joints of platform frame system construction (courtesy of Professor Ian Smith)	21
Figure 2.13	Schematic presentation of the timber frame panel construction following the platform frame technique; (a) exploded view of wood frame building; (b) shear wall layers; (c) shear wall panel module; (d) sections of shear wall panel module and mechanical fasteners of wood-based sheathing panels; (Pictures Modified from Premrov 2008)	22
Figure 2.14	wood frame resistance system: mechanism of lateral resisting system (modified from Ceccotti and Toulaiatos 1995)	23
Figure 2.15	Schematic presentation of the massive wood panel construction (XLAM system); (a) exploded view of massive wood panel system; (b) shear wall layers of cross-laminated solid wood panels	25
Figure 2.16	Illustration of XLAM lateral resisting system; Details of connections between the elements (modified from Binderholz 2010)	27
Figure 3.1	Fundamentals of Direct Displacement-Based Design (based on Priestley et al. 2007)	31
Figure 3.2	(a) Wayne Stewart degrading hysteresis rule described by Filiatrault et al. (2003); (b) The nine independent physical parameters of Wayne Stewart degrading hysteretic model	34
Figure 3.3	Single family house with two storeys, as in a modern residential construction in California (Curee 2008); (a) Structure finished before the test; (b) Lateral view after the test; (c) 3D view after the test	35

Figure 3.4	Global view of the four index buildings investigated (modified from Filiatrault et al. 2004)	36
Figure 3.5	Flowchart of Direct-DBD procedures developed for mid-rise wood frame buildings (modified from Pang and Rosowsky 2007)	38
Figure 3.6	(a) Elevation views of a three-storey wood frame structure, typical in America; (b) Three-dimensional nonlinear model for a three-story wood frame structure (modified from Pang and Rosowsky 2007)	39
Figure 4.1	Description of the case study; (a) 3D isometric view of the main resistant structure; (b) Geometrical description of the beam-to-column joint	42
Figure 4.2	Geometric features of the prototype portal	43
Figure 4.3	Design Force acting on a single dowel for knee joints made with two crowns of dowels; (a) Beam-to-column connection with no parallel elements and geometrical configuration; (b) Forces acting on dowels due to rigid body rotation (modified from Racher 1995b)	45
Figure 4.4	Failure modes provided by the European Yield Model for fasteners in double timber-to-timber shear planes (modified from Leijten 2008)	47
Figure 4.5	(a) Typical monotonic load-slip curves for a dowel-type timber connection; (b) Analytical models for the connections with main parameters	48
Figure 4.6	Definition of yielding parameters for a monotonic load-slip curve in two typical situations; (a) Load-slip curve with two well-defined linear parts; (b) Load-slip curve without two well-defined linear parts; (modified from CEN 2001)	49
Figure 4.7	Flow-of-forces in dowel-type fastener connections, embedment strength in timber elements and model of embedment strength (modified from Leijten 2008)	51
Figure 4.8	Embedment strength of a dowel-type fastener connection in parallel and perpendicular directions; (a) Test parallel to grain direction; (b) Test perpendicular to grain direction (modified from Sawata and Yasumura 2002)	52
Figure 4.9	(a) Test failure mode after reaching maximum load; (b) Normalized moment-angle diagram of a dowel-type fastener for different dowel diameters, d (modified from Blass et al. 2000)	53
Figure 4.10	(a) Analytical Load-Slip curve formulated; (b) Experimental Load-Slip curve after monotonic test (push out test of two-dowel-type connections of 12 mm; Piazza et al. 2009)	54
Figure 4.11	Möller's chart of dowel-type mechanical fasteners for different geometries and mechanical configurations	56

Figure 4.12	Conceptual model for estimating the design displacement Δ_d	58
Figure 4.13	Moment and shear stresses on dowels arranged in two concentric crowns	61
Figure 4.14	Spacings, edge distances and end distances for dowels on a knee joint made with two crowns of dowels	62
Figure 4.15	(a) Test on specimen with 12 dowels of 16 mm in diameter; (b) Connection failure mode after test (ultimate state for joint); (c) Dowel deformation after test (modified from Polastri et al. 2008)	63
Figure 4.16	Typical force-deformation loops for different load levels of dowelled joints under cyclic loading (modified from Ceccotti 1995)	69
Figure 4.17	Typical cyclical behaviour of a nailed connection with nail slenderness of 8.5; The red line shows the Envelope curve (Ceccotti 1995)	71
Figure 4.18	Failure of connections with metal dowel-type fasteners in double-shear; (a) Mode II in accordance with the EYM (CEN 2004a); (b) Mode III in accordance with the EYM (Courtesy of Professor Maurizio Piazza)	72
Figure 4.19	Qualitative trend of the cyclic response of a connection with dowel-type fasteners in double shear for failure mode III (European Yield Model; CEN 2004a)	73
Figure 4.20	Expected hysteretic loops of a connection with dowel-type fasteners in double shear subjected to cyclic loading (failure mode III in accordance of European Yield Model)	74
Figure 4.21	Analytical load-slip curve of a dowel-type fastener connection (black line); Expected load-slip curve of a dowel-type fastener connection (red line)	75
Figure 4.22	Failure Mode III dowel-type fastener connections in double shear; Johansen's model	76
Figure 4.23	Configuration of equilibrium (hypothetical) after the reaching of Failure Mode III, for a dowel-type fastener connection in double shear, on return to the undeformed situation	77
Figure 4.24	Idealization of the hysteretic loop for a dowel-type fastener connection based on three different loading histories; (a) Protocol I; (b) Protocol II; (c) Protocol III	81
Figure 4.25	Procedure for cyclic testing following EN 12512 (CEN 2001); Ratio between series of cycles	84
Figure 4.26	(a) Ultimate configuration of joint: slip of dowels due to inelastic deformation; (b) Dowelled cross-lapped joint; (c) Load-slip envelope curve of dowels	85

Figure 5.1	Hysteresis models developed for timber structures (modified from Dolan 1994); (a) Kivell et al. (1981) hysteresis model; (b) Dolan (1989) hysteresis model; (c) Stewart (1987) hysteresis model (d) Ceccotti and Vignoli (1990) hysteresis model	90
Figure 5.2	(a) Moment-rotation “Florence” model (Ceccotti and Vignoli 1989) of a semi-rigid joint with typical loop shape in cyclic response; (b) Parameters required by the proposed constitutive relation (modified from Dolan 1994)	91
Figure 5.3	(a) Finite element model implementation for structural model; (b) beam-to-column joints with an elastic-perfectly-plastic load-slip relationship of the dowels	92
Figure 5.4	(a) Ductile collapse mode; (b) brittle collapse mode	94
Figure 5.5	FEM II numerical model and joint definition for non-linear time-history analyses	95
Figure 5.6	Scheme of joints for the Moment-Rotation curve evaluation; (a) Yield of joints; (b) Ultimate state of joints	97
Figure 5.7	(a) Moment-Rotation law for dowelled cross-lapped joint with two crowns of dowels; (b) Yield moment formula; (c) Ultimate moment formula; (d) Yield rotation formula; (e) Ultimate rotation formula; (f) definition of rotational ductility	103
Figure 5.8	(a) Geometrical dimensions of the specimen tested by Polastri et al. (2008); (b) Static design of specimen	105
Figure 5.9	(a) Test arrangement; (b) Cyclic displacement sequence; (c) Moment versus rotation responses for cyclic loading	106
Figure 5.10	Inelastic displacement response curve for test based on the EN 12512 (CEN 2001) loading protocol	107
Figure 5.11	(a) Loading protocol in cyclic tests in accordance with the complete procedure of EN 12512; (b) Definition of equivalent viscous damping ratio in a cycle (modified from EN 12512; CEN 2001)	108
Figure 5.12	Fitting curves of equivalent viscous damping versus displacement ductility	110
Figure 5.13	Superposition of the the envelope Moment-rotation curves, theoretical and experimental, on the full cyclical response of the MR joint	111
Figure 5.14	Comparison of displacement between the pushover curve provided by the FEM I Model and the experimental curve	112
Figure 5.15	(a) Finite element model for non-linear time history analysis (FEM II); (b) moment-rotation Pivot hysteretic model with measured experimental values	113

Figure 5.16	Comparison of moment-rotation relationship, with the experimental dataset for two levels of displacement and three cyclic loading sequences	114
Figure 5.17	(a) Chart of stress-strain curve after tensile test of steel wire of dowels; (b) Mechanical properties of dowel measured (modified from Polastri et al. 2008)	118
Figure 5.18	Trends of input variables selected in the MC Simulation; Probability distribution $f(x)$ for the function x ; Probabilistic models for properties for glued laminated timber in accordance with JCSS (2007)	122
Figure 5.19	(a) Histogram of displacement error $E_{\%}(\Delta_d)(\%)$ (μ , average value; σ , standard deviation)	123
Figure 5.20	(a) Displacement error chart in function of the displacement ratio Δ_j (joint displacement) to Δ_d (total deformation) and histogram without gravity coefficient c_G ; (b) Displacement error chart in function of the displacement ratio Δ_j (joint displacement) to Δ_d (total deformation) and histogram with gravity coefficient c_G (μ , average value; σ , standard deviation, R^2 , coefficient of determination)	125
Figure 5.21	Displacement error $E_{\%}(\Delta_d)$ for the calibrated formula to estimate design displacement Δ_d	128
Figure 5.22	Geometrical dimensions of the three case studies investigated	131
Figure 5.23	(a) Selection of the accelerograms; (b) Elastic displacement response spectra	135
Figure 5.24	Pushover curve for the three case studies analyzed	136
Figure 6.1	(a) Load distribution for a group of dowels in a rhombic pattern due to bending (M) and shear (V); (b) Design scheme dowel-type MR joint	144
Figure 6.2	Load distribution for a group of dowels in a generic pattern due to bending (M) and shear (V)	148
Figure 6.3	(a) Failure mode of nails under cyclic actions: nails crush wood fibres and cavity is formed at the edges of joined material; (b) Impairment of the strength ΔF between the first and the third load cycles with the same deformation; (c) Energy dissipated during a cycle: due to embedment of wood and plasticity of the connections; (d) Global seismic response of a full-scale residential building (pictures modified from Ceccotti 1995)	149
Figure 6.4	Modified Möller's diagram for nails with diameter ranging from 2 mm to 3.1 mm and steel strength ranging from 5 th to 95 th	152
Figure 6.5	Displacement decomposition of shear walls	153
Figure 6.6	Displacement decomposition of shear walls, with the contribution of each component	154

Figure 6.7 Analytic model to evaluate bending displacement (Δ_b)	154
Figure 6.8 Analytic model to evaluate shear displacement (Δ_v)	155
Figure 6.9 Analytic model to evaluate displacement due to slip of nails (Δ_n)	156
Figure 6.10 Failure mode II of fasteners in single shear panel-to-timber connections	159
Figure 6.11 Restoring situation of fastener in single shear panel-to-timber connection	160
Figure 6.12 Description of the CASHEW model (modified from Filiatrault and Folz 2002)	164
Figure 6.13 Evolutionary Hysteretic Parameter Model (EPHM) developed during the NEESWood project (modified from Pei and van de Lindt 2007)	167
Figure 6.14 (a) Shear wall structure; (b) Mechanical parameters with defined probability density functions	168
Figure 6.15 (a) Shearwall backbone curve parameters; (b) Equivalent linearization of non-linear backbone curve (modified from Pang and Rosowsky 2007)	169
Figure 6.16 Backbone curve for a set of shear walls and in dots the corresponding design force/displacement analytical evaluation (adopted Judd & Fonseca modified model)	172

LIST OF TABLES

Table 4.1 Geometrical limits of the portals commonly adopted in Europe	43
Table 5.1 Experimental measured parameters and estimated equivalent viscous damping value	109
Table 5.2 Proposed equivalent viscous damping value for the test specimen	110
Table 5.3 Parameters of Priestley's viscous analytical model, calibrated using outcomes of test	110
Table 5.4 Error in the equivalent viscous damping in cycle 5 and cycle 6 of test. Experimental versus numerical data using FEM II Model	115
Table 5.5 Error in the equivalent viscous damping evaluated for the design displacement Δ_d ; Experimental versus analytical values with elastic-perfectly plastic curve of connectors	117
Table 5.6 Error in the equivalent viscous damping evaluated for the design displacement Δ_d ; Experimental versus analytical values with elasto-plastic hardening curve of connectors	118
Table 5.7 Summary of main statistical quantities for displacement error $E_{\%}(\Delta_d)$	128
Table 5.8 Geometrical and mechanical parameters of the three cases investigated	132
Table 5.9 Moment-rotation Pivot hysteretic curve parameters of the beam-to-column joint for the three cases	133
Table 5.10 Results of Non-Linear Time History Analyses (NLTHA)	137
Table 5.11 Pushover results of the three case studies (CASE A, B and C)	138
Table 5.12 Analytical EVD versus average value of EVD evaluated via non-linear time-history analyses (NLTHA)	138
Table 5.13 Numerical mean value of EVD versus analytical prediction of EVD for the three cases studied	139
Table 5.14 Final values of EVD for the three cases examined	141

Table 6.1	Backbone numerical parameters for shear walls built with different configurations of connectors (selection from Pang and Rosowsky 2007)	170
Table 6.2	Comparison between backbone parameters and estimated parameters for the selected shear walls	171
Table 6.3	Error in evaluation of shear wall design parameters	172
Table 6.4	Equivalent stiffness, k_{eq} (kN/mm) at target drift (% of wall height) for shear walls built with different configurations of connectors (selection from Pang and Rosowsky 2007)	173

NOMENCLATURE

The nomenclature used within this text is in agreement with the Safety Structural Code developed by the European Committee for Standardization, known as EUROCODE.

The following nomenclature is used throughout this thesis:

A	Area
a	half the length of the rhombic area in the horizontal direction
a_{eq}	Parameter to define pitch between two connectors
a_g	Ground acceleration
A_s	Cross-section area of studs
a_w	Aspect ratio of each sheathing panel
b	half the length of the rhombic area in vertical direction
b_b	Thickness of section of the beam
b_c	Thickness of section of the column
b_w	Wall panel width
C	Constant defined based on hysteretic model
c_2	Semi-empirical numerical parameter to define edge distances for dowels on a knee joint
c_{EVD}	Calibration coefficient for Equivalent Viscous damping model (EVD)
c_G	Coefficient to reduce inelastic displacement
C_J	Dimensionless configuration parameter of the beam-to-column joint
$c_{p,1}$	First calibration parameter
$c_{p,2}$	Second calibration parameter
c_{rwall}	Reduction factor
c_{scal}	Scaling factor of PGA
c_w	Number of sheathing panels along the length of edge of the frame
d	Diameter of connector
E	Timber elastic modulus
$E\%(\Delta_d)$	Error in displacement (percentage value)

$E_{dis,dowel,ext}$	Dissipated energy by internal connectors
$E_{dis,dowel,int}$	Dissipated energy by external connectors
$E_{dis,J}$	Dissipated energy by the beam-to-column joint
E_{diss}	Energy dissipated per half cycle
E_e	Energy dissipated between the instant in which the fastener regains stiffness from contact with the wooden surface and the instant when the previous displacement is reached
E_f	Energy dissipated by the effects of friction and plastic deformation of the connector in the recovery phase of the initial configuration
$E_{hyst,joint}$	Hysteretic energy dissipated by the beam-to-column Joint
$E_{hysteretic}$	Hysteretic dissipated energy by the structure
e_n	Slip of the nailed connection at a corner of the sheathing panel
E_p	Energy dissipated by plastic deformation of connector during the loading phase
E_{pot}	Available potential energy per half cycle
$E_{storage}$	Potential energy; Available potential energy
$E_{\dot{\epsilon}eq,JOINT}$	Error in equivalent viscous damping of the beam-to-column Joint
F	Force; Load
$F_{0,FBM}$	First parameter of Foschi and Bonac model
F_r	Restoring Force
f_h	Embedment strength
$f_{h,0,k}$	Characteristic embedment strength along the grain
$f_{h,1,k}$	Characteristic embedment strength of external timber member
$f_{h,2,k}$	Characteristic embedment strength of central timber member
$f_{h,\alpha_f,k}$	Characteristic embedment at an angle α_f to the grain
f_m	Bending strength
F_M	Component stress due to bending moment of the most critical dowels; Forces on the connectors due to bending moment
$F_{M,e}$	Forces on the connectors in external crown due to bending moment
$F_{M,i}$	Component stress due to bending moment of the i^{th} dowel
$f_{m,k}$	Characteristic bending strength
F_n	Yield Force
$F_{N,i}$	Component stress due to axial force of the i^{th} dowel
F_u	Ultimate Force
f_u	Ultimate strength of steel
$f_{u,exp}$	Experimental value of the ultimate strength of the connector
$f_{u,k}$	Characteristic tensile strength of connectors
F_V	Component stress due to shear of the most critical dowels; Forces on the connectors due to shear force
$F_{V,d,i}$	Total force acting on the i^{th} dowel
$F_{V,i}$	Component stress due to shear of the i^{th} dowel
$F_{V,w}$	Shear resisting force of the shear wall, Load-carrying capacity of the shear wall

F_w	Force at the top of shear wall
F_y	Bearing capacity; Load-carrying capacity of connector; Shear capacity
$F_{y,exp}$	Experimental value of the yield strength of the connector
$f_{y,exp}$	Experimental value of the yield strength of the connector
g	Acceleration of gravity
G_p	Shear modulus for the sheathing panels
h	Depth of section of the elements in beam-to-column Joint
h_b	Depth of section of the beam
h_c	Depth of section of the column
H_c	Column height
H_e	Effective height of building
H_i	Height of the i -mass locations of the structure
h_w	Wall panel height
i	Space between portals (pitch)
J_b	Moments of inertia of the beam
J_c	Moments of inertia of the column
$k_{0,FBM}$	Third parameter of Foschi and Bonac model
$k_{1,FBM}$	Second parameter of Foschi and Bonac model
$k_{d,i}$	Stiffness of the i^{th} dowel (slip direction)
k_e	Effective stiffness
k_{eq}	Equivalent stiffness
k_i	Initial stiffness of building; Initial stiffness
k_{rc}	Stiffness in recharge phase of loading
k_s	Secant stiffness
k_{SER}	Slip modulus
k_{ULS}	Ultimate slip modulus
k_{Φ}	Rotational stiffness
$k_{\Phi,u}$	Ultimate rotational stiffness
$k_{\Phi,y}$	Elastic rotational stiffness
L	Length
L_L	length in the longitudinal direction of warehouse
l_w	Diagonal length of the sheathing panel
m	Number of portals
M	Bending moment
m_e	Equivalent mass
m_i	Mass of the i -mass locations of the structure
M_J	Bending moment acting on the beam-to-column Joint
$M_{R,b}$	Yield moment of the beam; Resisting moment of the beam

$M_{R,J}$	Bending capacity of the beam-to-column Joint
M_s	Moment of equilibrium in the return of the configuration to its undeformed state
m_s	Number of nail spacing along the length of the sheathing panel
M_u	Ultimate bending moment of the beam-to-column joint
M_y	Yield moment
$M_{y,Rk}$	Characteristic fastener yield moment
n	Number of modes
n_1	Number of connectors in the first crown
n_2	Number of connectors in the second crown
n_{crowns}	number of crowns in the moment-resisting connections
$n_{eq,el}$	Equivalent number of dowels for the elastic range
$n_{eq,pl}$	Equivalent number of dowels for the plastic range
n_{ext}	Number of connectors in external crown
n_{int}	Number of connectors in internal crown
N_J	Axial Force acting on the beam-to-column Joint
n_j	Number of dowels in the j^{th} crown of the beam-to-column Joint
N_{nails}	Number of "resisting" connections
n_s	Number of nail spacing along the height of the sheathing panel
n_{tot}	Total number of connectors
P	Force; Base shear
PGA	Peak ground acceleration
q	Load acting on a structure in a quasi-permanent combination
q_{lim}	Vertical load leading to structure collapse due only to gravity load (ultimate static condition)
R	Internal beam radius
r	Radius of the crown
r_1	Radius of the first crown
r_2	Radius of the second crown
r_{ext}	External radius
r_j	Radius of the j^{th} dowel
r_{int}	Internal radius
r_j	Radius of the j^{th} crown of the moment-resisting connections
R_k	Characteristic load-carrying capacity
rk_i	Post yield stiffness
r_{max}	Maximum distance between the rotation centre C and the most critical dowel
$S_A(T)$	Period-dependent response acceleration coefficient from response spectrum
s_{nails}	Spacing of nails
t	Time
T	Period

t_1	External member thickness
t_2	Central member thickness
T_C	Upper limit of the period of the constant spectral acceleration branch
T_D	Value defining the beginning of the constant displacement response range of the spectrum
T_e	Effective period
t_p	Effective thickness of the sheathing panels
T_s	Fundamental period of structure
u	Slip
v	Displacement of the connections
V_B	Base shear; Design base shear
V_J	Shear stress acting on the beam-to-column Joint
v_y	Displacement at yield of the connections
W	Seismic weight
θ	inter-storey drift
Δ	Displacement
Δ_b	Elastic bending displacement of members
Δ_d	Design displacement
$\Delta_{d,experimental}$	Design displacement estimated via data tests
$\Delta_{d,NLTHA}$	Maximum (design value) displacement evaluated via Non-Linear Time-History Analyses
$\Delta_{d,numerical}$	Design displacement estimated via numerical analyses
$\Delta_{d,PUSH}$	Displacement extracted by the non-linear static analyses (pushover)
Δ_i	Design displacement of the i^{th} mass locations of the structure
Δ_j	Inelastic displacement
Δ_n	Non-linear displacement induced by the panel-to-frame connections
Δ_p	Plastic displacement; Inelastic displacement
Δ_s	Elastic displacement
Δ_t	Target displacement
$\Delta_{t,max}$	Maximum value of the target displacement
Δ_u	Ultimate displacement
Δ_v	Shear displacement of the panel
Δ_y	Yield displacement
$\Delta\delta/\delta$	Increase of slip compared to the past
Φ	Rotation
Φ_u	Ultimate rotation
Φ_y	Yield rotation
α	Angle
α_d	Over-strength design factor
α_f	Angle between a force and the direction of grain

α_{HHT}	Third coefficient of the Hilber Hughers-Taylor (HHT) method for numerical integration
α_n	n -eigenvalue
α_{Pivot}	First coefficient of Pivot model
α_r	Roof slope
α_R	Overstrength factor
α_{sh}	Hardening coefficient
$\alpha_{sh,measured}$	Hardening of steel on the connector
β	Ratio between the embedment strength of the members
β_{HHT}	Second coefficient of the Hilber Hughers-Taylor (HHT) method for numerical integration
β_k	Ratio between the initial stiffness and the stiffness in recharge phase
β_{Pivot}	Second coefficient of Pivot model
β_t	Ratio between the depth of timber section and radius of the moment-resisting connection
$\beta_{t,II}$	Geometrical dimensionless parameters
δ	Slip
δ_i	Tangential slip
δ_u	Ultimate slip
δ_y	Yield slip
ε	Strain
ε_y	Yield strain of timber
γ_{HHT}	First coefficient of the Hilber Hughers-Taylor (HHT) method for numerical integration
γ_{jn}	The n -participation factor of the j^{th} level of the building
γ_t	Ratio of timber portal length to section depth
η_{Pivot}	Third coefficient of Pivot model
μ_{Δ}	Ductility of the structure; Displacement ductility; Static ductility
μ_{ω}	Rotational ductility
μ_s	Static slip ductility
θ_t	Aspect ratio of portal frame
ρ_{exp}	Experimental value of the wood density
ρ_k	Characteristic density of wood
ρ_m	Mean density of glulam
σ	Stress
σ_F	Ratio between the restoring force and the bearing capacity
$\sigma_F=b/a$	Ratio between the half of sides of the perimeter that encloses the MR connection
ξ	Damping ratio
ξ_d	Design damping; Design value of Equivalent Viscous Damping(EVD)
ξ_{eq}	Equivalent viscous damping (EVD)
$\xi_{eq,dowel}$	Equivalent viscous damping of connectors

$\xi_{eq,i,dowel}$	Equivalent viscous damping of the i^{th} connector
$\xi_{eq,JOINT}$	Equivalent viscous damping of the joint
$\xi_{eq,NLTHA}$	Equivalent viscous damping evaluated via Non-Linear Time-History Analyses
ξ_{hyst}	Hysteretic viscous damping
ξ_0	Constant viscous component

1 INTRODUCTION

1.1 General

The performance of wooden buildings under very severe seismic forces was verified following the Northridge (1994) earthquake in the United States, and the earthquake in Kobe (1995), which affected a wide area of Japan in 1995. The former, in particular, highlighted the inadequacies of some wooden structures in regard to post-earthquake usability, as a result of significant structural and non-structural damage, especially when buildings were not appropriately designed (See Karacabeyli and Popovski 2003). Some images of earthquake consequences highlight structural problems and damage found to the buildings (Figure 1.1). Many of the structures that were seriously compromised by the earthquakes in Kobe and Northridge were later demolished in the phase of post-seismic operations.

It is clear that the cost of repair or reconstruction of buildings after an earthquake can be very high. For some classes of buildings, we need to ensure full or partial use after the earthquake, so that essential services can be maintained. Moreover, today's demand for more sustainable technologies has led to the rediscovery of building techniques and materials that better satisfy this condition. Wood is one of these materials and it is no coincidence that in North America two research projects have been financed, both aiming to mitigate the effect of earthquakes on wooden residential buildings (NEESWood Project; Seesl 2006 and CUREE-Caltech Woodframe Project; Curee 2008).

So the new challenge in seismic design is to build structures in which the acceptable level of damage caused by the earthquake is predetermined. This means implementing a reliable design code that relates the building performance, damage and the intensity of ground motion as much as possible (Karacabeyli and Popovski 2003).



(a) and (b): damage to wooden buildings after the Northridge Earthquake; California, 1994 (FEMA 2010)



(c) and (d): damage and collapse of wooden buildings after the Kobe Earthquake; (Kitagawa and Hiraishi 2004)



Figure 1.1. Overview of building damage after recent two earthquakes: Northridge 1994 with Magnitude of 6.7 and Kobe (Hanshin-Awaji) 1995 with Magnitude of 7.2 (Richter scale)

Laboratory work has helped to clarify the relation between damage to structural elements and the displacement/strain level. To identify the displacement as a criterion for design is, therefore, to control the damage mechanism and to predict the expected economic losses due to an earthquake (Calvi 2003).

In the seismic structure design, using displacement-based methods, design criteria are provided in terms of displacement. In displacement-based methods the problem is reduced to the evaluation of displacement available and displacement required for earthquake resistance (Calvi 2003). The safety of the structure is thus evaluated by the comparison of displacements. Figure 1.2 shows the typical Force-Displacement ($F-\Delta$) capacity curve of a structure in the post-elastic state of deformation. In the inelastic field, the displacement, Δ , increases without significant changes in the force, F , measured on the $F-\Delta$ curve. The trend of the convex curve $F-\Delta$ is very common in ductile structures, regardless of the material and the construction typology.

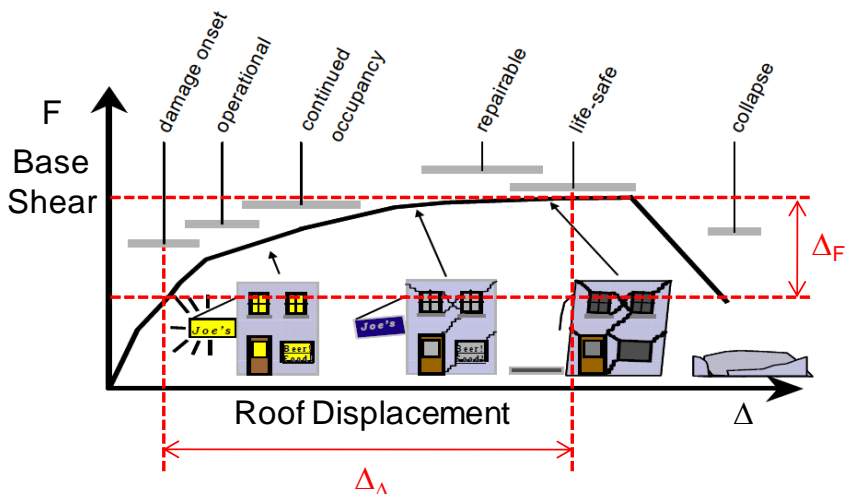


Figure 1.2 Typical performance curve for a structure with relation between displacement/force and damage (modified from Calvi 2003)

The red lines of Figure 1.2 show the efficiency of displacement in assessing structure performance in the inelastic range. It is otherwise very difficult to control the performance, based only on force.

Displacement-based design methods, as a class, are characterised by groups of algorithms which can differ significantly in their application. Currently, there is no agreement on which method is better in terms of reliability. A comprehensive review of the literature on the subject is reported in *Fib Bulletin 25* (Calvi 2003). The same author shows that it is difficult to evaluate the applicability of each procedure based on the state-of-the-art.

The following work is aimed at developing a seismic design procedure, applicable to wooden structures. The proposed procedure, for the design and evaluation of seismic vulnerability of timber buildings, is in the class of displacement-based methods and is known as Direct Displacement-Based Design (Direct-DBD) method. The Direct-DBD is a procedure in which the input design parameter is the displacement value and in which no iterative procedures are required in the computational phase. Priestley formulated the Direct-DBD procedure in 1993 and then codified it in 2003, for concrete structures (1993, 2003).

Recently Priestley *et al.* (2007) have published a book on the Direct-DBD approach, describing the state of development for different materials and construction typologies and presenting a first draft model code.

1.2 Objectives and scope

This work aims to allow the application of Direct-DBD to wooden structures. The analytical method developed focuses on buildings used in the European construction market.

The specific objectives are to:

- I. develop analytical expressions for the estimation of design parameters required by Direct Displacement-Based Design (Direct-DBD),
- II. validate the analytical model to predict with qualitative confidence the real values of design parameters,
- III. define guidelines to apply the Direct -DBD method to a generic structure in wood,

- IV. draft a model code, a commentary and some design examples on new built structures.

Although the analysis has been developed with reference to wooden structures identified as system with single degree of freedom (SDOF), the design model can be easily extended to structural systems with more degrees of freedom (MDOF). In this thesis the model has been extended to MDOF systems used in residential wooden construction.

The use of a Direct-DBD procedure implies some inherent difficulties in the design process, since assessing the safety is expressed in terms of displacement. This design philosophy is very different from the static design method, in which the safety verification utilizes the force or stress level reached in each structural element.

Displacement is a parameter related to the damage to the structural and non-structural elements. The use of displacement in the design process in the Direct-DBD method allows a prediction of the damage following an earthquake and, thus enables planning for the depreciation cost of buildings, repair costs, or demolition work, in the post-seismic conditions.

1.3 Dissertation overview

In Chapter 2 various aspects of the seismic response of timber constructions are described. The description of construction typologies, accompanied by the assembly design rules, highlights the role of connections in the global behaviour of a structure.

Chapter 3 presents the Direct-DBD method codified by Priestley (2003); the state-of-the-art of the Direct-DBD method applied to wooden buildings follows.

The limited literature on Direct-DBD applied to wooden structures does not yet allow a critical discussion, in contrast with that allowed by, for example, the literature on reinforced concrete structures. The introduction to the method and the explanation of the existing procedures support the formulation proposed in this thesis.

Chapter 4 discusses and presents the analytical formulation of the design parameters required by the Direct-DBD method. In this Chapter the design parameters are defined for the ultimate limit state (ULS) of the structure. The ULS condition is a particular level of performance which matches the maximum carrying capacity of the SDOF structure.

Chapter 5 addresses the validation of the mathematical model by using a Monte Carlo simulation (MC). The numerical-probabilistic MC simulation uses a specific finite element model (FEM) developed for connections with dowel-type metal fasteners. Outcomes of the FEM models correspond to those obtained experimentally on a specific configuration of the connection. In this Chapter the results of non-linear static and dynamic analysis are detailed. The Chapter closes by reporting the calibration of the design parameters.

Chapter 6 discusses guidelines for extension of the analytical model to other geometric configurations and other structural types, such as those commonly used in the construction of multi-storey buildings for residential use. The Chapter describes principles by which the mathematical model described at Chapter 4 can be applied to a variety of construction types using a modern type of connections, made with metal connectors with a cylindrical shank.

The conclusions of the research and recommendations for future work are presented in Chapter 7.

Appendix A describes the structure of the software written in Visual Basic to perform the Monte Carlo simulation. In Appendix B additional information is given on the glulam portal frame reference structure. Appendix C describes the additional model to evaluate equivalent viscous damping of dowel-type metal fasteners. Finally, Appendix D lists the publications produced during the research period.

2 EARTHQUAKES AND WOOD STRUCTURES

2.1 Performance of wood in earthquake conditions

The strength and reliability of wooden buildings in meeting the life safety demand under earthquake loads is recognized, especially when the structure is regular and extends evenly inside the building. However, to avoid collapse and reduce damage and casualties in timber buildings, an appropriate design, high quality workmanship and proper maintenance must be ensured (Karacabeyli and Popovsky 2003). In areas of high seismic risk, such as Japan and China, there are still buildings that testify to the construction techniques adopted to resist earthquakes (e.g. the Sakyamuni Pagoda built in 1056 in China, See Smith and Frangi 2008).

Residential buildings are normally limited in height to four storeys above ground. The height limit of residential buildings in wood is the effect of the restrictions imposed by some jurisdictions in respect of fire safety and, often, the ignorance shown by designers regarding the dynamic behaviour of systems with multiple degrees of freedom, MDOF (Smith and Frangi 2008).

Currently there are numerous analytical and numerical models formulated to describe the dynamic behaviour of timber structures. The study of the dynamic response of structures is often concerned with tall or slender buildings. In 2008, the international journal *Structural Engineering International* (IABSE) dedicated a special issue to tall buildings made of wood. Various authors who participated in the making of this edition emphasized the need to design tall timber buildings which prevent and limit the damage caused by earthquakes. Of particular interest were the contributions of: Teibinger (2008), Cheung (2008), Lam *et al.* (2008), Langenbach (2008a), Jorissen and Leijten (2008), Langenbach (2008b), Smith and Frangi (2008), Buchanan *et al.* (2008), Pang and Rosowsky (2008) and Heiduschke *et al.* (2008).

New timber civil buildings are built with different techniques and construction typologies. Many systems have undergone the normal process of evolution, such as the progression from traditional to modern methods of assembly of building elements and the use of engineered wood elements in place of solid wood elements. Wooden structures can be classified according to various criteria. This work focuses on the category of timber structures designed to respond to the effects of earthquakes; in particular, we focus on those structures normally used in Europe.

2.2 Suitable wood construction systems in seismic zones

Wood is a building material with good strength capacity compared to the strength-weight ratio of a generic element. The strength characteristics of wood are influenced by its anisotropy and its rheological behaviour (Piazza *et al.* 2005). The strength and stiffness of a wooden construction element vary depending on the defects and the orientation of the applied load compared to the fibre.

The stress-strain curves (σ - ε) of a wooden element show a behaviour which is markedly fragile, except for elements compressed perpendicular to the grain (Piazza *et al.* 2005), as illustrated in Figure 2.1(A). Failure mechanisms due to bending or shear actions are brittle and must therefore be avoided in seismic zones. To ensure a ductile response of the structure, the design of the connections should respect the *Capacity Design* rules (CD rules). The CD rules ensure that the connections are the weakest link between timber elements. The ductility of the system is thus achieved through the proper selection and design of connections (Dolan 1994).

Figure 2.1(B) shows the monotonic load-slip response (F - u) and the level of ductility obtained for a series of wood connections. The dissipative capacity of connections, under repeated loadings, is related to the strength of the materials and to the geometric configuration of the joints. Only certain types of connections give the level of ductility and the hysteretic behaviour desired.

The connections normally used in modern timber construction are elements or metal devices that work to ensure the transmission of forces between structural elements (Piazza *et al.* 2005). A set of wooden structures suitable to ensure ductile behaviour, for example, is that proposed in Figure 2.2. This selection represents construction systems used in the European construction market. Figure 2.3 shows a timber construction system developed in New Zealand and with good prospects of spreading elsewhere in the world, including Europe (Palermo *et al.* 2006).

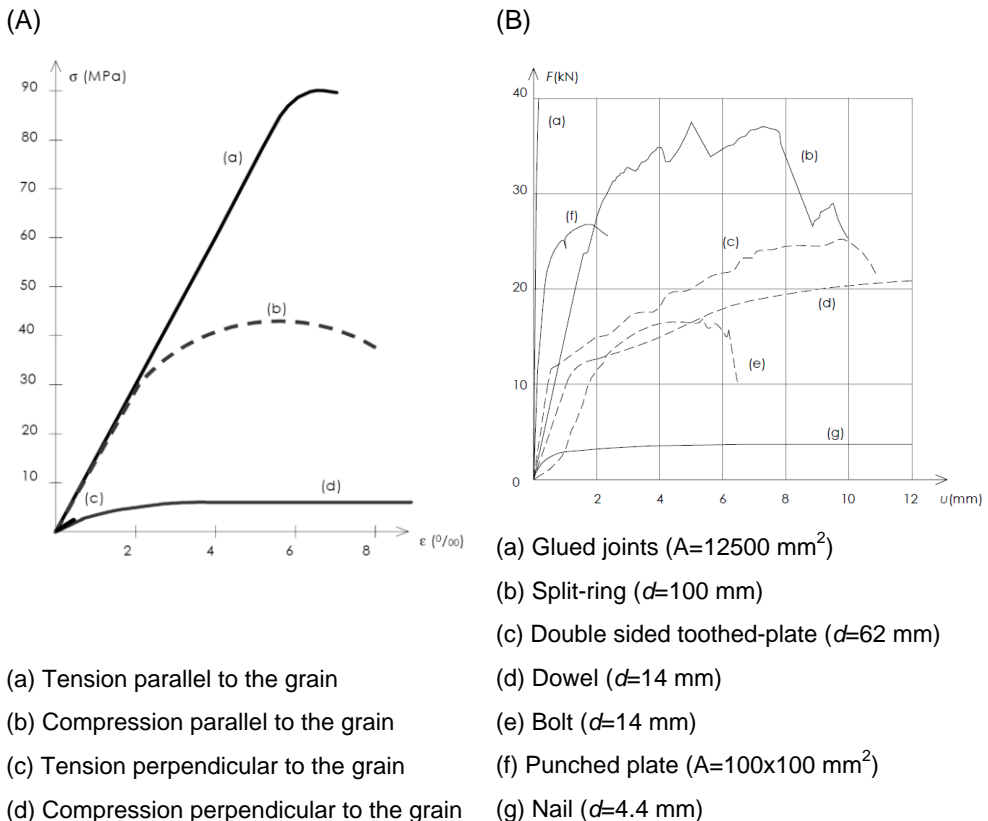


Figure 2.1 (A) Typical stress-strain curves for clear coniferous wood (Piazza *et al.* 2005); (B) Experimental load-slip curves for joints in tension parallel to the grain (Racher 1995a)

Figure 2.2(a) shows the simplified drawing of the construction system used for the construction of commercial, industrial and other open-space buildings. Buildings with a rectangular floor plant are normally built with a wooden frame in the main direction, to support the roof.

Bracing systems and the beams inserted between the frames ensure stability in the longitudinal direction. The main frames are made with portals, as illustrated in Figure 2.2(a), or by arches or trusses (Premrov and Tajnik 2008). The structures are built with solid wood, glued laminated wood or laminated veneer lumber (LVL), the latter also known as micro-glulam. The design of wooden portal frames is closely related to the design of the beam-to-column joint. Depending on the technology used and the construction costs, the length of portal frames covers the range 15-60 m. Portal frames can also adopt rigid beam-to-column joints, made with metal plates inserted between the elements (flanged joints) (Figure 2.4(a)) or large finger joints, bonded with epoxy resin (Figure 2.4(b)). The beam-to-column joint built by the overlapping of elements and the insertion of glued steel bars (Figure 2.4(c)) is a solution that has fallen into disuse.

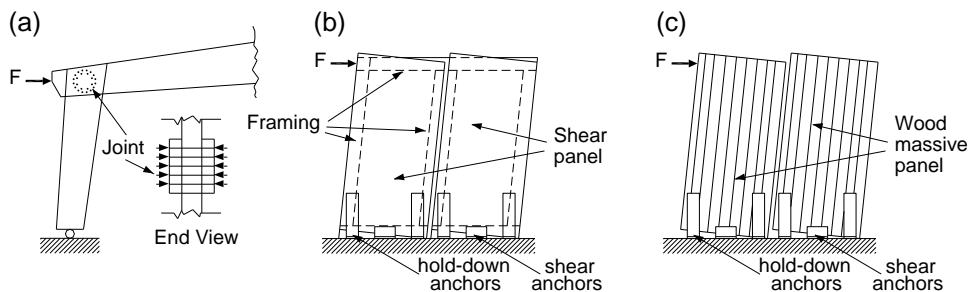


Figure 2.2 Selection of ductile timber structures; (a) Moment-resisting (MR) timber frame system; (b) Timber shear panel system; (c) Cross-laminated timber panel system; (modified from Priestley et al. 2007)

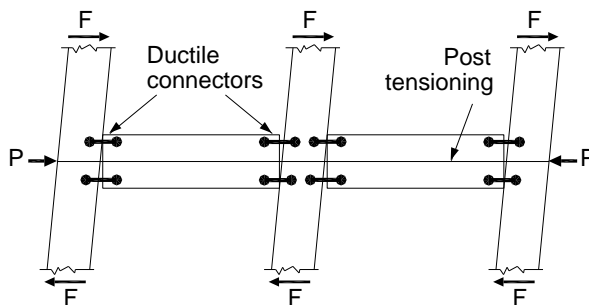


Figure 2.3 Post-tensioned timber frame system (modified from Priestley et al. 2007)

Bonded joints, which give continuity between the beam and columns, do not ensure the required ductility to the structures.

Flanged joints and connections with glued steel bars are still not very common, owing to the cost and to the difficulty of installation. An interesting work aimed at studying the seismic behaviour of joints made with flanged steel sections was recently published by Tomasi *et al.* (2008). Here, interest is directed at joints made with an arrangement of dowel-type metal fasteners.

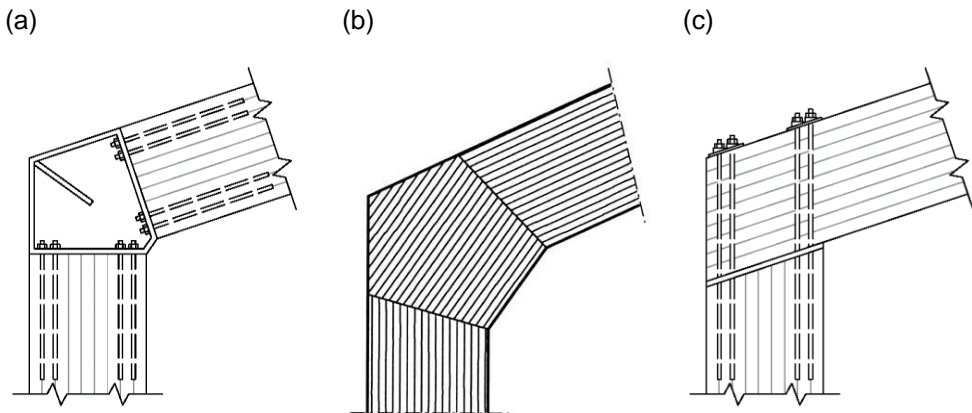


Figure 2.4 (a) MR joint built with flanged elements (from Piazza *et al.* 2005); (b) MR joint built with glued elements (from Racher 1995c); (c) MR joint built with epoxy steel rods (from Piazza *et al.* 2005)

The building systems commonly used to build multi-storey wooden buildings are the *timber frame panel system* (Figure 2.2(b)) and the *cross-laminated timber panel system* (the so-called *cross-laminated solid wood panel system*, also known as the *XLAM system*) (Figure 2.2(c)). In North America, a system still used for its low cost is *post and beams*; the structure is characterized by a skeleton of beams and columns that extend up to the roof (Premrov 2008). This system is also widespread in one-family buildings in Japan. The structure with the timber frame panel system is also known as the *wood frame system*, *light timber-frame system* and *2 by 4 system*. In New Zealand the *wood frame system* covers over 90% of the housing market with one or two storey (Fragiacomo 2009). In Europe, the *wood panel frame system* uses the same construction techniques as in North America and New Zealand. However, in Europe the geometric configuration of panel elements changes slightly, due to the different standard sizes of elements.

There are known two manufacturing techniques used to build structures with the *timber frame panel system*: the *platform frame* and the *balloon frame* system (American Forest and Paper Association 2001).

In the *platform frame* system each floor offers a work surface for subsequent levels, greatly facilitating the process of assembly of the elements (Figure 2.5(a)).

In the *balloon frame system* the exterior walls are continuous and extend from the first floor to the next levels without interruption (Figure 2.5(b)). The beams of each storey are hung on the studs and anchored with metal strips set into the wall surrounding the building. The time required in the process of construction and the difficulty in finding long-studs have led to a rapid abandonment of the *balloon frame system* (American Forest and Paper Association 2001).

In Europe, the *timber frame panel system* has undergone the inevitable process of prefabrication, thereby increasing the level of competition in the residential housing market. The walls are thus pre-assembled in the factory, by joining a series of panels and inserting the doors, windows, and other thermal-acoustic insulation materials (Premrov 2008).

The innovative building system that uses the *cross laminated solid wood panel system* has been introduced recently in the Alpine zone (North of Italy) and is a valid alternative to the traditional *timber frame panel system*.

The concept of global stability of the structure is very similar to that of the traditional *wood frame system* construction, except that the classic timber frame panels are replaced with cross-laminated massive wood panels (wall elements). Similarly, traditional floors made with beams and wood-based panels, are replaced by cross-laminated massive wood panels (plate elements).

The *timber frame panel system* and the *cross-laminated solid wood panel system* are ideal for creating buildings with a large number of partitions such as apartments, condominiums, hotels and other residential buildings (Fragiacomo 2009).

A promising type of construction, which could enter the European construction market, is a system that uses wooden prestressed elements with post-tensioned cables, known as *Prestressed Timber Buildings*. This system is still not very common, but it could be a viable alternative to traditional materials for the building of mid-rise open-space buildings, such as those used to house offices and commercial and recreational activities (Buchanan *et al.* 2008). A series of recent publications explain this construction system, including Buchanan *et al.* (2008), Newcombe *et al.* (2008), Palermo *et al.* (2006) and Kam *et al.* (2008).

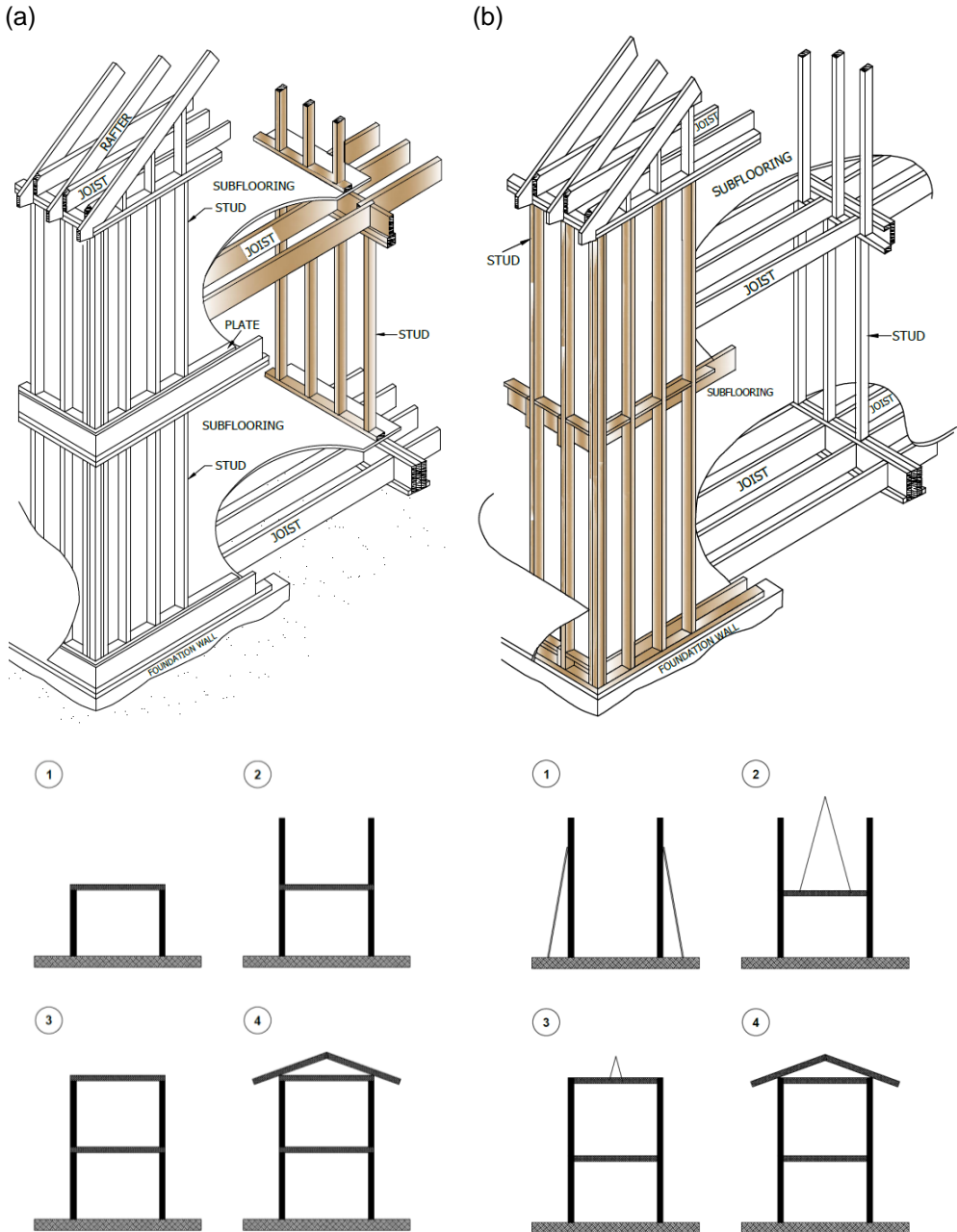


Figure 2.5 (a) Platform frame system (Common in 1940s in the USA): details of structure and construction sequence, from 1 to 4; (b) Balloon frame system: details of structure and construction sequence from 1 to 4 (modified from American Forest and Paper Association 2001)

The published results are the outcome of the project entitled “*Development of new generations of multi-storey timber buildings*”-Research consortium among the University of Auckland and University of Technology of Sydney and the participation of the University of Sassari and University of Milan- coordinated by Professor Buchanan. This structural system was recently introduced in the New Zealand construction market, gaining interest from those in the industry. Within the project coordinated by Buchanan a new type of connection was developed, that ensures the desirable resistance against seismic actions. As part of the research a six-storey building was designed (Figures 2.6(a) and (b)), and an evaluation was undertaken of aspects of its construction and construction costs.

Hybrid building systems represent a viable solution to accompany prestressed systems, in the construction of mid-rise open-space structures (Heiduschke *et al.* 2008). The assessment of the ductility and the dissipative capacity of hybrid systems are hard to deal with in a general manner. An extensive research work that investigates the seismic performance of the hybrid system was made by Sakamoto *et al.* (2004). Shaking table tests were performed to study the dynamic response of wood-concrete hybrid systems in full-scale. The project coordinated by Sakamoto was aimed at the preparation of guidelines for the structural design against earthquake and fire of mixed structures (Heiduschke *et al.* 2008). Particular attention was paid to the study of interaction force between the concrete core and the timber frame. Figure 2.7 shows the structural morphology of hybrid structures. Also in this case the careful design of the connections plays a key role in defining the seismic response of the whole building.

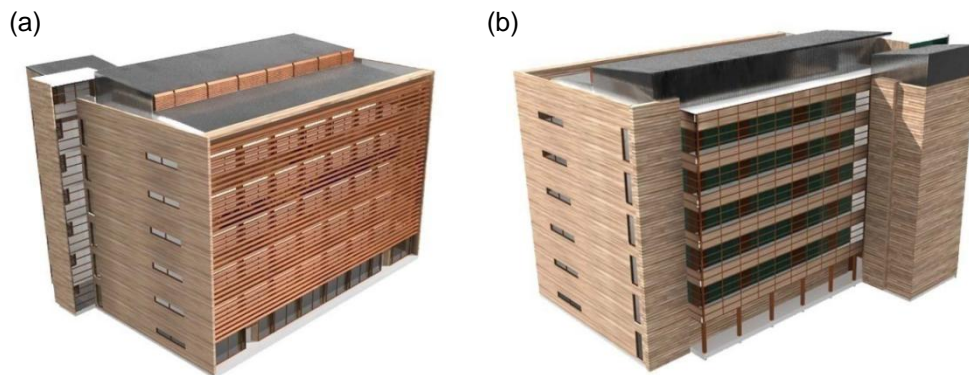


Figure 2.6 Prestressed System; (a) North-east perspective view of the University of Canterbury Biological Science building (modified from Fernandez 2008); (b) South-west perspective view of the University of Canterbury building (modified from Fernandez 2008)

The next three sections analyze the construction systems employed in the European building market. The discussion will be focused on how the forces are transferred between the components and from these to the foundations.

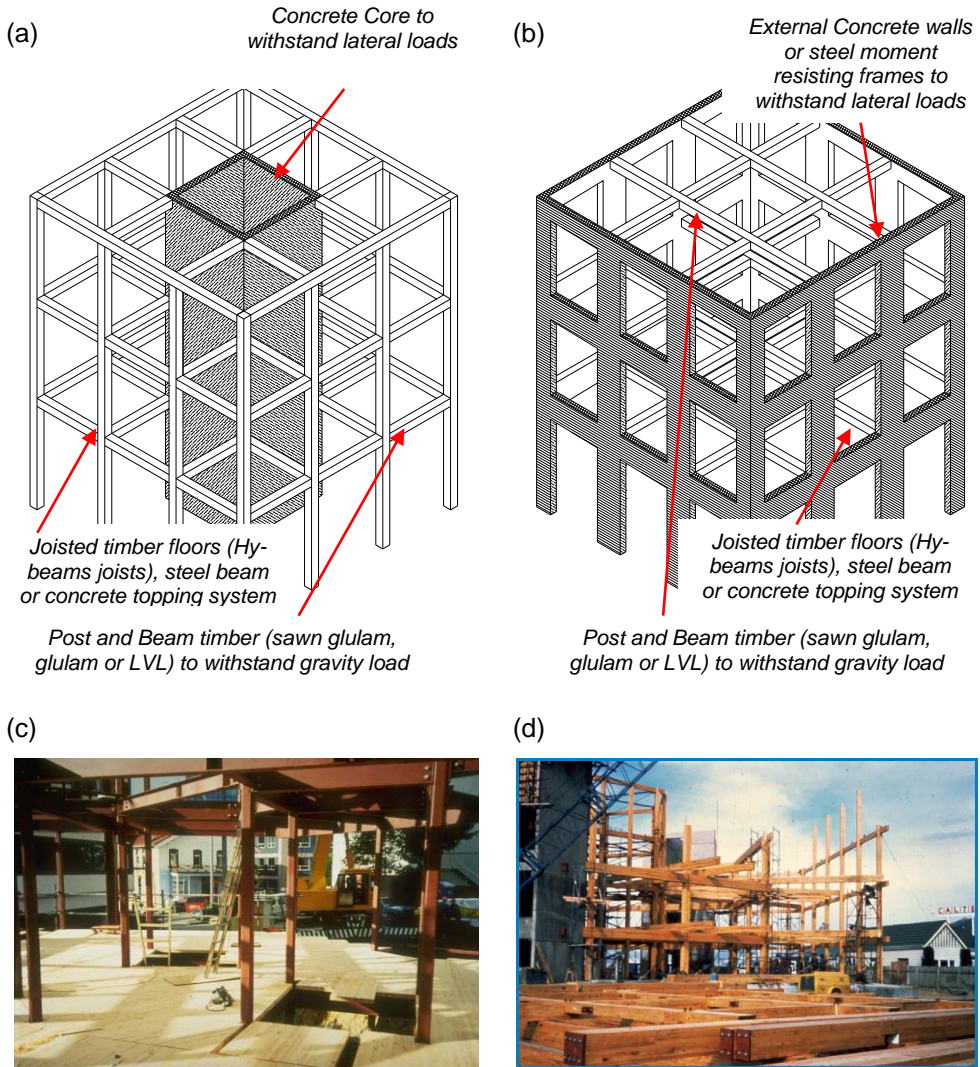


Figure 2.7 Hybrid systems, suitable for tall timber buildings up to 25 storeys; (a) Three-dimensional view of the whole resisting system in configuration No 1 (modified from Sakamoto et al. 2004); (b) Three-dimensional view of the whole resisting system in configuration No 2 (modified from Sakamoto et al. 2004); (c) Phase of realization of the **flooring** (from Fragiaco 2009); (d) Phase of erection of **post and beam** gravity load resisting element (from Fragiaco 2009)

Chapters 4 and 6 discuss in detail the ductility and dissipative capacity of connections, for the different typologies investigated in this research.

2.3 Timber frame systems with moment-resisting connections

The knee joint is a Moment-Resisting (MR) connection in which the forces on the connectors balance the external bending moment applied.

Portal frame systems with MR joints have hinged column-to-foundation restraints and only occasionally have fixed base joints. The construction components are made of laminated wood or LVL (micro-glulam) and are primarily subject to the stress due to bending moment. The main problem is the design of knee connections, with an appropriate solution selected according to the building technology used and the architectural design requirements (Premrov and Tajnik 2008).

Figure 2.8 (a), (b) and (c) show typical beam-to-columns MR joints built using an arrangement of dowel-type metal fasteners (Racher 1995c). In each case, a lateral load-resistance system is employed in the out-of-plane portal direction. Several types of bracing system are available as shown in Figure 2.9.

The construction technique used in Europe to build the joints of the portal frame requires the interposition of a beam between two conical section elements. The elements, in glued laminated timber, are joined with dowel-type metal fasteners placed along the cross-sections (Figure 2.8(a)). The fastener elements work in shear mode, with one or two sliding surfaces, and are subject to the stress on the joint (M_j , N_j and V_j). The design process should consider the effect of the difference in fibre direction between the column and the beam, which can trigger brittle fracture in the timber elements.

In New Zealand and Japan frequently the portal frames are built by joining individual elements (beam and column) with the use of internal metal plates, connected with dowels (Figure 2.8(b)), or external plates in plywood or metal, attached at the surface of elements with nails or dowels respectively (Figure 2.8 (c)).

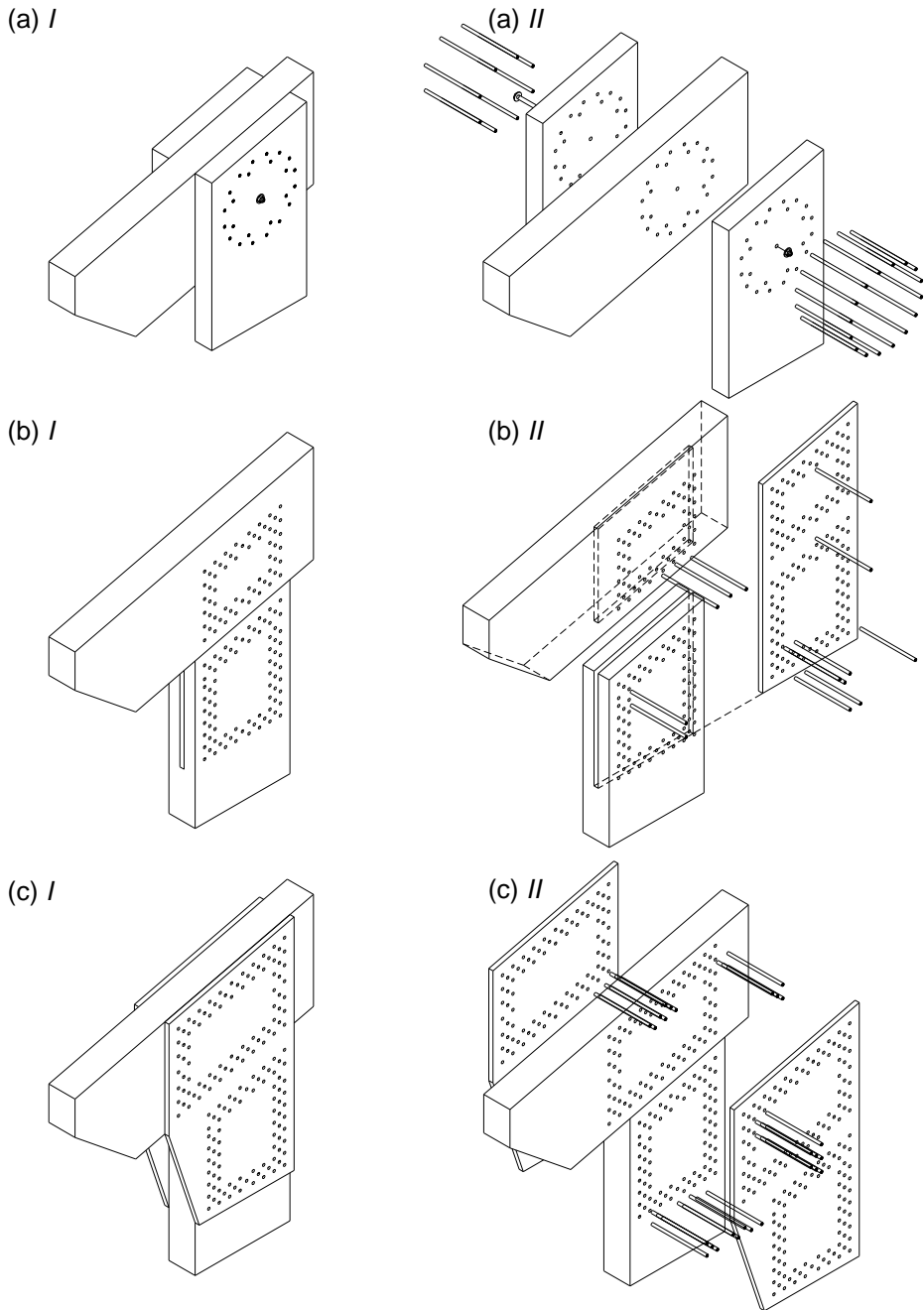


Figure 2.8 3D View (I) and exploded view of the scheme of assembly (II); (a) Dowelled cross-lapped joint; (b) Internal metal plates connected with fasteners; (c) Nailed plywood gussets or metal plate with fasteners

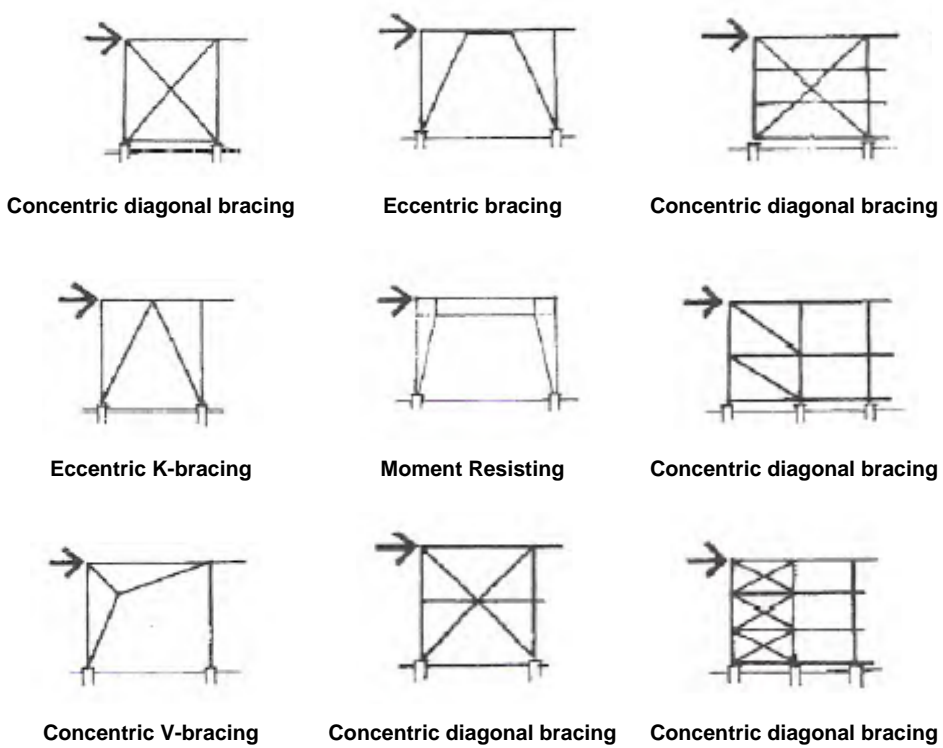


Figure 2.9 Drawing of the common bracing systems between timber frames (Gojkovic and Stojic 1996)

The timber portal frame system has received particular attention in recent years in many countries. Figure 2.10 shows a prefabricated portal frame proposed by a major multinational timber company. A real example of a portal frame system with MR joints made with two crowns of steel dowels is shown in Figure 2.11(a) and Figure 2.11(b). The building was built in Trentino (northern Italy) for the storage of building materials. Appendix B contains the architectural drawings for this industrial warehouse.

2.4 Timber frame panel systems

The *timber frame panel system* is normally used for the construction of residential buildings. The vertical structure, and in some cases the horizontal structure, is constructed through the use of a base module with standardized dimensions (Premrov 2008). The single panel module, known as a *shear wall*, is employed to withstand both the vertical loads and the horizontal loads.

In the *platform frame system*, a construction technique of the *timber frame panel system*, the wall-to-floor connections are made by blocking the beams between the studs of two successive levels of the building, as shown in Figure 2.12. Figure 2.13 shows the process of construction and the construction details of *shear walls* in the *platform frame technique*.

“Kerto” system portal frame: Standard trend of available dimension of members

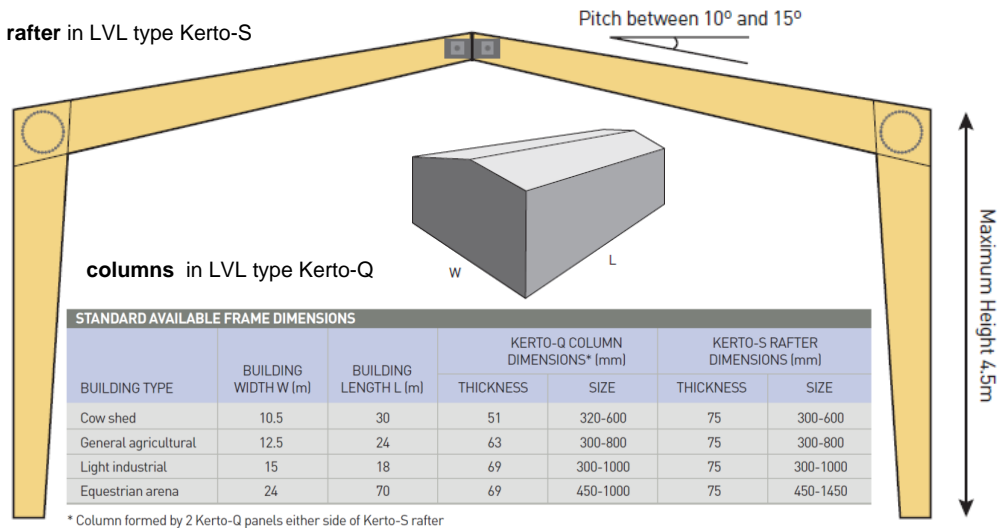


Figure 2.10 Commercial “Kerto” portal frame solution for light industrial, warehouse, agricultural or equestrian buildings; Three dimensional view of prefabricated elements (modified from Finnforest 2009)

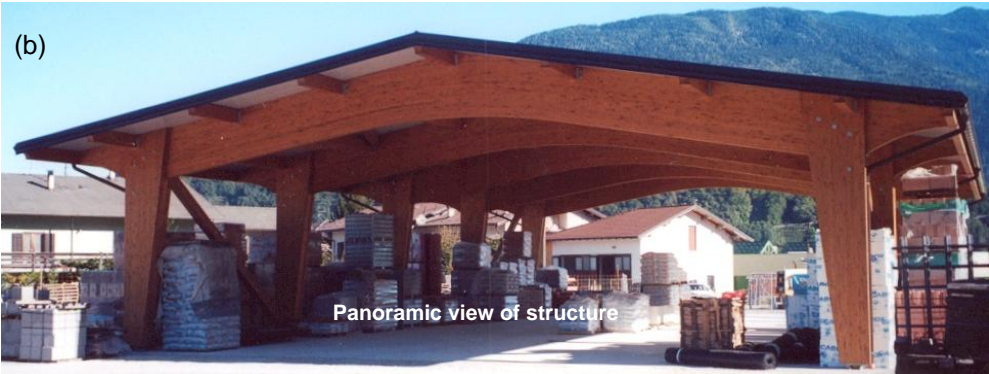
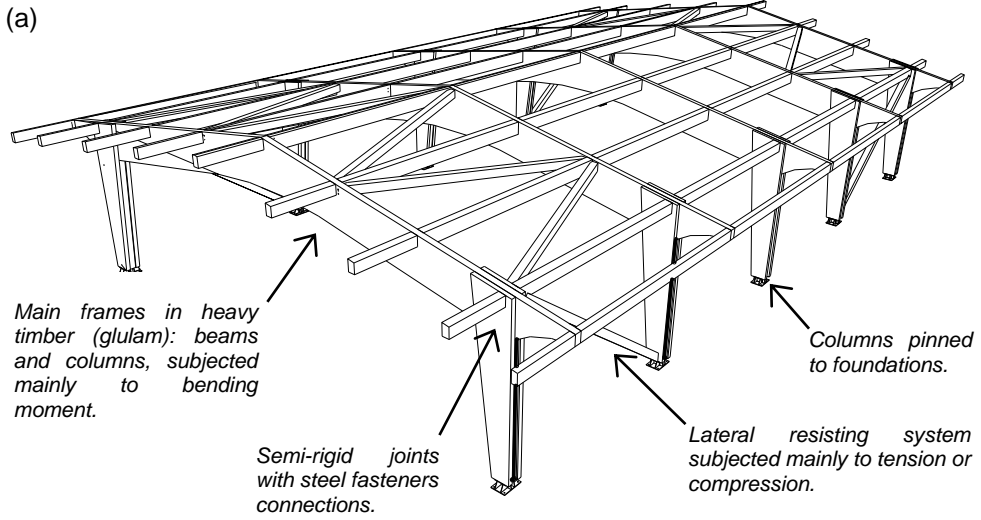


Figure 2.11 (a) Three-dimensional view of the Timber Portal frame system with dowelled cross-lapped joints (so-called “heavy timber structure”); (b) Details of an industrial warehouse built in Trentino (Italy)

Each wall of the building consists of a main timber frame, and wood-based panels mechanically fixed to one or both sides. Within each wall there is the single *shear wall*, replicated up to cover the length of wall in one direction. The typical *shear wall* is composed of three timber studs in sawn timber, LVL or glulam, upper and lower plate and sheathing panels in OSB, plywood, particleboard or other wood-based panels, fixed with mechanical connectors at the edges of the timber frame (Premrov 2008).

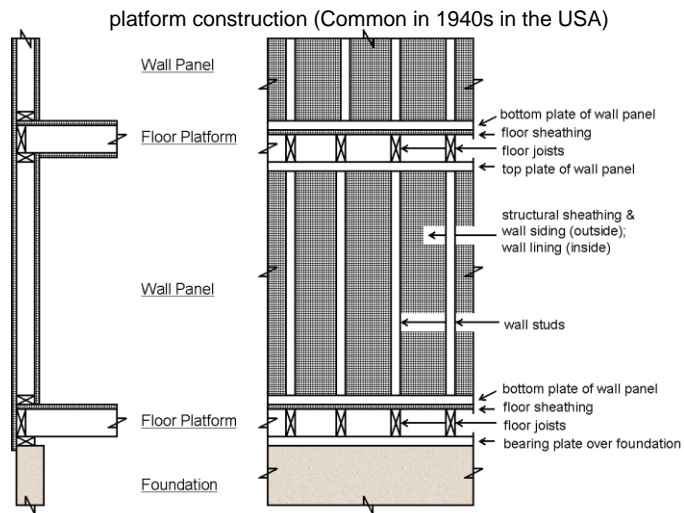


Figure 2.12 Details of wall-to-floor joints of platform frame system construction (courtesy of Professor Ian Smith)

A series of transverse reinforcements between the studs are used when sheathing panels are oriented horizontally or there is a need to stiffen the *shear wall* element.

In a *shear wall* the spacing of studs is a function of the standard dimensions of sheathing panels. The standard width of panels results is 1.25 meters in Europe, 1.2 meters in New Zealand and 1.22 meters in North America and Canada. The standard height of panels is double the width and ranges from 2.4 to 2.5 meters. Panels are generally fixed to the timber frames with mechanical fasteners such as nails or screws. To meet technical requirements, sheathing panels in gypsum or in wood-based composites are often used, while other thermal insulation materials are inserted between studs. The traditional technique described above is known as the *Micro-Panel Wall System* (Premrov 2008).

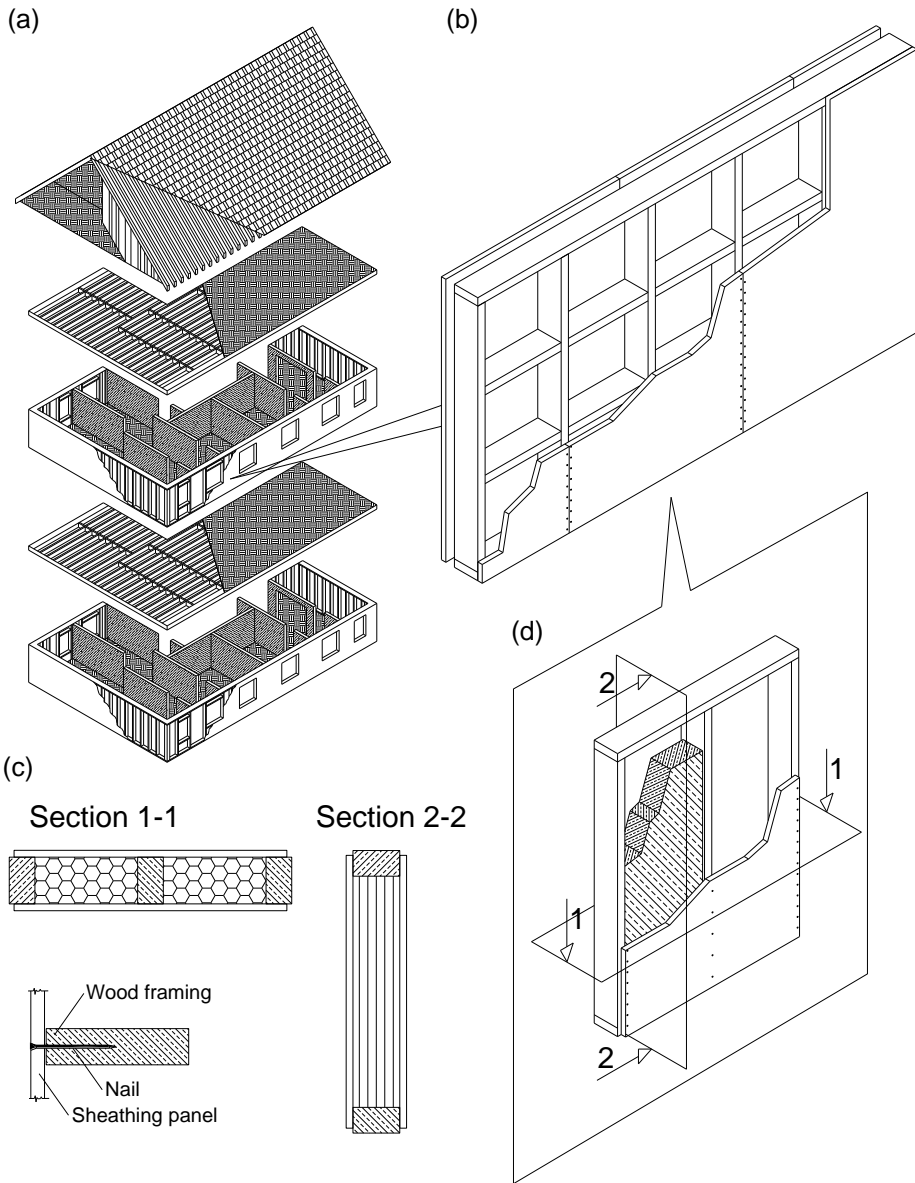


Figure 2.13 Schematic presentation of the timber frame panel construction following the platform frame technique; (a) exploded view of wood frame building; (b) shear wall layers; (c) shear wall panel module; (d) sections of shear wall panel module and mechanical fasteners of wood-based sheathing panels; (Pictures Modified from Premrov 2008)

Additional details on *shear walls* are given by Prion (2003). Nowadays it is increasingly common to use the *Macro-Panel Wall System* technique, in which the building is assembled on site, by connecting prefabricated macro *shear wall* elements, equipped with windows, doors and other technological devices (Premrov 2008).

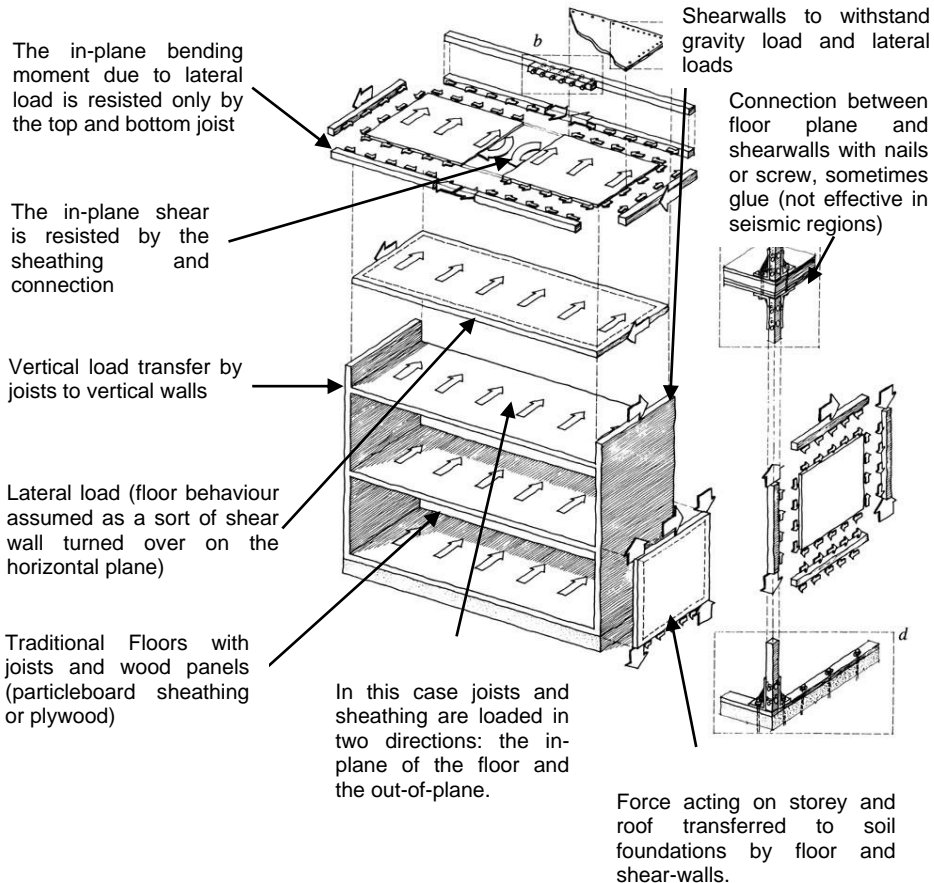


Figure 2.14 wood frame resistance system: mechanism of lateral resisting system (modified from Ceccotti and Toulaiatos 1995)

In seismic zones, a structure has to withstand seismic loads in addition to the gravity and wind actions present in a static situation. The horizontal elements of the storey have an important role in the seismic behaviour of buildings, due to their influence on the repartition of the seismic forces into each *shear wall*.

The floors should be rigid in-plane and strengthened enough to provide uniform distribution of storey force into the *shear walls*. The traditional floor is constructed with joists and wood fibre panels attached with nail connections. For the horizontal elements, use is also growing of prefabricated elements of variable width in the range 1.0÷1.3 m. The prefabricated modules of the floors are built with sawn beams, LVL or glulam, rigidly connected with resins or mechanically fastened to panels made of plywood, particle board or OSB on one or both sides (Premrov 2008).

Figure 2.13 shows, in detail, the seismic behaviour of the *timber frame panel system*. Horizontal forces are transferred to the foundation, starting from the horizontal floors, by means of the floor-to-wall connections and the elements that compose each *shear wall*. The energy dissipation and ductility of the structure is related to the behaviour of the *shear wall* elements and the connecting devices that anchor the wall at every level. A series of connections at each storey prevent the sliding and lifting of each wall due to the horizontal forces.

The performance of *shear wall* elements against seismic actions is internationally recognized, particularly in North America and Japan. Codes and numerous technical papers drawn for the *platform frame system* are the result of over twenty years of research. Several American institutions have been involved in producing technical documents useful for the designer and manufacturers. Among these is the “Wood Engineering Association” (APA), which has produced in recent years a series of technical documents specific to the American houses built with the platform frame system (APA 2007).

2.5 Massive wood panel system

In Europe, as an alternative to the traditional *wood frame system*, the *cross-laminated timber panel system* (XLAM system) was proposed. The *cross-laminated massive timber panels* are obtained by gluing wood boards of low quality in order to have the adjacent layers arranged at right angles (Augustin 2008).

A building built with XLAM technology is a box structure in which the horizontals and the walls are very stiff and strong elements of wood, connected with mechanical connections in predefined areas. In function of the load direction, the *wood-massive panels* can be subjected to an in-plane action (panel behaviour) or out-of-plane action (plate behaviour). In either case, the stress on the panels is affected by the number of layers that make it up and their orientation.

Massive wood XLAM wall, floor and roof elements can be precisely manufactured according to the architectural plans, including the holes for windows and doors.

The walls can be built with a single panel up to a maximum length of 10÷12 m and a height equal to the height of the storey (Augustin 2008).

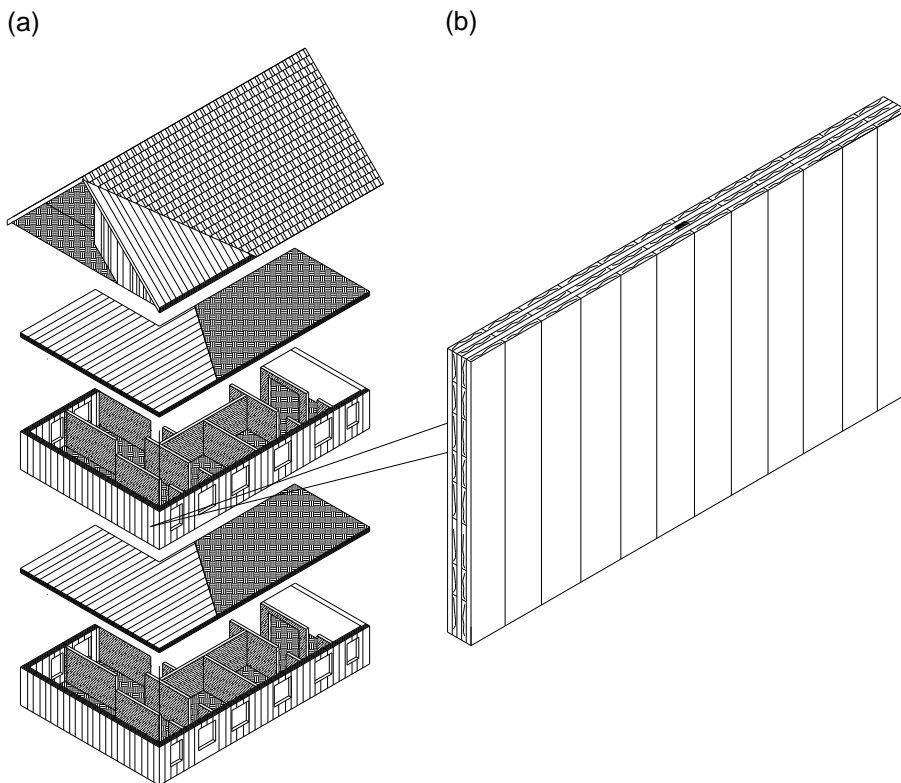


Figure 2.15 Schematic presentation of the massive wood panel construction (XLAM system); (a) exploded view of massive wood panel system; (b) shear wall layers of cross-laminated solid wood panels

More frequently, however, largely for the problems of transport, ease of handling, and assembly on site, walls are divided into panels of varying widths depending on the manufacturer and linked later with the creation of vertical joints. Vertical joints are made with the interposition of one or two strips of wood-based panelling, inserted into special grooves inside the wall or on its external surface.

Figure 2.15 shows an exploded view of a three-storey building with XLAM construction technology. The three-dimensional behaviour of the structure is provided by the connections between the wall elements that make up the wall and the joints between the horizontal and vertical elements. The horizontal forces are incurred by the massive panels positioned according to the geometry of the building. In this system connections play a strategic role in the control of the post-elastic capacity of the structure. The connectors and connecting devices are positioned so as to counter the uplift and sliding forces of an earthquake.

Connections are classified, in function of the elements connected, as Wall-to-Wall, Wall-to-Foundation, Wall-to-Floor-Wall and Floor-to-Floor (Figure 2.16). In general connections are made with mechanical dowel-type fasteners combined with retaining devices such as steel angle or hold-down devices. The metal fasteners normally employed are self-tapping wood screws, glued-in rods, nails, dowels and bolts (Augustin 2008).

The *massive wood panel system* differs significantly from the *timber frame panel system* in the mode of load transfer to the ground. In *timber frame panel system* the gravity loads are transferred to the foundation by means of each stud of the *shear walls*. The horizontal loads, generated by earthquakes or wind, are transferred to the soil by the development of a shear resistance mechanism, due to the sheathing panels and nails fixed on the frame of *shear wall*.

In the *massive wood panel system* the whole development of the wall resists the action of gravity, while the lateral forces are transferred to the ground primarily by the connections, in which the inelastic demand of the structure is concentrated. The *massive wood panels* are almost in the elastic range, as they are stiffer than the mechanical connections.

In comparison to the *timber frame panel system*, where mono-dimensional stud elements, bi-dimensional sheathing panels and an high number of fastener connections are employed, the *massive wood panel system*, uses solid laminated elements, and a smaller number of connections are used at the edges.

Chapter 6 describes in detail the global dissipative capacity of timber panel frame systems and the level of ductility achievable in the design phase.

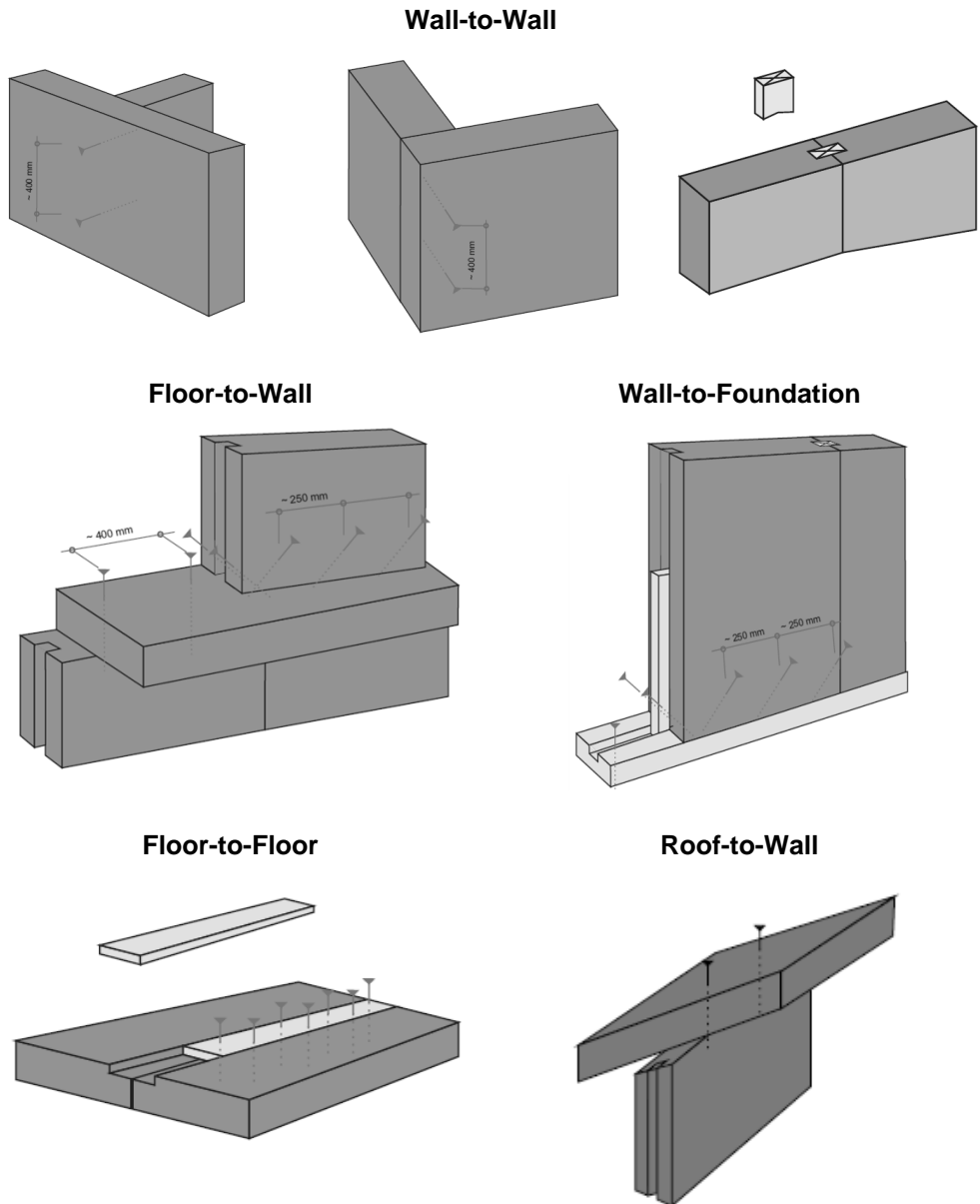


Figure 2.16 Illustration of XLAM lateral resisting system; Details of connections between the elements (modified from Binderholz 2010)

2.6 Conclusions

The seismic behaviour of wooden structures is strongly influenced by the behaviour of the connections. Some construction techniques are not suitable to design structures, with the desired dynamic behaviour. This Chapter has described earthquake-resistant building systems that cover the timber construction market. The selection of construction typologies must meet the requirements in terms of dissipation capacity and ductility, avoiding collapse of the structure after an earthquake. In this research we will refer to the modern connections that use dowel-type metal fasteners and metallic devices.

3 DIRECT DISPLACEMENT-BASED DESIGN METHODOLOGY

3.1 Introduction

The Direct Displacement-Based Design (Direct-DBD) approach was developed to design structures in seismic zones, using displacement as the input parameter. The Direct-DBD methodology, first codified by Priestley (2003) and subsequently developed by several other researchers (Priestley *et al.* 2007), presents itself as a real alternative to the "traditionals" methods in seismic design of structures.

The "traditional" procedures often relate to the Force-Based Design methods of calculation (FBD). FBD methods have been adopted by several international seismic design codes, including Eurocode 8 (CEN 2004b). In Eurocode 8 the FBD procedure has been calibrated to perform assessments of structural safety according to the semi-probabilistic limit states method (CEN 2004b).

In 2003 Priestley published a book (Priestley 2003) highlighting the various drawbacks of the traditional FBD method. The author demonstrates how the Direct-DBD method is not affected in these design situations. Calvi (2003) later published the state of the art of displacement-based design methods applied to reinforced concrete structures, concluding that the method of Direct-DBD is a valid and promising design tool for structural codes implementation.

In 2007, the authors Priestley *et al.* (2007) published a book on the displacement-based method, in which the first Direct-DBD procedure for some types of structures is presented. The extension of the Direct-DBD procedure to other materials and structural types is still an open research field. A first effort to upgrade and extend the applicability of the Direct-DBD method on a generic structure was completed in a recent Italian research project (**RELUIS** Project). The three-years project concluded with the drafting of a model code (DBD09; Calvi and Sullivan 2009), currently under public inquiry.

Nowadays, based on the state of the research it is premature to think that the Direct-DBD methods are more efficient or reliable than the FBD methods. However, the general opinion is increasingly insistent that current seismic design procedures should be updated according to the philosophy of Performance-Based Seismic Design (PBSD). The development of a Direct-DBD method, as a possible application of the PBSD, appears very promising in this respect (Calvi 2003).

3.2 Overview of the Direct-DBD procedure for MDOF System

The Direct-DBD procedure was codified by Priestley (2003) in four basic steps of calculation. Every step requires a different level of difficulty depending on the type of material and the structural typology of the building, due to the different knowledge acquired in the definition of the algorithms (Calvi and Sullivan 2009). Additional information on the Direct-DBD method can be found in Priestley *et al.* (2007) and in Calvi and Sullivan (2009). This review is taken from a paper by Sullivan *et al.* (2009) and is carried out with reference to Figure 3.1.

There are four components to the procedure:

- I. Representation of the MDOF structure (shown in Figure 3.1(I) as a frame building, though the procedure is identical for all structures) as an equivalent SDOF structure, in terms of equivalent mass and characteristic displacement.
- II. Representation of the force-displacement response of the equivalent SDOF structure by the secant stiffness to maximum design displacement response rather than the pre-yield elastic stiffness, as shown in Figure 3.1(II).
- III. Adoption of relationships between displacement ductility demand and equivalent viscous damping, based on results of non-linear time-history analyses (NLTHA), shown in Figure 3.1(III) instead of nominal elastic damping of (typically) 5% critical.
- IV. Use of design displacement spectra for different levels of equivalent viscous damping Figure 3.1(IV).

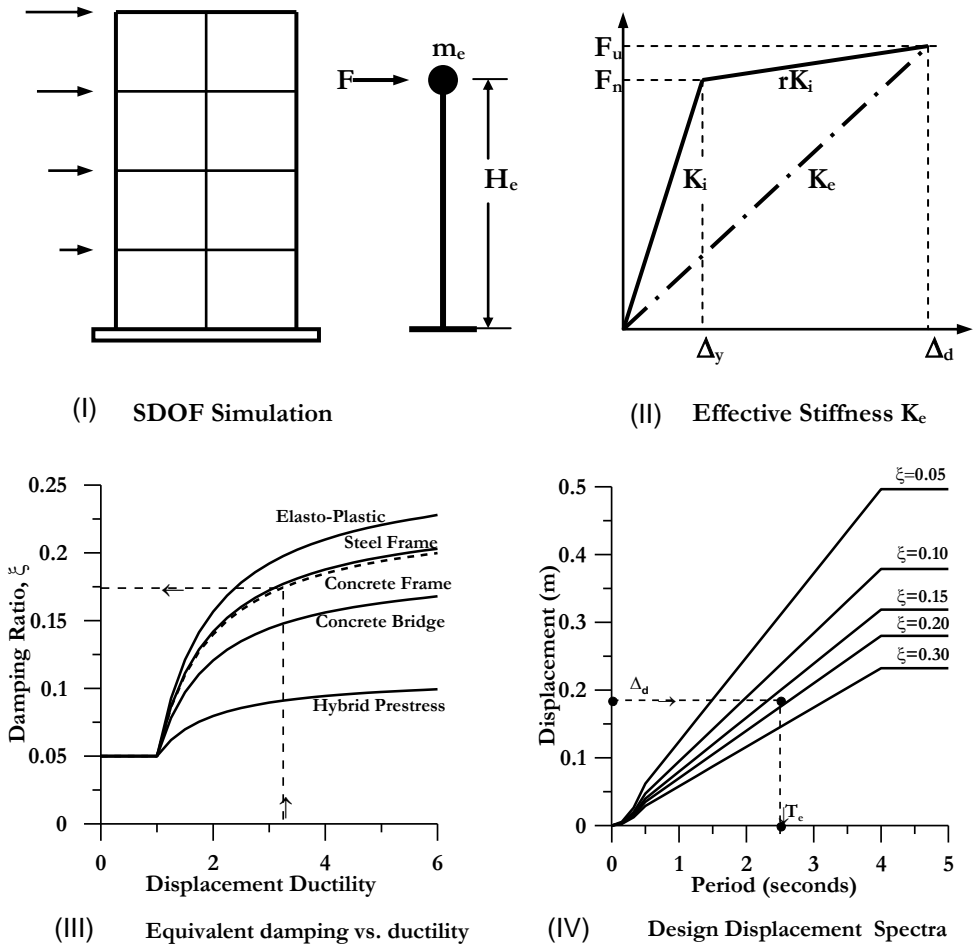


Figure 3.1 Fundamentals of Direct Displacement-Based Design (based on Priestley et al. 2007)

The following equations should be used to design the structures:

$$\Delta_d = \sum_{i=1}^n (m_i \Delta_i^2) / \sum_{i=1}^n (m_i \Delta_i) \rightarrow \text{Design displacement} \quad (3.1)$$

$$m_e = \sum_{i=1}^n (m_i \Delta_i) / \Delta_d \rightarrow \text{Equivalent mass} \quad (3.2)$$

$$H_e = \sum_{i=1}^n (m_i \Delta_i H_i) / \sum_{i=1}^n (m_i \Delta_i) \rightarrow \text{Effective height of building} \quad (3.3)$$

$$\mu_\Delta = \frac{\Delta_d}{\Delta_y} \rightarrow \text{Design displacement ductility} \quad (3.4)$$

$$\xi_{eq} = 0.05 + C \cdot \left(\frac{\mu - 1}{\mu \pi} \right) \rightarrow \text{Equivalent viscous damping} \quad (3.5)$$

$$K_e = 4\pi^2 m_e / T_e^2 \rightarrow \text{Effective stiffness} \quad (3.6)$$

$$V_B = k_e \Delta_d \rightarrow \text{Design base shear} \quad (3.7)$$

In Eqs. (3.1)÷(3.7) m_i , Δ_i , and H_i are respectively the mass, design displacement and height (for buildings) of the i -mass locations of the structure; Δ_y is the yield displacement of the equivalent SDOF system and C is a constant dependent on the hysteretic characteristics of the structure.

The effective period, T_e , is found from Figure 3.1(IV), entering from the characteristic displacement and selecting the appropriate level of damping given by Eq.(3.5). The procedure thus generally does not require iteration to achieve a valid solution (Sullivan *et al.* 2009); hence the procedure is termed “Direct” Displacement-Based Design. Full details are available in Priestley *et al.* (2007).

The applicability of the procedure is related to the identification of the inelastic deformed shape of the MDOF structure, for the selected performance level (limit state), the evaluation of design displacement and the definition of the matching hysteretic parameters (Sullivan *et al.* 2009). The design displacement (Δ_d) and the Equivalent Viscous Damping (ξ_{eq}) are the two design parameters. The analytical evaluation of design parameters is then related to the structural typology and to the building material.

The open area of research on Direct-DBD methods is precisely the formulation of analytical models for calculating the design parameters, through which it may be possible to find a solution to the seismic problem without iterative procedures.

3.3 State of development in timber systems

Over the last decade the study of dynamic behaviour of residential wooden structures has increased considerably (Foliente 1993). Nowadays, two design methods are available that follow the displacement-based approach, as will be explained in detail in this section.

The drafting of a displacement-based design method for the design of timber frame panel systems (*wood frame*) is one of the results obtained by two research projects in North America, the *CUREE-Caltech Woodframe Project* (Curee 2008) and the *NEESWood Project* (Seesl 2006).

The *CUREE-Caltech Woodframe Project* (CUREE-CWP) is financed by the U.S. Federal Emergency Management Agency (FEMA) in California and aims to reduce earthquake losses to *wood frame* construction.

The CUREE-CWP focuses on various types of wooden buildings, both new and existing, such as apartments, condominiums, schools, and buildings for commercial and recreational use. The project was divided into five integrated lines of research which include "Testing and Analysis" (Line I), "Field Investigations" (Line II), "Building Codes and Standards" (Line III), "Economic Aspects" (Line IV) and "Education and Outreach" (Line V). A shaking table test of a two-storey *wood frame* building, using data recorded during major earthquakes in the past, was presented as the result of the research project. About thirty scientific reports were released and published at the conclusion of CUREE-CWP Project (Curee 2008).

The objective of the NEESWood project is to develop a performance-based design philosophy for the economical design of low and mid-rise *wood frame* construction in regions of moderate to high seismicity (Seesl 2006). The NEESWood project was funded by the National Science Foundation of the U.S. and has involved five U.S. universities and two international research institutes. There are currently four scientific reports (MCEER 2010) describing the results obtained, and numerous articles published in journals or international conference proceedings.

A brief chronological overview of developments in the Direct-DBD method applied to wooden structures is presented in the following pages. The articles to which we refer are presented in chronological order of publication and were chosen for their significant impact on the applicability of Direct-DBD to wooden structures.

In 2002, Filiatrault and Folz (2002) presented and discussed the extension of the traditional method of Direct-DBD, proposed by Priestley (1998) for concrete structures to timber frame panel structures (*wood frame*).

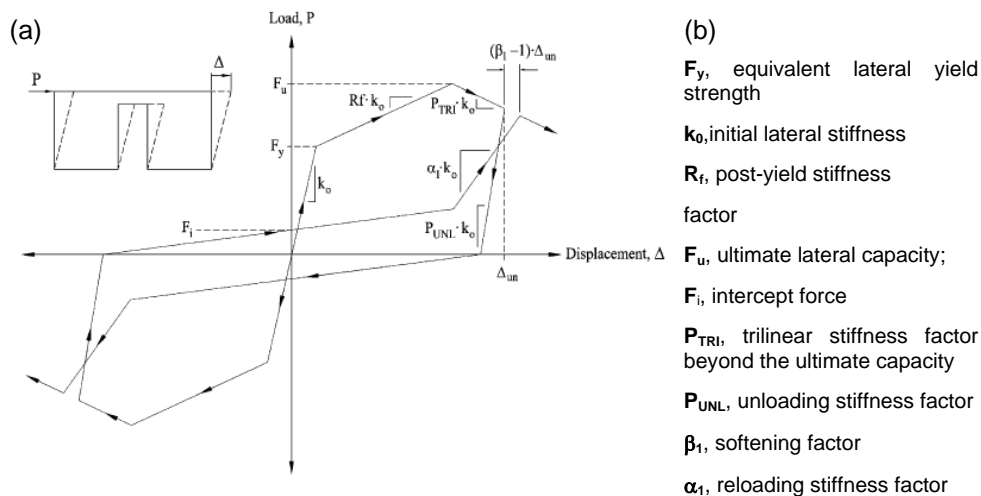


Figure 3.2 (a) Wayne Stewart degrading hysteresis rule described by Filiatrault et al. (2003); (b) The nine independent physical parameters of Wayne Stewart degrading hysteretic model

Filiatrault and Folz (2002) present a model for designing a *shear wall* panel using a displacement-based approach. The model is verified with a series of Non-Linear Time History Analyses (NLTHA), comparing the displacement value estimated at the top of the panel. The numerical model used to perform the NLTHA is the CASHEW model, which will be described in Chapter 6. To estimate the Equivalent Viscous Damping, the loading protocol proposed by Krawinkler et al. (2000) was used. The outcomes of the numerical analyses confirmed the validity of the proposed Direct-DBD methodology and the possibility of extending the model to the whole *wood frame* building.

In 2003, Filiatrault et al. (2003) proposed and calibrated a numerical model (Figure 3.2) to evaluate the load-displacement curve ($F-\Delta$) and the Equivalent Viscous Damping of a two-storey *wood frame* building. The “pancake numerical model” of Filiatrault et al. (2003) is the natural extension to the *wood frame* building of the CASHEW model used to describe the single *timber frame panel* (*wood shear wall*).

The validation of the numerical model was performed by comparing the values extrapolated from the numerical analyses with the results of shaking table tests, performed on a two-storey *wood frame* building in full-scale (Figure 3.3). In the "pancake numerical model" the in-plane response of the wall, exposed to seismic action, is modelled with a single non-linear shear spring and the Wayne Stewart hysteretic model (WS). The WS hysteretic model incorporates the degradation of stiffness and strength observed experimentally in the *shear walls*.

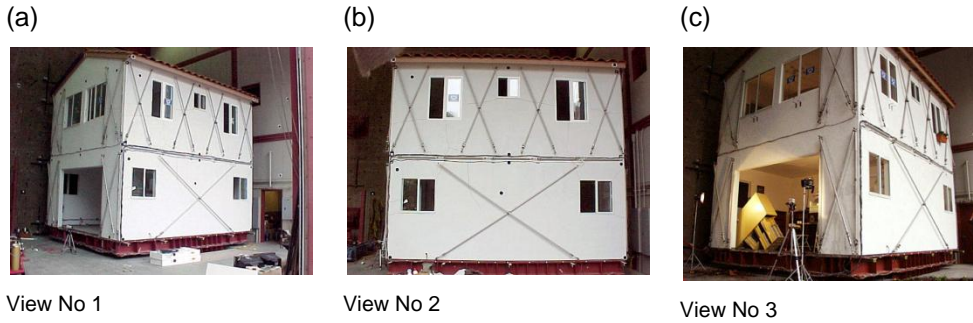


Figure 3.3 Single family house with two storeys, as in a modern residential construction in California (Curee 2008); (a) Structure finished before the test; (b) Lateral view after the test; (c) 3D view after the test

Finally, Filiatrault *et al.* (2003) propose two simple analytical expressions to calculate the hysteretic damping, ξ_{hyst} (Eq. (3.8)) and the Equivalent Viscous Damping value, ξ_{eq} (Eq. (3.9)).

$$\xi_{hyst} = \begin{cases} 0.5\Delta_t \rightarrow 0 \leq \Delta_t < 0.36\% \\ 0.18 \rightarrow 0.36\% \leq \Delta_t \end{cases} \quad (3.8)$$

$$\xi_{eq} = \begin{cases} 0.5\Delta_t + 0.02 \rightarrow 0 \leq \Delta_t < 0.36\% \\ 0.20 \rightarrow 0.36\% \leq \Delta_t \end{cases} \quad (3.9)$$

The analytical models to evaluate the damping are based on 24 monotonic and cyclic non-linear analyses considering four different structural configurations and, for each of these, three different construction variants representing superior-, typical- and poor-quality of execution of construction.

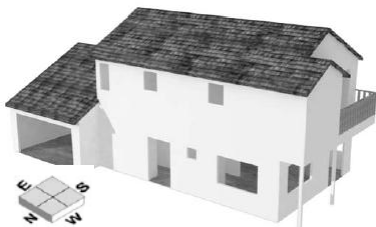
Case 1: Small house index building



Case 3: Townhouse index building



Case 2: Large house index building



Case 4: Apartment index building

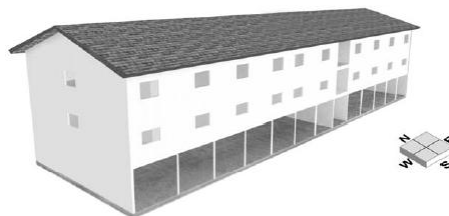


Figure 3.4 Global view of the four index buildings investigated (modified from Filiatrault *et al.* 2004)

In 2004 Filiatrault *et al.* (2004), presented the outcomes of an extensive numerical study carried out on characteristic structures and proposed an equivalent elastic model to estimate the dynamic behaviour of *wood frame* buildings. The equivalent elastic model takes into account the pinching effect, which causes a different response between the first virgin cycle of loading and the subsequent cycles for the same imposed displacement value. The structures studied are characterized by a structural detail typical of American constructions (Figure 3.4).

Outcomes have demonstrated that the equivalent viscous damping is sensitive to the history of deformation; in particular, passing from the first cycle to the subsequent cycles increases the degradation of the dissipative capacity of the structure. Independently of the loading protocol, the damping is stable for displacements in the range $\Delta_{t,max} \div \Delta_{t,max}/3$ and therefore can be assumed constant within these limits.

The first complete analytical formulation of the displacement-based design method, applied to mid-rise wood structures with the *timber frame panel system (wood frame)*, was presented in 2009 by the research group of the *NEESWood project* (Pang and Rosowsky 2009), coordinated by Professor John W. Van de Lindt of Colorado State University (USA). At the conclusion of the project two displacement-based design procedures for multi-story wooden buildings were issued.

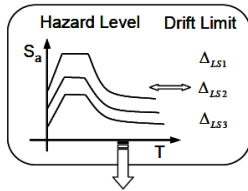
The first proposed “innovative displacement-based procedure” is based on the normalized modal analysis of building and the inter-storey drift spectra. The normalized modal analyses are used to evaluate the displacement capacity of the building, while the inter-storey drift spectra are used to evaluate the displacement demand. The Direct-DBD method proposed for mid-rise (commonly up to four stories) *wood frame* construction by Pang and Rosowsky (2009) was validated via non-linear time-history analyses. The second proposed displacement-based model (Pang *et al.* 2010) uses the same protocol as Priestley's approach, presented at the start of this Chapter and developed originally for concrete structures.

In brief, Figure 3.5 shows the “innovative displacement-based procedure” formulated by Pang and Rosowsky (2009), with comments at each step. In the evaluation of the design parameters, the performance levels, the i^{th} mass and the i^{th} stiffness are estimated using traditional methods. The particularity of the method is the introduction of the design spectrum expressed in terms of inter-storey drift for each level of the structure (storey). The inter-storey drift design spectra are scaled with the eigenvalues, α_n , and the modal participation factors γ_n (n , number of modes; j^{th} , level of the building). The secant period associated with the design displacement, which the structure has to ensure for a given level of performance, is obtained from the inter-storey drift spectrum associated to the j^{th} critical level. The minimum stiffness required at each level is then calculated using the design period of the structure corresponding to the design displacement.

In the Direct-DBD method of Pang and Rosowsky (2009), the equivalent elastic representation of the *shear wall* uses an alternative equivalent energy approach. In this Direct-DBD procedure the equivalent stiffness, k_{eq} , approximates the work done or the energy stored by the *shear wall* at a displacement level Δ_d . The method of Pang and Rosowsky (2009) does not require non-linear numerical analyses to estimate the effective stiffness and the Equivalent Viscous Damping, associated to the design displacement, Δ_d , as normally required in Priestley's approach (Priestley *et al.* 2007).

Step 1.

Define performance levels in terms of limiting inter-story drifts.

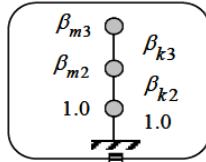


Earthquake Design Level	System Performance Level			
	Fully Operational	Operational	Life Safe	Near Collapse
Frequent (43 year)	○	x	x	x
Occasional (72 year)	○	○	x	x
Rare (475 year)	○	○	○	x
Very Rare (970 year)	○	○	○	○

Diagonal labels: Unacceptable Performance (for new construction), Basic Objective, Essential Objective, Safety Critical Objective.

Step 2.

Estimate mass and stiffness ratios (relative to first floor).



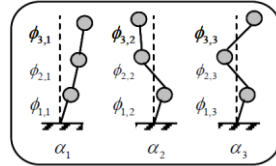
$$[K - \omega_n^2 M] \Phi_{jn} = 0$$

$$M = m \begin{bmatrix} 1 & 0 & 0 \\ 0 & \beta_{m2} & 0 \\ 0 & 0 & \beta_{m3} \end{bmatrix}$$

$$K = \begin{bmatrix} 1 + \beta_{k2} & -\beta_{k2} & 0 \\ -\beta_{k2} & \beta_{k2} + \beta_{k3} & -\beta_{k3} \\ 0 & -\beta_{k3} & \beta_{k3} \end{bmatrix}$$

Step 3.

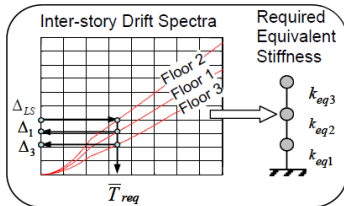
Perform normalized modal analysis on the equivalent linear MDOF system.



Obtaining inter-storey drift factors and natural frequency parameters.

Step 4.

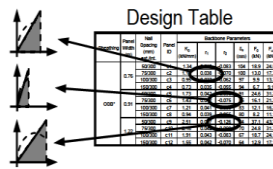
Construct inter-story drift spectra and determine required storey stiffness.



$$\Delta_j(T) = \frac{1}{H_j} \sqrt{\sum_n \left[\gamma_{jn} \left(\frac{T}{\alpha_n 2\pi} \right)^2 S_a(T/\alpha_n) \right]^2}$$

Step 5.

Select shear walls using shear wall backbone design table.



Wood shear wall design tables include information on shear wall backbone response and equivalent stiffness at various drift levels.

Step 6.

Check the design using the actual stiffness ratios and revise the shearwall selection if necessary.

Step 7.

Repeat steps 2÷6 for each performance level using the actual stiffness ratios of the selected shear walls. Revise the design if drift limits are exceeded at any performance level.

Step 8.

Compute design base shear, storey shear and uplift force using the actual nonlinear backbone curves of shear walls.

Figure 3.5 Flowchart of Direct-DBD procedures developed for mid-rise wood frame buildings (modified from Pang and Rosowsky 2007)

The method of Pang and Rosowsky (2009) was validated on a three-story wood frame building, shown in Figure 3.6(a), comparing the expected displacement at each level, with the inelastic deformed shape obtained from a series of dynamic time-history analyses.

The non-linear dynamic analyses were performed with the SAWS-software developed by Folz and Filiatrault (2004a,b) for the study of the seismic response of *wood frame* systems (Figure 3.6(b)). The SAWS-software (Seismic Analysis of Wood Structures) describes the response curve of each *shear wall* using the same algorithm as CASHEW, developed during the CUREE-CWP Project. To validate the innovative method of Direct-DBD three groups of accelerograms were selected in two main directions, each consisting of a set of 20 spectrum-compatible accelerograms, representative of the seismic hazard of the area and of the performance levels selected for the building.

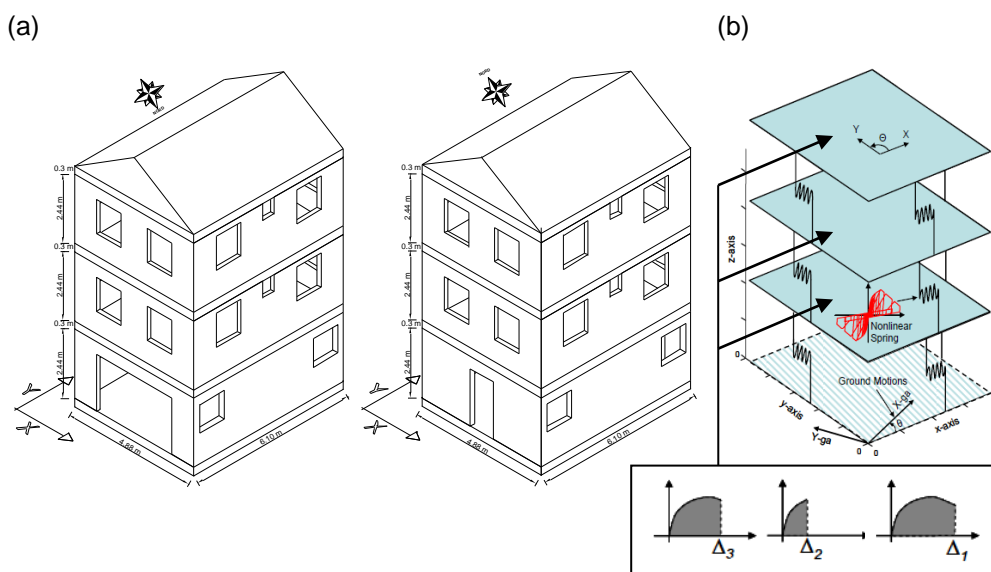


Figure 3.6 (a) Elevation views of a three-storey wood frame structure, typical in America; (b) Three-dimensional nonlinear model for a three-storey wood frame structure (modified from Pang and Rosowsky 2007)

In the traditional method of Direct-DBD, according to the formulation of Priestley (2003), Pang *et al.* (2010) presented the procedure to design a six-storey building with a *timber frame panel system*. The Direct-DBD procedure assumes an inelastic profile of displacements that interpolates the first modal elastic shape, and evaluates the design displacement as a function of the inter-storey drift limits required in the U.S. Code (e.g. FEMA 2000).

The same authors propose an expression for calculating hysteretic damping, Eq. (3.10) from which we can estimate the Equivalent Viscous Damping, adding an elastic component assumed equal to 5%.

$$\xi_{hyst} = 0.32e^{-1.38\frac{k_s}{k_i}} \quad (3.10)$$

wherein k_s/k_i is the ratio between the secant stiffness and the initial stiffness of the building.

The numerical validation is based on the outcomes of the Non-Linear Time History Analyses (NLTHA), in which the input parameters are a series of ground motions (accelerograms), scaled in function of the performance level required.

3.4 Conclusions

The overview of Direct Displacement-Based seismic Design methods (Direct-DBD) highlights the full development of the procedure for buildings constructed with the *wood frame* system. However, the state of development of the Direct-DBD method for structures which differ from the multi-storey *wood frame* American buildings is not clear. The feeling is that, while for some types of structures general displacement-based methods and Direct-DBD methods are available, for others we are still far from their full applicability. This is the case, for example, with open-plan single-storey buildings, used to cover large commercial and industrial areas.

This research opens starting precisely from the study of single-storey buildings which fall into the category of "heavy timber structures", as will be presented in the next Chapters.

4 PROPOSED DIRECT-DBD METHOD FOR TIMBER SYSTEMS

4.1 General

This Chapter deals with the formulation of the Direct Displacement-Based Design (Direct-DBD) procedure for the portal frame structure, identified as a system with one degree of freedom (SDOF). The Direct-DBD method requires the estimation a priori of the design displacement, Δ_d , and the associated Equivalent Viscous Damping of the structure, ξ_{eq} , for a specific performance level.

In this Chapter the analytical models to evaluate the design parameters Δ_d and ξ_{eq} at the ultimate limit state (ULS) are presented.

4.2 Structure description

The prototype structure selected is designed with the portal system using glulam elements in class GL24h (CEN 2000) for the realization of industrial buildings (Figure 4.1(a)). The corner connections of the frame are made using dowel-type metal fasteners arranged in two concentric crowns (Figure 4.1(b)).

The construction details of the structure are presented in Appendix A, while additional details on the secondary structure can be found in Piazza *et al.* (2005). The building is in accordance with the appropriate building codes regularity requirements in plan and in elevation, as defined by the seismic design procedures (e.g. Eurocode 8; CEN 2004b).

The bearing structures are a series of m portals equally spaced at pitch, i , equal to 6.5 m. Each portal is made with a continuous curved beam with a slope $\alpha_r=10.2^\circ$ inserted between the columns, hinged at the base on the concrete foundation.

The analysis concerns the seismic response of the structure in the in-plane direction of the portal. Due to the symmetry of the structure, the number of portals, m , and the building length in the longitudinal direction, L_L , do not affect the final result of the analysis.

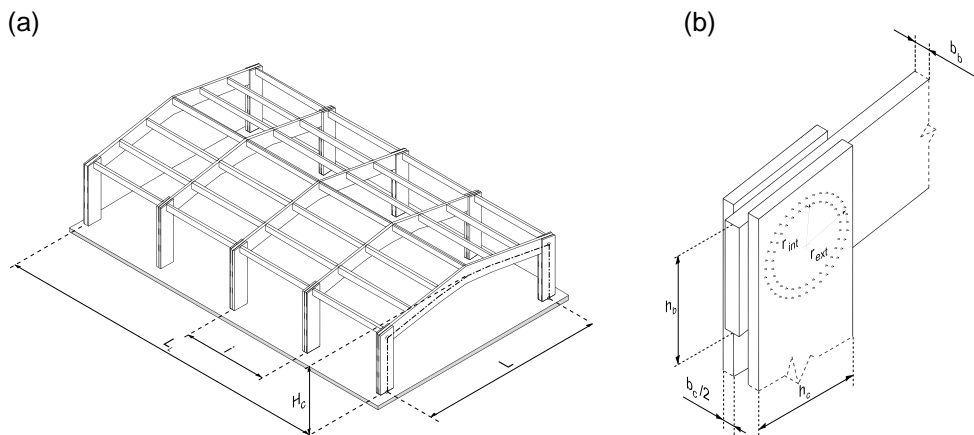


Figure 4.1 Description of the case study; (a) 3D isometric view of the main resistant structure; (b) Geometrical description of the beam-to-column joint

The length and the height of the portal are parameters defined depending on the architectural requirements and technical-economic limits. The current sizes in the European market are within the limits listed in Table 4.1. For structures over the geometrical limits in Table 4.1, different classes of construction system are adopted, such as portals with rigid joints, arches or truss systems.

Timber elements of the building are designed and verified in accordance with the current standard, Eurocode 5 (CEN 2004a), assuming a service class 1. The elastic design of a portal made with Moment-Resisting (MR) connections (Figure 4.1(b)) is a known problem and well described in Racher (Racher 1995b). In static conditions the portal is designed with the use of linear-elastic analyses (Figure 4.3). The force acting on each fastener within the MR joint is calculated via the linear combination of the shear stress component ($F_{V,i}$), normal stress component ($F_{N,i}$) and bending moment stress ($F_{M,i}$) acting on joint (N_J , V_J , M_J), calculated according to the static design of the structure.

A brief summary of the procedure taken from Racher (1995b) is given below.

Table 4.1 Geometrical limits of the portals commonly adopted in Europe

PARAMETER		MIN	MAX
Length	L m	10	25
Column height	H_c m	3.8	9.0
Typical commercial cross-section	h (h_c, h_b) mm	501	2209
Internal beam radius	R m	6.6	143.0
Roof slope	α_r °	5	20
Space between portals	i m	5	8

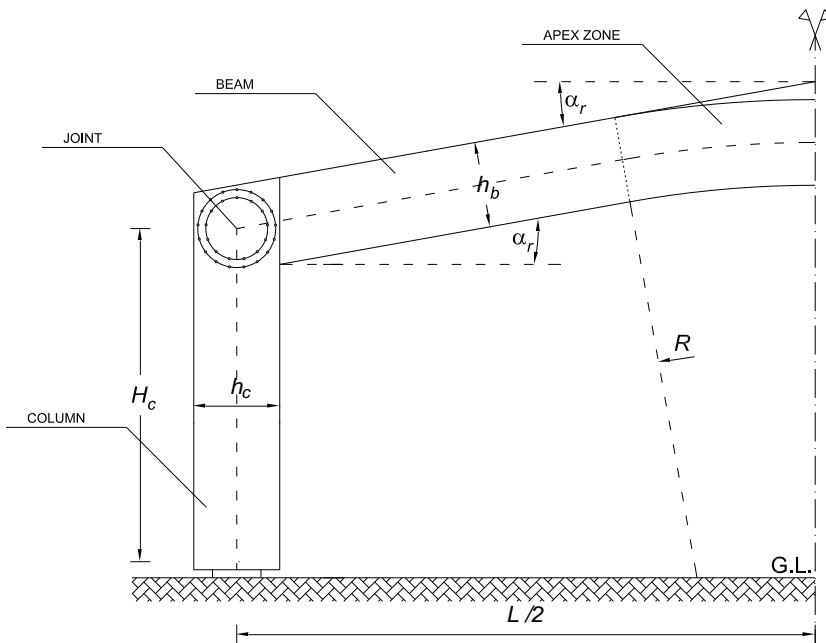


Figure 4.2 Geometric features of the prototype portal

Each component force on a dowel is calculated as:

$$F_{M,i} = \frac{k_{d,i}r_i}{k_{\Phi}} M_J = \frac{r_i}{n_1r_1^2 + n_2r_2^2} M_J \quad (4.1)$$

$$F_{V,i} = \frac{V_J}{n_{tot}} \quad (4.2)$$

$$F_{N,i} = \frac{N_J}{n_{tot}} \quad (4.3)$$

Eq. (4.1) is the stress due to bending moment (M_J), Eq. (4.2) is the stress due to shear (V_J) and Eq. (4.3) is the stress due to axial force (N_J).

The total force ($F_{V,d,i}$) acting on the dowels are equal to (Eq. (4.4)):

$$F_{V,d,i} = \sqrt{(F_{M,i} + F_{V,i})^2 + F_{N,i}^2} \quad (4.4)$$

Where N_J , V_J and M_J are, respectively, design axial force, shear and bending moment acting on the joint, n_{tot} is the total number of dowels, r_i is the radius of the i^{th} dowel, while subscripts 1 and 2 refer to the first and second crown respectively.

In the current codes for static and seismic design of timber structures, e.g. Eurocode 5 (CEN 2004a) and Eurocode 8 (CEN 2004b), the verification of the timber connections follows safety criteria expressed in terms of strength. The design of the connection is reduced to the definition and evaluation of the bearing capacity of each connector of the beam-to-column joint. The behaviour of the single connector also becomes a key point in the formulation of the design displacement, Δ_d , defined in the post-yielding deformed configuration. The next Section describes the mechanical model used for the single connecting element, based on the state of the art of dowel-type metal fastener devices.

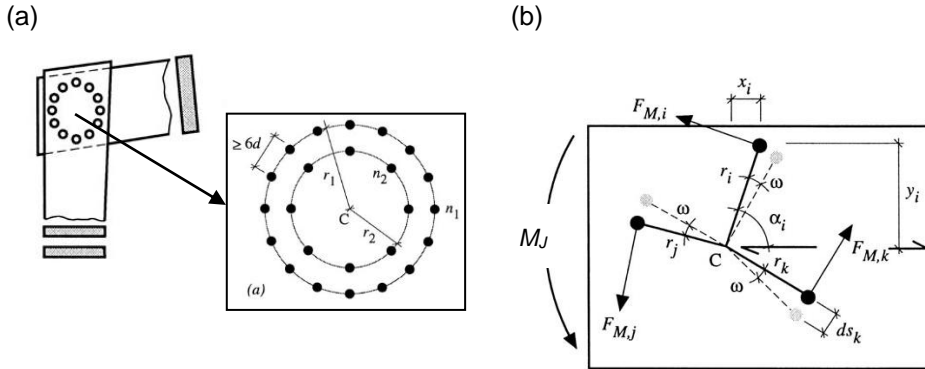


Figure 4.3 Design Force acting on a single dowel for knee joints made with two crowns of dowels; (a) Beam-to-column connection with no parallel elements and geometrical configuration; (b) Forces acting on dowels due to rigid body rotation (modified from Racher 1995b)

4.3 Load-slip monotonic curve for fasteners

The monotonic load-slip relationship (F - δ) for dowel-type metal fasteners has been the subject of numerous experimental and analytical studies. One of the accepted models which describes the F - δ curve of ductile connections was proposed by Foschi and Bonac (1977). In the Foschi and Bonac model, the non-linear monotonic response of the connections made with a single connector, laterally loaded, is formulated and described by means of Eq. (4.5):

$$F = \left(F_{0,FBM} + k_{1,FBM} \delta \right) \left(1 - e^{-\frac{k_{0,FBM}}{F_{0,FBM}} \delta} \right) \quad (4.5)$$

in which parameters $F_{0,FBM}$, $k_{0,FBM}$ and $k_{1,FBM}$ of the $F-\delta$ curve are calibrated to agree with the results of laboratory tests.

Blass (1994), subsequently to the proposal of Foschi and Bonac (1977) presented an analytical model applicable to the other connections made with dowel-type metal fasteners. In addition, alternative formulations of the load-slip curve ($F-\delta$) can be found in Lantos (1969) and Cramer (1968).

There are also some numerical studies of the load-slip curve of dowel-type metal fasteners. Numerical finite element models (FEM) have recently been proposed to describe the interaction between the timber matrix and the metal fasteners. In the FEM models the strength properties of the material and the geometry of the connection are formulated locally, with constitutive relations and curves chosen in an appropriate manner, increasing the difficulty of the solution process. Regardless of the model chosen to describe the $F-\delta$ curve, in this work a general model is required in which parameters are directly estimated via analytical expressions.

The recognized analytical model for the design of connections made with dowel-type metal fasteners, laterally loaded, is known as the “European Yield Model” (EYM). The EYM is currently adopted in several design codes for wood building, e.g. Eurocode 5 (CEN 2004a), the Canadian Code and other international codes.

The EYM is normally used to design according to the semi-probabilistic limit state method. The EYM is the natural extension of the model presented by Johansen in 1949 (1949). Based on Johansen’s model the EYM is defined by simply adding to the analytical expressions the numerical coefficients, calibrated with the experimental results of tests conducted on a series of connections (Hilson 1995). The calibration coefficients are evaluated to minimize the difference between the expected value and the experimental value.

The load-carrying capacity of a connection in accordance with the EYM is analytically evaluated with one of the three failure modes expected. The model is not able to identify other brittle failure mechanisms, such as those observed experimentally on some configurations of connections. Hence, the EYM model is always accompanied by a series of restrictions on the relative distance between fasteners and the edges of the elements connected, to avoid unexpected mechanisms occurring.

The European Yield Model (EYM), as shown in Figure 4.4, calculates only the load-carrying capacity of connections (known as the R_k , characteristic value) through equations proposed for three different failure modes, associated to four corresponding geometric configurations.

The first failure mode is characterized by the embedment strength of wood in the area surrounding the single dowel-type metal fasteners; failure modes II and III, which generally occur with increasing slenderness of the connectors, are caused instead by the embedment strength of the wood and the yielding of the connectors. In failure mode I, the expected behaviour of connections is brittle, while in failure modes II and III the expected behaviour is ductile. The ductile mode with the maximum number of plastic hinges in the connector is failure mode III.

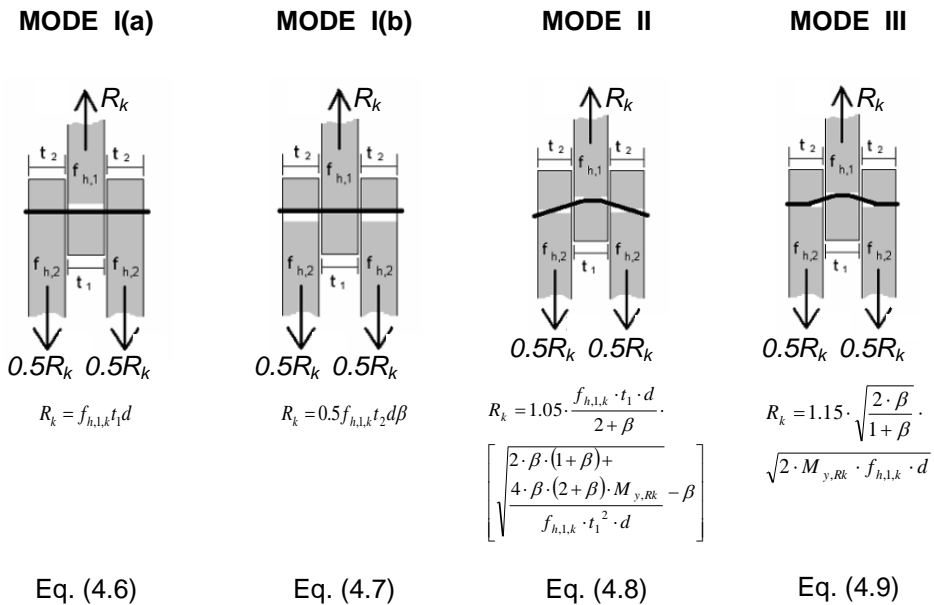


Figure 4.4 Failure modes provided by the European Yield Model for fasteners in double timber-to-timber shear planes (modified from Leijten 2008)

The EYM model was created as an application of limit analysis (lower bound theory) to the problem of wooden connections. Figure 4.5(a) shows the expected load-slip curves ($F-\delta$) of a dowel-type fastener connections and the load-carrying prediction of the EYM model.

As proposed in Racher (1995a), in function of the static slip ductility (μ_δ), connection elements can be identified by an appropriate design model. Figure 4.5(b) shows the possible analytical models that describe the mechanical behaviour of connections for different design situations.

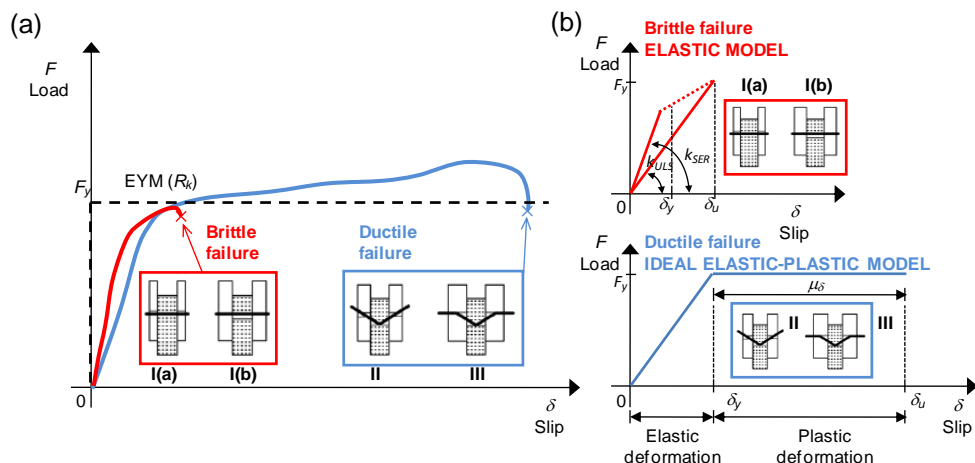


Figure 4.5 (a) Typical monotonic load-slip curves for a dowel-type timber connection; (b) Analytical models for the connections with main parameters

For well-designed connections the expected behaviour is ductile and therefore the ideal elastic-plastic curve can be used to design in the ultimate limit state condition. The ductility ensures plastic deformation in the connection before it reaches the ultimate bearing capacity. The load-slip curve ($F-\delta$) is identified by the parameters: static slip ductility (μ_δ), as the ratio between the ultimate slip (δ_u) and the yield slip (δ_y), the bearing capacity, F_y (known as R_k in EYM) and the ultimate slip modulus, k_{ULS} , for the ultimate limit state condition, defined in function of the slip modulus k_{SER} .

In an ideal elastic-plastic model of the connection, the ultimate slip of the single connector (δ_u) can be calculated indirectly by multiplying the yield slip (δ_y) by the static slip ductility (μ_δ). The yield slip (δ_y) is appropriately defined for connections that show a well-defined change of slope in the $F-\delta$ curve.

Unlike other materials, in wood connections the yield point is not always easily distinguishable in the experimental curves. Figure 4.6 shows the two typical situations defined by the standard EN 12512 (CEN 2001). For connections built with a single element, designed in high ductility ($\mu_\delta \geq 6$), it is simple to show that the yield point is that of Figure 4.6(a). In fact, the ideal model that interpolates the expected curve of Figure 4.6(a) is precisely the elastic-perfect plastic model, wherein the change of slope coincides with the formation of the plastic hinge in the connector. The test protocol according to EN 12512, in fact, was defined for the generic connection made up of several components. It is intuitive to understand that, in the connection made with several dowels, the yield point changes depending on the

sequence of the formation of plastic hinges in the connectors. In the design phase, the yield slip of the connection (δ_y) is calculated by the ratio of the load-carrying capacity (F_y assumed equal to R_k) and the slip modulus (k_{ULS}) of the connection, evaluated at the ultimate limit state condition (ULS).

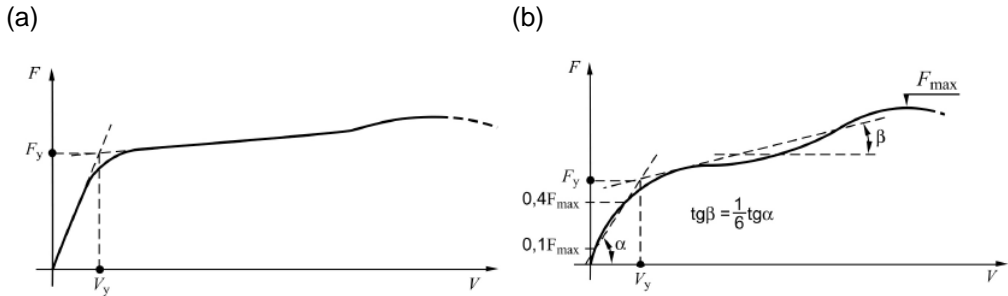


Figure 4.6 Definition of yielding parameters for a monotonic load-slip curve in two typical situations; (a) Load-slip curve with two well-defined linear parts; (b) Load-slip curve without two well-defined linear parts; (modified from CEN 2001)

The slip modulus at the ultimate limit state (k_{ULS}) and at the elastic limit state (k_{SER}) is calculated using respectively Eq. (4.10) and l'Eq. (4.11), proposed in Eurocode 5 (CEN 2004a).

$$k_{ULS} = 2/3k_{SER} \quad (4.10)$$

$$k_{SER} = \rho_k^{1.5} \frac{d}{20} \quad (4.11)$$

Equation (4.11) is an analytical expression that interpolates the results obtained by experimental tests on dowel-type metal fastener connections, performed with variable angle of loading compared to the grain. The slip modulus of the connector at the ultimate limit state is defined conventionally in Eurocode 8 (CEN 2004b), as a simple multiple of the elastic slip modulus, estimated from the mechanical properties of the connection. The uncertainty about the actual value of the slip modulus at the ultimate limit state, experimentally measured, is reflected in the

assessment of the yielding slip and therefore, in the ductility available. This work takes into account the effect of this uncertainty on the final evaluation of the design parameters.

In dissipative zones, where the inelastic capacity of the structure is concentrated, Eurocode 8 (CEN 2004b) imposes a minimum value of static slip ductility, to consider the connections in high ductility class (DCH). The structural behaviour in high ductility is ensured if static ductility on connections is at least 6 or if limits of geometric relationships between the connector and wooden elements connected are followed. The properties of dissipative zones should be determined by tests in accordance with EN 12512 (CEN 2001).

Therefore, in the design process it is possible to assume a static slip ductility of 6 to design a structure in DCH class. The ultimate slip of the connection, δ_u , is conventionally defined by Eq. (4.12) and directly evaluated in function of the mechanical properties of materials and the geometry of the connection.

$$\delta_u = \delta_y \cdot \mu_\delta \tag{4.12}$$

The evaluation of the bearing capacity of the connector ($F_y=R_k$) is immediate with the use of Eqs. (4.6)÷(4.9) of the EYM. The EYM is always accompanied by a series of supporting expressions that allow the numerical calculation of R_k . The bearing capacity of the connection is, in fact, lower than the resistance of the elements connected and is based on the mechanism known as "flow-of-forces" affecting the contact areas surrounding the metal connection element (Augustin 2008b).

The model of stress of modern connections with dowel-type metal fasteners has a simplified distribution of stress. The stress that balances and supports the connector is assumed constant on an area that has the short side defined by the diameter of the fasteners (Figure 4.7). The maximum allowable stress in the plastic field is defined as the embedment strength and is experimentally evaluated using the standard EN 383 (CEN 2007). The mechanism of the "flow-of-forces" explains and demonstrates that large contact areas can produce a high level of stress on the wooden elements and should consequently be avoided, so as not to cause brittle failure of connections.

The embedment strength of connectors with various diameters, in the two main directions, was investigated by Sawata and Yasumura (2002) and is shown in Figure 4.8.

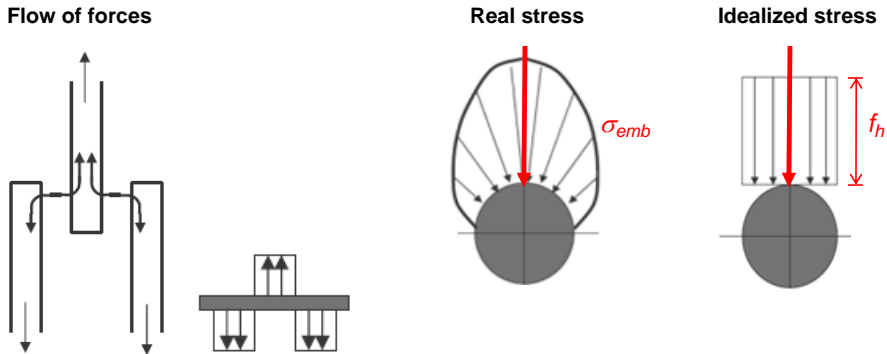


Figure 4.7 Flow-of-forces in dowel-type fastener connections, embedment strength in timber elements and model of embedment strength (modified from Leijten 2008)

The embedment strength in the fibre direction is analytically defined by Eq. (4.13) (characteristic value). This is an interpolating function that was calibrated by experimental tests and is contained in the European standard for wooden structures, Eurocode 5 (CEN 2004a).

$$f_{h,0,k} = 0.082(1 - 0.01d)\rho_k \quad (4.13)$$

For an angle α_f between stress and grain, the embedment strength is given by Eq. (4.14).

$$f_{h,\alpha_f,k} = \frac{f_{h,0,k}}{K_{90} \sin^2 \alpha_f + \cos^2 \alpha_f} \quad (4.14)$$

With $K_{90}=1.35+0.015d$ for softwood

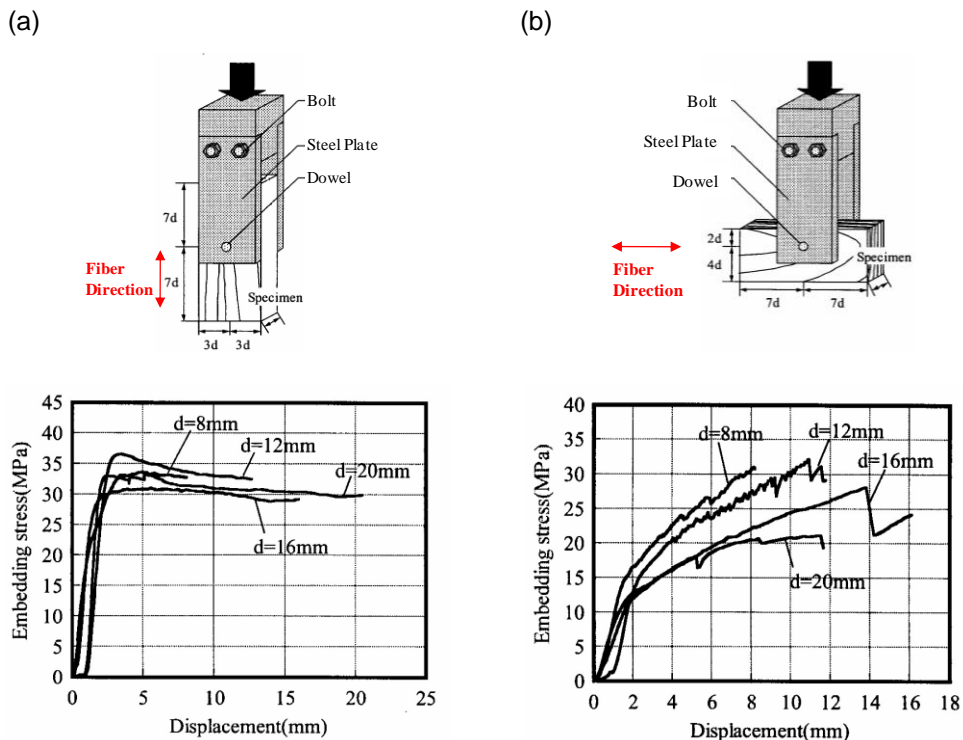


Figure 4.8 Embedment strength of a dowel-type fastener connection in parallel and perpendicular directions; (a) Test parallel to grain direction; (b) Test perpendicular to grain direction (modified from Sawata and Yasumura 2002)

The bearing capacity of the connection (R_k , characteristic value) is also a function of the post-yield strength of fasteners. The fastener yield moment is analytically evaluated based on the hypothesis of fully-developed plasticity of the section of the dowels. The final formula is nevertheless calibrated numerically to consider the real situation where the total development of the plastic hinge in the connector is not reached, as presented in Eq. (4.15) and (Figure 4.9):

$$M_{y,Rk} = 0.3 \cdot f_{u,k} \cdot d^{2.6} \tag{4.15}$$

The final calibration of Eq. (4.15) was done by Blass *et al.* in 2000 (2000).

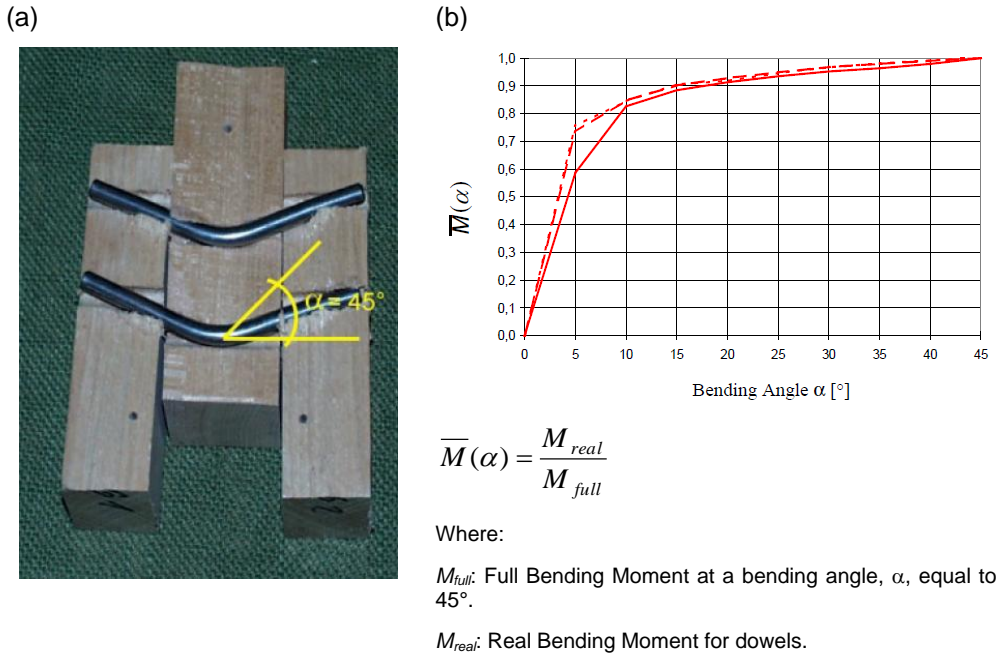


Figure 4.9 (a) Test failure mode after reaching maximum load; (b) Normalized moment-angle diagram of a dowel-type fastener for different dowel diameters, d (modified from Blass *et al.* 2000)

The monotonic load-slip curve ($F-\delta$), formulated in high ductility (DCH according to Eurocode 8, CEN 2004b) to describe the behaviour of a single connector under a static and quasi-static load, is shown in Figure 4.10(a). The perfect elastic-plastic model fits very well with numerical results obtained by tests. Figure 4.10(b) shows the development of a real load-slip curve for a connection built with two dowels of 12 mm diameter after a push-out test (Piazza *et al.* 2009). The perfect elastic-plastic model greatly simplifies the formulation of the overall response of a connection, achieved by placing some elements according to a given geometry, starting from the behaviour of a single connecting element.

The proposed analytical model can be used when ductile failure modes, type II and III according to the European Yield Model (EYM), are reached. From the equations of the EYM theory it is easy to show that there are geometric conditions that ensure the type III ductile failure mode independently of the mechanical properties of connected elements.

The transition from the first to the third failure mechanism is directly influenced by the slenderness of the fasteners, defined as the ratio between the thickness of the i^{th} wood elements connected and the diameter of the connector.

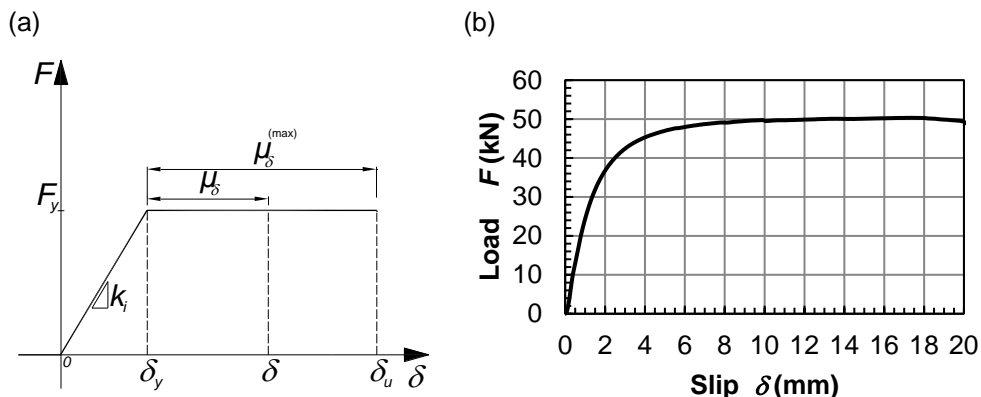


Figure 4.10 (a) Analytical Load-Slip curve formulated; (b) Experimental Load-Slip curve after monotonic test (push out test of two-dowel-type connections of 12 mm; Piazza et al. 2009)

As an alternative to checking the minimum value of the static ductility, Eurocode 8 (CEN 2004b), for this type of connection, sets an upper limit of dowel diameter and a minimum slenderness of the dowel. In this way the high ductility level and the expected cyclical behaviour are ensured, as will be shown in the next Section. For connections with fasteners in timber-to-timber shear plane mode the minimum value of slenderness is 10, while the maximum diameter of the dowels is 12 mm.

The use of the geometrical rules proposed in Eurocode 8 (CEN 2004b), allows the type III failure mechanism of fastener connections to be ensured, regardless of the materials used. Möller's algorithm (Möller 1951) can be used to validate the hypothesis of the type III failure mode (EYM) of connections made with fasteners in timber-to-timber shear mode. Figure 4.11 shows Möller's points diagrams, one for each diameter of dowel, where the solid lines represent the boundaries of each of the three failure modes defined for the connection. The diagrams have been modified here to consider the improvement of the capacity model of connectors, from the Johansen model (Johansen 1949) to the EYM. The current European Yield Model is contained in Eurocode 5 (CEN 2004a). The cloud of points on each diagram represents the variability of the materials wood and steel for the same geometric configuration.

Each point corresponds therefore to a specific configuration of the joint, expressed in terms of wood strength class and steel strength class.

The graphs of Figure 4.11 show that, regardless of the dowel diameter, based on the characteristic values (5th percentile) of timber and the 95th percentile of steel, only the strength class of 8.8 dowels does not ensure the type III failure mechanism. The strength class of bolts (EN 20898-2; CEN 1993) is also considered here because dowels are frequently used that are produced with the same resistance requirements as bolts. Normally, the strength class of the dowels must be in accordance with EN 10025 (CEN 2004).

The non-dimensional parameters of Figure 4.11 are defined as:

$$\lambda_1 = t_1 / \sqrt{M_{y,Rk} / f_{h,1,k} d}$$

and

$$\lambda_2 = t_2 / \sqrt{M_{y,Rk} / f_{h,1,k} d}$$

while parameter β is defined as:

$$\beta = \frac{f_{h,2,k}}{f_{h,1,k}}$$

and represents the ratio between the embedment strengths of the elements connected.

As explained above, in the design of connections with high ductility the mechanical model of Figure 4.10(a) is accepted, numerically evaluated with the expressions included in this Section.

The model is based on simple geometric relationships, contained in Eurocode 8 (CEN 2004b), that define the minimum thickness of the connected elements and the maximum diameter of the connectors employed.

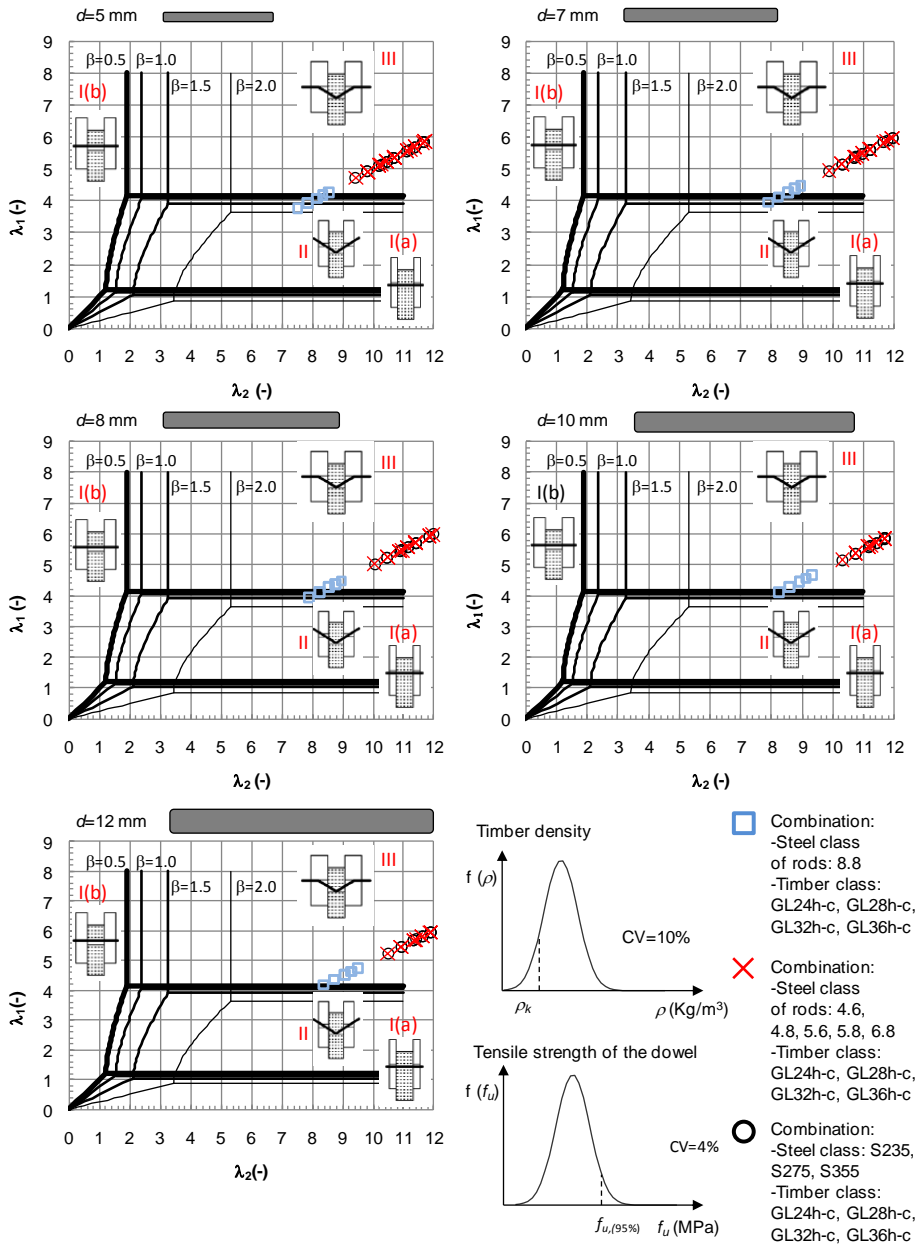


Figure 4.11 Möller's chart of dowel-type mechanical fasteners for different geometries and mechanical configurations

The failure mode III (EYM) involves the maximum static slip ductility and the maximum energy dissipation capacity of connections. The next section, which deals with the formulation of the design displacement of the portal, Δ_d , will clarify the role of the load-slip curve of fasteners ($F-\delta$) and in particular the ultimate slip of the dowel δ_u .

4.4 Design displacement formulation

In the Direct-DBD method the design starts with the estimation of the design displacement, Δ_d , usually having unknown geometrical dimensions of elements and joints. The design displacement of the structure at the serviceability limit state is easy to estimate, since normally we are required to comply with the requirements expressed in terms of inter-storey drift or deformation of the material, *e. g.* Eurocode 8 (CEN 2004b) and FEMA 356 (2000). At the ultimate limit state, defined as the maximum capacity of the structure, the design displacement is a function of the geometry of the elements, construction details of the connections and the properties of the material used.

The portal structure hinged at the base, presented in Figure 4.1(a) and Figure 4.1(b), has semi-rigid ductile joints made by placing the dowels according to a given geometry. The analytical model formulated for the calculation of the design displacement assumes that the inelastic deformation is concentrated in the beam-to-column joints. The assumption about inelastic displacement is true when the elements and connections are properly sized. The elements must be oversized with respect to the connections (Capacity Design rules), while the connectors should ensure a ductile failure mode. In accordance with the previous section it is assumed that the connectors possess a type III mechanism of failure (EYM).

The design displacement (Δ_d), with reference to Figure 4.12, can be estimated as the sum of the direct inelastic displacement for rigid rotation of the columns, following the yielding of the connectors (Δ_j), and the elastic deformation of the portal (Δ_s) calculated assuming rigid beam-to-column joints (Eq. (4.16)):

The design assumptions in which wooden elements are considered more rigid than the joints, usually accepted in the elastic range, can be extended to the plastic

range, as in the post-yield phase there is always a reduction in stiffness due in large part to structural damage. The rotation in the joint is then given by a rigid deformation with slip of fasteners mainly in the tangential direction.

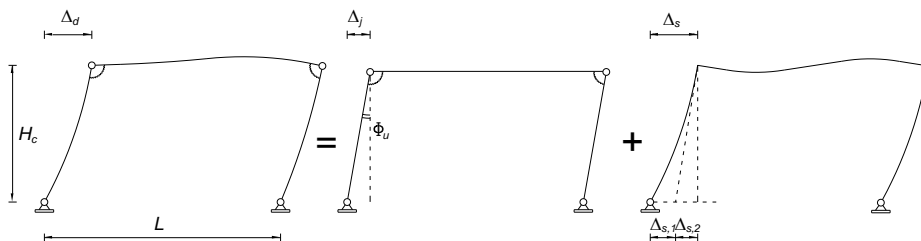


Figure 4.12 Conceptual model for estimating the design displacement Δ_d

$$\Delta_d = \Delta_j + \Delta_s \tag{4.16}$$

In the case of a circular configuration of dowels it is demonstrated experimentally that a rotation Φ produces, in each fastener, a tangential slip δ_i proportional to the distance from the joint centre of rotation **C** (Racher 1995b).

The ultimate slip of dowels is analytically evaluated as:

$$\delta_u = r_{max} \Phi_u \tag{4.17}$$

where r_{max} is the maximum distance between the rotation centre **C** and the most critical dowel, while Φ_u is the ultimate rotation of the joint.

In the analysis of joints we consider the effect of the shear and bending moment force, while the effect of axial force is neglected. The instantaneous centre of rotation **C** does not coincide with the geometrical centre **O** of the node.

In the ultimate plastic configuration, the distribution of internal forces is a distribution in equilibrium with the external forces and in which the ductility ensures the reaching of capacity in each dowel. The shear force is distributed uniformly over all

the connectors, while the force induced by the bending moment is distributed in function of the radius, evaluated from the centre of rotation O .

The connection of the portal of Figure 4.1(b) has a geometric configuration in which steel dowels, of the same diameter and with the same properties of strength, are arranged on two concentric crowns. The forces acting on the connectors induce a compression parallel and perpendicular to the fibre on the columns and the beam, variable depending on the position of the dowel within the joint.

Assuming that all fasteners are in the outer circle of radius r_{ext} , the shear and moment components on each dowel are given by (Eqs. (4.18) and (4.19)):

$$F_M = \frac{M_J}{n_{eq,pl} r_{ext}}; \quad F_V = \frac{V_J}{n_{tot}} \quad (4.18)$$

wherein:

$$n_{eq,pl} = n_{ext} + n_{int} \frac{r_{int}}{r_{ext}} \quad (4.19)$$

where M_J is the bending moment acting on the joint, V_J is the shear force on the joint, n_{tot} is the total number of dowels in the connection, r_{ext} and r_{int} are the external and internal radius respectively, n_{ext} and n_{int} are the external and internal numbers of dowels respectively and $n_{eq,pl}$ is defined as the equivalent number of dowels for the plastic range.

The criterion that defines the maximum capacity of the joint is that for which the maximum slip is reached in the most stressed dowel. In the elastic range, Racher (1995b) demonstrated that the critical location for a dowel in elastic range is the location close to the longitudinal axis of the elements connected.

For the symmetry of the connection it is possible to assume that this condition is valid also in the plastic field. Therefore, the condition of ultimate limit state on the joint is reached when, in the most stressed dowel, the ultimate slip is reached. In an analytical way the ultimate rotation of the joint is formulated taking into account the effect of shear forces, which shift the centre of instantaneous rotation.

Using simple geometrical relations, with reference to Figure 4.13 and keeping in mind that $M_J=V_J H_c$, we obtain the following estimate of r_{max} (Eq. (4.20)):

$$\Delta r = r_{ext} \frac{F_V}{F_M} = r_{ext}^2 \frac{V_J}{M_J} \cdot \frac{n_{eq,pl}}{n_{tot}} = \frac{r_{ext}^2}{H_c} \cdot \frac{n_{eq,pl}}{n_{tot}}$$

$$\rightarrow r_{max} = r_{ext} + \Delta r = r_{ext} \left(1 + \frac{r_{ext}}{H_c} \cdot \frac{n_{eq,pl}}{n_{tot}} \right) \quad (4.20)$$

In Eq. (4.20) the contribution of axial force is neglected. Hence, the following expression for the ultimate rotation is found:

$$\Phi_u = \frac{\delta_u}{r_{ext} \left(1 + \frac{r_{ext}}{H_c} \cdot \frac{n_{eq,pl}}{n_{tot}} \right)} \quad (4.21)$$

At the ultimate rotation of the joint, Φ_u , there is a corresponding displacement of the frame of $\Delta_f = \Phi_u H_c$, where H_c is the height of the column.

Finally, the inelastic displacement of the portal, Δ_j , can be written as:

$$\Delta_j = \Phi_u H_c = \frac{\delta_u}{r_{ext} \left(1 + \frac{r_{ext}}{H_c} \cdot \frac{n_{eq,pl}}{n_{tot}} \right)} H_c = \frac{\delta_u}{1 + \frac{L}{H_c} \frac{h}{L} \frac{r_{ext}}{h} \cdot \frac{n_{eq,pl}}{n_{tot}}} \frac{H_c}{L} \frac{L}{h} \frac{h}{r_{ext}} =$$

$$= \delta_u \frac{\theta_t \gamma_t \beta_t}{1 + 1/\theta_t \gamma_t \beta_t \cdot n_{eq,pl} / n_{tot}} \quad (4.22)$$

where h is the minimum section height of a member, beam (h_b) or column (h_c); $\theta_t = H/L$ is the aspect ratio of the building; $\gamma_t = L/h$ and $\beta_t = h/r_{ext}$ are dimensionless design parameters.

The extension of the formula for connections built with several crowns of dowels is immediate, by redefining the generalized parameter $n_{eq,pl}$ as:

$$n_{eq,pl} = n_{ext} + \sum_{j=2}^{n_{crowns}} n_j \frac{r_j}{r_{ext}} \tag{4.23}$$

where n_{crown} is the number of crowns in the joint, r_j is the radius of the j^{th} crown while r_{ext} is still defined as the radius of the external crowns.

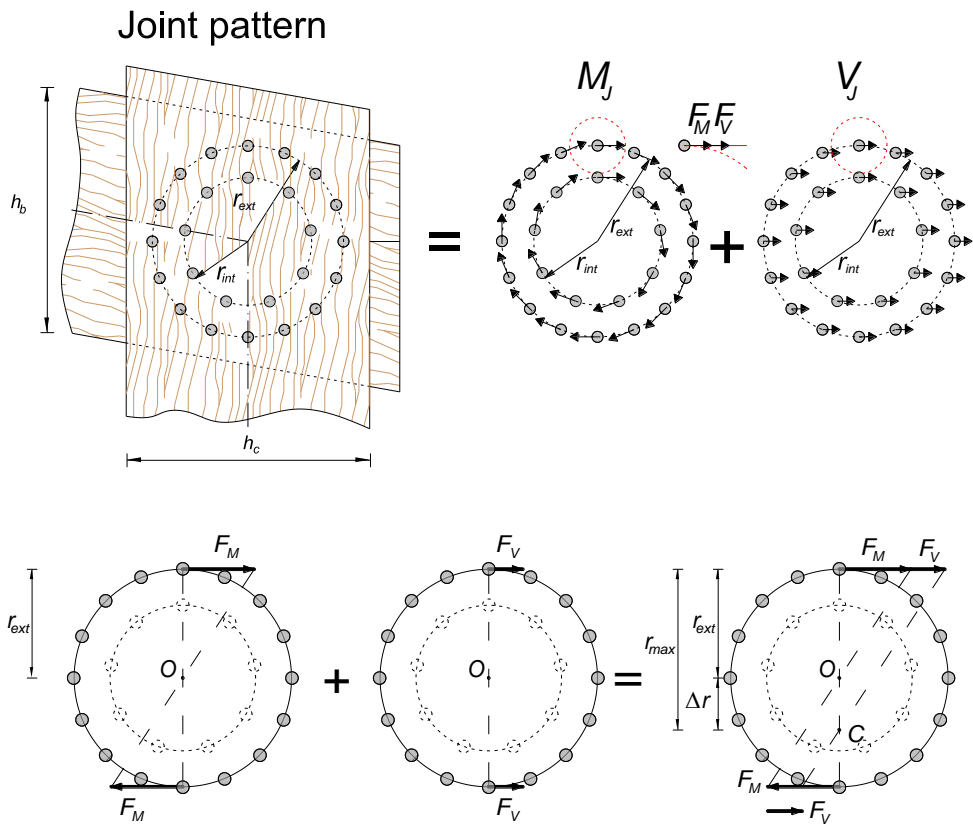


Figure 4.13 Moment and shear stresses on dowels arranged in two concentric crowns

In the design process the parameter β_t of Eq. (4.22) is calculated directly as a function of the inter-distance between dowels and of the distance of dowels from edges (Figure 4.14). The parameter β_t is defined by $\beta_t = h/r_{ext}$. For this geometrical configuration of the joint r_{ext} is equal to $r_{ext} = h/2 - c_2 \cdot d$. Referring to Eq.(4.24) the dimensionless parameter β_t is then defined according to the diameter of the dowel d :

$$\beta_t = h / r_{ext} = 1 / (0.5 - (c_2 \cdot d \cdot \gamma_t) / L) \tag{4.24}$$

The c_2 parameter is a semi-empirical numerical value (Figure 4.14) expressed as a function of the type of fasteners used in connections, and defined in Eurocode 5 (CEN 2004a) or other regulatory codes.

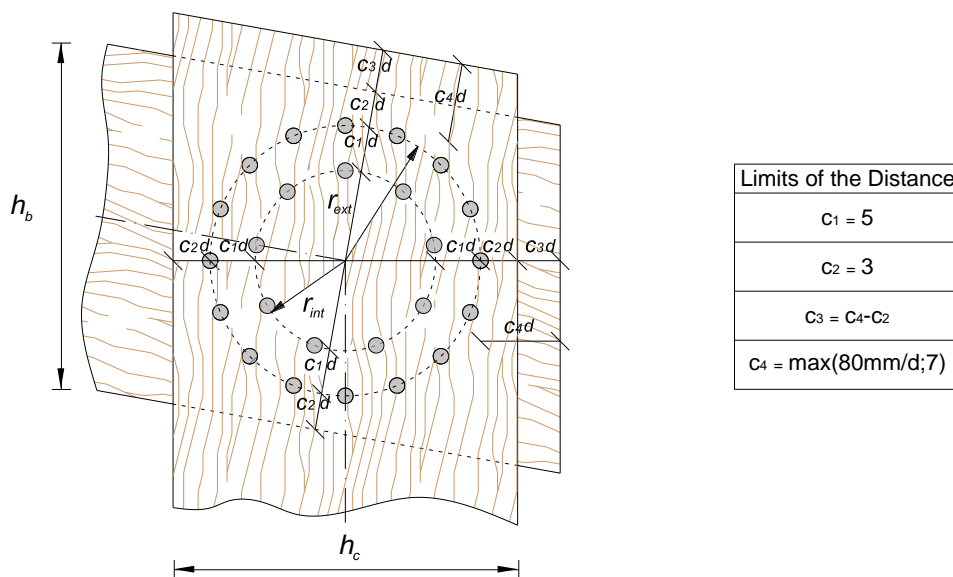


Figure 4.14 Spacings, edge distances and end distances for dowels on a knee joint made with two crowns of dowels

Figure 4.15 shows the final deformed configuration of a connection arranged with one crown of dowels, after a full-scale test performed with a monotonic test protocol (Polastri *et al.* 2008). The test results show that the plastic deformation of the joint is influenced mainly by the bending, validating the assumptions from which we started to formulate the displacement model of the portal.

The elastic displacement of the portal can be calculated by a simple overlapping of displacements due to element deformation, considering that the beam-to-column joint has reached a state of stress equal to the maximum possible, assuming rigid MR joints.

(a)



(b)



SPECIMEN PROPERTIES:

Mechanical properties

Mean density of glulam ρ_m equal to 467 kg/m³

Ultimate strength of steel (for dowels) f_u equal to 580 MPa

Geometrical properties

One crown with r equal to 240 mm

12 dowels with diameter of 16 mm

(c)



Figure 4.15 (a) Test on specimen with 12 dowels of 16 mm in diameter; (b) Connection failure mode after test (ultimate state for joint); (c) Dowel deformation after test (modified from Polastri *et al.* 2008)

The displacement of the assumed rigid portal (Δ_s), can be evaluated by the theory of elastic beams and is independent of the configuration of the connection (Eq. (4.25)):

$$\Delta_s = \Delta_{s,1} + \Delta_{s,2} = \frac{M_J H_c^2}{3EJ_c} + \frac{M_J}{6EJ_b} LH_c \quad (4.25)$$

where E is the timber elastic modulus, and J_b and J_c are the moments of inertia of the beam and the column, respectively.

The geometrical dimensions parameters can be removed in Eq. (4.25) by recalling the rules for seismic design of timber structures. In a well-designed portal, the yield moment of the beam, $M_{R,b}$, must be greater than the ultimate moment of the joint $M_J = M_u$. Thus, we can write $M_u = M_{R,b}/\alpha_R$, where α_R is defined as the coefficient of overstrength.

The displacement of the portal is given by (Eq. (4.26)):

$$\begin{aligned} \Delta_s &= \frac{M_u}{3EJ_b} \left(\frac{J_b}{J_c} H_c^2 + \frac{H_c L}{2} \right) = \\ &= \frac{H_c L}{3\alpha_R} \frac{M_{R,b}}{EJ_b} \left(\frac{H_c}{L} \frac{J_b}{J_c} + \frac{1}{2} \right) = \frac{2}{3\alpha_R} \left(\theta_t \frac{J_b}{J_c} + \frac{1}{2} \right) H_c \gamma_t \varepsilon_y \end{aligned} \quad (4.26)$$

where ε_y is a conventional yield strain of timber (calculated as the ratio of nominal strength f_m to Young's modulus).

The yield deformation of wood is little sensitive to the strength class of the elements (CEN 2000) and can be assumed to be $\varepsilon_y = 0.002$. A reasonable value of the coefficient of over-strength is 1.3, similar to that employed for other traditional materials treated in Eurocode 8 (CEN 2004b).

The timber portal system built for commercial use is generally performed with tapered columns and beams with curvilinear development in the apex zone. The cross-section of elements near the joint, however, is constant in height for reasons mainly related to its implementation.

For the type III failure mode of connectors (EYM) a ratio of inertia beam-column, J_b/J_c ($\approx b_b/b_c$) which is between 1.0÷0.5 is implicitly assumed. We can assume a conservative value of $J_b/J_c=0.5$.

The final expression for the calculation of the elastic displacement of the portal (Δ_s) is:

$$\Delta_s \cong \frac{H_c}{2000} \gamma_t (\theta_t + 1) \quad (4.27)$$

Thus, summing Eq. (4.22) and Eq. (4.27), the design displacement (also ultimate displacement) can be estimated using the following simple equation (Eq. (4.28)):

$$\Delta_d = \delta_u \frac{\theta_t \gamma_t \beta_t}{1 + 1/\theta_t \gamma_t \beta_t} + \frac{H_c}{2000} (\theta_t + 1) \gamma_t \quad (4.28)$$

Parameters that control the design displacement formula of the portal (Δ_d) are basically the ultimate slip of the dowel (δ_u), the height of the portal frame (H_c), the portal aspect ratio ($\theta_t=H_c/L$), the ratio between the length of the portal and the height of the cross-section of the beam ($\gamma_t=L/h$), and the ratio between the cross-section of the beam and the external radius of the joint ($\beta_t=h/r_{ext}$). The dimensionless parameter β_t ($=h/r_{ext}$) can be estimated in the design process, while H_c and θ_t are obviously known at the design stage. Lastly, the adimensional geometric parameter under normal design assumptions, γ_t ($=L/h$), is expected to be between 10 and 15.

4.5 Ductility

A similar expression to that for the calculation of the design displacement of the portal can be formulated to calculate the elastic displacement at yield (Eq. (4.29)):

$$\Delta_y = \delta_y \frac{\theta_t \gamma_t \beta_t}{1 + 1/\theta_t \gamma_t \beta_t} + \frac{H_c}{2000} (\theta_t + 1) \gamma_t \quad (4.29)$$

where now δ_y is the dowel yield slip, while the other parameters are defined in the previous section.

As usual, the static ductility capacity of the structure μ_Δ can be calculated as the ratio of Δ_d to Δ_y . As mentioned in the Section above, the assessment of the yield slip of the dowel, δ_y , reflects the uncertainty in the estimation of the ultimate slip modulus k_{ULS} . The value of the displacement ductility, μ_Δ , of the structure is, therefore, influenced by the conventional definition of the yield point of the single connector. In the model, defined in the next Section and validated in Chapter 5, to estimate the equivalent viscous damping, the effect of uncertainty in the displacement ductility (μ_Δ) is attenuated by the hysteretic model formulated. In the high ductility state of connections, the slip ductility is 6. Due to the uncertainty on slip modulus, the slip ductility of the dowel can reach the lower limit expected when $k_{ULS} \rightarrow k_{SER}$ and then $\mu_\delta = 4$ (factor 2/3 of Eurocode 8; CEN 2004b). The Equivalent Viscous Damping of the structure, with the hysteretic model formulated in the next Section, is affected little (less than 5% error) by the exact value of ductility in the final evaluation of the damping. This is true, however, when the high ductility mechanism of connections is ensured ($\mu_\delta \geq 4$, Eurocode 8; CEN 2004b). More details are reported in Chapter 5.

4.6 Equivalent viscous damping

The next step in the application of the Direct-DBD method is to define the design damping, ξ_d , i. e. the Equivalent Viscous Damping (EVD) ξ_{eq} of the structure matching the design displacement Δ_d . The use of the EVD parameter simplifies the dynamic problem greatly, passing from a non-linear solution of the system to a simple linear-elastic one (Chopra 1995). Works specifically intended to study the damping of some types of wood structures are those of Foliente (1995) and Filiatrault *et al.* (2003).

The literature shows very few works that deal specifically with damping in wood structures. Nailed connections are the most studied, due to their widespread use in wooden structures. Chui and Smith (1990) have demonstrated that the structures with nailed connections can reach equivalent viscous damping values of about 30%, in function of the constraints imposed between the elements. In Yeh *et al.* (1971) it is demonstrated that the viscous damping of the material is independent of the type of wood used and ranges from 2.5 to 10%.

In Yasumura (1996) and Polensek and Bastendorff (1987), referring again to nailed connections, acceptable values are discussed for the equivalent viscous damping, on the order of 10÷20% and 10÷30% respectively. Other authors, such as Dolan (1995) and Karacebeyli and Ceccotti (1996), have examined and compared the influence of the loading protocol on the results obtained from tests.

Frequently the Equivalent Viscous Damping of the structure, ξ_{eq} , is defined as the sum of a constant viscous component (ξ_0) and an hysteretic component (ξ_{hyst}) which increases with displacement amplitude Δ_d . It is also customary to express the hysteretic component of damping with a non-linear function of the structural ductility μ_Δ .

An often used general formulation of this kind is that suggested by Priestley *et al.* (2007), based on the equivalent energy absorbed approach - Jacobsen's approach - Eq. (4.30):

$$\xi_d = \xi_{eq} = \xi_0 + \xi_{hyst} = \xi_0 + \frac{C}{\pi} \left(\frac{\mu_\Delta - 1}{\mu_\Delta} \right) \quad (4.30)$$

wherein C and ξ_0 are constants that depend on the material and structural type, while μ_{Δ} is the displacement ductility. In particular, the parameter C is a function of the hysteretic model chosen for the structure. This expression generalizes the formulation originally proposed by Gulkan and Sozen (1974) for concrete structures. The model of Eq. (4.30) is commonly used for steel and reinforced concrete, while almost no application is found in the technical literature in the case of timber.

The Equivalent Viscous Damping (ξ_{eq}) is influenced by the fundamental period of the system, by the characteristics of ground motion and by the ductility level (Blandon and Priestley 2005). The Eq. (4.30) must therefore be validated through a series of non-linear dynamic analyses, with a set of accelerograms selected to measure the influence of these factors on the analytical model. Blandon and Priestley (2005) describe and propose a procedure for the calibration of analytical expressions to estimate the equivalent viscous damping (EVD, ξ_{eq}) of some hysteretic models used to describe the behaviour of traditional materials. More details of EVD can be found in Priestley *et al.* (2007).

The analytical expression of the equivalent viscous damping, based on parameters known at the beginning of the design process, is formulated within this Chapter. The final expression is consistent with the model selected to describe the mechanical response of the single connector. The next Section shows the state-of-the-art of cyclic load-slip ($F-\delta$) curves of dowel-type metal fastener connections.

4.6.1 Cyclic behaviour of dowel type fastener connections

The energy dissipation of structures is essentially the result of the cyclic behaviour of connections. The hysteretic behaviour of connections, the weak link of the structure, is influenced by the capacity of the metal fasteners and the strength properties of wood. Wood has mechanical properties that vary depending on the orientation of the load relative to the direction of the grain (Piazza *et al.* 2005). The design complexity of connections increases when the buildings are subject to a seismic force, which by its nature is unpredictable (Karacabeyli and Popovski 2003).

Experimental tests have shown that the shape of hysteresis loops in connections with dowel-type metal fasteners is sensitive to the amplitude of the imposed displacement.

Figure 4.16 shows the expected response of a dowelled connection designed for various levels of displacement. In Karacabeyli and Popovski (2003) some recent cyclic tests carried out on modern connections, including those of dowel-type, are discussed. Results of tests showed that the failure mechanism that involves the yielding of the dowel and the embedment strength of wood is able to provide high ductility and excellent energy dissipation under the effect of repeated cycles of loading. These performances are ensured, in particular, when the dowels are slender and the relative distance between elements is high.

The study of cyclic and dynamic behaviour of a wooden connection with a metal dowel is a field which has been explored for only a few years. Two major publications submitted by Allotey (1999) and Lo (2002) deal with the definition of a mechanical model capable of accurately describing the cyclic load-slip curve for a single connector. Allotey's model is an improvement on one previously proposed by Foschi and Bonac (1977) to describe the monotonic load-slip curve. The mechanical model takes account of local force of friction generated by contact between the metal surface of the dowel and the wooden element. Formulation of the load-slip curve is based on the theory of a flexible beam on deformable soil (an analogy of a beam on a deformable foundation) with non-linear behaviour. This model takes into account effects of friction at the interface between connector and wood, the pressure imposed on the wood and the connector cavity formed after the first load cycle, which affects the behaviour of subsequent cycles of loading.

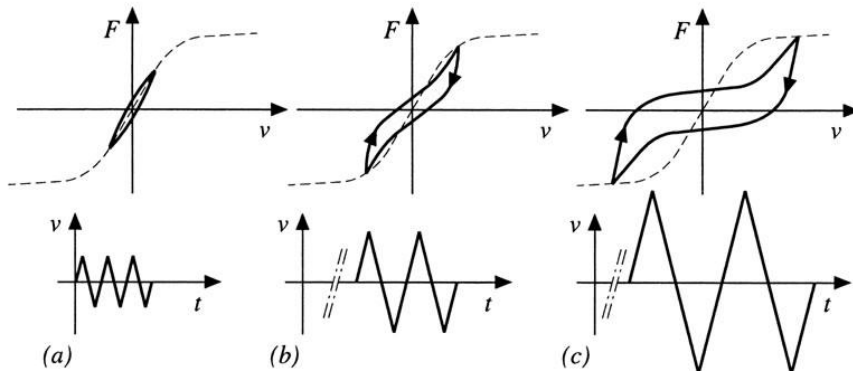


Figure 4.16 Typical force-deformation loops for different load levels of dowelled joints under cyclic loading (modified from Ceccotti 1995)

Lo (2002) remarks on some important aspects of the applicability of Allotey's model and proposes an interesting comparison with the simplified Bouc-Wen-Baber-Noori (BNW) model type, based on the evaluation of 13 parameters.

The models presented above are very sophisticated and allow a proper investigation of the whole dynamic response of wooden connections as displacement increases, up to failure. This research, on the other hand, focuses on the study of the dynamic response of a structure in the ultimate limit state, a highly non-linear situation that can be treated with limit analysis tools.

This work proposes an analytical expression for estimating the Equivalent Viscous Damping, ξ_{eq} , using known design parameters, in a similar way to the formulation of the design displacement. Hence, we assume connections with dowel-type metal fasteners in double shear plane timber-to-timber joints, ductile independently (see Figure 4.11) of geometry and mechanical properties. The failure mode is highly ductile, type III according to the European Yield Model. It was demonstrated in the previous paragraph that, regardless of the mechanical properties of steel and wood, mode III is always ensured for dowels with a slenderness (=ratio between thickness of the timber member to be connected and the diameter of the fastener) of at least 10. The slenderness of dowels controls the plastic behaviour of the connection, and the effects of flexural deformation of the metallic element (Ceccotti 1995). Under the effect of repeated cycles of loading with the same amplitude, the connection is controlled by the rotation mechanism of the plastic hinges of dowels. In other words, the mechanism whereby only the crushing of the wood occurs is avoided. In the latter case the connection is fragile and shows loss of stiffness during the return to the undeformed situation.

The typical expected load-displacement (slip) curve (F-v), under cyclic loading, of a connection with dowel-type metal fasteners is shown in detail in Figure 4.17.

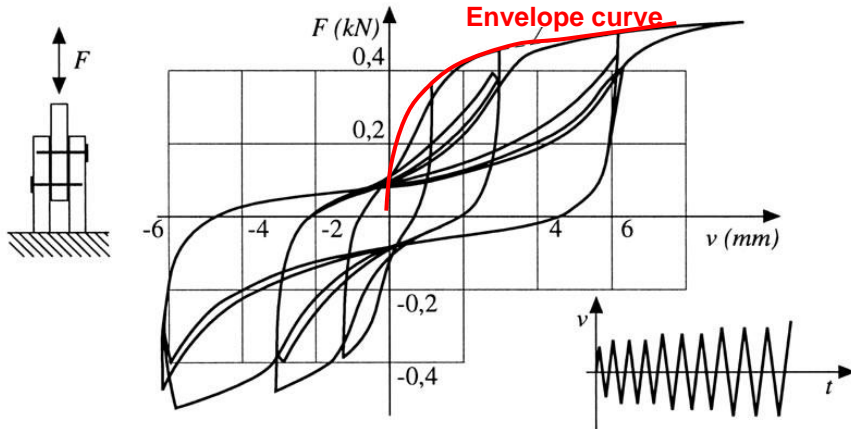


Figure 4.17 Typical cyclical behaviour of a nailed connection with nail slenderness of 8.5; The red line shows the Envelope curve (Ceccotti 1995)

The expected trend shows an envelope curve that, regardless of the load history, differs little from that for monotonic loading (Ceccotti 1995). For well-designed connections the difference between curves is always less than 10%. Connections in wood are characterized by two important phenomena: the *pinching effect* and the *memory of the material*. The *pinching effect phenomenon* modifies the hysteresis cycles in the transition from first to subsequent cycles for the same amplitude range of loading. The typical pinched hysteretic cycle is characterized by a thinner loop in the middle compared to the ends. This phenomenon is caused by the cavity formed around the fasteners during plastic deformation. The *memory of the material phenomenon* implies that the load-slip curve of the connection at a given time is a function of the instantaneous displacement and of the loading history (Dolan 1994).

Both these phenomena lead to a reduction in the energy dissipated in hysteresis loops and must be properly taken into account. The cyclical response of the connector can be idealized by decomposing the motion into a series of ultimate situations, occurring before and after the phase of inversion of motion. This assumption is satisfied if the state of deformation involves the development, at least in part, of plastic hinges on dowels (Figure 4.18) and then is consistent with the evaluation of design displacement as formulated in the previous Section.

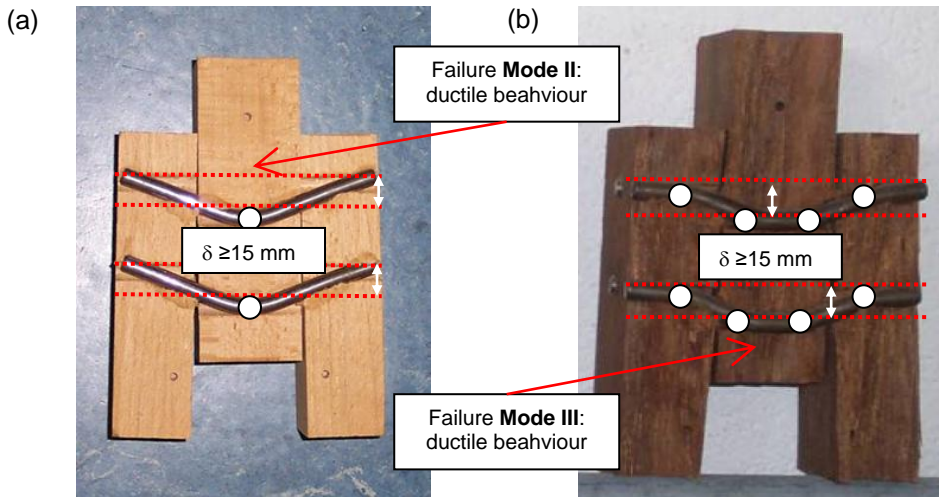


Figure 4.18 Failure of connections with metal dowel-type fasteners in double-shear; (a) Mode II in accordance with the EYM (CEN 2004a); (b) Mode III in accordance with the EYM (Courtesy of Professor Maurizio Piazza)

For fully-developed plastic hinges on connectors, failure mode III, Figure 4.19 shows the instants of the mechanism, under a cyclic history of loading scaled on two levels of slip δ_1 and δ_2 , in which $\delta_2 > \delta_1$.

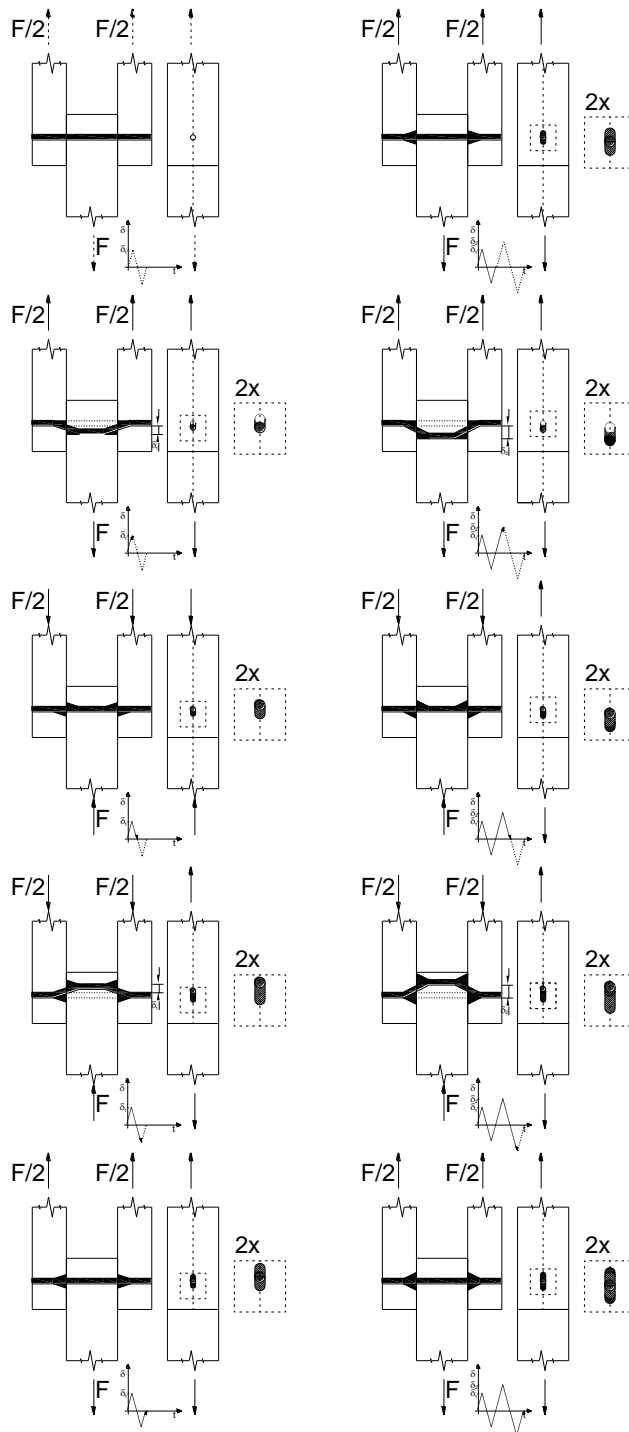


Figure 4.19 Qualitative trend of the cyclic response of a connection with dowel-type fasteners in double shear for failure mode III (European Yield Model; CEN 2004a)

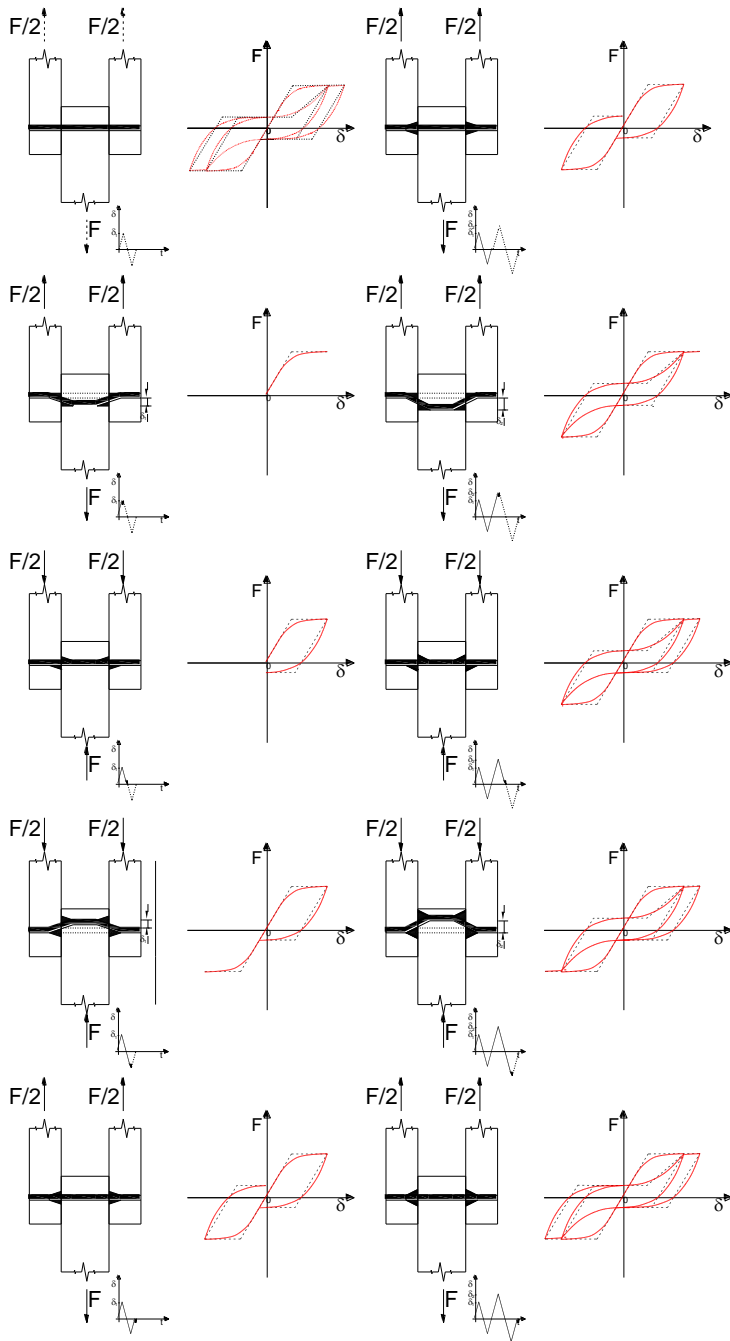


Figure 4.20 Expected hysteretic loops of a connection with dowel-type fasteners in double shear subjected to cyclic loading (failure mode III in accordance of European Yield Model)

Expected load-slip curves for these connections are shown in red on Figure 4.20 and have typical “drop” form behaviour. The theoretical load-slip charts (dashed lines in Figure 4.20), however, are formulated based on the monotonic curve, described in the previous Section, and use some experimental observations. The load-slip model for dowels, under cyclic response, does not consider the loss of strength that can occur under consecutive cycles of loading for a given level of displacement. This assumption implies a negligible error in conditions of high ductility, since the energy dissipated at the ends of the hysteresis curve becomes small compared with the energy dissipated in the central part of the cycle. The analytical model adopted in the cyclic response of a single dowel is that shown in Figure 4.21.

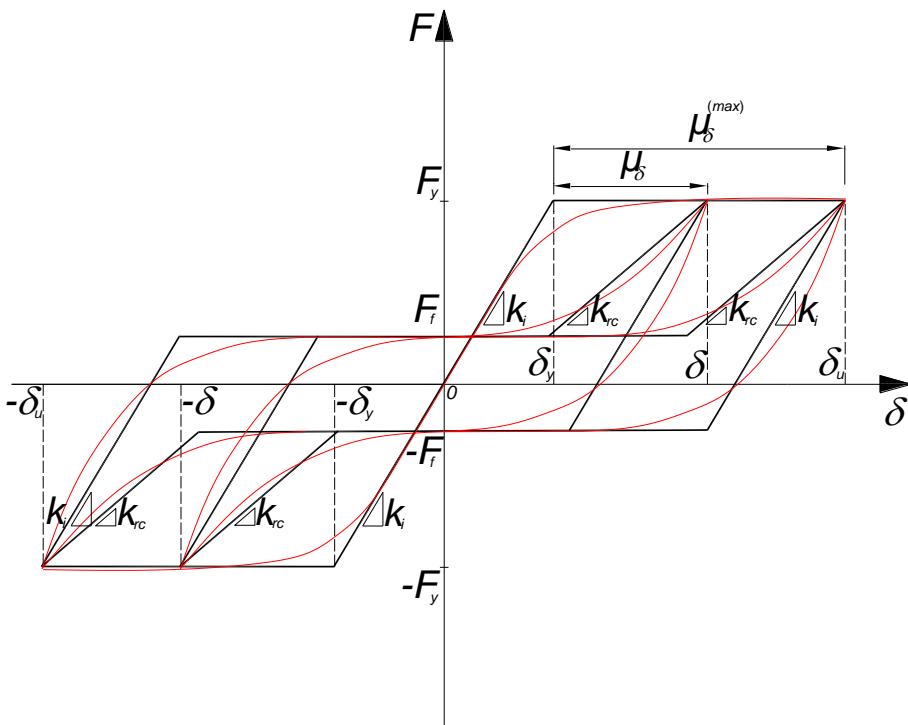


Figure 4.21 Analytical load-slip curve of a dowel-type fastener connection (black line); Expected load-slip curve of a dowel-type fastener connection (red line)

The model in Figure 4.21 is correct for displacement amplitudes close to the design displacement.

In the final representation, the generic hysteresis curve consists of an elastic-perfectly plastic branch in the loading phase, unloading with a slope equal to the elastic stiffness, and residual plastic deformation restored by a force equal to that required for plasticizing the dowel and overcoming the friction generated between the wooden and steel surfaces of the elements. Subsequently to the first cycle, the response is based on a curve where the plateau branch is set to the restoring force F_f , while in the final part it has stiffness equal to k_{rc} , whereby the bearing capacity F_y is restored.

The parameters required for the cyclic load-slip curve are: F_y , δ_y , μ_δ (or δ_u), F_f , k_i ($=k_{ULS}$) and k_{rs} . Here we describe the method for evaluating the bearing capacity of the single dowel F_y (shear force) and the restoring force to the undeformed situation, here noted as F_f (restoring force). Parameters μ_δ , k_i and k_{rc} are obtained immediately with the data available in the literature.

The bearing capacity that is generated as a result of the yielding of the dowel (F_y) is estimated by imposing the equilibrium of the forces acting on the wooden connection in the ultimate situation. The analytical evaluation is based on the European Yield Model (EYM; CEN 2004a), as discussed in the previous Section.

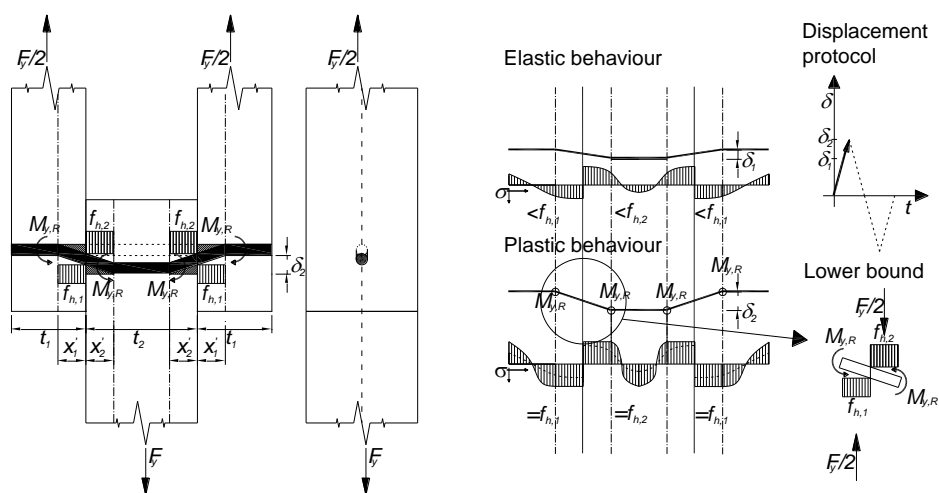


Figure 4.22 Failure Mode III dowel-type fastener connections in double shear; Johansen's model

Here we recall the final form of the expression required to evaluate the force F_y (Eq. (4.31)).

$$F_y = \sqrt{\frac{2\beta}{1+\beta}} \sqrt{2M_{y,Rk} f_{h,1,k} d} \quad (4.31)$$

in which, the lengths x_1' and x_2' , required for stress equilibrium on the dowel, are equal to (Piazza *et al.* 2005):

$$x_1' = \sqrt{\frac{2M_{y,Rk}}{f_{h,1,k} d}} \sqrt{\frac{2\beta}{1+\beta}}; \quad x_2' = \frac{x_1'}{\beta} \quad (4.32)a,b$$

Starting from a new equilibrium for the dowel, which no longer has wooden support in the zone between two successive plastic hinges, we can calculate the restoring force F_f in a similar manner to the force F_y (Figure 4.23).

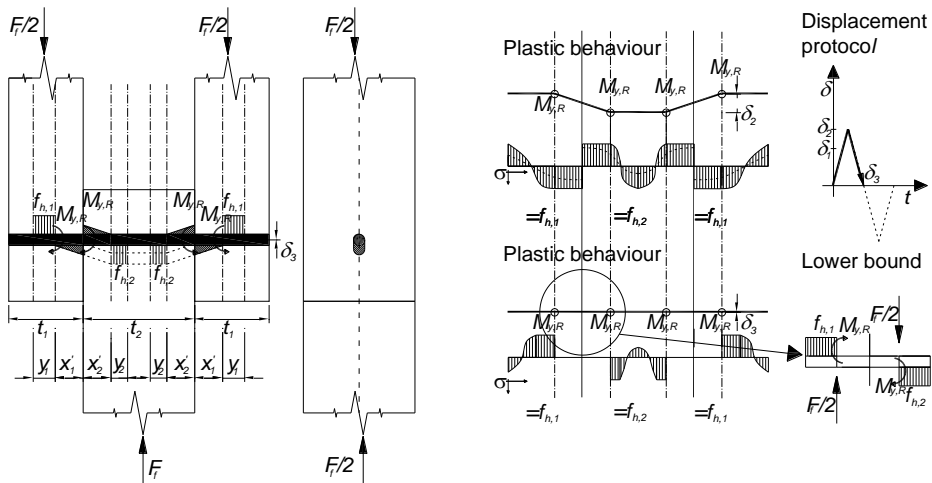


Figure 4.23 Configuration of equilibrium (hypothetical) after the reaching of Failure Mode III, for a dowel-type fastener connection in double shear, on return to the undeformed situation

The restoring force F_f is given by the sum of the force due to plastic deformation of the dowel and by the friction between the dowel and wood. Neglecting the latter contribution, we can write the following equation (Eq. (4.33)) according to the lower bound limit theorem of limit analysis. Assuming a stress distribution in equilibrium in the connector and the inelastic deformation of the dowel that follows by formation of plastic hinges, we can determine directly the force F_f .

For the equilibrium in rotation imposed on half connection, we can write:

$$-M_{y,Rk} - M_{y,Rk} + F_f \left(\frac{y_1}{2} + x_1' + x_2' + \frac{y_2}{2} \right) = 0 \quad (4.33)$$

For the translational equilibrium on each i^{th} wooden element we can write instead:

$$F_f = f_{h,1,k} \cdot d \cdot y_1 = f_{h,2,k} \cdot d \cdot y_2 \quad (4.34)$$

which yields Eq. (4.35):

$$y_2 = y_1 / \beta \quad (4.35)$$

Substituting Eqs. (4.34) and (4.35) in Eq. (4.33) and remembering how quantities x_1' and x_2' are defined, we find a second order equation in variable y_1 :

$$y_1^2 + 2x_1' y_1 - x_1'^2 = 0 \quad (4.36)$$

The only real solution that ensures a value of $\sigma_F (= F_f / F_y)$ less than one is that of Eq. (4.37):

$$y_1 = (\sqrt{2} - 1)x_1' \quad (4.37)$$

Considering the numerical coefficient of calibration, 1.15, provided by the EYM Eq. (4.31) and the instantaneous load condition (increase of 10% in F_y), we obtain:

$$\sigma_F = \frac{F_f}{F_y} \cong 0.33 \quad (4.38)$$

Therefore:

$$F_f = \sigma_F F_y \cong 0.33 F_y \quad (4.39)$$

In conclusion, the restoring force to the undeformed state is about 33% of the shear force produced by the yielding of the dowel and the embedment strength of wood in the loading phase.

4.6.2 Formulation of the equivalent viscous damping analytical model

As demonstrated in this Section, the hysteretic model selected to describe the behaviour of the dowel-type fastener connections is that of Figure 4.21. The generic cycle of loading for a given amplitude of displacement is described by five parameters which are expressed analytically through Eqs. (4.31) and (4.39) or have a numeric value, as described previously. The analytical expressions to calculate the equivalent viscous damping, developed in function of these five design parameters, are presented in the next pages.

The evaluation of the equivalent viscous damping, ξ_{eq} , is based on Jacobsen's energy approach (Jacobsen 1930).

The damping is calculated as the ratio between hysteresis energy dissipated in a mid-cycle and the potential energy stored by an equivalent simple oscillator for the same displacement amplitude.

We must remember at this point that, for fastened connections, the hysteretic dissipation is partially due to the steel dowels that embed in the wood during the load action, as explained previously. Because this mechanism implies reduction of energy dissipation after each cycle, the total amount of energy dissipated depends largely on the load protocol: and therefore, we do not expect the relationship between equivalent damping and ductility to be unique. Taking account of this issue, it is possible to identify one of three typical damping-to-ductility curves here labelled *Protocol I*, *Protocol II* and *Protocol III*, in function of the loading history imposed on the connection.

For the loading protocol I (*Protocol I*), with the help of Figure 4.24(a), through simple mathematical operations we can calculate the final value of the damping as the direct sum of two components, Eqs. (4.40) and (4.41):

$$\xi_p = \frac{E_p}{2\pi E_{storage}} = \frac{1}{\pi} \left(1 - \frac{1}{\mu_\delta} \right) \quad (4.40)$$

$$\xi_f = \frac{E_f}{2\pi E_{storage}} = \frac{\sigma_F}{\pi} \left(1 - \frac{1}{\mu_\delta} - \frac{\sigma_F}{2\mu_\delta} \right) \quad (4.41)$$

Equation (4.40) is the energy dissipated by plastic deformation during the loading phase (wood and steel) (E_p), while Eq. (4.41) is the energy dissipated by the effects of friction and plastic deformation of the fastener (E_f), in the recovery phase of the initial configuration.

The final equation for calculating the damping value is (Eq. (4.42)):

$$\xi_{eq,dowel} = \xi_p + \xi_f = \frac{1}{\pi} (1 + \sigma_F) \left(1 - \frac{1}{\mu_\delta} \right) \quad (4.42)$$

$$\xi_e = \frac{E_e}{2\pi E_{storage}} = \frac{(\beta_k - 1)}{2\pi\mu_\delta} (1 - \sigma_F)^2 \quad (4.43)$$

$$\xi_f = \frac{E_f}{2\pi E_{storage}} = \frac{2\sigma_F}{\pi} \left(1 - \frac{1}{\mu_\delta}\right) \quad (4.44)$$

Equation (4.43) estimates the energy dissipated between the instant in which the fastener regains stiffness from contact with the wooden surface and the instant when the previous displacement is reached (E_e).

With Eq. (4.44) we estimate the effects of friction and the plasticity of the fastener during the loading and unloading phases (E_f).

In conclusion, the final damping is given by:

$$\xi_{eq,dowel} = \xi_e + \xi_f = \frac{(\beta_k - 1)}{2\pi\mu_\delta} (1 - \sigma_F)^2 + \frac{2\sigma_F}{\pi} \left(1 - \frac{1}{\mu_\delta}\right) \quad (4.45)$$

in which the numerical values of $\sigma_F (=F_y/F_y)$, $\beta_k (=k/k_{rc})$ and $\mu_\delta (= \delta_u/\delta_y)$ are used to calculate the equivalent viscous damping.

Finally, for the loading protocol III (*Protocol III*), with clear reference to Figure 4.24(c), the damping is defined for the generic situation in which the connection has undergone a displacement previously. This condition represents an intermediate situation between the two given above. The increase in slip compared to the past is defined by means of the parameter $\Delta\delta/\delta$.

Also in this case, each contribution can be analytically modelled in terms of the energy dissipated, and the damping calculated as the sum of three parts (Eq. (4.46), Eq. (4.47) and Eq. (4.48)):

$$\xi_e = \frac{E_e}{2\pi E_{storage}} = (\beta_k - 1) \frac{(1 - \sigma_F)^2}{2\pi\mu_\delta} \quad (4.46)$$

$$\xi_p = \frac{E_p}{2\pi E_{storage}} = \frac{\Delta\delta}{\delta} \left(\frac{1 - \sigma_F}{\pi} \right) \quad (4.47)$$

$$\xi_f = \frac{E_f}{2\pi E_{storage}} = \frac{2\sigma_F}{\pi} \left(1 - \frac{1}{\mu_\delta} \right) \quad (4.48)$$

The meaning of E_p , E_f and E_e is as seen above. In conclusion, the final damping is given by Eq. (4.49).

$$\xi_{eq,dowel} = \xi_e + \xi_p + \xi_f = (\beta_k - 1) \frac{(1 - \sigma_F)^2}{2\pi\mu_\delta} + \frac{\Delta\delta}{\delta} \left(\frac{1 - \sigma_F}{\pi} \right) + \frac{2\sigma_F}{\pi} \left(1 - \frac{1}{\mu_\delta} \right) \quad (4.49)$$

The equations (4.42), (4.45) and (4.49) require the numerical value of the parameters β_k , σ_F and $\Delta\delta/\delta$ to assess the equivalent viscous damping $\xi_{eq,dowel}$. The parameter σ_F is defined as the ratio between the force required to move the connector to its initial undeformed position and the bearing capacity at ultimate limit state (F_y). As shown above this value can be assumed to be $\sigma_F \sim 0.33$ when a local failure mechanism type III is ensured, according to the EYM (CEN 2004a).

The parameter β_k can be assumed equal to 2, since the stiffness during the reloading phase is half of the initial stiffness (Ceccotti and Vignoli 1989). This point requires a more detailed discussion even though its estimation may lead to small errors in the final value of $\xi_{eq,dowel}$.

The parameter $\Delta\delta/\delta$ deserves an in-depth discussion, given its weight in the calculation of the final value of the damping. This parameter is closely related to factors that are a function of the loading history imposed on the connection.

The loading history of a connection is related to the seismic hazard in a given geographical area. In safety terms, it is clear that this parameter, related to events that are unpredictable by nature, can be defined in non-deterministic mode (Foliente 1993).

Given a certain seismic risk, it is possible to define a numerical value of $\Delta\delta/\delta$. In this way the cyclic quasi-static test protocol provided by the EN 12512 (CEN 2001) defines a loading history that must be used to estimate the dissipative properties of the connection (Figure 4.25).

The ratio of slip $\Delta\delta/\delta$, consistent with the test protocol of the UNI EN 12512 (CEN 2001) can be taken as $\Delta\delta/\delta = \Delta v_y/v_y = 0.5$. Usually an earthquake is represented by a number of whole cycles interrupted by a culminating instant in which the highest energy content is released, and followed by a phase of adjustment still with minor fluctuations. Less conservative values for the parameter $\Delta\delta/\delta$ could be around 0.8.

When the equivalent viscous damping ($\xi_{eq,dowel}$) value of one connector is known, we can estimate the final value of the joint damping, in a similar way to what was done in the definition of design displacement. Starting from the same assumptions, the Moment-Resisting (MR) connection is seen as a set of non-linear springs that work in parallel and are subject to the same slip if equal distant from the centre of instant rotation.

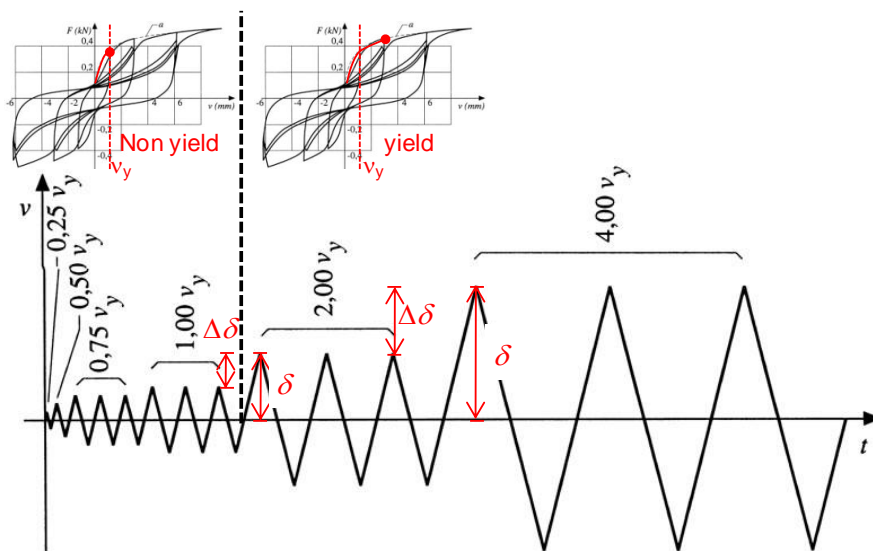


Figure 4.25 Procedure for cyclic testing following EN 12512 (CEN 2001); Ratio between series of cycles

By definition, the equivalent viscous damping of the MR connection, at the ultimate limit state (ULS), is given by Eq. (4.50):

$$\xi_{eq,JOINT} = \frac{(E_{dis,J})^{1/2cycle}}{2\pi E_{storage}} = \frac{(E_{dis,J})^{1/2cycle}}{2\pi M_u \Phi_u / 2} \quad (4.50)$$

Referring to Figure 4.26, for connections with two concentric crowns of dowels, we can estimate the energy dissipated by the connectors as (Eq. (4.51)):

$$\xi_{eq,JOINT} = \frac{n_{ext} (E_{dis,dowel,ext})^{1/2cycle} + n_{int} r_{int} / r_{ext} (E_{dis,dowel,int})^{1/2cycle}}{2\pi M_u \Phi_u / 2} \quad (4.51)$$

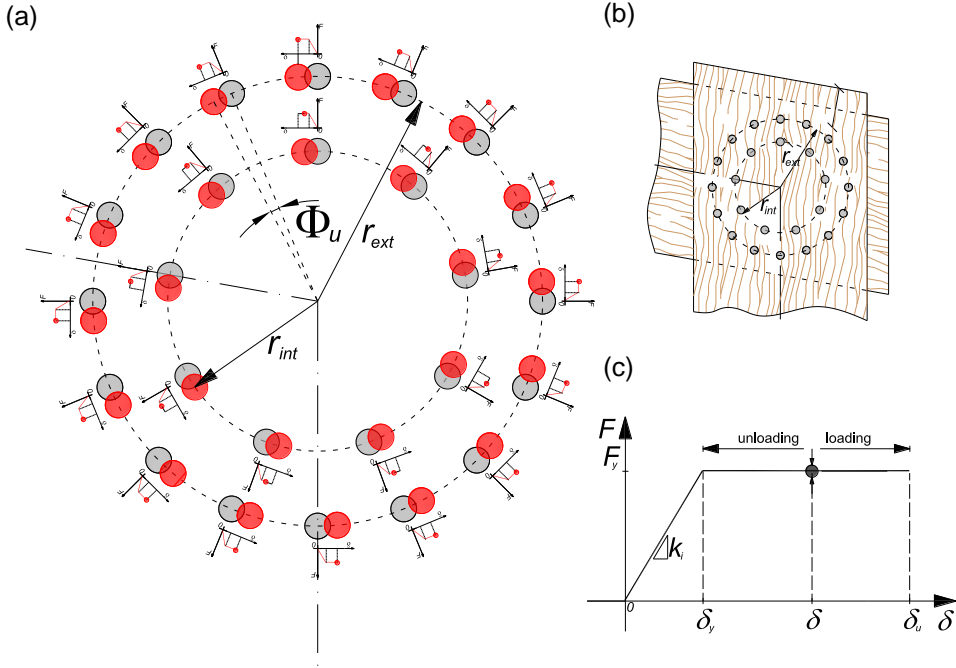


Figure 4.26 (a) Ultimate configuration of joint: slip of dowels due to inelastic deformation; (b) Dowelled cross-lapped joint; (c) Load-slip envelope curve of dowels

By manipulating the expression (4.51) we can write again:

$$\xi_{eq,JOINT} = \frac{2\pi F_y \delta_u / 2 (n_{ext} \xi_{eq,dowel,ext} + n_{int} r_{int} / r_{ext} \xi_{eq,dowel,int})}{2\pi M_u \Phi_u / 2} \quad (4.52)$$

The terms M_u and Φ_u , ultimate bending moment and ultimate rotation of the connection, will be defined analytically in Chapter 5 with Eqs. (5.15) and (5.19). In Eqs. (5.15) and (5.19) the effect of shear is included by the dimensionless term r_e/H_c . Neglecting the effect of shear and substituting the analytical expressions of M_u and Φ_u in Eq. (4.52) we obtain:

$$\begin{aligned} \xi_{eq,JOINT} &= \frac{n_{ext} \xi_{eq,dowel,ext} \delta_u + n_{int} \xi_{eq,dowel,int} \delta_u r_{int} / r_{ext}}{n_{ext} \delta_u + n_{int} \delta_u r_{int} / r_{ext}} = \\ &= \frac{n_{ext} \xi_{eq,dowel}(\mu_\delta) + n_{int} \xi_{eq,dowel}(\mu_\delta r_{int} / r_{ext}) r_{int} / r_{ext}}{n_{ext} + n_{int} r_{int} / r_{ext}} \end{aligned} \quad (4.53)$$

The final value of the equivalent viscous damping of the single beam-column connection of the portal can be estimated using Eq. (4.53), with the geometric and mechanical design parameters.

The extension of Eq. (4.53) to a generic connection made by a finite number of crowns of dowels, n_{crowns} (Eq. (4.54)) is simply:

$$\begin{aligned} \xi_{eq,JOINT} &= \frac{\sum_{n_{crowns}} \left(\sum_{i=1}^n \xi_{eq,i,dowel}(\mu_i) \delta_{u,i} + \dots \right)}{\sum_{i=1}^n \delta_i + \sum_{j=1}^m \delta_j r_j / r_e} + \\ &= \frac{\sum_{n_{crowns}} \left(\dots + \sum_{j=1}^m \xi_{eq,j,dowel}(\mu_j r_j / r_{ext}) \delta_{u,j} r_j / r_{ext} \right)}{\sum_{i=1}^n \delta_i + \sum_{j=1}^m \delta_j r_j / r_{ext}} \end{aligned} \quad (4.54)$$

From the equivalent viscous damping of the connections we can evaluate the EVD of the structure via simple direct assessment. Consistently with the Direct-DBD approach of Priestley *et al.* (2007), ignoring the contribution of gravity loads, we can assume a symmetrical deformation of the portal.

By definition, the Equivalent Viscous Damping of structure (EVD, ξ_{eq}) is estimated via Eq. (4.55):

$$\xi_{eq} = \frac{E_{hysteretic}^{(1/2cycle)}}{2\pi \cdot E_{storage}} \quad (4.55)$$

Given the hypothesis that all the dissipation capacity is concentrated into the beam-to-column joints of the portal, Eq. (4.55) can be rewritten as (Eq. (4.56)):

$$\begin{aligned} \xi_{eq} &= \frac{2E_{dis,J}^{(1/2cycle)}}{2\pi \frac{F\Delta_d}{2}} = \frac{2(\xi_{eq,JOINT} \cdot 2\pi \cdot M_u \cdot \Phi_u)^{(1/2cycle)}}{2\pi \frac{2 \cdot V_J \Delta_d}{2}} = \\ &= \xi_{eq,JOINT} \left(\frac{\Delta_j}{\Delta_d} \right) = \xi_{eq,JOINT} \left(\frac{1}{1 + \Delta_s / \Delta_j} \right) \end{aligned} \quad (4.56)$$

The final expression for the evaluation of the equivalent viscous damping of the structure is that of Eq. (4.57):

$$\xi_{eq} = \xi_{eq,JOINT} \left(\frac{1}{1 + \frac{\Delta_s}{\Delta_j}} \right) \quad (4.57)$$

Where $\xi_{eq,JOINT}$ is estimated with Eq. (4.53), Δ_j with Eq. (4.22) and Δ_s with Eq. (4.26).

To manipulate Eq. (4.55) all the definitions of the parameters defined in this Chapter were considered.

4.7 Conclusions

The model presented in this Section allows the assessment of the Equivalent Viscous Damping of the structure (EVD, ξ_{eq}) in a simple and direct manner, based on the physical description of connections made with the use of dowel-type metal fasteners. This makes it possible to extend the formulation to other configurations and types of connections and thus constructive systems.

5 VALIDATION OF THE PROPOSED DIRECT-DBD METHOD

5.1 Dynamic behaviour of timber structures

The evaluation of the dynamic behaviour of the portal frame system (presented in Chapter 4) in the time domain is possible through structural analysis software. The dynamic behaviour of the system is strongly influenced by the non-linearity of the connections with changes in the state of stress-strain reached in the deformed configuration.

In the literature there are several hysteretic models developed to describe the mechanical behaviour of timber connections (Figure 5.1). A brief state-of-the-art on modelling and on non-linear analyses of timber structures was published by Foliente (1997). The most widely used tool in the study of non-linear response of structures subjected to actions variable in time is finite element analysis (known as the FEM method). FEM analyses are normally performed with numerical models implemented with an appropriate balance between accuracy and computational efficiency.

A first numerical model of a portal structure, with hinged bases and semi-rigid joints, was presented by Ceccotti and Vignoli (1989, 1990). The model of Ceccotti and Vignoli was experimentally validated on glulam portal frames. This model was then implemented by the authors in the DRAIN-2D software using special subroutines. Figure 5.2 summarizes the parameters required by the moment-rotation hysteretic curve ($M-\Phi$) adopted in the DRAIN-2D software. In the design process these parameters are all unknown and in general should be predicted or estimated from test results, in function of the configurations of wooden joints and using system identification techniques (Ceccotti and Vignoli 1989).

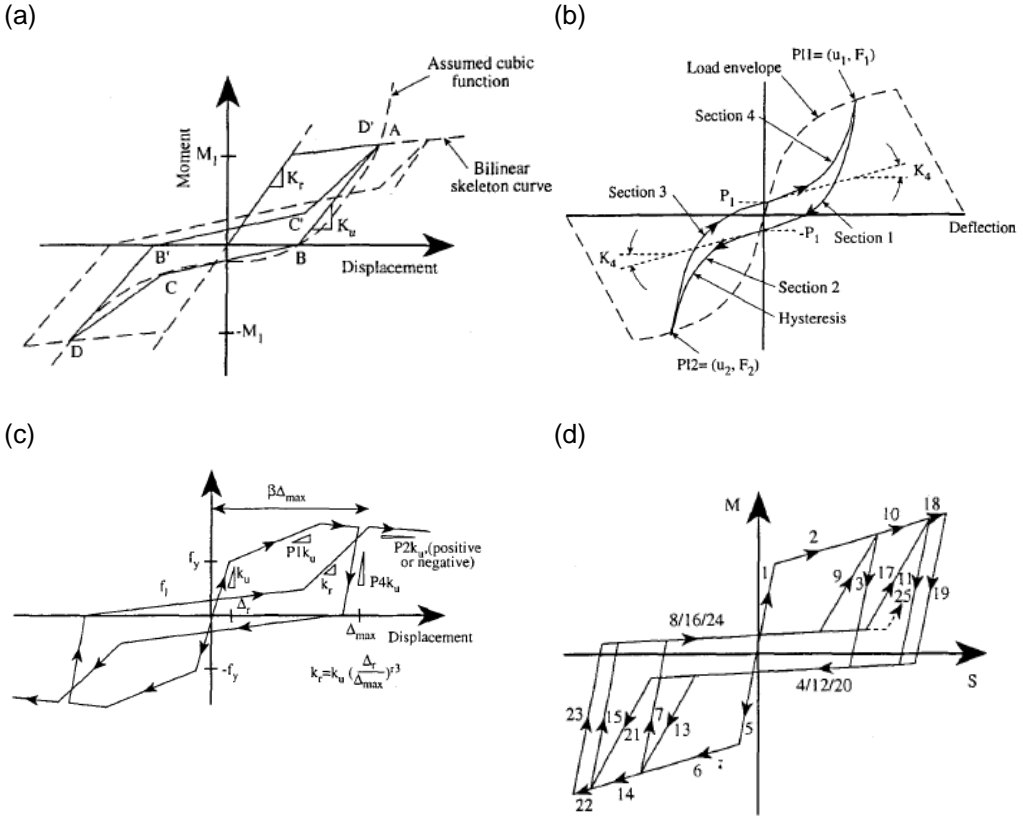
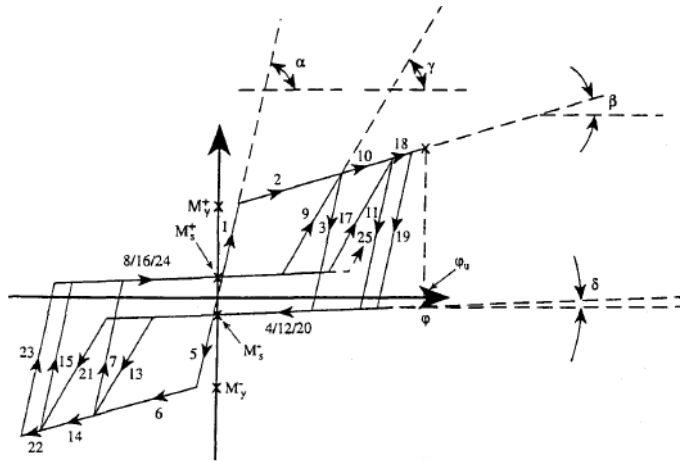


Figure 5.1 Hysteresis models developed for timber structures (modified from Dolan 1994); (a) Kivell et al. (1981) hysteresis model; (b) Dolan (1989) hysteresis model; (c) Stewart (1987) hysteresis model (d) Ceccotti and Vignoli (1990) hysteresis model

In this research two simple finite element models (FEM Models) have been developed to perform non-linear static and dynamic analyses of portal structures. These FEM models are based on mechanical and geometrical parameters that are known in the design process, and avoid the use of iterative procedures to converge on experimentally measured values.

(a)



(b)

- | | |
|--|---|
| $\tan \alpha = K^* \Phi_0$, Rotational initial elastic stiffness | $\tan \delta = K^* \Phi_1 / 10$, Slip stiffness |
| $\tan \beta = K^* \Phi_1$, stiffness corresponding to the yielding phases | $M_s^+ = M_y^+ / 10$, Positive slip moment |
| M_y^+ , Positive yielding moment | $M_s^- = M_y^- / 10$, Negative slip moment |
| M_y^- , Negative yielding moment | $\tan \gamma = K^* \Phi_0 / 2$, Degradation of stiffness |
| | ϕ_u , Ultimate rotation |

Figure 5.2 (a) Moment-rotation "Florence" model (Ceccotti and Vignoli 1989) of a semi-rigid joint with typical loop shape in cyclic response; (b) Parameters required by the proposed constitutive relation (modified from Dolan 1994)

5.2 Numerical model for non-linear static analysis

5.2.1 General aspects

To perform static non-linear analyses of a portal frame structure a refined Finite Element Model has been developed (**FEM I** Model).

Numerical simulations have been performed using the commercial finite element integrated software for structural analysis SAP2000® (2006). From non-linear analyses the load-displacement ($F-\Delta$) capacity curves have been extracted.

The model has been developed taking account of the exact geometry of elements and connections, balancing the accuracy and computational efficiency required (Figure 5.3). Timber elements of the portal are constructed by combining several finite elements, *frames*, (26÷42) in function of the beam and column length. The geometry of the beam-to-column joint and its inelastic response is reproduced with a set of non-linear spring elements, *N-link*, one per dowel, distributed on the double-crown configuration. The load-slip curve of the dowel has elastic-perfectly plastic behaviour, based on the European Yield Model, as presented in Chapter 4.

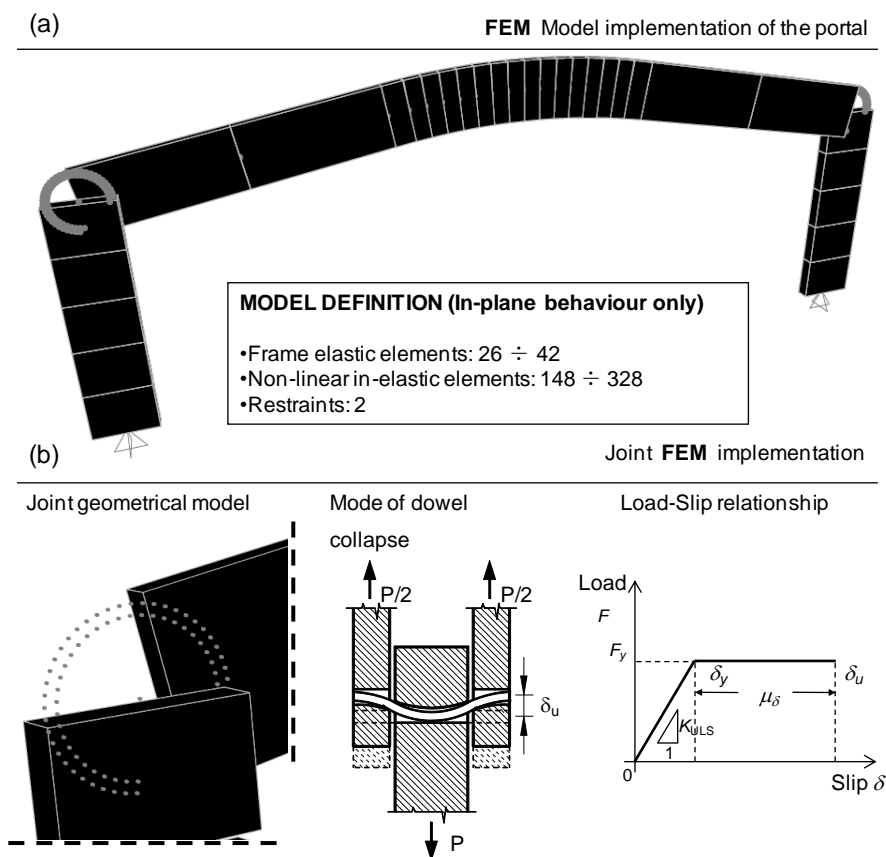


Figure 5.3 (a) Finite element model implementation for structural model; (b) beam-to-column joints with an elastic-perfectly-plastic load-slip relationship of the dowels

The *N-link* elements have a shear mechanism along the two main directions, radial and tangential, reproducing the expected slip on each dowel arranged inside the beam-to-column joint. The portal is anchored to the ground with two hinges and analyses are limited to studying its in-plane behaviour.

5.2.2 Pushover analysis and results

Non-linear static analysis (*pushover analysis*) is a reliable numerical method to evaluate the force-displacement capacity of structures (Dolan 1994). The analysis consists in pushing the structure, under a normalized loading protocol, up to a specific level of displacement measured on a control point. As a result of the static *pushover analysis* we have the capacity curve, or so called *pushover curve*, which represents the load-displacement relationship of an equivalent substitute SDOF system to the structure under investigation.

The non-linear analyses were performed considering the effect of gravity loads and second-order effects (P- Δ effects). To consider P- Δ effects on numerical outcomes more analyses were carried out on the same model, considering or neglecting the effect of gravity loads and the deformed shape of the portal.

The procedure for the seismic design of the portal structure, from Eurocode 8 (CEN 2004b), gives no guidance on how to prevent brittle failure of elements. The ductile failure mechanism of the beam-column joint is therefore not always ensured in the design stage. Thus, the ultimate displacement extracted from the capacity curve cannot be directly compared with the design displacement estimated using Eq. (4.28), formulated implicitly assuming a ductile mechanism of the portal. We must, therefore, first find the failure mode of the portal-frame structure, and then calculate the displacement on the basis of the lower value of two limit states: the *ductile limit state* (ULS1) and the *brittle limit state* (ULS2).

The ductile limit state (ULS1) has been conventionally defined assuming that the slip limit is reached on one dowel of the beam-to-column joint (Figure 5.4(a)). In the brittle limit state the deformed shape of portal is limited by the maximum bending moment developed by the beam or the column (Figure 5.4(b)). In ULS2 the design displacement is then lower than in ULS1, thus the latter is the more suitable mechanism in the seismic field.

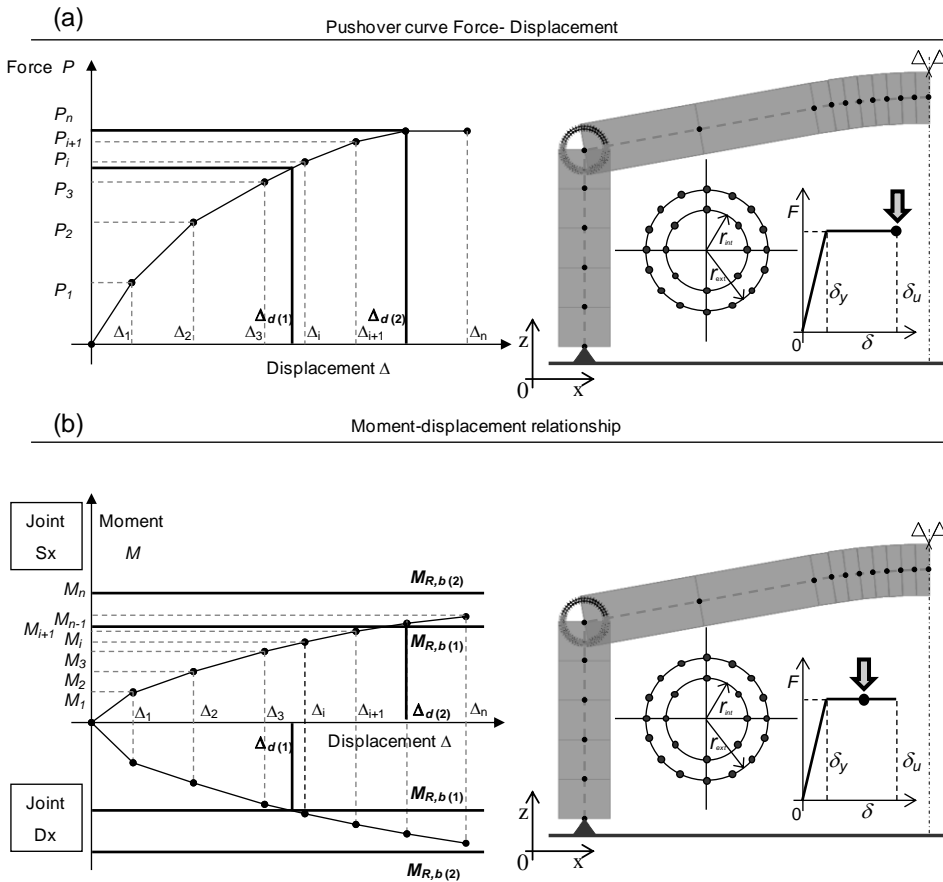


Figure 5.4 (a) Ductile collapse mode; (b) brittle collapse mode

In the normal seismic design process the overstrength coefficient (α_R) for the beam-to-column joint is not defined. Thus, the model formulated to evaluate the design displacement does not cover the brittle failure mode of the portal, although this could occur, due to the aleatory nature of the materials employed during the construction of the structure. This concept will be explained in the Section of this Chapter that deals with the validation of the Direct-DBD method.

5.3 Numerical model for non-linear dynamic analysis

5.3.1 General

The finite element model (**FEM II**) employed to perform non-linear dynamic analyses differs from the static one in the mechanical definition of the beam-to-column joint. In the **FEM model II**, the beam-to-column joint is described with a hysteretic rotational element, through a constitutive moment-rotation curve ($M-\Phi$), to reduce the computational time required in the calculation (Figure 5.5). The hysteretic moment-rotation relationship selected for this application is the so-called Pivot model introduced by Dowell *et al.* (1998), to which the reader is referred for more details.

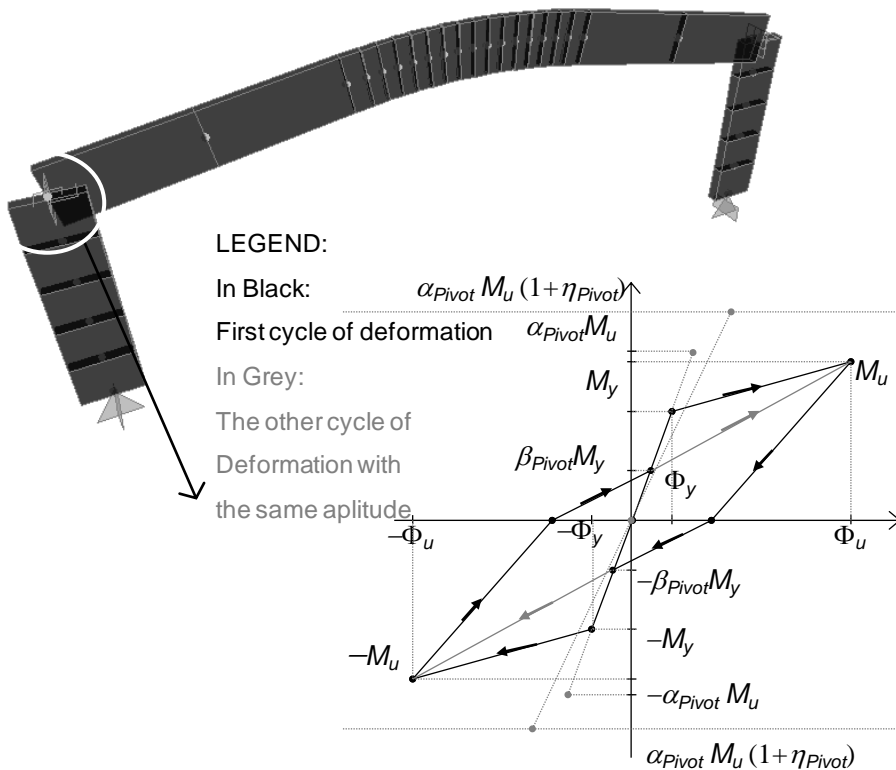


Figure 5.5 FEM II numerical model and joint definition for non-linear time-history analyses

More sophisticated numerical models, which require open-source software, have been proposed in the literature, such as those of Foliente (1995), Ceccotti and Vignoli (1989, 1990) and Chui and Yantao (2005). The Pivot hysteretic moment-rotation relationship is suited to the objectives of this work, although it was originally proposed for the beam-to-column joints of reinforced concrete frames. The parameters required for the envelope curve of the Pivot model are the yield moment (M_y), the ultimate moment (M_u), the yield rotation (Φ_y) and the ultimate rotation (Φ_u).

In this research, the proposed analytical expressions to evaluate the parameters M_y , M_u , Φ_y and Φ_u , with the known quantities of the design process will be explained. The additional parameters that describe the cyclical behaviour of the bi-linear hysteretic model are the coefficients α_{Pivot} , β_{Pivot} and η_{Pivot} . The discretization of the portal frame system, the constraints, and the mechanical description of the timber elements are the same as for non-linear static analysis (pushover analysis). The **FEM II model** allows the evaluation of the dynamic response of the structure against an imposed ground motion, in the time domain. The algorithm of calculation is in the class of *deterministic dynamic analysis* methods (Foliente 1993).

5.3.2 Analytical evaluation of the moment-rotation curve for joint connections

In this Section we propose the bi-linear moment-rotation (M - Φ) analytical envelope curve for semi-rigid portal frames with dowels arranged in two concentric crowns. The implementation of the M - Φ curve is based on the same assumptions used in Chapter 4 for the formulation of the design displacement Δ_d (Figure 5.6). Each connector exhibits an elastic-perfectly plastic behaviour, consistent with the expected failure mode III of the European Yield Model (Eurocode 5; CEN 2004a).

The analytical M - Φ curve, of the elastic-plastic type with hardening, is well suited to the experimental outcomes, and is a common model in the formulation of design methods according to Direct Displacement-Based Design (see Priestley *et al.* 2007).

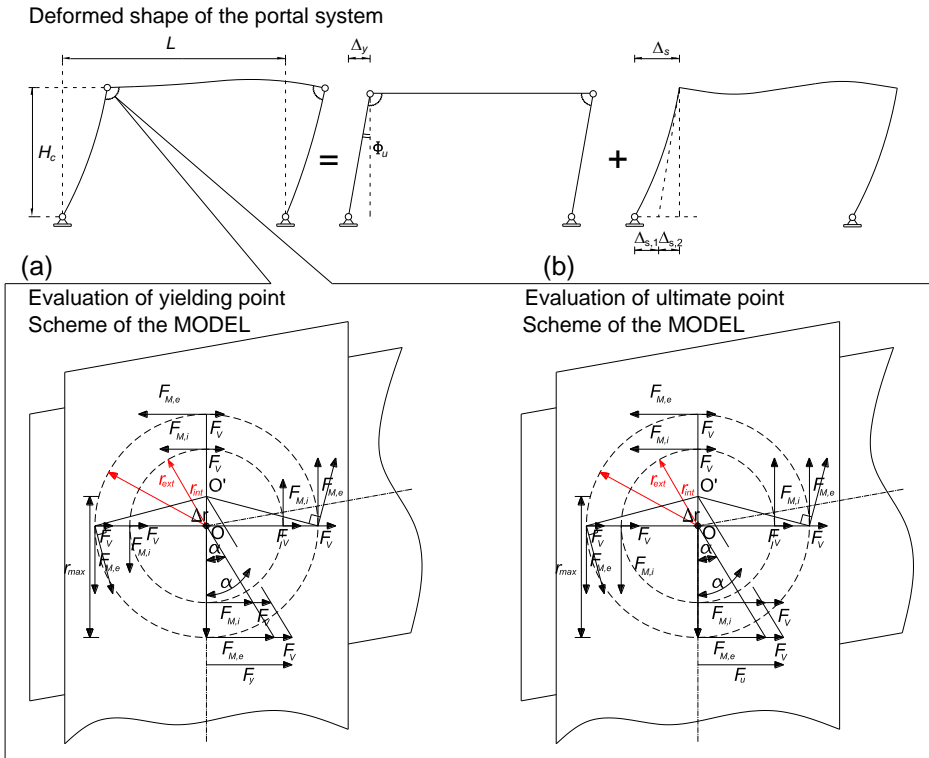


Figure 5.6 Scheme of joints for the Moment-Rotation curve evaluation; (a) Yield of joints; (b) Ultimate state of joints

The parameters shown in Figure 5.6 are defined as:

- r_{ext} , r_{int} external radius and internal radius respectively
- n_{ext} , n_{int} number of connectors in external and internal crown respectively
- $n_{tot}=n_{ext}+n_{int}$ total number of connectors
- F_M forces on the connectors due to bending moment
- F_V forces on the connectors due to shear force
- M_J external bending moment on beam-to-column joint
- V_J shear on beam-to-column joint

$H_c = M_J / V_J$ height of columns (ratio between bending moment and shear at beam-to-column joint)

The yield moment (M_y) is defined as the value associated with the elastic limit reached in the most stressed connector. The elastic limit is reached first in the connector with stresses M_J and V_J parallel and in the same direction (Figure 5.6(a)).

For the equilibrium we can write the following expressions:

$$F_M = \frac{M_J}{r_{ext} n_{eq,el}} = \frac{M_y}{r_{ext} n_{eq,el}} \quad (5.1)$$

$$F_V = \frac{V_J}{n_{tot}} = \frac{M_J}{n_{tot} H_c} = \frac{M_y}{n_{tot} H_c} \quad (5.2)$$

whereby the equivalent number of dowels in the elastic range is:

$$n_{eq,el} = n_{ext} + n_{int} \left(\frac{r_{int}}{r_{ext}} \right)^2 \quad (5.3)$$

With a simple linear combination we obtain:

$$F_y = F_M + F_V = \frac{M_y}{r_{ext} n_{eq,el}} + \frac{M_y}{H_c n_{tot}} = \left(\frac{1}{r_{ext} n_{eq,el}} + \frac{1}{H_c n_{tot}} \right) M_y \quad (5.4)$$

In conclusion, M_y is evaluated with Eq. (5.5):

$$\begin{aligned}
 M_y &= \frac{F_y}{\left(\frac{1}{r_{ext} n_{eq,el}} + \frac{1}{H_c n_{tot}} \right)} = \\
 &= \frac{F_y n_{eq,el} r_{ext} H_c}{H_c + r_{ext} \frac{n_{eq,el}}{n_{tot}}}
 \end{aligned} \tag{5.5}$$

The yield rotation (Φ_y) corresponds to the achievement of the yield slip (δ_y) in the most stressed dowel. The formulation considers the shift of the instantaneous centre of rotation from the geometric centre due to the effect of shear stresses.

Referring to Figure 5.6(a), we can calculate the final rotation at yield from the instantaneous centre of rotation by the following equations:

$$r_{max} = r_{ext} + \Delta r \tag{5.6}$$

$$r_{ext} + \Delta r = \frac{F_M + F_V}{F_M / r_{ext}} \tag{5.7}$$

$$r_{ext} + \Delta r = r_{ext} (1 + F_V / F_M)$$

The tangent of the angle α can be written as:

$$\tan \alpha = \frac{F_M}{r_{ext}} \text{ and } \tan \alpha = \frac{F_M + F_V}{r_{ext} + \Delta r} \tag{5.8}$$

The expressions above lead to Eq. (5.9):

$$r_{ext} + \Delta r = r_{ext} (M_J / (n_{tot} H_c)) = r_{ext} \left(1 + \frac{r_{ext} n_{eq,el}}{H_c n_{tot}} \right) \quad (5.9)$$

For small rotations, the tangent of the angle α is equal to the rotation at yield (Φ_y):

$$\Phi_y \approx \tan \alpha = \frac{\delta_y}{r_{ext} + \Delta r} = \frac{\delta_y}{r_{ext} \left(1 + \frac{r_{ext} n_{eq,el}}{H_c n_{tot}} \right)} \quad (5.10)$$

where δ_y is the yield slip of the connector while $n_{eq,el}$ is defined by Eq. (5.3).

The ultimate moment of the beam-to-column joint is calculated referring to Figure 5.6(b). Thus, all connectors have reached or exceeded the yield point and have a shear force equal to the load-carrying capacity F_y (EYM). The orientation of the force at yield (F_y) will differ in function of the location of the i^{th} dowel within the connection.

The projection of the ultimate force F_y (coinciding with the yield strength, F_y) in the direction perpendicular to the radius (Figure 5.6(b)) is expressed by Eq. (5.11):

$$F_{u\perp} = \sqrt{F_y^2 - \left(\frac{V_J}{n_{tot}} \right)^2} = \sqrt{F_y^2 - \left(\frac{M_J}{n_{tot} H_c} \right)^2} \quad (5.11)$$

The equilibrium moment of the connection can be written by Eq. (5.12):

$$M_u = \left(r_{ext}n_{ext} + r_{int}n_{int} \sqrt{F_y^2 - \left(\frac{M_J}{n_{tot}H_c} \right)^2} \right) \quad (5.12)$$

Squaring and solving for F_y^2 yields:

$$\frac{M_J^2}{(r_{ext}n_{ext} + r_{int}n_{int})^2} + \left(\frac{M_J}{n_{tot}H_c} \right)^2 = F_y^2 \quad (5.13)$$

In conclusion, the ultimate moment is defined as:

$$M_u = \frac{F_y}{\sqrt{\frac{1}{(r_{ext}n_{ext} + r_{int}n_{int})^2} + \frac{1}{(n_{tot}H_c)^2}}} \quad (5.14)$$

In compact form Eq. (5.14) becomes:

$$M_u = \frac{F_y}{\sqrt{\frac{1}{(r_{ext}n_{eq,pl})^2} + \frac{1}{(n_{tot}H_c)^2}}} \quad (5.15)$$

The accepted expression for calculating the ultimate moment (M_u), neglecting the shear effect, is given by Eq. (5.16):

$$M_u = \left(n_{ext} + n_{int} \frac{r_{int}}{r_{ext}} \right) F_y = n_{eq,pl} r_{ext} F_y \quad (5.16)$$

where the number of equivalent plastic dowels $n_{eq,pl}$ is given by Eq. (5.17):

$$n_{eq,pl} = n_{ext} + n_{int} \frac{r_{int}}{r_{ext}} \quad (5.17)$$

The ultimate strength of the connector (F_u) is equal to the yield strength (F_y), from the elastic-perfectly plastic relationship assumed for dowels.

The procedure adopted to find the yield rotation (Φ_y) can be used to get the ultimate rotation (Φ_u) of the connection. In this case it is permissible to assume that all connectors are plasticised, and thus, the stress on each element is obtained using Eq. (5.18):

$$F_M = \frac{M_J}{r_{ext} n_{eq,pl}} \quad (5.18)$$

The ultimate rotation, similar to the above, can be calculated through Eq. (5.19):

$$\Phi_u = \frac{\delta_u}{r_{ext} + \Delta r} = \frac{\delta_u}{r_{ext} \left(1 + \frac{r_{ext}}{H_c} + \frac{n_{eq,pl}}{n_{tot}} \right)} \quad (5.19)$$

Equations (5.5), (5.10), (5.14) and (5.19), for standard values of r_{ext}/H_c (~ 0.20), can be simplified assuming the ratio $n_{eq,pl}/n_{tot}$ to be equal to 1. In reality the ratio $n_{eq,pl}/n_{tot}$ is always less than 1 for connections made with several crowns of dowels.

The final model of the moment-rotation curve ($M-\Phi$) of the connection is that of Figure 5.7, with associated analytical formulas for the evaluation of design parameters.

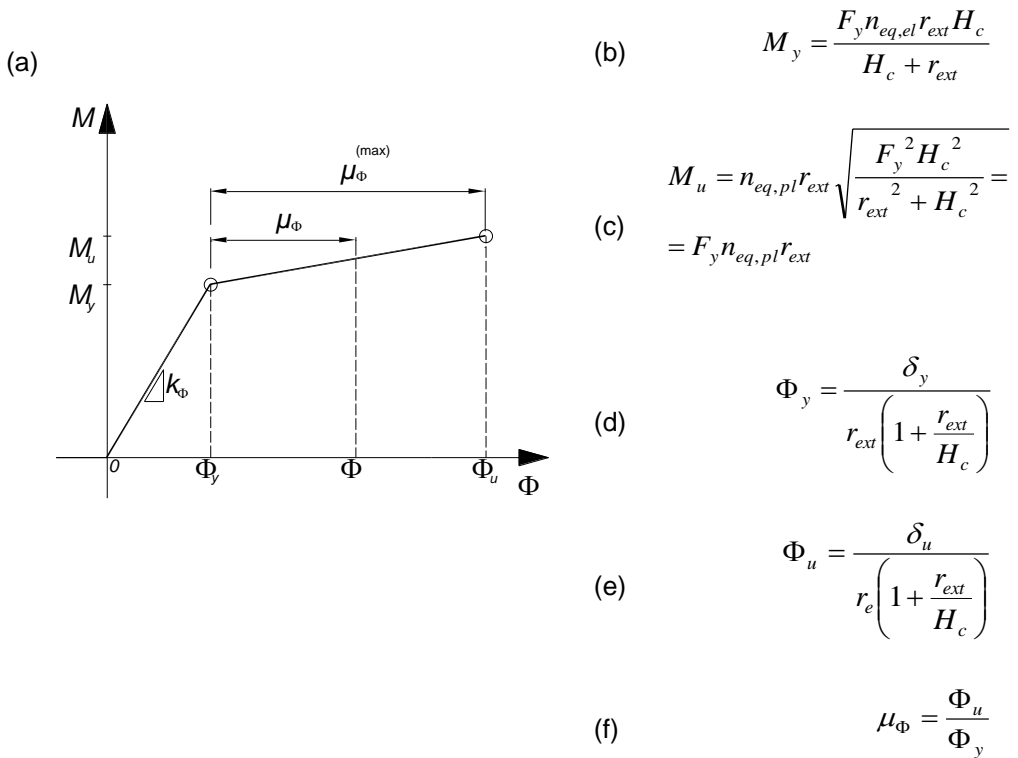


Figure 5.7 (a) Moment-Rotation law for dowelled cross-lapped joint with two crowns of dowels; (b) Yield moment formula; (c) Ultimate moment formula; (d) Yield rotation formula; (e) Ultimate rotation formula; (f) definition of rotational ductility

5.3.3 Time-history analysis

Non-linear dynamic analyses were performed to predict the response of the structure considering all the non-linearity, geometrical and mechanical, including the irregular shape of ground motion. An ensemble of mono-dimensional accelerograms was selected to define the seismic input, in function of the seismic hazard in the area. The selection and the scaling of accelerograms is based on the European protocol, given by Eurocode 8 (CEN 2004b) and is consistent with the current Italian standard “DM 14 gennaio 2008” (CS.LL.PP. 2008).

The structure was subjected to seven spectrum-compatible accelerograms, based on the elastic response spectrum of Eurocode 8 (CEN 2004b), scaled to a damping value of 5%. The spectrum-compatible accelerograms are generated using SIMQKE-II software (Vanmarcke *et al.* 1997) and then individually scaled to produce a maximum displacement response equal to the ultimate displacement for the structure. The ultimate displacement, here understood as the design displacement, (Δ_d) is numerically estimated from the capacity (pushover) curves, obtained from the non-linear static analyses.

The time history analyses use the Hilber Hughes-Taylor (HHT) method for numerical integration ($\gamma_{HHT}=0.5$, $\beta_{HHT}=0.25$ and $\alpha_{HHT}=0$), to solve the general differential equation of motion. In the general equation of motion, stiffness, mass and damping values are expressed in matrix form, and are assembled numerically via the finite element algorithm (FEM Analysis).

On a characteristic sample of three portal structures non-linear dynamic analyses were performed. The Equivalent Viscous Damping, as an average value, was compared with the equivalent damping calculated by the analytical model proposed in Chapter 4 (Eq. (4.53)).

5.4 EXPERIMENTAL RESULTS

The numerical finite element models (**FEM I** and **FEM II**), implemented to evaluate the design displacement (Δ_d) and the Equivalent Viscous Damping (ξ_{eq}) of the portal frame structure are validated in this Section with the outcomes of experimental

tests. The reference test was taken from a research project aimed at investigating the ductility and the dissipative capacity of Moment-Resisting (MR) connections on an ensemble of joint configurations. Tests were performed at the Laboratory of Materials and Structural Testing of the Department of Mechanical and Structural Engineering of the University of Trento (Italy). The results were presented and published recently by Polastri *et al.* (2008).

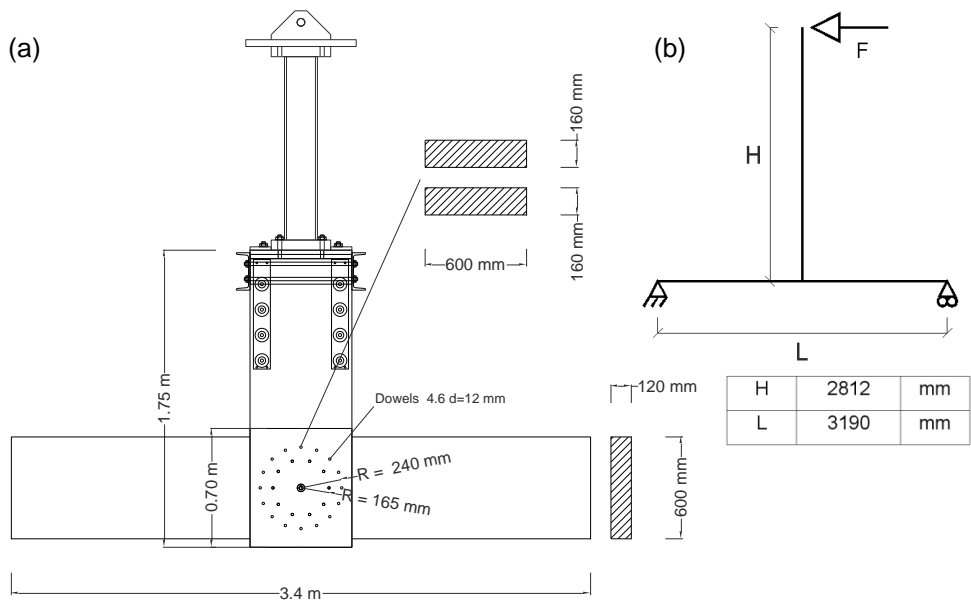


Figure 5.8 (a) Geometrical dimensions of the specimen tested by Polastri *et al.* (2008); (b) Static design of specimen

The reference test is a frame consisting of a full-scale beam-column made of two crowns of dowels with a diameter $d=12$ mm and radii of 165 mm and 240 mm. The wooden elements are made of class GL24h glulam (CEN 2000), while the dowels are 4.6 steel grade (CEN 1993). The wood density measured in the laboratory is $\rho_{exp}=467$ Kg/m³, while the ultimate strength of the connector is equal to $f_{u,exp}=566.3$ Mpa. The geometrical dimensions of the frame tested are those of Figure 5.8(a). The measured values are in agreement with average values derived using the "Probabilistic Model Code" (JCSS 2007), taking the probability distribution function known a posteriori, the covariance value and the nominal (characteristic) value for the strength class of materials.

Tests were carried out in accordance with the test protocol of EN 12512 (CEN 2001) and allow assessment of the non-linear response of the MR connection up to a static displacement ductility value, μ_{Δ} , equal to 4.

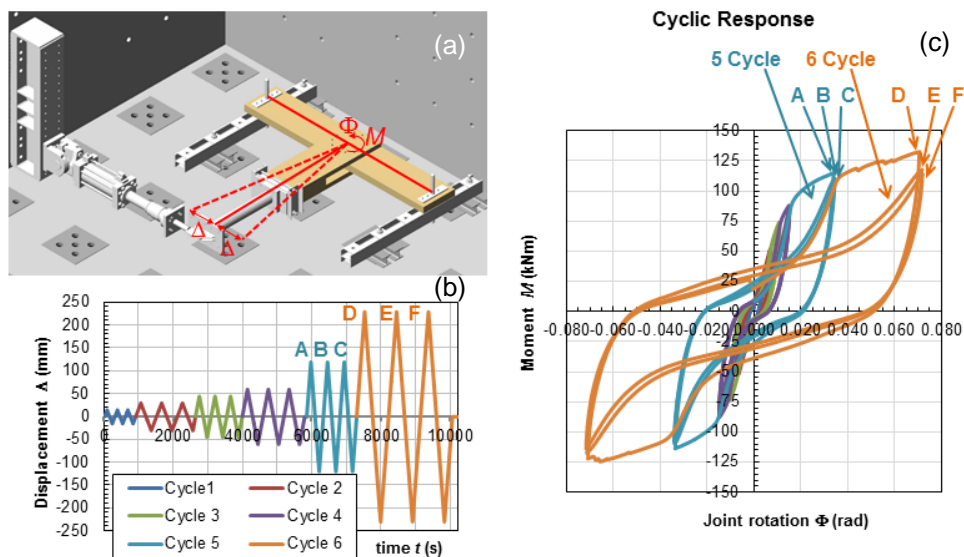


Figure 5.9 (a) Test arrangement; (b) Cyclic displacement sequence; (c) Moment versus rotation responses for cyclic loading

Figure 5.9(a) shows the set up of the test to run cyclic protocol loading and unloading, Figure 5.9(b) the protocol of the test in accordance with EN 12512 (CEN 2001) and Figure 5.9(c) the moment-rotation diagram ($M-\Phi$). The outcomes of the reference test have been adjusted to remove the instrumental errors and unexpected slips occurring in the specimen-to-ground constraints.

Figure 5.10 shows the three load cycles in the inelastic range, each repeated three times for each level of pre-defined amplitude (v_y , $2v_y$ and $4v_y$). These three levels represent respectively the displacement at yield, v_y , displacement with static ductility μ_{Δ} of 2, $2v_y$, and displacement with static ductility μ_{Δ} of 4, $4v_y$.

From the results of the reference test, with the test protocol defined by EN 12512 (CEN 2001) shown in Figure 5.11(a), it is possible to estimate a conventional value of Equivalent Viscous Damping, ξ_{eq} , using the energy approach of Jacobsen (1930) (Figure 5.11(b)).

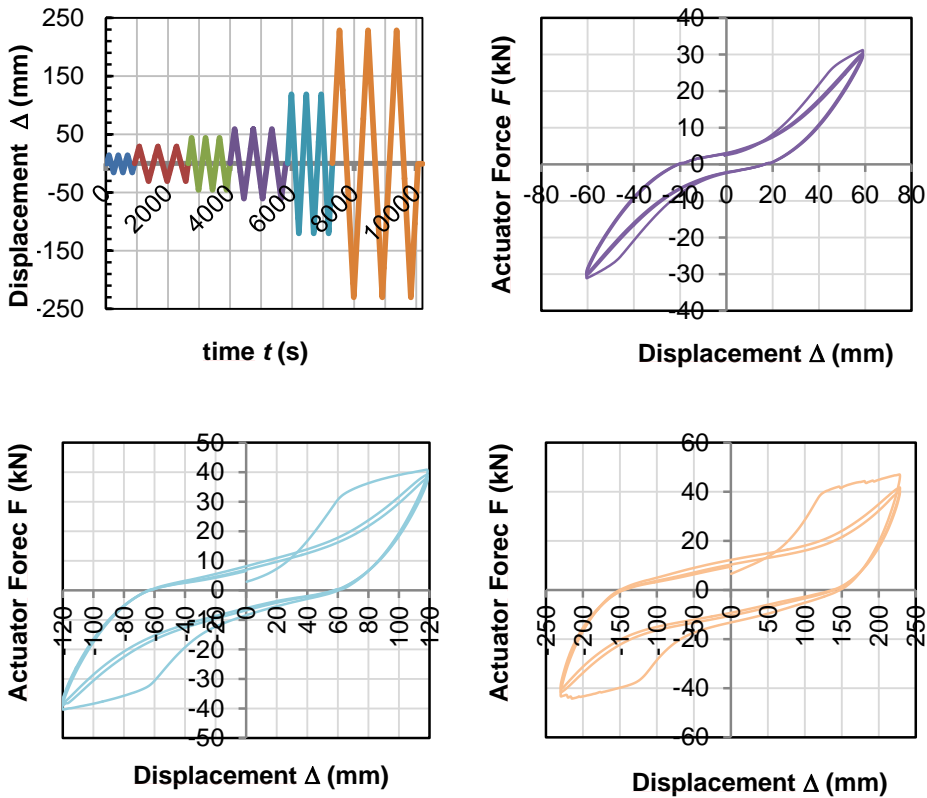


Figure 5.10 Inelastic displacement response curve for test based on the EN 12512 (CEN 2001) loading protocol

In the $M-\Phi$ response chart of Figure 5.9(c) it is possible to identify the two typical situations defined in Chapter 4 and labelled respectively *Protocol II* and *Protocol III*. The situation labelled *Protocol I* can be estimated from the test results by artificially removing the dependency of each hysteresis loop from the displacement history. The damping extracted in the situation of *Protocol I* is not considered of interest in this work and remains the upper limit of the Equivalent Viscous Damping for the connection.

Table 5.1 shows data measured in the test and the value of equivalent viscous damping estimated for each load cycle calculated in both directions.

From Table 5.1 it is possible to assess the value of equivalent viscous damping on a full cycle of loading, by averaging the values of the positive and negative cycles (Table 5.2). From Eq. (4.30), taken here as a generic interpolating function, the parameters C and ξ_0 , can be calibrated for each cycle and level of displacement reached in the test (Table 5.3).

Figure 5.12 shows the trend of damping as the displacement ductility μ_Δ changes, both in the experimental and the numerical situation. The numerical model uses the expression (4.30) calibrated with the values of Table 5.3. In the reference values of Table 5.3 and Figure 5.12 the contributions of elastic deformation of wooden elements have been weighted, in a coherent expression (4.26), since the configuration of the frame tested in the laboratory is different from that of the portal presented in Chapter 4. Priestley's model, Eq. (4.30), to calculate the equivalent viscous damping of the beam-column connection, predicts the experimental results well.

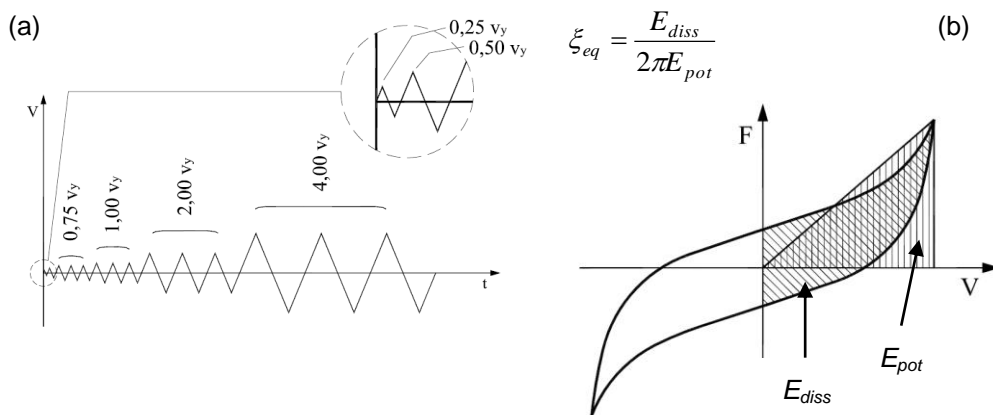


Figure 5.11 (a) Loading protocol in cyclic tests in accordance with the complete procedure of EN 12512; (b) Definition of equivalent viscous damping ratio in a cycle (modified from EN 12512; CEN 2001)

Figure 5.13 shows a part (Quadrant I) of the moment-rotation envelope curve ($M-\Phi$) of the cyclic test performed according to EN 12512 (CEN 2001), the theoretical curve estimated by the analytical relations developed in the previous section (Eq.(5.1)÷Eq. (5.19)) and the experimental envelope curve calculated according to the algorithm of EN 12512 (CEN 2001).

With the test results, the following are estimated experimentally: $M_y=105.74$ kNm, $M_u=132.6$ kNm, $\Phi_y= 0.014$ rad and $\Phi_u=0.071$ rad. The analytical curve of Figure 5.13 is evaluated instead with Eqs.(5.5), (5.10), (5.14) and (5.19), assuming an average value of the load bearing capacity of the dowel equal to $F_y=21.09$ kN, yield slip of dowel of 2.61 mm and slip ductility of dowel equal to 6 ($\delta_u=15.67$ mm). The parameters $M_u=116.13$ kNm, $M_y=96.95$ kNm, $\Phi_y=0.010$ rad e $\Phi_u=0.060$ rad have been evaluated for the analytical curve.

Table 5.1 Experimental measured parameters and estimated equivalent viscous damping value

		Δ (mm)	F (kN)	M_U (kNm)	Φ (rad)	$E_{hyst,joint}$ (J)	$\xi_{eq,JOINT}$ (%)
4 CYCLE	1 ^{pos}	58.94	31.20	87.92	0.015	454.20	7.86
	1 ^{neg}	-60.44	-31.10	-87.65	-0.015	503.15	8.52
	2 ^{pos}	58.93	30.40	85.66	0.015	364.03	6.47
	2 ^{neg}	-60.44	-30.38	-85.62	-0.015	380.71	6.60
	3 ^{pos}	58.93	29.98	84.47	0.015	341.74	6.16
	3 ^{neg}	-60.44	-29.98	-84.47	-0.015	360.16	6.33
5 CYCLE	1 ^{pos}	118.21	40.85	115.11	0.034	2399.22	15.82
	1 ^{neg}	-120.23	-40.38	-113.79	-0.034	2684.91	17.60
	2 ^{pos}	118.21	39.17	110.37	0.034	1757.15	12.08
	2 ^{neg}	-119.71	-38.83	-109.43	-0.034	1748.86	11.98
	3 ^{pos}	118.73	38.04	107.20	0.034	1560.19	11.00
	3 ^{neg}	-120.13	-38.20	-107.64	-0.034	1584.19	10.99
6 CYCLE	1 ^{pos}	228.07	47.04	132.56	0.071	6670.82	19.79
	1 ^{neg}	-214.56	-44.23	-124.65	-0.066	6900.34	23.14
	2 ^{pos}	228.06	41.78	117.75	0.072	4667.89	15.59
	2 ^{neg}	-229.54	-41.70	-117.51	-0.071	4464.87	14.85
	3 ^{pos}	228.49	40.33	113.66	0.072	4077.37	14.08
	3 ^{neg}	-229.53	-40.30	-113.55	-0.072	4044.36	13.92

The offset of the two curves (always less than 15%) can be explained by the effects of friction at the interface of the joint area, and hardening of steel that occurs from the increasing of the displacement Δ . These effects generate an overstrength in the connection, lost in the subsequent cycles for a given level of displacement reached.

Table 5.2 Proposed equivalent viscous damping value for the test specimen

μ_{Δ}	1 cycle	2 cycle	3 cycle
	$\xi_{eq,JOINT}$	$\xi_{eq,JOINT}$	$\xi_{eq,JOINT}$
(-)	(%)	(%)	(%)
1	8.19	6.53	6.24
2	16.71	12.03	10.99
4	21.47	15.22	14.00

Table 5.3 Parameters of Priestley's viscous analytical model, calibrated using outcomes of test

Parameter		1 cycle	2 cycle	3 cycle
C	(-)	55.00	36.00	32.00
ξ_0	(%)	8.19	6.53	6.24

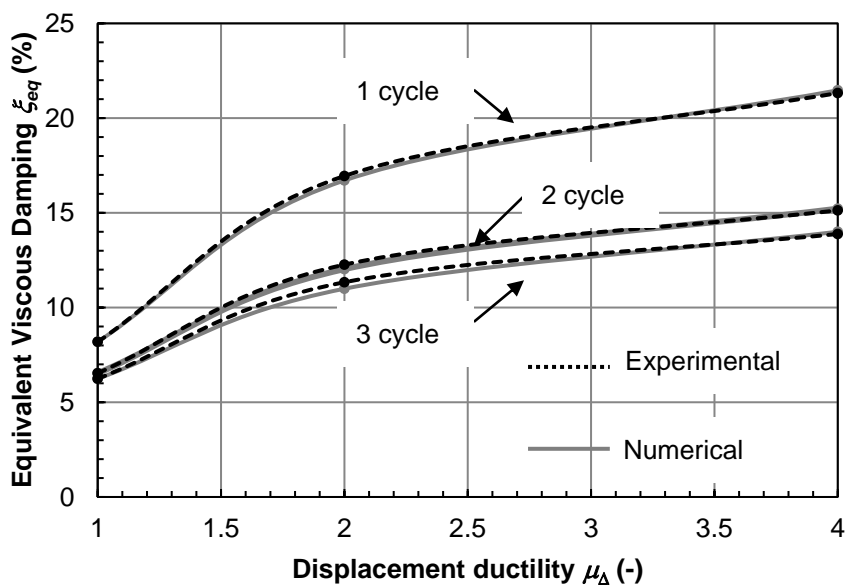


Figure 5.12 Fitting curves of equivalent viscous damping versus displacement ductility

This degradation of strength in subsequent cycles of loading is due to the loss of contact between the sliding surfaces. The analytical $M-\Phi$ curve, however, is held to be consistent with the results measured as a result of the experimental test. The effect of friction, in fact, is a phenomenon known in the field of testing of timber connections, which changes the values expected from those actually measured (Hilson 1995). Similarly, the hardening of steel is a phenomenon observed in many experimental tests. The analytic formulation of the effects of friction and the hardening of steel complicate the design of connectors, and this complication outweighs the gains in terms of reliability.

To verify the finite element model (*FEM I*) used to perform non-linear static analyses (pushover), the design displacement value estimated at the ultimate slip, $\delta_u=15.67$ mm, reached in the most stressed dowel of the test specimen is compared. In line with what has been outlined above, the finite element model of the experimental test was developed and a pushover analysis was performed.

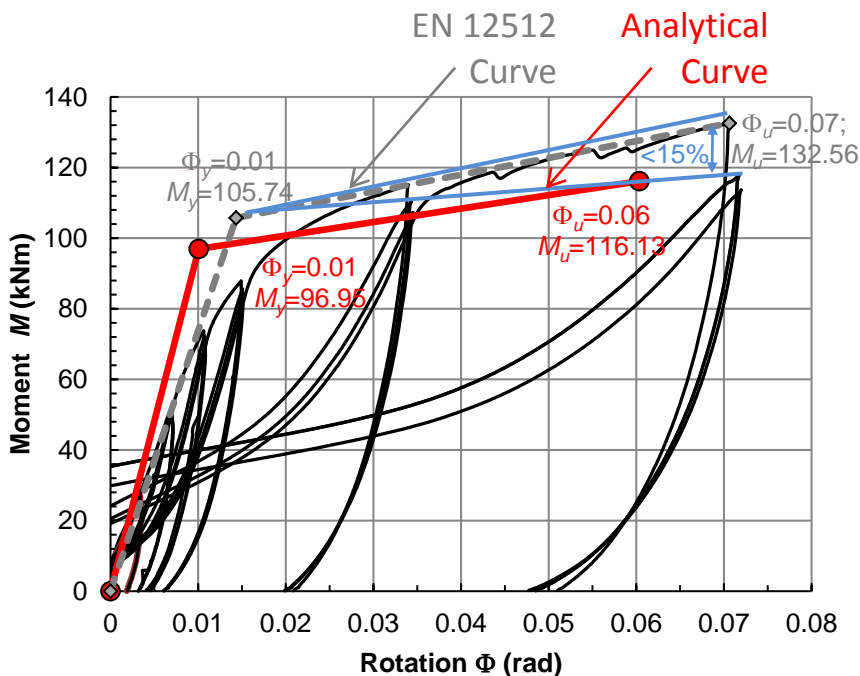


Figure 5.13 Superposition of the the envelope Moment-rotation curves, theoretical and experimental, on the full cyclical response of the MR joint

Figure 5.14 shows the pushover curve, the force–displacement diagram, $F-\Delta$, evaluated with the values measured in the test, and the design displacement value estimated in the $F-\Delta$ cycles at an ultimate slip of $\delta_u=15.67$ mm. The design displacement is estimated numerically at $\Delta_{d,numerical}\sim 198$ mm, while from the experimental curve $F-\Delta$ a design displacement of $\Delta_{d,experimental}\sim 189$ mm is extrapolated. The analytical design displacement is estimated by Eq.(4.16), presented in Chapter 4, at $\Delta_d=195$ mm ($\Delta_f=170$ mm and $\Delta_s=25$ mm).

The error in the evaluation of the design displacement is approximately 4.7%. In these terms, the error is considered acceptable (lower than 10%) and validates the **FEM I** model.

The verification of the finite element model (**FEM II**) for the prediction of the equivalent viscous damping is obtained by comparing the experimental value of the damping, measured at each cycle, with the expected value from the model, starting from the geometrical and mechanical characteristics measured on the experimental test.

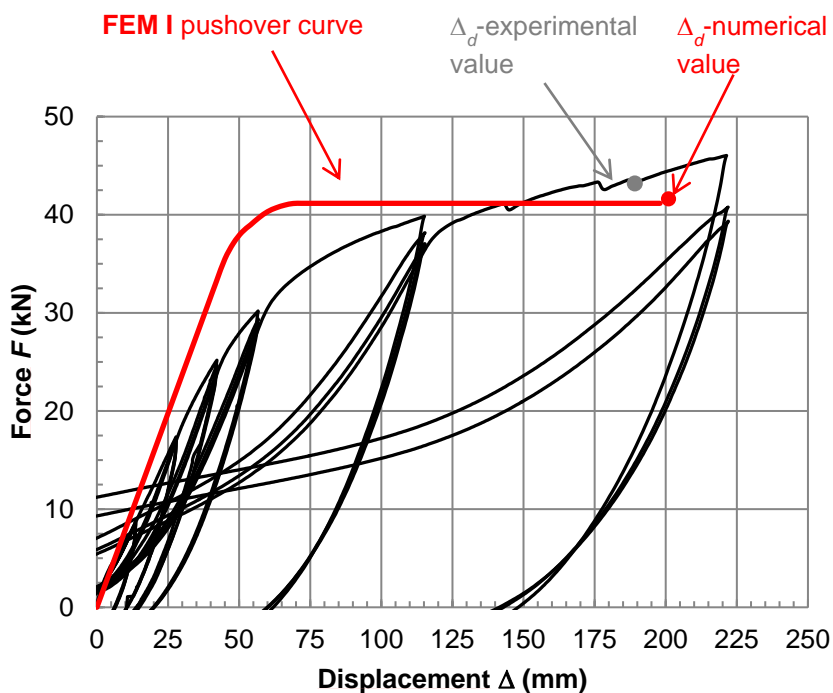


Figure 5.14 Comparison of displacement between the pushover curve provided by the FEM I Model and the experimental curve

The non-linear analysis of the experimental test was performed by imposing the same loading protocol (EN 12512; CEN 2001). In the bi-linear moment-rotation envelope curve the parameters M_u , M_y , Φ_u and Φ_y measured directly in the test are inserted. The parameters α_{Pivot} and η_{Pivot} of the Pivot model (Dowell *et al.* 1998) were calibrated to obtain an hysteretic curve of the connection similar to the experimental one. The parameter β_{Pivot} is calibrated so as to minimize the error in the estimation of the hysteretic energy in each cycle.

Figure 5.15(a) and Figure 5.15(b) briefly describe the **FEM II** model and the non-linear curve with the Pivot hysteretic model, while Figure 5.16 shows a brief comparison between the equivalence of the numerical model and experimental results with the same imposed loading on the specimen.

The error in the estimation of equivalent viscous damping between the **FEM II** numerical model and the experimental results is reported in Table 5.4 for the reference cycles of the test. The average error committed in the medium-high ductility level, μ_{Δ} , loop 5 and loop 6 of the test, is equal to about 2% and is considered acceptable for our purposes.

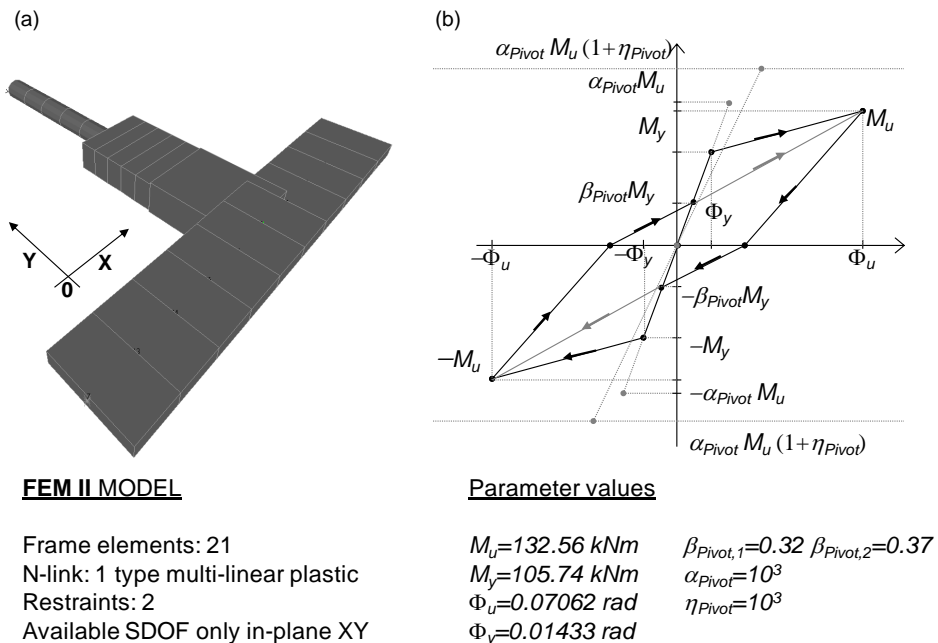


Figure 5.15 (a) Finite element model for non-linear time history analysis (**FEM II**); (b) moment-rotation Pivot hysteretic model with measured experimental values

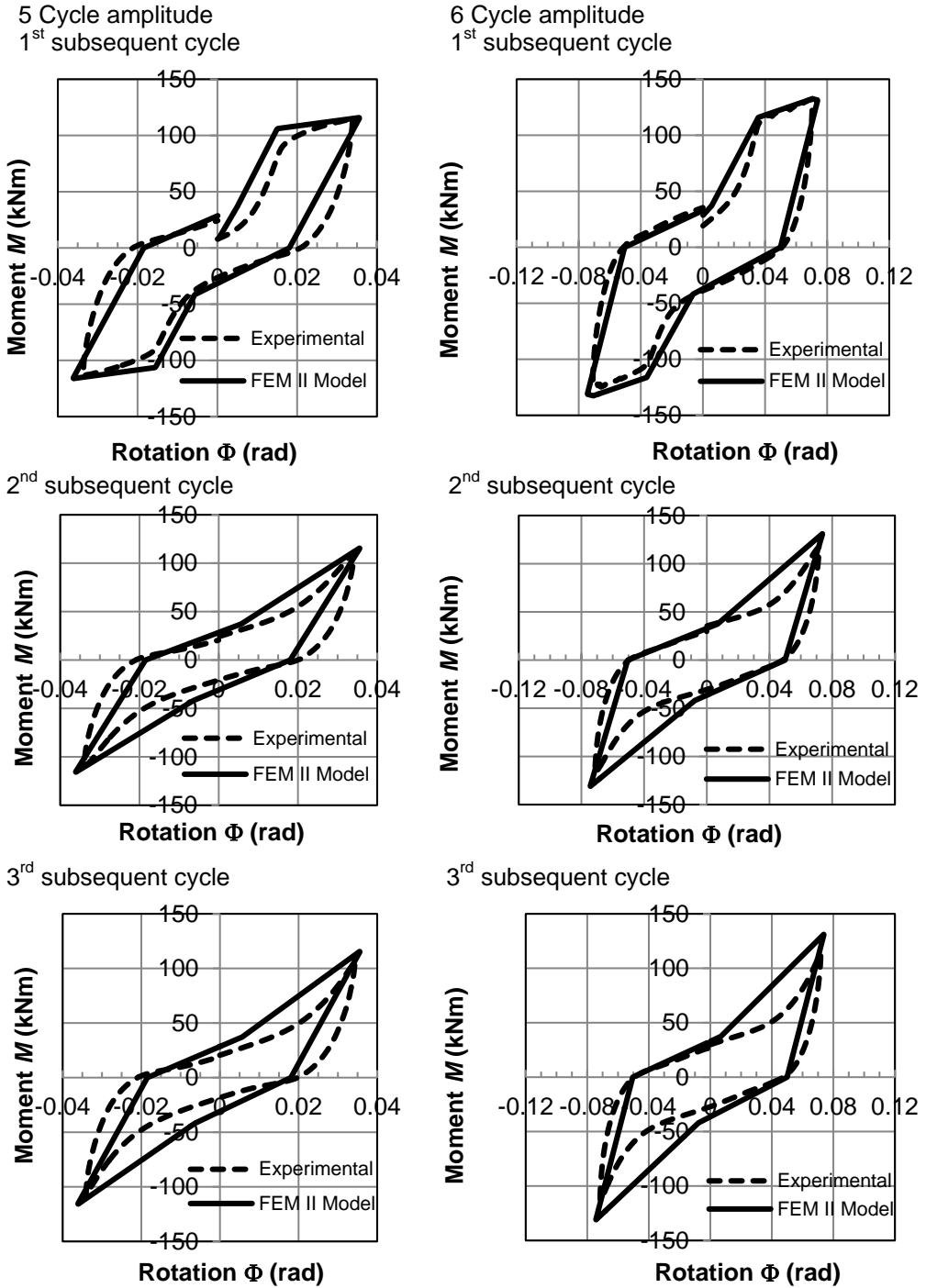


Figure 5.16 Comparison of moment-rotation relationship, with the experimental dataset for two levels of displacement and three cyclic loading sequences

Table 5.4 Error in the equivalent viscous damping in cycle 5 and cycle 6 of test. Experimental versus numerical data using **FEM II** Model

		Experimental			Numerical with NLTHA			Error
		$\xi_{eq,JOINT}$ (%)	Δ (mm)	F (kN)	$\xi_{eq,JOINT}$ (%)	Δ (mm)	F (kN)	$E_{\xi_{eq,JOINT}}$ (%)
5 CYCLE	1 ^{pos}	15.82	118.21	40.85	15.39	118.23	41.20	2.68
	1 ^{neg}	17.60	-120.23	-40.38	16.29	-119.73	-40.99	7.49
	2 ^{pos}	12.08	118.21	39.17	11.90	118.23	40.91	1.49
	2 ^{neg}	11.98	-119.71	-38.83	11.81	-119.73	-41.00	1.36
	3 ^{pos}	11.00	118.73	38.04	11.43	118.23	40.89	-3.97
	3 ^{neg}	10.99	-120.13	-38.20	11.83	-119.75	-40.97	-7.62
6 CYCLE	1 ^{pos}	19.79	228.07	47.04	19.79	228.15	46.457	-0.01
	1 ^{neg}	23.14	-214.56	-44.23	22.32	-229.62	-46.39	3.56
	2 ^{pos}	15.59	228.06	41.78	15.70	228.152	46.456	-0.66
	2 ^{neg}	14.85	-229.54	-41.70	15.77	-229.62	-46.37	-6.22
	3 ^{pos}	14.08	228.49	40.33	15.51	228.152	46.44	-10.13
	3 ^{neg}	13.92	-229.53	-40.30	15.73	-229.837	-46.403	-12.99

Mean error between 5th cycle and 6th cycle is equal to 2 %

NLTHA: Non-linear time history analysis

The **FEM II** model was validated experimentally (error less of 10%) with the values measured directly in the experimental test. For the non-linear response curve of the connection, the average value of the parameter β_{Pivot} is approximately 0.35. The β_{Pivot} parameter of the Pivot moment-rotation model is defined as the ratio between the ultimate moment (M_u) and the moment of equilibrium in the return of the configuration to its undeformed state (M_s).

In a manner consistent with the analytical model for the evaluation of the moment-rotation monotonous curve we can assume:

$$\beta_{Pivot} = \frac{M_u}{M_s} \approx \frac{F_u}{F_f} = \frac{F_y}{F_f} = \sigma_F \quad (5.20)$$

As demonstrated in Chapter 4, the parameter σ_F is analytically estimated at 0.33 and is consistent with the assumption in Eq. (5.20). For the reference configuration we can assume values of $\beta_{Pivot}=0.33$, $\alpha_{Pivot}=10^3$ and $\eta_{Pivot}=10^3$. The numerical model proposed and validated in this Section allows the extension of the numerical evaluation to other mechanical-geometric configurations of the portal frame. In the analysis of other geometric configurations we can assume the parameters $\alpha_{Pivot}=10^3$ and $\eta_{Pivot}=10^3$, or at least three orders of magnitude higher than the value used for β_{Pivot} . For the meaning of the parameters α_{Pivot} and η_{Pivot} the reader is referred to Dowell *et al.* (1998).

This Section ends with a direct comparison between the analytical model to calculate the equivalent viscous damping, presented in Chapter 4, and the experimental results of the reference test. Table 5.5 shows the comparison for the two situations of *Protocol II* and *Protocol III*.

Eq. (4.53) has been formulated for the ultimate limit state (ULS), in which the ultimate slip, δ_u , has been reached in the most stressed dowel within the joint. For the ultimate slip, δ_u , on the dowel there is a corresponding ultimate rotation in the beam-to-column joint and an ultimate displacement of the structure.

The rotation ductility of the joint, μ_Φ , is given by:

$$\begin{aligned} \mu_\Phi &= \Phi_u / \Phi_y = \\ &= \mu_\delta \frac{1 + \frac{r_e}{H_c} \frac{n_{eq,el}}{n_{tot}}}{1 + \frac{r_e}{H_c} \frac{n_{eq,pl}}{n_{tot}}} \\ &\approx \mu_\delta \end{aligned} \tag{5.21}$$

The results of Table 5.5 are based on the geometric and mechanical values of the connection measured on the experimental test. The value of the ultimate slip, to be assumed in the design phase, is estimated at $\delta_u=15.67$ mm. The ultimate rotation evaluated by the analytical model is equal to $\Phi_u=0.06035$ rad, while the ultimate displacement (here the design displacement), Δ_u , is equal to 189.14 mm.

To evaluate the analytical equivalent viscous damping value, the following should be substituted into Eq.(4.53) $\beta_k=2$, $\sigma_F=0.33$, $n_1=16$, $n_2=10$, $r_1=240$ mm, $r_2=165$ mm, $\mu_\delta=4.21$ and $\Delta\delta/\delta=0.37$, as measured by the test.

The equivalent viscous damping experimental value is calculated instead with the EN 12512 (CEN 2001) procedure, at a slip ductility level μ_{Δ} of 3.17.

Table 5.5 Error in the equivalent viscous damping evaluated for the design displacement Δ_d ; Experimental versus analytical values with elastic-perfectly plastic curve of connectors

Situation	Analytical	Experimental			Error		
	Estimate $\xi_{eq,Th}$ JOINT (%)	Min $\xi_{eq,min}$ JOINT (%)	Max $\xi_{eq,max}$ JOINT (%)	Mean $\xi_{eq,mean}$ JOINT (%)	Error _{min} $E_{\xi_{eq,min}}$ JOINT (%)	Error _{max} $E_{\xi_{eq,max}}$ JOINT (%)	Error _{mean} $E_{\xi_{eq,mean}}$ JOINT (%)
Protocol II	17.16	14.11	14.80	14.46	-21.59	-15.92	-18.69
Protocol III	25.06	18.75	21.86	20.30	-33.71	-14.66	-23.45

The error between the analytical model and experimental results, reported in Table 5.5, is explained by the simple model for predicting the equivalent viscous damping of the beam-to-column joint ($\xi_{eq,JOINT}$), formulated in Chapter 4, from the $F-\delta$ curve assumed for the connector. Eq. (4.53), in fact, is based on the simultaneous achievement of the ultimate slip on all dowels placed in the l^{th} crown of the joints. The model of Eq. (4.53) then evaluates the maximum equivalent viscous damping of the connection. The average error committed varies in the range 14÷16% in the comparison between the maximum and reaches more than 30% for the most unfavorable case.

The effect of the error on the evaluation of the equivalent viscous damping, $\xi_{eq,JOINT}$, is reduced in the calculation of the Equivalent Viscous Damping of the structure (EVD, ξ_{eq}), as discussed in the Section of this Chapter dedicated to the numerical validation of EVD. The expression (4.57) evaluates the damping of the structure, ξ_{eq} , taking into account the ratio of displacement Δ_s/Δ_j . The elastic displacement component of the design displacement, Δ_s , thereby reduces the effect of the damping error of the connection. The mechanical model of the dowels, formulated in Chapter 4 to assess the Equivalent Viscous Damping (EVD), ξ_{eq} , is therefore considered consistent with the results from laboratory tests.

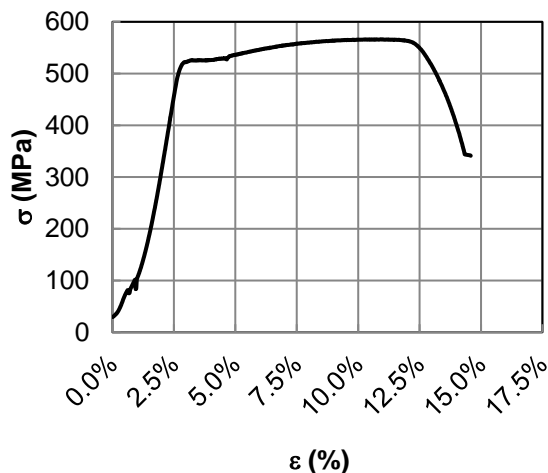
The analytical model for estimating the equivalent viscous damping of the connector, formulated in Chapter 4, can be refined by introducing an elastic-plastic hardening curve instead of the elastic-perfectly plastic curve to take into account the effect of steel hardening.

If we limit ourselves solely to the change of the analytical viscous model (Eq. (4.40)÷(4.49)), neglecting the effect of strain hardening on analytical models for calculating the design displacement, Δ_d , and the $M-\Phi$ of the connection, we obtain the results of Table 5.6. The error in the estimation of $\xi_{eq,JOINT}$, as an absolute maximum, then, is reduced to about 5% and still suffers the effects of friction, difficult to consider without significantly increasing the cost of calculation in the design process. The modified equations for estimating the equivalent viscous damping are shown in Appendix C.

Table 5.6 Error in the equivalent viscous damping evaluated for the design displacement Δ_d ; Experimental versus analytical values with elasto-plastic hardening curve of connectors

Situation	Analytical	Experimental			Error		
	Estimate	Min	Max	Mean	Error _{min}	Error _{max}	Error _{mean}
	$\xi_{eq,Th}$ %	$\xi_{eq,min,JOINT}$ (%)	$\xi_{eq,max,JOINT}$ (%)	$\xi_{eq,mean,JOINT}$ (%)	$E_{\xi_{eq,min,JOINT}}$ (%)	$E_{\xi_{eq,max,JOINT}}$ (%)	$E_{\xi_{eq,mean,JOINT}}$ (%)
Protocol II	15.65	14.11	14.80	14.46	-10.91	-5.74	-8.26
Protocol III	23.09	18.75	21.86	20.30	-23.17	-5.62	-13.72

(a)



(b)

Dowel in class 4.6 (CEN 1993)

Measured value:

$$f_{u,exp} = 566.3 \text{ MPa}$$

$$f_{y,exp} = 525.9 \text{ MPa}$$

$$\alpha_{sh,measured} = 1.077$$

$$\sim 1.1$$

Figure 5.17 (a) Chart of stress-strain curve after tensile test of steel wire of dowels; (b) Mechanical properties of dowel measured (modified from Polastri et al. 2008)

The values of damping and the relative errors of Table 5.6 are calculated using a value of α_{sh} (hardening coefficient) of 1.1, which is the hardening of steel experimentally observed after tension tests. Figure 5.17 shows the stress-strain relationship of a connector tested by Polastri *et al.* (2008) during the experimental tests to which we refer.

In this research, the estimation model of EVD remains that of Eq. (4.57), which will then be calibrated to consider errors in the model as compared to the real situation. The calibration coefficient of EVD will be presented in Section 5.6 of this Chapter, which explains the entire process of numerical validation of the EVD (ξ_{eq}). The gain in the final estimate of the design parameters does not justify, thus, the introduction of sophisticated design expressions, which stem from the compatibility of the model assumed for the dowel.

The next section presents the procedure for validating the analytical model for estimating the design displacement Δ_d .

5.5 VALIDATION OF DESIGN DISPLACEMENT

The analytical model for the evaluation of design displacement, Δ_d , (Eq. (4.28)) has been numerically validated by applying the numerical-statistical procedure known as a Monte Carlo simulation (MC). The MC method makes it possible to evaluate the effect of design uncertainties on the model implemented for the calculation of Δ_d .

In the current design process, the parameters of the timber elements and connections are known as a deterministic value. The Design Code, *e.g.* Eurocode 5 (CEN 2004a) controls the effect of uncertainties using probabilistic analyses, defined for different levels of reliability and difficulty in the calculation. The Force Based Design (FBD) procedure, for example, implicitly uses the approach known as the semi-probabilistic method of partial coefficients (Eurocode 8; CEN 2004b), which represents a level 1 procedure of probabilistic methods.

The analytical formula to predict design displacement, Δ_d , (Eq. (4.28)), as a deterministic approach, cannot directly assess the effect of uncertainties in the geometrical and mechanical parameters of the portal frame.

However, the proposed analytical model must be compatible with the real situation, independently of the strength class of the wood and steel and of the geometrical configuration of the portal. Therefore, utilizing the Monte Carlo (MC) approach, wherein the geometry of the members and their mechanical properties are selected in an aleatory manner, we can validate the predictions of Eq.(4.28) by comparing its values with the numerical pushover (non-linear static) results.

In the Monte Carlo method all the mechanical and geometrical variables and other uncertainties associated with the design process are described with probabilistic curves to take into account the effect of uncertainties.

The basic concepts of the Monte Carlo Method can be found in Robert and Casella (2004), while to understand the philosophy of the method, Elishakoff (2003) is recommended. In this work a Monte Carlo simulation with $N=1000$ case studies is carried out to consider a statistically representative group and to reduce computation time.

Obviously, in this case the simulation needs to be controlled automatically. To achieve this we have created a software program using VBA (Visual Basic for Applications) called "Wood Seismic Software Control" (WSSC), which controls the structural analysis program SAP 2000® (2006) and Microsoft Excel® (2007).

The WSSC software has been organized in blocks, to simplify its extension to other geometric configurations and types of wooden structures. Additional details on the WSSC software are given in Appendix A. WSSC generates all the parameters of the FEM model, runs the analysis and extracts the displacement value for each model from the capacity curve. WSSC then compares the displacement estimated via the analytical formula (Eq. (4.28)) to the displacement provided by non-linear static analysis. Finally, WSSC creates a statistical distribution of the final data value, including the main statistical indices, and creates a database file.

The extraction process of aleatory values of input variables follows the normal process of design to define timber elements and beam-to-column connections. The extraction, operated by the WSSC software, is done through an internal algorithm that uses pseudo-random numbers (distribution in the range 0 to 1) and the inverse distribution function method. From the probability density function the associated distribution function, $F(x)$, is defined, and its analytically inverse function $F^{-1}(u)$ is obtained. The generic i^{th} random number, x_i , is evaluated from the pseudo-random value, u_i , directly from the curve of $F^{-1}(u_i)$. The problem of correlation between input variables is treated according to the "subjective method" proposed by Hertz (conditional sampling).

Thus in carrying out the Monte Carlo simulation, for each iteration a value for the independent variable is first generated; then the specific distribution function is selected and the dependent variable value extracted. The extraction process is managed by the WSSC software in an implicit manner.

In the Monte Carlo Method the final result is most influenced by the probabilistic distribution of the input variable and the parameter values selected.

Figure 5.18 shows the probabilistic curve selected for any variable and its correlations, while the fixed parameters used are: diameter of the dowels, $d=12$ mm, strength class of wood, GL24h (CEN 2000), type of steel, S355 (CEN 2004c) and static slip ductility of the dowel, $\mu_s=6$, as a characteristic value (5th percentile). The probability curves of the strength properties of the materials were selected based on the “Probabilistic Model Code”, presented at the COST Action E24 meeting (COST 2004) and published in 2007 by the Joint Committee on Structural Safety (JCSS 2007). The part of the probabilistic model code concerning timber elements is based on the outcomes of tests and investigations carried out in accordance with European and American standards. In the MC simulation the variability of the geometric properties of the portal in space and of the mechanical properties over time is not taken into account.

After the MC Simulation, to verify the validity of the analytical formula we compare the design displacement predicted with Eq. (4.28) and the design displacement extracted by non-linear static analysis for each portal configuration investigated ($N=1000$).

The error in displacement, as an index to quantify the predictive capacity of the analytical formula, is defined as a percentage by Eq. (5.22):

$$E_{\%}(\Delta_d)=100 (\Delta_{d,PUSH}-\Delta_d)/\Delta_{d,PUSH} \quad (5.22)$$

where $\Delta_{d,PUSH}$ is the displacement extracted by the non-linear static analysis and Δ_d is the design displacement predicted with Eq. (4.28).

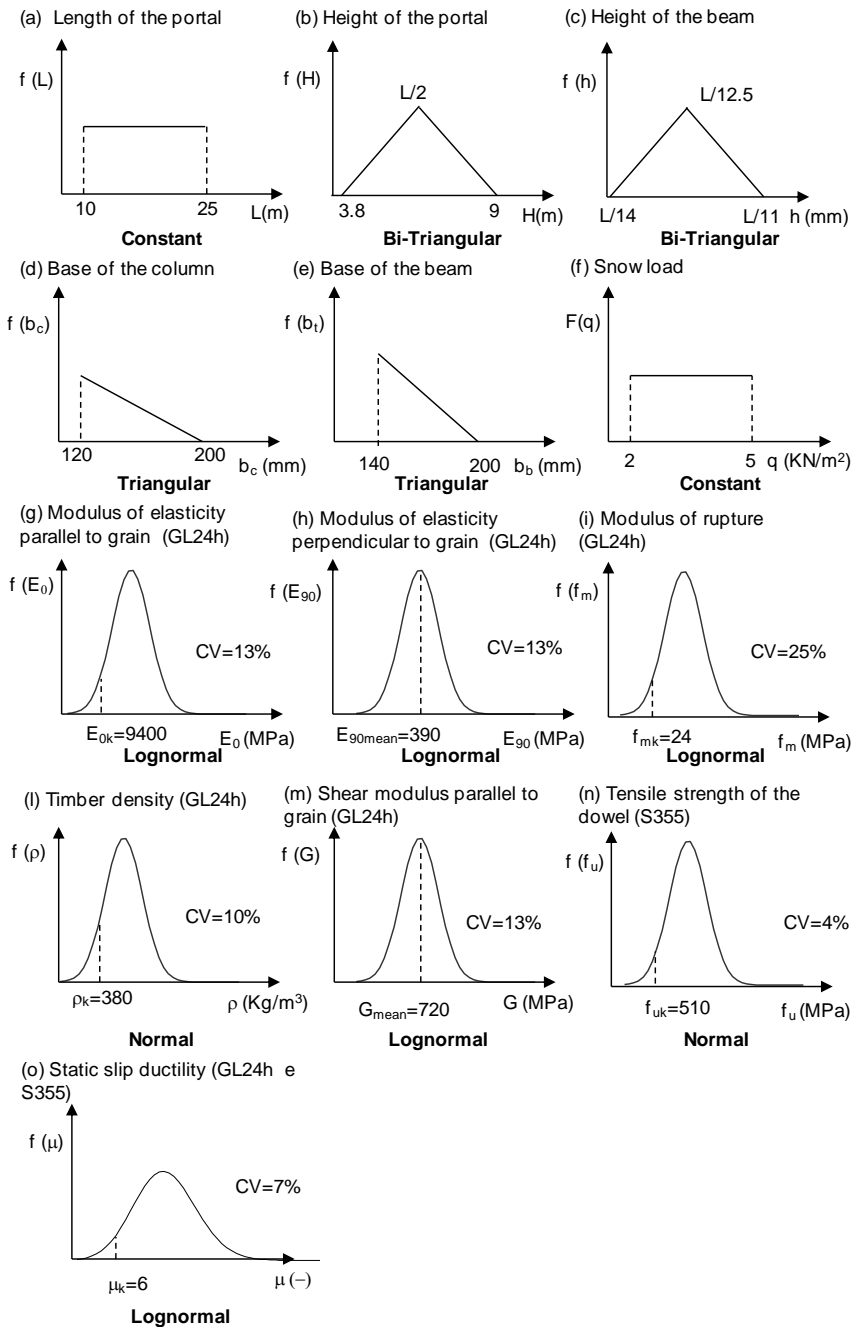


Figure 5.18 Trends of input variables selected in the MC Simulation; Probability distribution $f(x)$ for the function x ; Probabilistic models for properties for glued laminated timber in accordance with JCSS (2007)

5.5.1 Analysis results

In the absence of errors in the prediction model for design displacement (Eq. (4.28)), using the input variables curve defined above, the statistical distribution of error in displacement $E_{\%}(\Delta_d)$ is expected to be approximately symmetrical and centred on the Y Axis.

The absence of rules that control the geometrical and mechanical properties of the portal members, and the geometrical details of joints, can create a number of cases with brittle failure mode. If the design moment at joints is greater than the resisting moment of members, the failure mode of the portal is brittle and the displacement capacity is limited.

The outcomes of the MC Simulation have highlighted the considerable influence of the portal failure mechanism (ductile or brittle) on the value of the design displacement error. In particular, the post-elastic behaviour idealized for design displacement of the portal, appropriately designed, is not always confirmed in the real behaviour of the portal. Figure 5.19 shows the non-symmetrical trend of the design displacement error $E_{\%}(\Delta_d)$, skewed to the left.

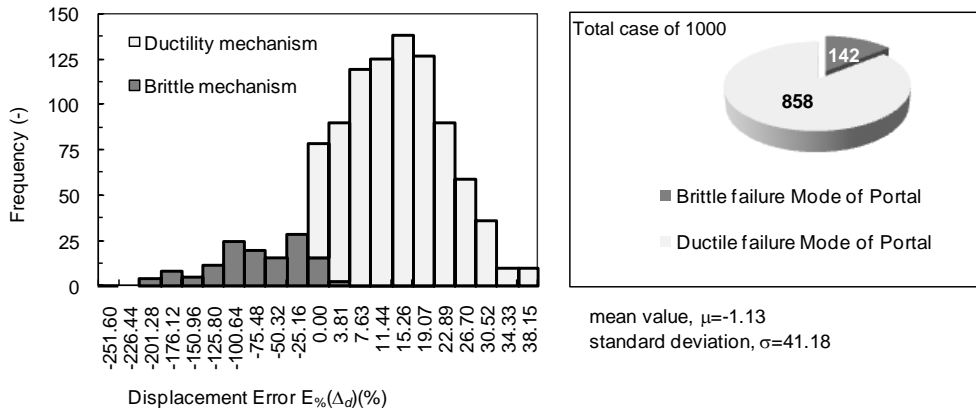


Figure 5.19 (a) Histogram of displacement error $E_{\%}(\Delta_d)$ (%) (μ , average value; σ , standard deviation)

Actual procedures for seismic design of timber structures, e.g. Eurocode 8 (CEN 2004b), the DM 14 gennaio 2008 (CS. LL. PP. 2008) and other international design codes, provide criteria and rules for the design of reinforced concrete and steel elements according to the Design Capacity philosophy (CD), but not for the design of wood structures.

This is a problem because the portal collapse mechanism is not guaranteed in the deformation phase. To design elements of the structural system able to maintain energy dissipation under severe deformation and in the failure mode, we suggest the introduction of an overstrength design factor, defined as (Eq. (5.23)):

$$\alpha_d = M_{R,b} / M_{R,j}$$

wherein:

$$M_{R,b} = (b_b \cdot h^2) / 6 \cdot f_{m,k} \quad (5.23)$$

$$M_{R,j} = n_{ext} \cdot r_{ext} \cdot F_y + n_{int} \cdot r_{int} \cdot F_y$$

where b_b and h are respectively the base and height of cross-section members, $f_{m,k}$ is the characteristic bending strength, n_{ext} and n_{int} are respectively the number of external dowels and internal dowels for the joint, r_{ext} and r_{int} are respectively the external radius and the internal radius of the joint and F_y is the characteristic load-carrying capacity of the dowel. These parameters are known in the design process phase.

It has been proven that we cannot ensure the proper conditions for structural ductility, regardless of control over the geometrical configuration of joints and the selection of materials. In general, the use of an overstrength factor also helps in avoiding loss of strength of the structure under cyclic loading conditions.

With a sample composed of 1000 case studies and a parametric analysis in α_d , we can evaluate the contribution of α_d in terms of displacement error $E\%(\Delta_d)$. Figure 5.20(a) summarizes the trend of $E\%(\Delta_d)$ and the main statistical parameters as the overstrength design factor, α_d , changes for the sample, and shows three characteristic histograms. The parametric analysis was performed in the range 1 to 1.5 with an incremental step of 0.5. It is noted that a coefficient α_d of 1.2 enables design without excessive over-design and ensures a ductile mechanism of the portal.

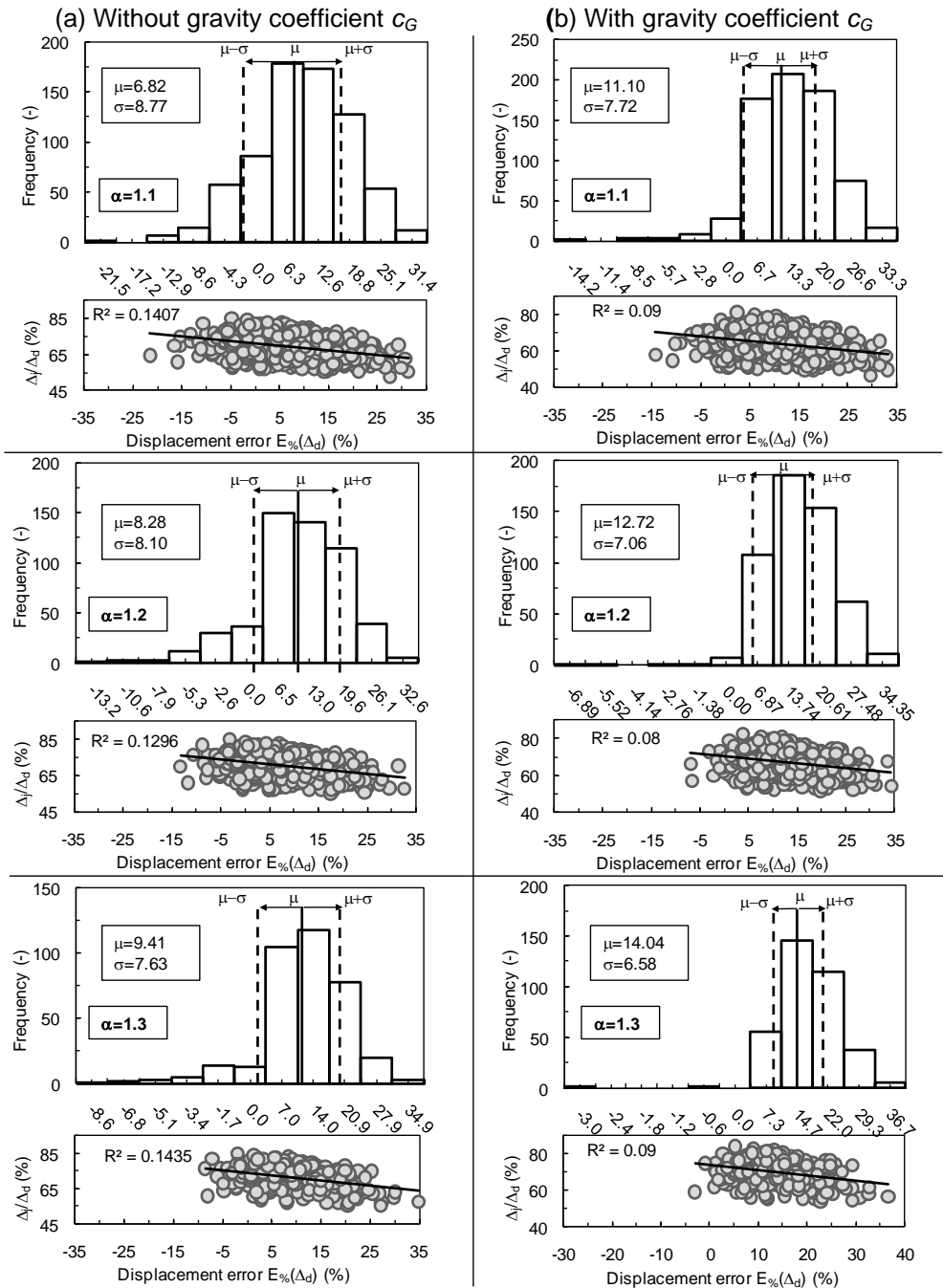


Figure 5.20 (a) Displacement error chart in function of the displacement ratio Δ_j (joint displacement) to Δ_d (total deformation) and histogram without gravity coefficient c_G ; (b) Displacement error chart in function of the displacement ratio Δ_j (joint displacement) to Δ_d (total deformation) and histogram with gravity coefficient c_G (μ , average value; σ , standard deviation, R^2 , coefficient of determination)

To minimize the effects of gravity on the displacement error, the analytical formula is corrected by introducing a coefficient that reduces inelastic displacement, called c_G . The c_G coefficient is based on a linear model to reduce plastic deformation of the dowels as a function of the vertical loading ratio of the portal, evaluated with Eq. (5.24):

$$c_G = q/q_{lim} \quad (5.24)$$

The parameter q_{lim} is defined as the vertical load leading to structure collapse due only to gravity load (ultimate static condition). The maximum value of the bending moment on the joints is assumed equal to $M_J = q_{lim} \cdot L^2/12$ and the associated shear is $V_J = q_{lim} \cdot L/2$. The load-carrying capacity of the single dowel is calculated using the European Yield Model (Eurocode 5; CEN 2004a), considering the acceptable minimum space between dowels.

The final formula proposed here to estimate q_{lim} is (Eq.(5.25)):

$$q_{lim} = \frac{24 \cdot \pi}{a_{eq}} \cdot \frac{F_y}{(\gamma_t \cdot \beta_t)^2 \cdot d} \quad (5.25)$$

where the coefficient a_{eq} is assumed to be of 5, while other parameters are as previously defined.

In Eq. (5.24) q is the load acting on a structure in a quasi-permanent combination (Eurocode 8, CEN 2004b) and could be considered as concentrated at the roof level.

The coefficient c_G reduces the slip ductility available on the single dowel and then the corresponding inelastic design displacement of the portal. Figure 5.20(b) presents the design displacement error as the overstrength factor changes, and introduces the coefficient c_G in Eq. (4.28) for the data collected.

5.5.2 Numerical calibration of design displacement

To validate the model to evaluate design displacement, Δ_d , we have introduced two numerical calibration parameters in Eq. (4.28), calibrated from the data of the sample. The use of numerical calibration parameters modifies the distribution of the design displacement error, $E_{\%}(\Delta_d)$, in function of the criteria imposed.

The criteria selected to re-centre $E_{\%}(\Delta_d)$ are:

1. The mean value of the design displacement (Δ_d) estimated with the analytical formula, is equal to the mean design displacement extracted by the non-linear static analysis, for the sample ($N=1000$);
2. With a sample of design displacement composed of 1000 case studies, the statistical distribution of displacement error $E_{\%}(\Delta_d)$ is as low as possible.

Thus, the numerical parameters that calibrate Eq. (4.28) are defined as the result of minimum problem for the data collected, from the MC Simulation, and finally Eq. (4.28) becomes Eq.(5.26):

$$\Delta_d = c_{p,1} \cdot \Delta_j \cdot \frac{\delta_y}{\delta_u} \cdot (\mu_{\delta} - c_G) + c_{p,2} \cdot \Delta_s \quad (5.26)$$

where parameter $c_{p,1}$ and $c_{p,2}$ are estimated equal to 1.10 and 1.18 respectively, δ_y and δ_u are respectively dowel yield slip and dowel ultimate slip (See Chapter 4), μ_{δ} is static slip ductility, c_G is the gravity reduction factor and Δ_j and Δ_s are as previously defined in Chapter 4 (Eq. (4.22) and Eq. (4.27)).

Using the gravity reduction factor c_G , an overstrength design factor α_d equal to 1.2, the first calibration parameter $c_{p,1}$ and the second calibration parameter $c_{p,2}$, we can see the histogram of displacement error $E_{\%}(\Delta_d)$ for the sample obtained from the MC Simulation (Figure 5.21).

Table 5.7 reviews the statistical index of position, the statistical index of dispersion, index of shape and other parameters that summarize the sample of 1000 portal configurations (from the MC Simulation).

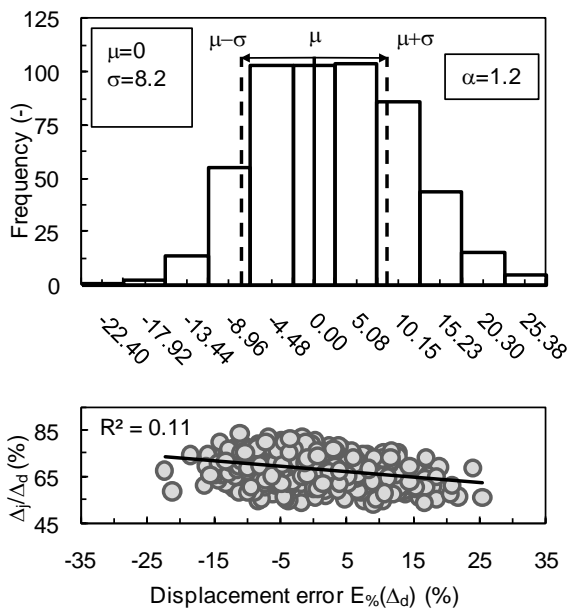


Figure 5.21 Displacement error $E_{\%}(\Delta_d)$ for the calibrated formula to estimate design displacement Δ_d

Table 5.7 Summary of main statistical quantities for displacement error $E_{\%}(\Delta_d)$

Median	$\text{med}(E_{\%}(\Delta_d))$	-0.51 %
Average	$m(E_{\%}(\Delta_d))$	0.00 %
Standard deviation	$ds(E_{\%}(\Delta_d))$	8.20 %
Percentile 5%	$P_{5\%}(E_{\%}(\Delta_d))$	-12.49 %
Percentile 2%	$P_{2\%}(E_{\%}(\Delta_d))$	-14.30 %
No. of cases ($\alpha \geq 1.2$)	N_{TOT}	532
No. of cases $E_{\%}(\Delta_d) < 0$	$N(E_{\%}(\Delta_d) < 0)$	278

The final analytical model calibrated and proposed here to evaluate the design displacement, Δ_d , has been validated with the results of non-linear static analyses and is proposed for the design of timber portal frame buildings.

5.6 Validation of Equivalent Viscous Damping

The cyclical behaviour of timber joints is markedly influenced by the history of deformation undergone. To perform reliable comparisons between test results on timber connections a standardized procedure, provided by reference standards, is usually defined (Dolan 1994). In Europe, the reference standard is EN 12512 (CEN 2001), while in North America it is the D1761 (ASTM 2006). Another known standard is the AS1649 (Australian Standard 2001). The standardized testing protocols are defined to evaluate the structures and connections under quasi-static loading.

In Chapter 4 of this thesis, a model was presented to estimate the Equivalent Viscous Damping of the portal, based on the expected behaviour on the connector, Eqs. (4.42), (4.45) and (4.49). The parameters required to evaluate Eq. (4.49), defined for the single connector (*Protocol III*), are partly dependent on the loading protocol required by the standard. For the European standard (EN 12512; CEN 2001), in the expression (4.49) we can assume $\Delta\delta/\delta \sim \Delta v_y/v_y = 0.5$. For dowel-type metal connectors in double shear, timber-to-timber with failure mode III (EYM; Eurocode 5, CEN 2004a), we can take the following values for each of the other parameters: $\sigma_F = 0.3274 \sim 0.33$ and $\beta_k = 2$.

To substitute the numerical values of the parameters $\Delta\delta/\delta$, σ_F and β_k in Eqs. (4.45) and (4.49), the final expression is simplified in the form of Eqs.(5.27) and (5.28) respectively for *Protocol II* and *Protocol III*.

$$\xi_{eq,dowel} = 0.072 + \frac{0.4287}{\pi} \left(\frac{\mu_\delta - 1}{\mu_\delta} \right) \quad (5.27)$$

and

$$\xi_{eq,dowel} = 0.179 + \frac{0.4287}{\pi} \left(\frac{\mu_\delta - 1}{\mu_\delta} \right) \quad (5.28)$$

wherein μ_δ is the static slip ductility of the dowel.

The equivalent viscous damping of the beam-to-column joint, made of two concentric crowns of dowels, can be estimated with Eq. (4.53). For the configuration of the portal frame, under *Protocol II*, Eq. (4.53) simplifies to Eq. (5.29):

$$\xi_{eq,JOINT} = (0.2085 - 0.1365C_J) + \frac{0.4287}{\pi} \left(\frac{\mu_\delta - 1}{\mu_\delta} \right) C_J \quad (5.29)$$

in which C_J is the dimensionless configuration parameter of the joints and is given by Eq. (5.30), while μ_δ is still the slip ductility of the dowel.

$$C_J = \frac{n_{ext} + n_{int}}{n_{ext} + n_{int} \frac{r_{int}}{r_{ext}}} = \frac{n_{tot}}{n_{eq,pl}} \quad (5.30)$$

Similarly to the *Protocol III* situation, the damping of the beam-to-column joints can be estimated with Eq. (5.31):

$$\xi_{eq,JOINT} = (0.3155 - 0.1365C_J) + \frac{0.4287}{\pi} \left(\frac{\mu_\delta - 1}{\mu_\delta} \right) C_J \quad (5.31)$$

wherein C_J is still defined by Eq. (5.30).

The evaluation of the EVD (ξ_{eq}) of the structure can be done once the value of equivalent viscous damping of nodes is known, as has been presented in Chapter 4. It then replaces the expressions of estimated damping of the connection in the two situations *Protocol II* and *Protocol III*, respectively Eqs.(5.29) and (5.31), in the final model of the EVD in Eq. (4.57).

In a real situation the structure is subject to the effect of an earthquake and its irregular load cycles.

Recent research has shown that the Jacobsen's energy approach tends to overestimate the value of hysteretic damping, and thus the Equivalent Viscous Damping (EVD) value, especially in models that have a high hysteretic energy dissipation capacity. A comprehensive discussion of the problem can be found in Blandon and Priestley (2005) and in Priestley *et al.* (2007).

In this work non-linear dynamic analyses have been performed to validate the proposed analytical model for estimating the EVD. Inputs are represented by an ensemble of spectrum-compatible accelerograms selected to have characteristic frequency content for the structure. The Equivalent Viscous Damping (EVD) calibration approach is based on time-history analyses, as proposed in Blandon and Priestley (2005).

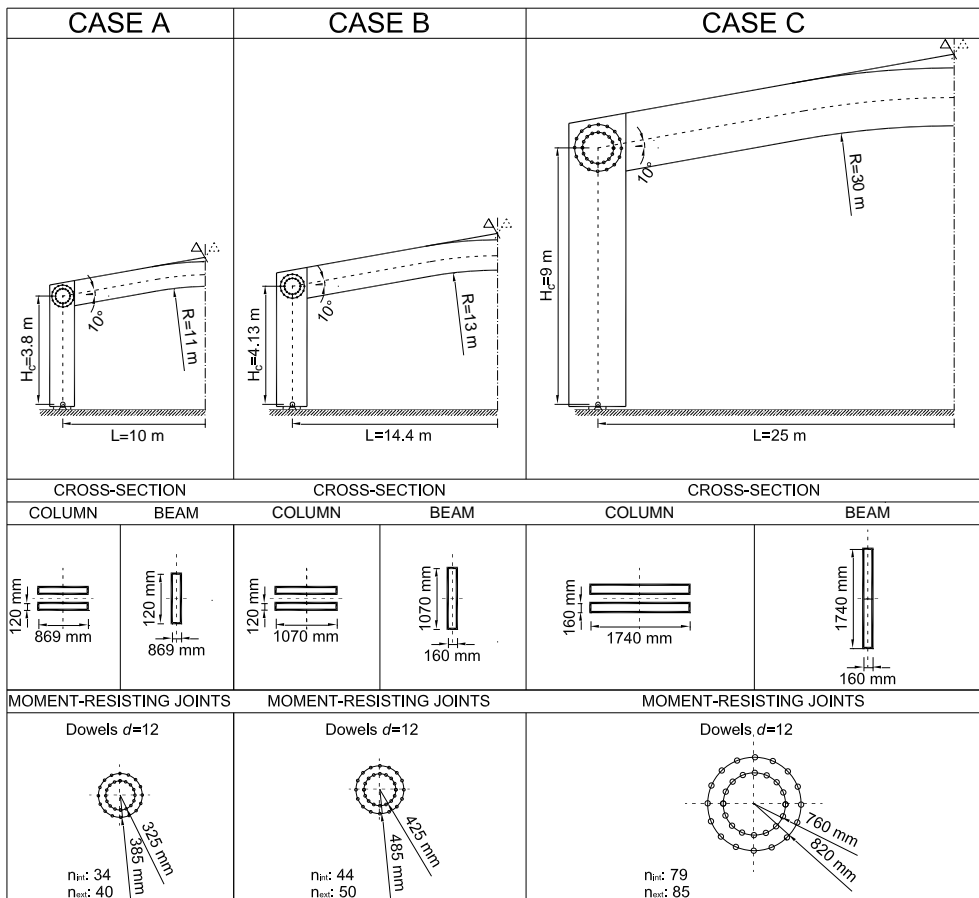


Figure 5.22 Geometrical dimensions of the three case studies investigated

The non-linear analyses were conducted on a sample of three finite element models (**FEM I** and **FEM II**). The three portal structures are representative of the range of possible geometrical configurations and are named CASE A, CASE B and CASE C. Figure 5.22 and Table 5.8 show the dimensions of the elements and connections of the portal frames, designed in static conditions in accordance with Eurocode 5 (CEN 2004a). The problem is limited compared to the general case presented in Priestley *et al.* (2007), since the EVD analytical model has been formulated only for the ultimate limit state condition corresponding to the maximum capacity level of the structure (ULS).

Table 5.8 Geometrical and mechanical parameters of the three cases investigated

	CASE A	CASE B	CASE C
Geometrical dimensions of the portal			
Nominal height of the portal – H_c (m)	3.8	4.1	9
Nominal width of the portal – L (m)	10	14.4	25
Slope of the roof beam – α_r (°)	10.2	10.2	10.2
Radius of the roof beam – R (m)	11	13	30
Thickness of the beam – b_b (mm)	160	160	160
Thickness of the column – b_c (mm)	2 x 120	2 x 120	2 x 120
Height of the beam cross-section – h_b (mm)	869	1070	1740
Height of the column cross-section – h_c (mm)	869	1070	1740
Geometrical dimensions and mechanical properties of the joint			
Dowel diameter – d [mm]	12	12	12
Radius of the internal dowel crown – r_{int} (mm)	325	425	760
Radius of the external dowel crown – r_{ext} (mm)	385	485	820
Number of internal dowels – n_{int}	34	44	79
Number of external dowels – n_{ext}	40	50	85
Elastic rotational stiffness – $k_{\Phi,y}$ (kNm rd ⁻¹)	84600	175200	913700
Ultimate rotational stiffness – $k_{\Phi,u}$ (kNm rd ⁻¹)	56400	116800	609100

For the three portal frame structures, finite element models (**FEM I** and **FEM II**) were developed based on the procedure described in the previous sections and assuming a load-slip curve, $F-\delta$, of dowels calculated with the characteristic strength of materials. In order, we estimated (see Chapter 4) $\delta_y=2.9$ mm (dowel yielding slip), $\delta_u=17.1$ mm (dowel ultimate slip) and $\mu_\delta=6$ (dowel ductility).

Table 5.8 shows the values of the parameters of the moment-rotation curve ($M-\Phi$) of the beam-to-column joints of the portals, estimated by the analytical model.

The time-history analyses employ a set of seven spectrum compatible accelerograms generated by the code SIMQKE-II (SIMulation of earthQuaKE ground motions).

Table 5.9 Moment-rotation Pivot hysteretic curve parameters of the beam-to-column joint for the three cases

	CASE A	CASE B	CASE C
Ultimate Moment - M_u (kNm)	449.65	730.15	2205.58
Yielding Moment - M_y (kNm)	381.70	618.22	1952.96
Ultimate Rotation - Φ_u (rad)	0.0405	0.032	0.0192
Yielding Rotation - Φ_y (rad)	0.0067	0.0053	0.0032
Rotation Ductility - μ_Φ (-)	6	6	6
Pivot hysteresis first parameter - α_{Pivot} (-)	10^3	10^3	10^3
Pivot hysteresis second parameter - β_{Pivot} (-)	0.33	0.33	0.33
Pivot hysteresis third parameter - η_{Pivot} (-)	10^3	10^3	10^3

The artificial accelerograms are generated by SIMQKE-II (Vanmarcke *et al.* 1997), setting the parameters of the program as follows: TS=0.02 s (Smallest period of desired response spectrum), TL=4 s (Largest period of desired response spectrum), TRISE=2 s (Start of the stationary part of the accelerogram), TLVL=10 s (Duration of the stationary part), DUR=20 s (Duration of the stationary part), NCYCLE=30 (Number of cycles to smoothen the response spectrum), AGMX=0.42 s (Maximum ground acceleration), NPA=1 s (Number of artificial earthquakes), IIX=1235 (Arbitrary odd integer), AMOR=0.05 s (Damping coefficient).

The value of each parameter was selected in a manner consistent with the indications of Eurocode 8 (CEN 2004b).

Figure 5.23(a) shows the accelerograms artificially generated and used in the analyses. The elastic displacement response spectrum, adjusted to a viscous damping of 5% ($\xi=5\%$), is of the class type 1 proposed by Eurocode 8 (CEN 2004b), considering a PGA of 0.35g and a soil class type B. Figure 5.23(b) illustrates the spectrum-compatibility of the elastic displacement response spectra generated by the accelerograms. Each color represents an accelerogram and its elastic displacement response spectrum. Note how the average value of the displacement response spectra obtained from each accelerogram tends to coincide with the shape of the spectrum encoded in Eurocode 8 (CEN 2004b).

The analyses carried out refer only to the in-plane direction of the portal studied. Thus, the accelerograms were applied only in that direction. After the time-history analyses the Equivalent Viscous Damping value was estimated in the loop which achieves the maximum displacement of the structure. Table 5.10 summarizes the values of Equivalent Viscous Damping, calculated based on Jacobsen's equivalent energy approach, as a function of the seismic input and of the reference structure (CASE A, B or C). The accelerograms were scaled to achieve the displacement for the structure corresponding to the design level, estimated a priori via the non-linear static analysis (pushover analysis). Figure 5.24 shows the pushover curves, drawn with the outcomes of the finite element models **FEM I**, corresponding to the three case studies.

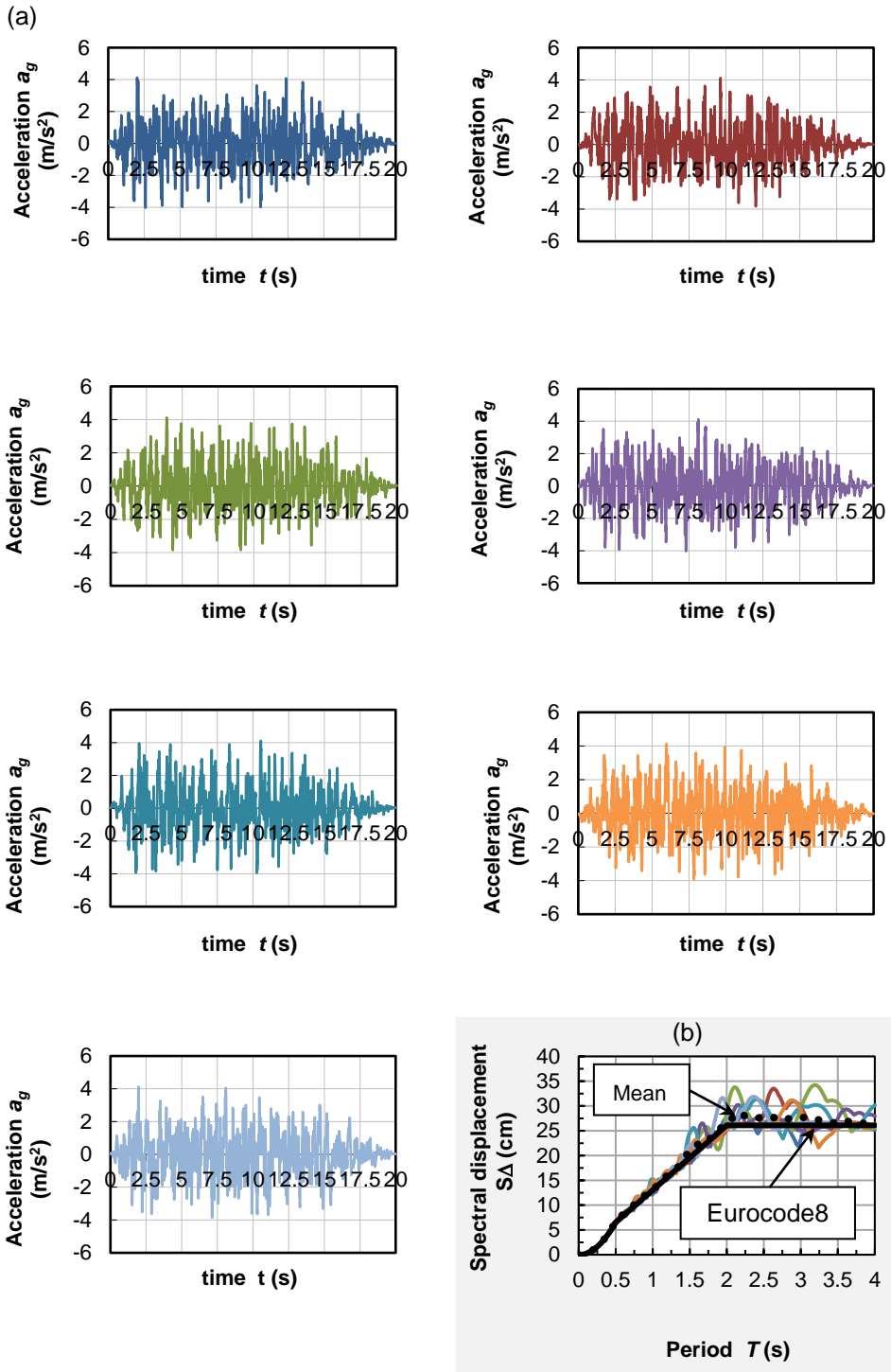


Figure 5.23 (a) Selection of the accelerograms; (b) Elastic displacement response spectra

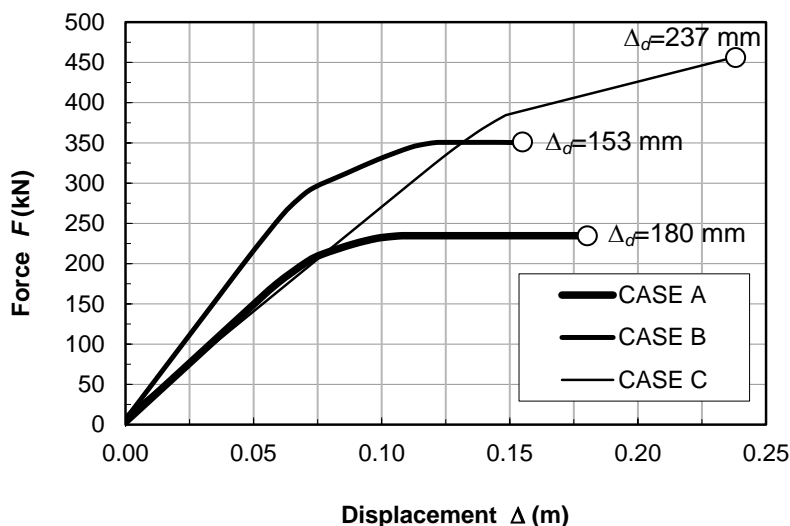


Figure 5.24 Pushover curve for the three case studies analyzed

Table 5.11 shows the measured values of the parameters of the capacity curves after the pushover analyses performed on the three portals defined above.

Table 5.12 shows, instead, the final outcomes expressed in terms of Equivalent Viscous Damping (EVD): the value averaged on the seven accelerograms, and the minimum and maximum measured for the three case studies. In addition, Table 5.12 shows the average value of design displacements evaluated via non-linear dynamic analyses for the three situations A, B and C and the coefficient of variation for the set of accelerograms used.

Table 5.13 shows the comparison of the Equivalent Viscous Damping (EVD, ξ_{eq}), estimated a priori with the analytical model (formulated in Chapter 4) and the average value estimated via time-history analyses. In the analytical model for estimating the EVD, the ratio Δ_s/Δ_j is extracted from the capacity curves (see Table 5.11).

Table 5.10 Results of Non-Linear Time History Analyses (NLTHA)

			CASE A	CASE B	CASE C
Seismic Weight (according to Eurocode 8)	W	(kg)	13630	19780	35490
Fundamental period of structure	T_s	(s)	0.4328	0.4482	0.747
First Accelerogram- No1					
Scaling factor of PGA	C_{scal}	(-)	3	2.6	1.4
Maximum Displacement Evaluated	$\Delta_{d,NLTHA}$	(mm)	180.95	144.50	239.21
Equivalent viscous damping evaluated via NLTHA	$\xi_{eq,NLTHA}$	(%)	17.02	12.51	13.53
Second Accelerogram- No2					
Scaling factor of PGA	C_{scal}	(-)	2.85	2	1.5
Maximum Displacement Evaluated	$\Delta_{d,NLTHA}$	(mm)	171.60	151.26	236.02
Equivalent viscous damping evaluated via NLTHA	$\xi_{eq,NLTHA}$	(%)	15.62	15.08	13.34
Third Accelerogram- No3					
Scaling factor of PGA	C_{scal}	(-)	3.5	2.7	2.6
Maximum Displacement Evaluated	$\Delta_{d,NLTHA}$	(mm)	189.33	157.29	237.30
Equivalent viscous damping evaluated via NLTHA	$\xi_{eq,NLTHA}$	(%)	12.57	12.07	12.91
Fourth Accelerogram- No4					
Scaling factor of PGA	C_{scal}	(-)	3.2	2.6	1.45
Maximum Displacement Evaluated	$\Delta_{d,NLTHA}$	(mm)	180.16	151.71	233.18
Equivalent viscous damping evaluated via NLTHA	$\xi_{eq,NLTHA}$	(%)	14.51	12.76	12.86
Fifth Accelerogram- No5					
Scaling factor of PGA	C_{scal}	(-)	3.15	2.3	1.40
Maximum Displacement Evaluated	$\Delta_{d,NLTHA}$	(mm)	182.28	157.97	238.26
Equivalent viscous damping evaluated via NLTHA	$\xi_{eq,NLTHA}$	(%)	12.84	12.47	11.02
Sixth Accelerogram- No6					
Scaling factor of PGA	C_{scal}	(-)	3.75	2.55	1.7
Maximum Displacement Evaluated	$\Delta_{d,NLTHA}$	(mm)	203.07	152.53	243.04
Equivalent viscous damping evaluated via NLTHA	$\xi_{eq,NLTHA}$	(%)	15.84	13.13	12.10
Seventh Accelerogram- No7					
Scaling factor of PGA	C_{scal}	(-)	3.1	2.5	1.8
Maximum Displacement Evaluated	$\Delta_{d,NLTHA}$	(mm)	174.37	154.51	226.62
Equivalent viscous damping evaluated via NLTHA	$\xi_{eq,NLTHA}$	(%)	14.18	13.39	12.26

Table 5.11 Pushover results of the three case studies (CASE A, B and C)

			CASE A	CASE B	CASE C
Yielding displacement via pushover analysis	$\Delta_{y,PUSH}$	(mm)	52.82	54.71	115.79
Ultimate displacement via pushover analysis (here the design value)	$\Delta_{d,PUSH}$	(mm)	180.29	153.32	236.79
Displacement ductility via pushover analysis	$\mu_{\Delta,PUSH}$	(-)	3.41	2.80	2.05
Elastic displacement via pushover analysis	$\Delta_{s,PUSH}$ (CHAPTER 4)	(mm)	29.86	36.96	99.08
Plastic displacement via pushover analysis	$\Delta_{j,PUSH}$ (CHAPTER 4)	(mm)	150.43	116.36	137.71
Elastic-to-plastic displacement ratio via pushover analysis	$\Delta_{s,PUSH} / \Delta_{j,PUSH}$	(-)	0.20	0.32	0.72

Table 5.12 Analytical EVD versus average value of EVD evaluated via non-linear time-history analyses (NLTHA)

			CASE A	CASE B	CASE C
Mean of ultimate displacement via NLTHA analysis (here the design value)	$\Delta_{d,NLTHA}$	(mm)	183.11	152.82	236.23
Mean value of EVD estimated via NLTHA	$\xi_{eq,NLTHA,Mean}$	(%)	14.65	13.06	12.57
Maximum Value of EVD estimated via NLTHA	$\xi_{eq,NLTHA,max}$	(%)	12.57	12.07	11.02
Minimum Value of EVD estimated via NLTHA	$\xi_{eq,NLTHA,min}$	(%)	17.02	15.08	13.53
Coefficient of variation	CV	(%)	11.09	7.60	6.85

Table 5.13 Numerical mean value of EVD versus analytical prediction of EVD for the three cases studied

			CASE A	CASE B	CASE C
Mean Value of EVD estimated via NLTHA	$\xi_{eq,NLTHA,Mean}$	(%)	14.65	13.06	12.57
Equivalent viscous damping (<i>Protocol II</i>)	$\xi_{eq,P-II}$	(%)	15.28	13.99	10.75
Error in EVD using <i>Protocol II</i>	$E\xi_{eq,P-II}$	(%)	-4.30	-7.11	14.50

The analytical model for calculating the Equivalent Viscous Damping considers the loading *Protocol II*, defined in Chapter 4. The loading *Protocol II* is consistent with the EN 12512 (CEN 2001) provisions for the calculation of the dissipative capacity of the structure or the connections. According to the EN 12512 code, in fact, the Equivalent Viscous Damping should be measured at the third cycle of loading for any given level of ductility, $\mu_{\Delta} = \Delta_d / \Delta_y$. Under these conditions, *Protocol II* is the one that meets this requirement, and will be used in the design stage.

The comparison shows an error of EVD equal to -4.30%, -7.11% and 14.50%, respectively for CASE A, CASE B and CASE C. The average value of error is equal to 1.03%. Thus, the analytical model has been validated on a representative sample of portal structures.

In the design process it is useful to have a model that links the EVD value to the displacement ductility of the structure ($\mu_{\Delta} = \Delta_d / \Delta_y$). In a similar way to that proposed in Chapter 3 of the book by Priestley *et al.* (2007), in the following we present the modified analytical expression for estimating the EVD.

The original formula (Eq. (4.57)) is modified by introducing the reduction factor $c_{\mu\Delta}$, defined by Eq. (5.32), in place of the parameter $(1/1 + \Delta_d / \Delta_y)$ that appears in Eq. (4.57):

$$c_{\mu\Delta} = \frac{\mu_{\Delta} - 1}{\mu_{\Delta}} \tag{5.32}$$

In addition, it introduces a calibration coefficient, c_{EVD} , in order to minimize the error of the model on the numerical sample.

Thus, the analytical expression for calculating the Equivalent Viscous Damping becomes (Eq. (5.33)):

$$\xi_{eq} = c_{EVD} \left((0.2085 - 0.1365C_J) + \frac{0.4287}{\pi} \left(\frac{\mu_\delta - 1}{\mu_\delta} \right) C_J \right) \left(\frac{\mu_\Delta - 1}{\mu_\Delta} \right) \quad (5.33)$$

wherein $\mu_\Delta = \Delta_d / \Delta_y$, while the other parameters have been defined above.

For a well-designed structure, the coefficient C_J is in the range 1 to 1.15, so on average we can assume $C_J = 1.1$. In addition, in connections designed according to failure mechanism type III (EYM), at a high ductility level, we can assume $\mu_\delta = 6$.

The expression above simplifies and becomes (Eq. (5.34)):

$$\xi_{eq} = c_{EVD} \frac{0.5763}{\pi} \left(\frac{\mu_\Delta - 1}{\mu_\Delta} \right) \quad (5.34)$$

The final calibration of the model proposes a correction factor, c_{EVD} , estimated to minimize the error on the sample of structures, with the same criteria as defined in the previous Section. The value of c_{EVD} that minimizes the variance and leads to a zero mean error on the three cases is estimated as 1.1790 (~1.18).

The final model to estimate Equivalent Viscous Damping, Eq. (5.34) is assumed to be independent of the actual period of the structure (T_s). This condition usually occurs with an effective period, T_e , greater than 1 (Priestley *et al.* 2007). This makes it possible to evaluate the damping of the structure, ξ_{eq} , without resorting to iterative procedures in the design stage.

After the calibration process, the analytical values of EVD evaluated based on Eq. (5.34) were compared with the results of the NLTH-analyses and the experimental values measured on the reference test.

Table 5.14 shows the values of EVD, as an average, obtained from the time history analyses, in accordance with Eq. (5.34) and, using interpolated expressions of experimental data (Eq. (5.35) a,b). Eqs. (5.35) a and b, are derived by substitution of the parameters C and ξ_0 , of Table 5.3 into the mathematical model of Priestley (Eq. (4.30)):

$$\begin{aligned}
 \text{(a) } \xi_{eq,EXPERIMENTAL} &= 6.53 + \frac{35.81}{\pi} \left(\frac{\mu_{\Delta} - 1}{\mu_{\Delta}} \right) \quad (\%) \\
 \text{(b) } \xi_{eq,EXPERIMENTAL} &= 6.24 + \frac{31.68}{\pi} \left(\frac{\mu_{\Delta} - 1}{\mu_{\Delta}} \right) \quad (\%)
 \end{aligned}
 \tag{5.35} \text{ a,b}$$

In Table 5.14, $\xi_{eq,EXPERIMENTAL}$ is the lower limit of the damping measured on the reference test and refers to the load cycles 2 and 3, according to the protocol of testing required by EN 12512 (CEN 2001).

Table 5.14 Final values of EVD for the three cases examined

			CASE A	CASE B	CASE C
Mean value of EVD estimated via NLTHA	$\xi_{eq,NLTHA,Mean}$	(%)	14.65	13.06	12.57
Equivalent viscous damping (Eq. 5.34)	$\xi_{eq,PROPOSAL}$	(%)	15.28	13.99	10.75
Equivalent viscous damping (Eq. 5.35a)	$\xi_{eq,EXPERIMENTAL, 2\text{ CYCLE}}$	(%)	14.59	13.86	12.37
Equivalent viscous damping (Eq. 5.35b)	$\xi_{eq,EXPERIMENTAL, 3\text{ CYCLE}}$	(%)	13.37	12.73	11.40

The values of Table 5.14 further validate the mechanical model formulated to evaluate the Equivalent Viscous Damping of the structure.

5.7 Conclusions

In this Section, the hysteretic model for estimating the Equivalent Viscous Damping (EVD) has been validated on an ensemble of cases that cover the geometric variability of the structure. The applicability of the model to other types of construction with dowel-type metal fasteners connections should now extended and verified.

6 EXTENSION OF DIRECT-DBD METHOD TO OTHER TIMBER BUILDINGS

6.1 General

The analytical formulation for the estimation of design displacement and the Equivalent Viscous Damping (Δ_d, ξ_{eq}) is based on a mechanical model of the single connector. The connections discussed in this work are "modern" type (so called engineer-joints), using an arrangement of dowel-type metal fasteners.

The extension of the formulation of the Direct-DBD procedure to other geometric configurations of portals and other types of wooden structures with dowelled connections is quite straightforward. This Chapter deals with the case of the glulam portal frame with Moment-Resisting (MR) joints, and the generic *shear wall* that defines the response of the *wood frame* building.

6.2 Moment-resisting joint for general dowel configuration

The formulation of the design displacement (Δ_d) presented in Chapter 4 for portals with semi-rigid joints made with two concentric crowns of dowels, can be extended to other geometric configurations of beam-to-column connections.

Figure 6.1(a) shows the case of the portal with connections made by placing a set of dowels according to a rhombic geometry. The aid of Figure 6.1(b) allows the analytical formula of design displacement (Δ_d) to be defined.

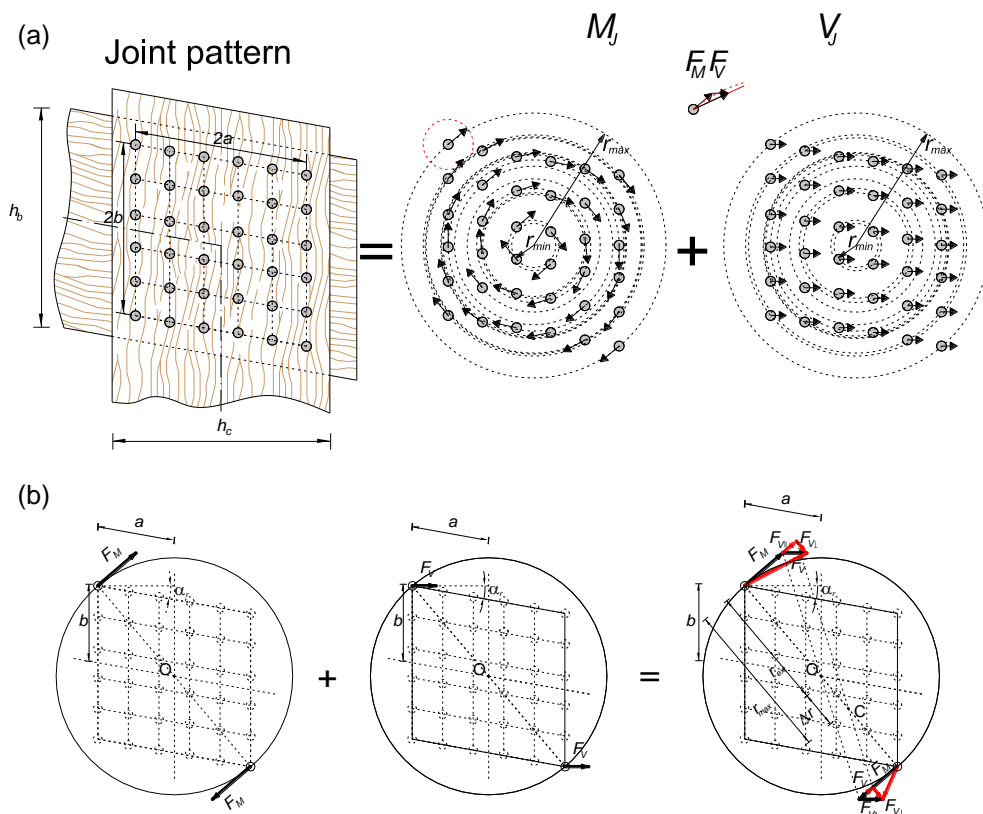


Figure 6.1 (a) Load distribution for a group of dowels in a rhombic pattern due to bending (M) and shear (V); (b) Design scheme dowel-type MR joint

In the elastic range, the critical element for the design of the Moment-Resisting (MR) joint is the farthest dowel from the geometric centre of the connection. The symmetry of the geometric configuration and the hypothesis of rigid rotation in connection simplify the study in the plastic range.

The instantaneous centre of rotation in the plastic range is shifted from the geometric centre by the effect of the shear stresses (V_j). The ultimate slip will be reached by dowels placed at the apex of the rhombic distribution (Figure 6.1(b)).

The use of the same model and assumptions presented in Chapter 4 allows the calculation of the ultimate rotation of the joint and then the corresponding displacement of the portal. The ultimate rotation (Φ_u) is still derived from the ultimate slip of the dowel and is calculated by solving Eq.(6.1).

$$\Phi_u = \delta_u / r_{\max} \quad (6.1)$$

where

$$r_{\max} = r_{\text{ext}} + \Delta r \quad (6.2)$$

and

$$\Delta r = r_{\text{ext}} \frac{F_V}{F_M} = \frac{r_{\text{ext}} \cdot (b + a \sin \alpha_r)}{H_c} \cdot \frac{n_{\text{eq,pl}}}{n_{\text{tot}}} \quad (6.3)$$

The final expression to calculate the ultimate rotation becomes:

$$\Phi_u = \frac{\delta_u}{\sqrt{a^2 + b^2 + 2ab \sin \alpha_r} \cdot \left(1 + \frac{(b + a \sin \alpha_r)}{H_c} \cdot \frac{n_{\text{eq,pl}}}{n_{\text{tot}}} \right)} \quad (6.4)$$

The displacement of the portal for inelastic deformation of the MR joint is given by:

$$\begin{aligned} \Delta_j = \Phi_u H_c &= \frac{\delta_u}{\sqrt{a^2 + b^2 + 2ab \sin \alpha_r} \cdot \left(1 + \frac{(b + a \sin \alpha_r)}{H_c} \cdot \frac{n_{\text{eq,pl}}}{n_{\text{tot}}} \right)} H_c \\ &= \frac{1}{\sqrt{1 + \sigma_f^2 + 2\sigma_f \sin \alpha_r}} \frac{\delta_u}{1 + \frac{n_{\text{eq,pl}}}{n_{\text{tot}}} \frac{L}{H_c} \frac{h}{L} \frac{a}{h} (b + a \sin \alpha_r)} \frac{H_c}{L} \frac{L}{h} \frac{h}{a} = \\ &= \frac{\delta_u}{\sqrt{1 + \sigma_f^2 + 2\sigma_f \sin \alpha_r}} \frac{1}{\left(1 + (\sigma_f + \sin \alpha_r) / \theta_t \gamma_t \beta_{t,II} \cdot n_{\text{eq,pl}} / n_{\text{tot}} \right)} \end{aligned} \quad (6.5)$$

where $\theta_r=H_c/L$ is the aspect ratio of the portal, $\sigma_r=b/a$ is the ratio between the half of sides of the perimeter that encloses the MR connection (rhombus geometry), $\gamma_r=L/h$ and $\beta_{r,II}=h/a$ are geometrical dimensionless parameters, h is the height of the cross-section of the column, a is half the length of the rhombic area in the horizontal direction, b is half the length of the rhombic area in vertical direction and n_{tot} is the total number of dowels.

The parameter $n_{eq,pl}$, which defines the equivalence of the connectors on the outer circumcircle, is defined by Eq. (4.23). For this configuration, the radius of the j^{th} connector becomes a function of the spacing between the dowels in both directions, of the distances from the edges and of the distances from the ends. The spacing of the connectors are usually expressed as a function of their diameter, which greatly simplifies the calculations.

When α_r equals zero, the beam-to-column joint combines square elements, and the configuration of the dowels becomes rectangular. Under these conditions, the inelastic displacement of the portal, Δ_j , is directly estimated by Eq. (6.6):

$$\Delta_j = \delta_u \frac{1}{\sqrt{1 + \sigma_f^2}} \left(\frac{\theta_r \gamma_r \beta_{r,II}}{1 + \sigma_f / \theta_r \gamma_r \beta_{r,II} \cdot n_{eq,pl} / n_{tot}} \right) \quad (6.6)$$

Eq. (6.9) is numerically evaluated with the parameters defined above.

For an un-defined geometric configuration of the MR joint, in the absence of symmetry, it is still possible to extend the procedure to evaluate the design displacement of the MR joint.

The basic steps of calculation are in order:

- i. Define a geometric configuration of dowels in the crossover region between the beam and columns (Figure 6.2).
- ii. Evaluate the instantaneous centre of rotation in the elastic and plastic range, assuming a rigid body rotation of the connection. For all elements of connection the same force-slip ($F-\delta$) relationship is assumed, regardless of the j^{th} position. The instantaneous centre of rotation is shifted as a result of shear stresses. The slip of the j^{th} dowel is in the direction of force F_j .

The ensemble of the slips, δ_j , in the generic configuration must ensure the equilibrium of the joint. From the rotational equilibrium and from the direction of the dowel slip δ_j , the instantaneous centre of rotation (Eq. (6.7)) is uniquely identified.

Equilibrium of rotation

$$M_J = \sum_{i=1}^{n_{tot}} F_{M,i} r_i = F_y \sum_{i=1}^{n_{tot}} r_i \quad (6.7)$$

- iii. Identification of the dowel farthest from the instantaneous centre of rotation in the plastic range (r_{max}).
- iv. Analytical computation of the maximum (ultimate) rotation of the joint, given the ultimate slip of the most stressed dowel (Eq. (6.8)):

$$\Phi_u = \frac{\delta_u}{r_{max}} \quad (6.8)$$

- v. Evaluation of the inelastic displacement of the portal, as a product of the joint rotation and the portal height (Eq. (6.9)):

$$\Delta_j = \Phi_u H_c \quad (6.9)$$

The parameters defining the F - δ curve of the dowel within the connection should be evaluated to take into account the variability of the mechanical properties of wood due to the angle between the stress and the fibre. It is reasonable to assume a value of F_y and δ_y (δ_u) as a mean of the actual values, calculated for each dowel within the joint in function of the stress-grain angle.

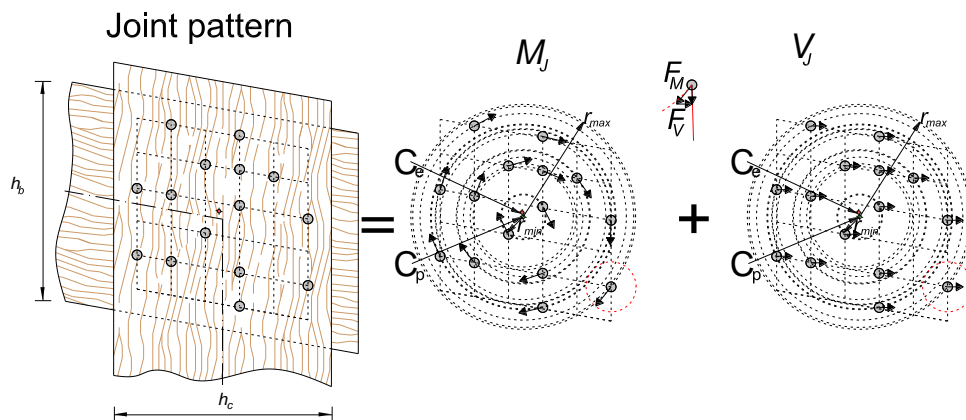


Figure 6.2 Load distribution for a group of dowels in a generic pattern due to bending (M) and shear (V)

6.3 Wood light-frame system

6.3.1 General

The seismic response of *wood frame* buildings, with *platform frame* technology, is directly related to the *shear wall* response at each storey (Ceccotti and Toulaiatos 1995). Figure 6.3 shows the role of panel-to-frame connections in the expected seismic behaviour of the building. This Section shows how it is possible to get the final evaluation of the structure, in terms of displacement and Equivalent Viscous Damping, starting from the local response of a single nail.

Timber *wood frame* buildings are made by assembling *shear walls* in such a way as to download the seismic forces and the dynamic forces induced by wind onto the ground (Prion 2003).

The evaluation of the load-displacement ($F-\Delta$) response of each *shear wall* is difficult to perform, since the behaviour is highly non-linear and hysteresis loops are affected by deterioration and the pinching effect.

The assessment of the $F-\Delta$ relationship is affected by the aleatory variability of material properties and the geometric uncertainty of the component elements (Ceccotti and Toulaitos 1995). The latter often is due to incomplete knowledge of how the system has been assembled or the poor quality of execution.

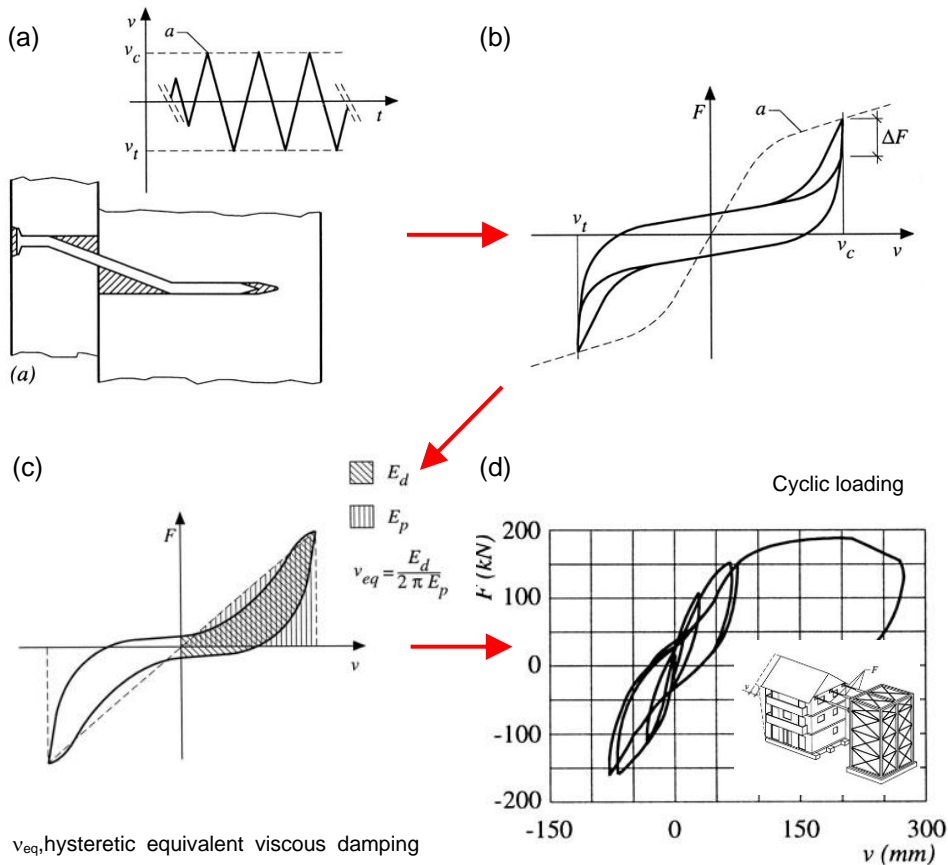


Figure 6.3 (a) Failure mode of nails under cyclic actions: nails crush wood fibres and cavity is formed at the edges of joined material; (b) Impairment of the strength ΔF between the first and the third load cycles with the same deformation; (c) Energy dissipated during a cycle: due to embedment of wood and plasticity of the connections; (d) Global seismic response of a full-scale residential building (pictures modified from Ceccotti 1995)

The uncertainty of the behaviour of the *shear wall* is reflected directly in the inelastic response of the *wood frame* building. Experiments have shown that the non-linear response of *shear walls* is a function primarily of the local behaviour of each element of connection between the panel and the frame, expressed as a load-slip curve; (Prion 2003) and (Karacabeyli and Popovski 2003). Thus, the analytical formulas for calculating the design displacement (Δ_d) and the Equivalent Viscous Damping (ξ_{eq}) can be extrapolated in a similar way to that presented in Chapter 4.

6.3.2 *Direct-DBD: formulation of design displacement*

The design displacement (Δ_d) corresponds to the maximum deformation capacity of the *shear wall*. The Δ_d matches the performance level necessary for preservation of life, known as the ultimate limit state (ULS) in Eurocode 8 (CEN 2004b).

The buildings investigated are constructed by combining a series of wood-based panels attached to the edges of the frame structure with steel nails, to ensure an adequate cyclic behaviour. Nails are elements widely used in wood structures for ease of installation and for their favourable dynamic response against the effects of the earthquake (Dolan 1994).

The formulation of the design displacement is based on a failure mode in the *shear wall*, in the inelastic deformation range, known as the "shear type mechanism". To prevent overturning and sliding on the storeys, at each level, anchoring devices at the ends of each wall are provided. The expression for the calculation of the design displacement, Δ_d , is formulated by the simple linear combination of displacements due to each component element of the *shear wall*: the frame, panels, sheathing (or bracing) wood-based panels and connections between panels and frame (nails).

To ensure cyclic behaviour of the *shear walls*, Eurocode 8 (CEN 2004b) specifies requirements in terms of the thickness and minimum density of the panels, diameter of nails and spacing between the connectors. The design rules provided in Eurocode 8 ensure ductility and the energy dissipation capacity of *shear walls* and thus the ultimate plastic deformation of the construction (Toratti 2006).

In addition, this work uses outcomes presented by Smith *et al.* (1998) on the performance of nailed connections exposed to seismic effects. The load-slip curve of nails has a similar trend to that presented in Chapter 4 for dowels. Nails, in fact, are a class of dowel-type fasteners (Augustin 2008b).

In Europe, as in North America, the design code was developed to evaluate the load-carrying capacity of connections, following the limit state design philosophy (evaluation of strength). The prediction model for fastener connections is known as European Yield Model (EYM) and is an improvement of Johansen's theory (Johansen 1949), as explained in Chapter 4. A series of supporting provisions are included to find the modulus of slip of fasteners. To evaluate the slip of a nail it is assumed that slip modulus is independent of the angle between the stress and the grain direction of the wooden element.

Outcomes of experimental tests performed on a single-shear plane nailed connection highlight that the yield point occurs for a small slip of the connector (Smith *et al.* 1998). Under monotonic loading conditions the post-yield curve has a slight hardening and a high value of static slip ductility, $\mu_{\delta} \sim 20$. For cyclic loading the envelope curve shows a significant hardening and the maximum load is achieved on a slip value about 10 times the yield slip, $\mu_{\delta} \sim 10$. Beyond this load level, it highlights the progressive loss of available capacity (Smith *et al.* 1998). From this experimental evidence it is possible to define a load-slip curve ($F-\delta$) for elastic-perfectly plastic type nail connections as done for dowel connectors.

In Eurocode 8 (CEN 2004b) some geometric rules are provided to ensure the minimum level of ductility available and the dissipative capacity of *shear walls* (nailed wall panels). Following the rules of detail provided in Eurocode 8 ensures that each *shear wall* is in the high ductility state (DCH) or in the average ductility state (DCM). In line with the approach to calculation presented in Chapter 4, this work considers the rules corresponding to the DCH situation.

To ensure the expected load-slip curve for nails ($F-\delta$), defined in function of the analytical values known in the design process, extensive parametric analysis has been performed on a possible set of mechanical parameters, such as the wood density of the panel (sheathing or bracing) and the tensile strength of the steel wire used to produce the nails.

Figure 6.4 summarizes the results of the sensitivity analysis, via Möller's charts representing the nailed connection, in which each point represents a mechanical configuration of the connection. The outcomes are valid for connections made with nails up to 3.1 mm in diameter and a thickness of panel bracing equal to or greater than $4d$.

In Figure 6.4, t_2/t_1 is defined as the dimensionless ratio between the thickness of the frame elements (point-side penetration of nail) and the bracing wood-based panel, while λ_1 is defined as (Eq. (6.10)):

$$\lambda_1 = t_1 / \sqrt{M_{y,Rk} / (f_{h,k,1} d)} \tag{6.10}$$

At this point there is evidence that the requirements of Eurocode 8 (CEN 2004b) provide a type II ductile failure mode for the dowel (EYM). Figure 6.4 shows that the slenderness of fasteners (=the ratio between the thickness of the wood members and diameter of the fasteners) is a good index to measure the ductility capacity and therefore the possibility to dissipate the energy of the connectors. Common nails are made of hardened steel, thus, the slenderness of nails should be at least 4.

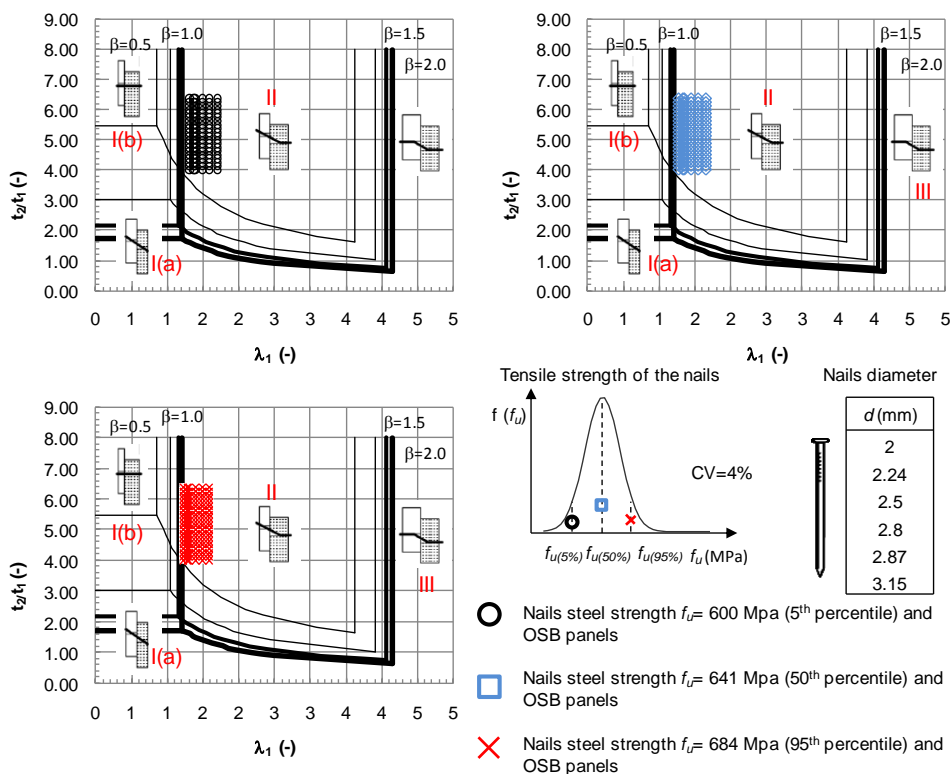


Figure 6.4 Modified Möller's diagram for nails with diameter ranging from 2 mm to 3.1 mm and steel strength ranging from 5th to 95th

Assuming a type II failure mode (EYM) of nails we can estimate the capacity of each *shear wall* using simple geometric rules and the lower bound theorem of limit analysis. The equivalent identification of each *shear wall* with an SDOF system, considers all the mechanical and geometric parameters of structural elements that compose the *shear wall*.

The design displacement (ultimate value) is estimated as the sum of an elastic part and an inelastic part of displacement mainly due to post-yield of connectors (Figure 6.5). The analytical model assumes that the inelastic deformation of the panel is concentrated in the connections. The failure mode is identified by the deformed shape of the *shear wall*, in the absence of rigid rotations and sliding in the devices provided at the base. The hypothesis is consistent with the expected response of the building observed experimentally (Prion 2003). Each *shear wall* panel can be considered as a separate cantilever element.

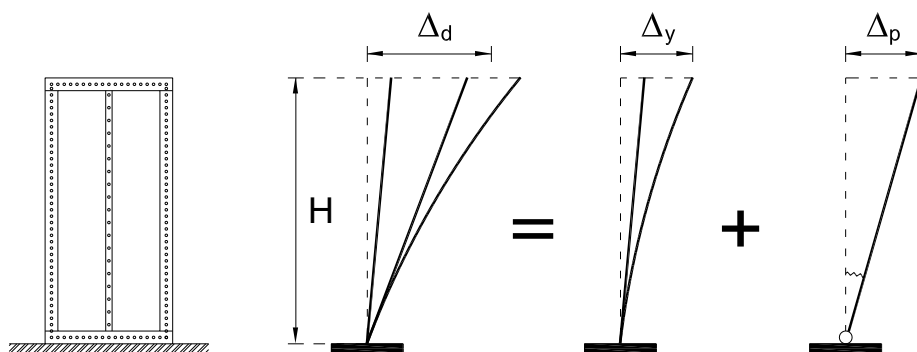


Figure 6.5 Displacement decomposition of shear walls

The inelastic displacement of the *shear wall* can be estimated according to the load-slip curve assumed for the nails, elastic-perfectly plastic type in accordance with what has been demonstrated above.

To derive the analytical model for estimating the design displacement, Δ_d , of *shear walls*, the contributions of deformation of each structural component are added up. The design displacement of the *shear wall* is the sum (Figure 6.6) of the elastic bending displacement (Δ_b) of members, the shear displacement (Δ_v) of the panel, and non-linear displacement induced by the panel-to-frame connections (Δ_n).

The elastic deformation is calculated on the basis of the theory of elastic beams.

The contributions of deformation due to the bending and shear stresses are obtained using the virtual unit load method. The displacement due to bending deformation can be calculated with Eq. (6.11) and the annexed scheme of calculation (Figure 6.7):

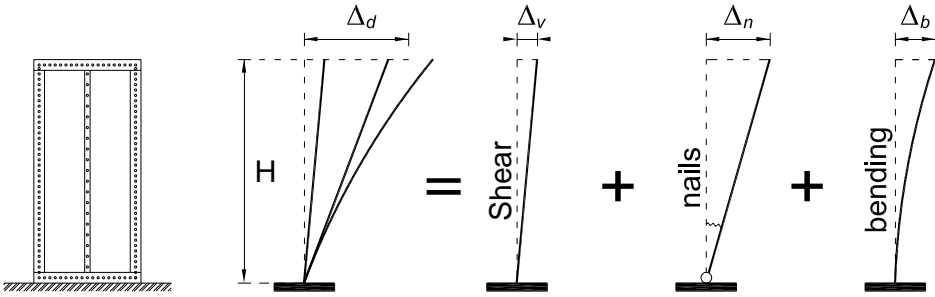


Figure 6.6 Displacement decomposition of shear walls, with the contribution of each component

$$\Delta_b = \frac{2F_w h_w^3}{3E A_s b_w^2} \tag{6.11}$$

where E is the modulus of elasticity of the framed timber elements, A_s is the cross-section area of studs, h_w is the wall panel height; b_w is the wall panel width and F_w is the force acting at the top of wall (the maximum resisting force $F_{V,w}$).

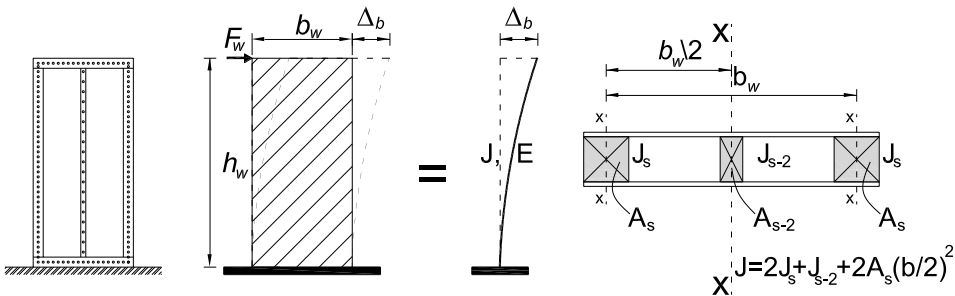


Figure 6.7 Analytic model to evaluate bending displacement (Δ_b)

The displacement due to shear panel deflection can be calculated by Eq.(6.12) and referring to Figure 6.8:

$$\Delta_v = \frac{F_w h_w}{G_p b_w t_p} \tag{6.12}$$

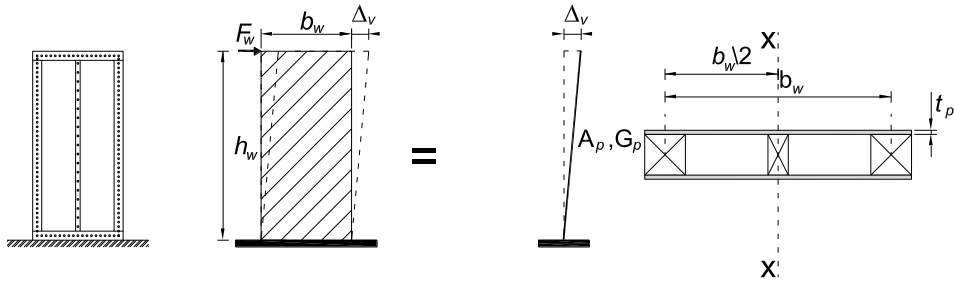


Figure 6.8 Analytic model to evaluate shear displacement (Δ_v)

where G_p is the shear modulus for the sheathing panels, t_p is the effective thickness of the sheathing panels, b_w is the wall panel width and F_w is the force at the top of wall (the maximum resisting force $F_{V,w}$).

The inelastic displacement due to the slip of nails, Δ_n , can be analytically calculated by upgrading one of the equivalent models for the elastic range proposed by these authors: Judd and Fonseca (2006), Yasumura (2000) or, more simply, by applying the relation provided in Chapter 5 of NZS 3603 (New Zealand Standard 1993). In any case all these models, defined to evaluate elastic *shear wall* deflection due to nail slip, should be extended using the non-linear relationship assumed for nails, described in this work.

Eq. (6.13), Eq. (6.14) and Eq. (6.15) represent the models to evaluate displacement due to nails respectively for the Judd and Fonseca model, Yasumura’s model and for the NZS 3603 model (New Zealand standard 1993) (referring to Figure 6.9):

$$\Delta_n = \frac{4\sqrt{2} \cos\phi}{l_w \cos 2\phi} h_w e_n \tag{6.13}$$

$$\Delta_n = \frac{2\left(1 + Ah_w^2 / Bb_w^2\right)}{\sqrt{1 + (Ah_w / Bb_w)^2}} e_n \quad (6.14)$$

$$\Delta_n = 2(1 + a_w)c_w e_n \quad (6.15)$$

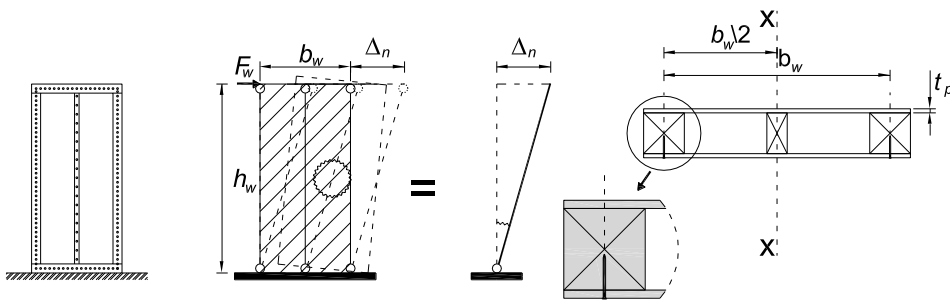


Figure 6.9 Analytic model to evaluate displacement due to slip of nails (Δ_n)

where l_w is the diagonal length of the panel, h_w is the wall height, $\phi=45^\circ-\arctan(b_w/h_w)$, e_n is the slip of the nailed connection at a corner of the sheathing, b_w is the width of the sheathing panels, c_w is the number of sheathing panels along the length of edge of the frame, a_w is the aspect ratio of each sheathing panel, $A=(n_s^2+3m_s n_s+2)/(3n_s)$, $B=(n_s^2+3m_s n_s+2)/(3n_s)$, m_s is the number of nail spacing along the length of the sheathing and n_s is the number of nail spacings along the height of the sheathing.

The procedure to calculate the nail slip displacement of *shear walls* in accordance with Judd and Fonseca's model (Judd and Fonseca 2006) provides results very close to those estimated with the NZS 3603 model (New Zealand Standard 1993), extended either to the non-linear inelastic range.

The value of the shear resisting force of the *shear wall*, $F_{V,w}$, used in static design, can be roughly calculated by the product of the number of “resisting” connectors (N_{nails}) to the load-carrying capacity of the connector (F_y): $F_{V,w}= N_{nails}F_y$, since the main frame elements are considered pinned.

For a *shear wall* loaded along the top edge, the “resisting” connections are the perimeter connections (on the top and bottom). Otherwise, according to Eurocode 5 (CEN 2004a), the racking load-carrying capacity of each *shear wall* can be calculated based on the capacity of the connector, using a reduction parameter, c_{rwall} , that takes into account the aspect ratio of the sheathing panels (Eq. (6.16)):

$$F_{V,w} = F_y b_w / s_{nails} c_{rwall} \quad (6.16)$$

where F_y is the load-carrying capacity of the connector, b_w is the wall panel (sheathing) width, s_{nails} is the fastener spacing and c_{rwall} is the reduction factor.

Other more refined models can be found in the literature. In this work, force is not the primary parameter of design, and thus we have accepted the unconditional use of one of the two models outlined above.

The evaluation of the load-carrying capacity ($F_{V,w}$) of the *shear wall* allows the calculation of the stiffness, as the ratio between the strength capacity and the ultimate displacement, which must be controlled within the design process to ensure the stiffness required for a given design displacement value Δ_d .

The *shear wall* displacement capacity (Δ_d) is strictly related to the arrangement of nails and the type of nails selected (strength of the steel wire, diameter and length), as well as the aspect ratio of sheathing panels h_w/b_w .

From the design displacement of the single *shear wall* panel it is possible to obtain the design displacement of the whole structure, with one or more to levels, by simple addition of the displacement value of each panel. This recognized design method of *shear walls* is known as the "segmented shear wall design approach". In this approach only the full-height segments are considered in the lateral resisting system while sheathing panels above and below the openings are neglected. The procedure to apply the "segmented shearwall design approach" can be found in Pang and Rosowsky (2007) and in Eurocode 5 (CEN 2004a). The total stiffness of the structure in one direction, for a given displacement, is equal to the sum of the stiffness of the panels that make up the walls.

6.3.3 Direct-DBD: formulation of the equivalent viscous damping

The tests performed on nailed connections showed a hysteretic response under the effect of cyclic loading protocols, with a similar trend to that of common dowel-type fasteners (Karacabeyli and Popovski 2003). The hysteretic behaviour is affected by the typical pinching effect which leads to flattening of the hysteresis loops for repeated loading over time. A noticeable degradation occurs between the first and second cycle and the response tends to stabilize after several cycles (Dolan 1994).

In the following we will present the procedure to apply the analytical model of equivalent viscous damping, presented in Chapter 4, to the *shear wall* element.

The ductility and capacity in terms of energy dissipation of the *shear wall* can be evaluated as a function of the behaviour of the single connector, as shown for the portal structure in Chapter 4. The load-slip curve of the nail can be described by the same elastic-perfectly plastic law as the dowel-type fasteners (Figure 4.21 of Chapter 4).

For connecting elements that come under the category of nails, in the design phase, the five parameters F_y , F_f , μ_{δ} , δ_y and k_{rc} of the elastic-perfectly plastic curve (Figure 4.21 of Chapter 4) can be numerically estimated. For nailed connections in a single shear plane, the type II failure mechanism (EYM) is anticipated regardless of the mechanical properties, as has been demonstrated in the previous Section.

The bearing strength of the nail, F_y , for failure mode II can be estimated according to the theory of Johansen (1949) through Eq. (6.17) and increased by 5% in accordance with the current European Yield Model (EYM).

$$F_y = R_k = \frac{f_{h,k,1} dt_1}{2 + \beta} \left[\sqrt{2\beta(1 + \beta) + \frac{4\beta(2 + \beta)M_{y,Rk}}{f_{h,k,1} dt_1^2}} - \beta \right] \quad (6.17)$$

Eq. (6.17), to estimate the bearing strength of the nail (F_y), is the result of the equilibrium conditions imposed in ultimate state on the connection, here, timber-to-timber with connections with a single shear plane (Figure 6.10).

The analytical expression for calculating the restoring force to return to the undeformed situation, F_f , is formulated based on the ultimate equilibrium in Figure 6.11.

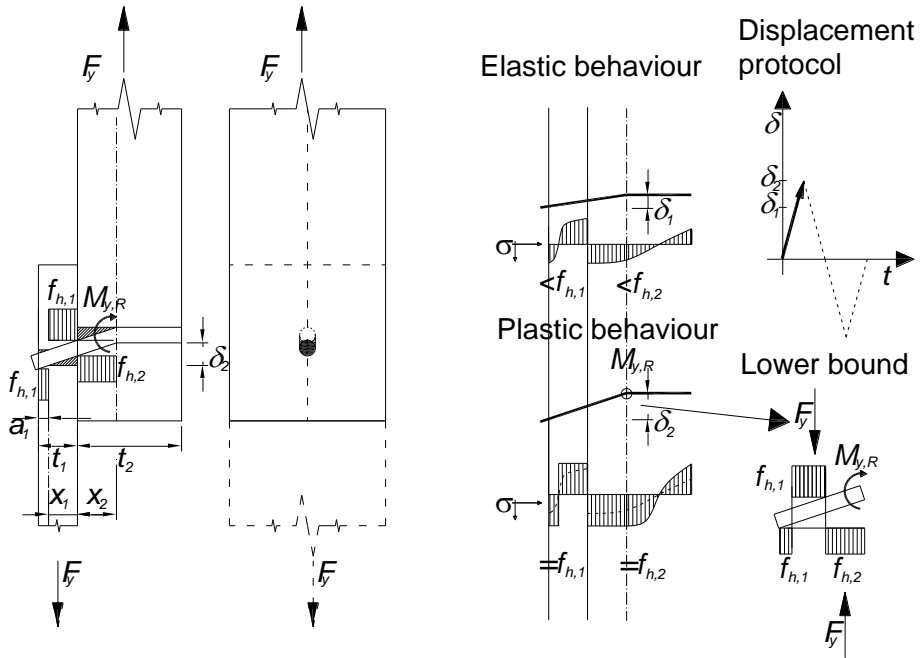


Figure 6.10 Failure mode II of fasteners in single shear panel-to-timber connections

The equations of equilibrium in the deformed state are (Eq. (6.18) and Eq. (6.19)):

$$F_f \left(t_1 - a_1 - \frac{y_1}{2} + x_2 + \frac{y_2}{2} \right) = M_{y,Rk} \quad (6.18)$$

Eq.(6.18) defines the equilibrium to the rotation imposed on the centre of failure tensions of the wooden frame elements (embedment strength $f_{h,k,2}$):

$$F_f = f_{h,k,1} dy_1 = f_{h,k,2} dy_2 \quad (6.19)$$

Eq.(6.19) defines the equilibrium in force imposed on both elements connected (panel and frame).

By manipulating expressions we find a quadratic equation in y_1 that solved, leads to the only real solution given by Eq. (6.20).

$$y_1 = \frac{(2 + \beta)}{2(\beta - 1)} x_1 + \frac{t_1 \beta}{2(\beta - 1)} - \frac{1}{2(\beta - 1)} \sqrt{(t_1 \beta + \beta x_1 + 2)^2 + \frac{8M_{Ry} \beta (1 - \beta)}{f_{h,k,1} d}} \quad (6.20)$$

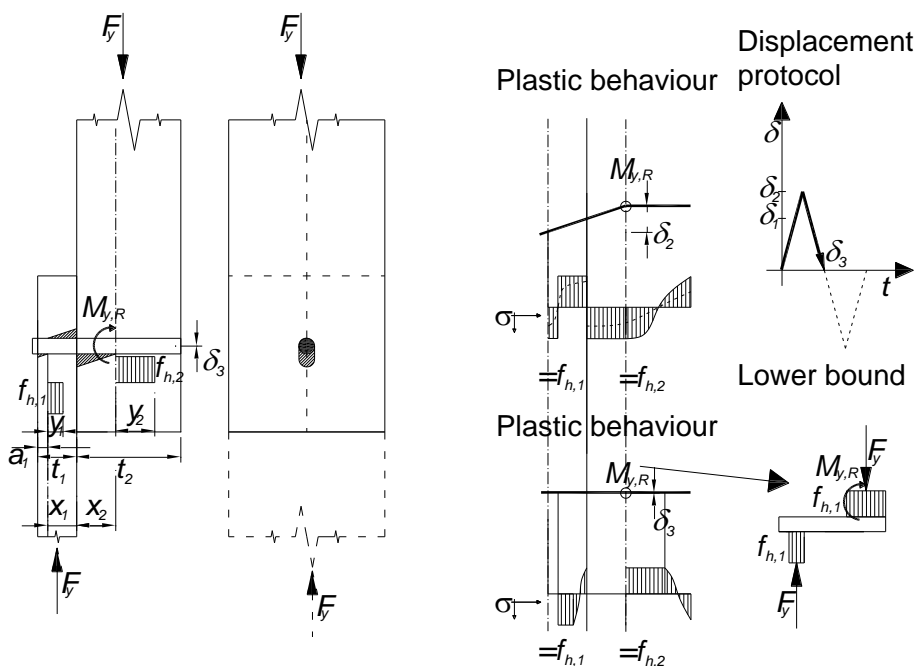


Figure 6.11 Restoring situation of fastener in single shear panel-to-timber connection

Eq. (6.20) brings in the parameter x_1 , defined by the analytical model of Johansen (1949) and subsequently calibrated according to the European Yield Model (EYM) (Eq. (6.21)).

$$x_1 = \frac{t_1}{2 + \beta} \left[\sqrt{2\beta(1 + \beta) + \frac{4\beta(2 + \beta)M_{y,Rk}}{f_{h,k,1} d t_1^2}} - \beta \right] \quad (6.21)$$

In conclusion, by manipulating and simplifying, we estimate the dimensionless ratio σ_F by Eq. (6.22) as follows:

$$\sigma_F = \frac{F_f}{F_y} = \frac{f_{h,k,1} dy_1}{f_{h,k,1} dx_1} = \frac{y_1}{x_1} \quad (6.22)$$

Therefore:

$$\sigma_F = \frac{y_1}{x_1} = \frac{(2+\beta)}{2(\beta-1)} + \frac{t_1\beta}{2(\beta-1)} - \frac{1}{2(\beta-1)} \sqrt{\left(\frac{t_1}{x_1}\beta + \beta + 2\right)^2 + \frac{8M_{y,Rk}\beta(1-\beta)}{f_{h,k,1}dx_1}} \quad (6.23)$$

Consistent with the EYM (Eurocode 5, CEN 2004a), parameter σ_F calculated using the expression (6.23) should be amplified with a calibration coefficient equal to 1.05. The calibration coefficient increases the theoretical capacity of the connector by 5%, so as to reduce the gap between the analytical model and experimental results.

For the other model parameters k_{rc} , μ_δ and δ_y , the reader is referred to the data available in the bibliography in accordance with the EYM model.

For the three situations covered in Chapter 4 labelled as *Protocol I*, *Protocol II* and *Protocol III*, it is possible to identify the equivalent viscous damping value of the single nail, $\xi_{eq,dowel}$ by solving the same equations (Eq. 4.35÷Eq. 4.44).

In accordance with the strain model assumed for the estimation of the design displacement, Δ_d , we can calculate the equivalent viscous damping to a simple linear combination of all the connectors that define the capacity of the single framed panel. From the analytical model employed for each *shear wall* we have a uniform slip and a force that are equally divided over every nail.

Without recourse to Jacobsen's formula it is possible to estimate the damping of the system (*shear walls*) directly from the linear combination of dampings associated with each connection. The expression for the combination of structural systems composed of elements with different capacities, proposed by Priestley *et al.* (2007) for the generic case, specializes in the case of a *shear wall* in Eq.(6.24):

$$\xi_{eq,wall} = \frac{\sum_{i=1}^{N_{nails}} \xi_{eq,i,dowel}(\mu_{\delta_i}) F_i \delta_{u,i}}{\sum_{i=1}^{N_{nails}} F_i \delta_{u,i}} = \quad (6.24)$$

wherein F_i , $\delta_{u,i}$, μ_{δ_i} and $\xi_{eq,i,dowel}$ are respectively the design force, the ultimate slip, the ultimate slip ductility and the equivalent viscous damping of the i^{th} nail in the *shear wall*, while N_{nails} is the number of “resisting” connectors.

Eq. (6.20) simplifies to Eq. (6.21):

$$\xi_{eq,wall} = \frac{\xi_{eq,dowel}(\mu_{\delta}) \sum_{i=1}^{n_{nails}} F_i \delta_{u,i}}{\sum_{i=1}^{n_{nails}} F_i \delta_{u,i}} = \xi_{eq,dowel}(\mu_{\delta}) \quad (6.25)$$

Eq. (6.24) performs a weighted average on the dissipation capacity of each structural element in the design situation. The model of Priestley *et al.* (2007) applies to the case of *shear walls* since the elastic deformation component ($\Delta_v + \Delta_b$) is negligible compared to the inelastic (Δ_n) (ULS condition).

The Equivalent Viscous Damping of *shear walls*, in the ultimate situation (ξ_{eq}) is equal to the equivalent viscous damping of a single nail ($\xi_{eq,dowel}$), regardless of the number of connectors in the walls.

6.3.4 Non-linear model for wood shear walls buildings

The response to the horizontal actions of multi-storey buildings with a *wood frame* system is strongly influenced by the capacity of a single wall in the main direction, defined by the addition of the load-displacement curves ($F-\Delta$) of the sheathing panels that compose the wall (*shear walls*) (Prion 2003). The following pages briefly outline the state-of-the-art on non-linear numerical models implemented to study the lateral load-displacement relationship of *shear walls*.

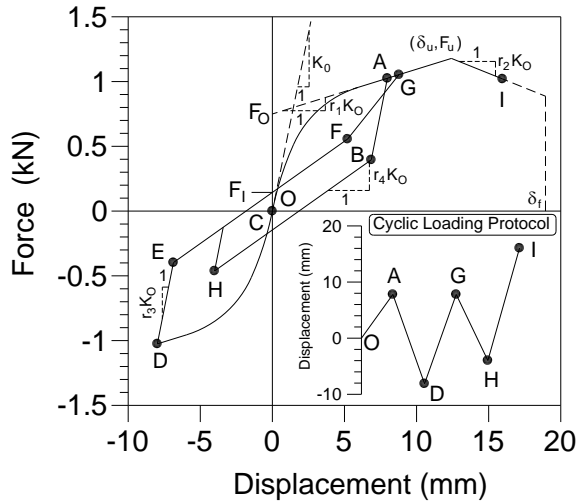
In the past three decades, several experimental tests and analytical studies have been performed on timber *shear walls*, and numerical models have been proposed to describe them. A general overview on the available numerical models to describe the dynamic response of *shear walls* was published recently by Ashraf (2007).

Nowadays, a large number of numerical models with different levels of complexity are available to predict the static racking response of wood *shear walls*, but only a few consider all dynamic effects. In general, the models use the finite element algorithm to model the behaviour of each element that makes up *shear walls*, such as: sheathing panels, framing members and sheathing-to-framing connectors, and to model the local deformation of all of these contributions. Some of these models are described in Filiatrault *et al.* (2003) and in Ashraf (2007). Obviously, these models are very sophisticated and can well reproduce the overall behaviour of the panel as deformation increases. On the other hand, the complexity in defining each parameter of the model and the computational time required to analyze a complex structure make these models rarely used outside of scientific research.

The model currently accepted within scientific community to represent the dynamic behaviour of *shear walls* is the CASHEW (Cyclic Analysis of wood SHEar Walls) model proposed by Folz and Filiatrault (2001a,b). In the CASHEW model the non-linear load-displacement hysteretic curve is modelled with an SDOF spring described with ten parameters. The monotonic load-displacement response is well-described with only five parameters. The ascending branch of the load-displacement curve in the CASHEW model is based on Foschi's curve proposed in 1977 (Foschi 1977) for the evaluation of nailed connections. In general, parameters are estimated in function of outcomes of test data, performed on *shear wall* specimens.

The model was originally validated by the comparison of the prediction of the numerical value of the load-displacement curve and numerical data extracted from full-scale shaking tests. The model was later improved to extend its applicability to general *wood frame* buildings. The CASHEW load-displacement model is shown in Figure 6.12, for the single panel-to-frame connection. The CASHEW model is based on the assumption of rigid timber frame elements, bracing panels with linear-elastic behaviour and panel-to-frame connections with non-linear behaviour, described by an equivalent single degree of freedom model (Folz and Filiatrault 2001a,b).

CASHEW model: SDOF representation of shear walls.
Hysteretic behaviour described with ten parameters. Backbone behaviour described with five parameters



Equation of Envelope Load-displacement curve of CASHEW Model:

$$F = \begin{cases} \operatorname{sgn}(\delta)(F_0 + r_1 k_0 |\delta|) [1 - \exp(-k_0 |\delta| / F_0)] & |\delta| \leq |\delta_u| \\ \operatorname{sgn}(\delta) F_u + r_2 k_0 [\delta - \operatorname{sgn}(\delta) \delta_u] & |\delta_u| < |\delta| \leq |\delta_F| \\ 0 & |\delta| > |\delta_F| \end{cases}$$

F , load on shearwalls δ , displacement for shearwalls

- K_0 , initial tangent stiffness r_2 , ratio of the degrading backbone stiffness to K_0 (typically a negative value)
- F_0 , resistance force parameter
- r_1 , stiffness ratio parameter of the backbone curve (typically a small positive value)
- δ_u , maximum displacement (corresponding to maximum restoring force)
- δ_F , ultimate displacement

Hysteretic behaviour with required ten parameters: Six parameters above with the four parameters listed below

- $r_3 k_0$, stiffness in unloading path (typically close to 1)
- α , hysteretic model parameter for stiffness degradation (usually takes a value between 0.5-0.9)
- $k_p = k_0 \left(\frac{\delta_0}{\delta_{\max}} \right)^\alpha$ with $\delta_{\max} = \beta \delta_{un}$ with δ_{un} as the last unloading displacement
- β , another hysteretic model parameter (usually takes a value between 1.01-1.5).
- $\delta_0 = F_0 / k_0$ and
- $r_4 F_0$, reduced stiffness in unloading path (typically under 0.1)

Figure 6.12 Description of the CASHEW model (modified from Filiatrault and Folz 2002)

The response of a connector under monotonic loading is modelled by the non-linear load-deformation curve originally proposed by Foschi (1977). In the original version of the CASHEW model only the stiffness degradation was included. Recently, this model has been refined to replicate as best as possible the actual behaviour of the shear wall panel.

The final release of the CASHEW program includes the ability to study the generic multi-storey structural system with a system platform frame and was included in the SAWS (Seismic Analysis of Wood Structures) calculation software for wooden structures. The SAWS software was developed during the CUREE-Caltech Woodframe Project (Folz and Filiatrault 2003). The SAWS model assumes that, along a defined direction, all the wood *shear walls* exhibit the same lateral displacement. Therefore, the final response of a multi-degree-of-freedom system (MDOF) is simply the mechanical addition of the response of each *shear wall*. In SAWS, the building structure response is decomposed by two primary components: rigid horizontal diaphragms and the non-linear lateral load resisting system (*shear wall* elements). The actual three-dimensional behaviour of a building is represented in a two-dimensional planar model with only three-degrees-of-freedom per floor, using zero-height *shear wall* spring elements connected between the diaphragms and the foundation. The hysteretic behaviour of the CASHEW model takes account of the pinching effect, the strength degradation and the stiffness degradation. A new version of SAWS (version 2) was developed by researchers at SUNY Buffalo during the NEESWood project and includes modifications of the code to incorporate modelling of viscous damping elements such as rubber systems or isolator systems.

A more detailed description of the CASHEW model can be found in Folz and Filiatrault (2001), while for the SAWS program we refer to Folz and Filiatrault (2003) and Folz and Filiatrault (2004a,b).

Models used to evaluate the non-linear hysteretic behaviour of *shear walls*, such as Folz and Filiatrault (2001), consider only the stiffness degradation and strength reduction and no other typical degradation of wooden structures. In this way the complexity of the model is limited and a direct analytical interpretation is possible. A numerical model of *shear walls* that considers all types of degradation was presented recently by Ashraf (2007).

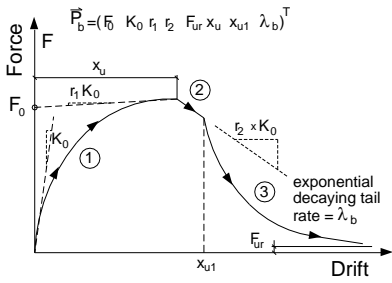
The proposed *shear wall* response curve takes into account the degradations observed in experimental testing, such as strength degradation (decrease of yielding force), unloading stiffness degradation (decreases as a function of the number of cycles), accelerated stiffness degradation (in reloading the target stiffness decreases) and cap degradation (onset of strength softening is reached earlier). The numerical model proposed by Ashraf (2007) can be easily added to the normal library of commercial finite element packages. The degrading constitutive laws are based on a four-parameter peak-oriented pinched hysteretic model. The parameters of degradation are calibrated from experimental data using an equivalent energy approach.

Nowadays a new "SAPWood" program is available (Pei and van de Lindt 2007) in which a new hysteretic model is implemented called the "Evolutionary Hysteretic Parameter Model" (EPHM). The SAPWood program was developed during the three-year research project called "NEESWood". The SAPWood program is the natural extension of the CASHEW and SAWS software, and was developed by NEESWood team to create a user-friendly tool to evaluate seismic effects on a timber *wood frame* building. SAPWood software runs the common seismic analyses such as single and multi-record uni/bi-directional incremental dynamic analysis (IDA), traditional nonlinear time domain analysis (NLTHA) and uni/bi-directional incremental mass analysis (IMA), system identification and loss analysis. The SAPWood program is capable of utilizing an array of hysteretic spring elements, ranging from linear spring, ten parameter element (CUREE) to the 16-parameter evolutionary hysteretic parameter model spring. More details of this program package are available in its user's manual (Pei and van de Lindt 2007).

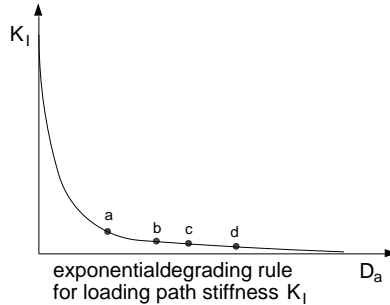
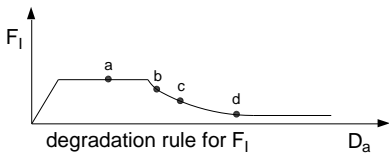
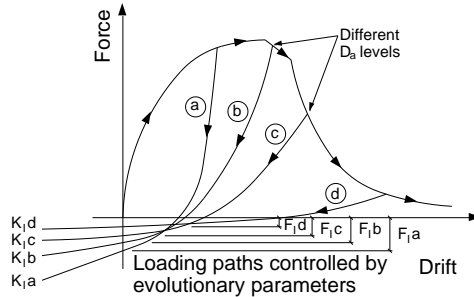
Each of the numerical models presented above is difficult to use directly in the design process: These models are much more useful to verify the structural system when details of elements, geometry and material properties are well known. Numerical models are very useful for performing validation of the proposed analytical model to evaluate the load-displacement curve, $F-\Delta$, of the single panel and its dissipative properties for a given load history.

Numerical models developed for the *shear wall* are various and have reached a satisfactory level of accuracy, in terms of reliability and prediction of experimental results. Thus, this work considers the state of development of *shear wall* elements.

EPHM Model backbone curve



Loading paths at different damage levels (a,b,c and d) follows different boundary conditions defined by dynamic parameters F_I and K_I



F- δ curve

F restoring force

δ , displacement

The 16 hysteretic parameters

$F_{I,r}$, minimum value of the residual pinching force in severe damage stage. A local parameter for evolutionary parameter F_I .

DF1a, tracking damage index (average maximum drift) corresponding to the starting point of the plateau portion of the F_I degrading function. $F_{I,II}$ varies linearly before this point.

DF1b, tracking damage index (average maximum drift) corresponding to the end point of the plateau portion of the F_I degrading function. F_I degrades exponentially after this point.

F_{ur} , residual resistance force value of the backbone in severe damage stage.

β , strength degradation parameter, usually takes a value between 1.01~1.5.

r_{4r} , ratio of the residual K_I value to initial stiffness.

K_0 , initial tangent stiffness

F_0 , resistance force parameter of the backbone

r_1 , the stiffness ratio parameter of the backbone (typically be a small positive value).

x_u , the drift corresponding to the maximum restoring force of the backbone curve.

r_2 , the ratio of the degrading backbone stiffness (linear portion) to K_0 , typically a negative value

x_{u1} , the drift corresponding to the end of the linear portion of the degrading backbone. The backbone degrades exponentially after this point.

P_1 , the exponential degrading rate parameter of the backbone, λ_b .

$F_{I,m}$, maximum value that the residual pinching force can reach. A local parameter for evolutionary parameter F_I (residual pinching force).

p_{F1} , the exponential degrading rate parameter of the F_I degradation function.

p_{r4} , the exponential degrading rate parameter of the K_I (the tangent stiffness at the point where loading paths intersect with the Y axis) degradation function.

Figure 6.13 Evolutionary Hysteretic Parameter Model (EPHM) developed during the NEESWood project (modified from Pei and van de Lindt 2007)

6.4 Comparison of results for the proposed analytical model

The analytical model to predict the design parameters of *shear walls* has been tested on a series of *shear walls* covered with full-size wood-based sheathing panels. The estimated values with the analytical expressions proposed in the previous sections are compared with results from tests on an ensemble of *shear walls*. The walls are made with 2.44 m x 1.22 m OSB (Oriented Strand Board) sheathing panels 11 mm thick and connected to nominal 50 mm x 100 mm Hem-Fir studs spaced at 400 mm on-centre using 8d common nails (63.5 mm long x 3.3 mm diameter) (Figure 6.14 (a)). Nails are arranged at variable distances in the range 50÷150 mm along the external perimeter and 300 mm on the inside of the panel.

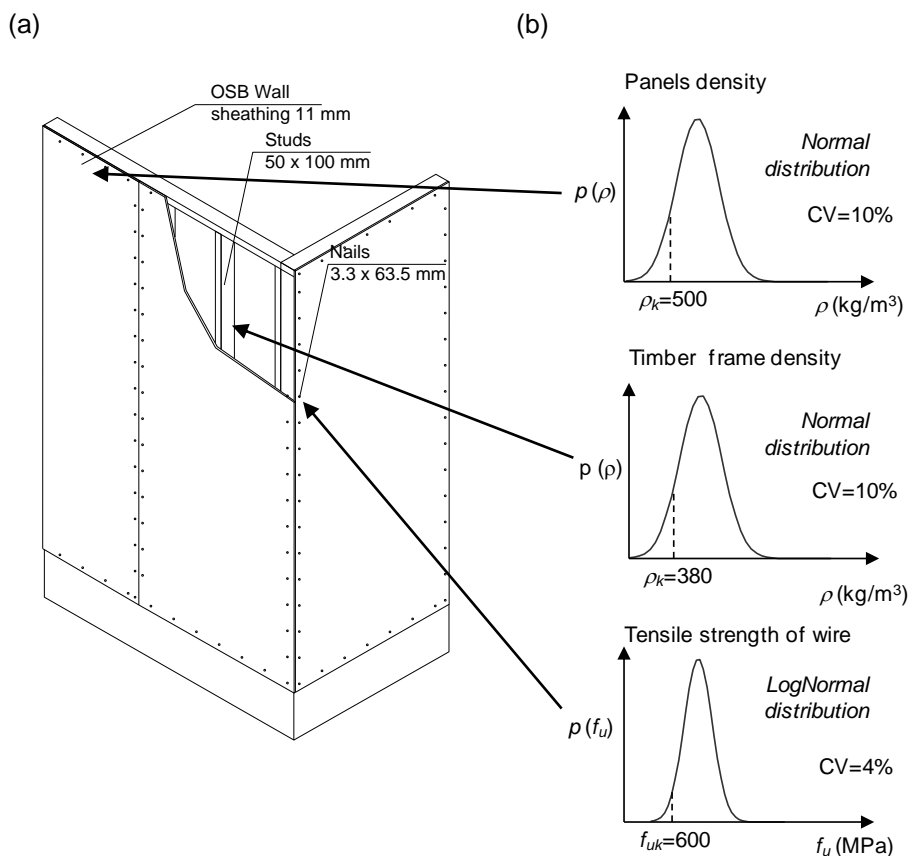


Figure 6.14 (a) Shear wall structure; (b) Mechanical parameters with defined probability density functions

The design parameters of *shear walls* were estimated during the NEESWood project (Pang and Rosowsky 2007).

Table 6.1 lists the numerical values that implement the envelope curve for the selected *shear walls*. The values were calibrated according to the CASHEW model (Folz and Filiatrault 2001a,b), presented in the previous Section, based on the experimental values. The envelope force-displacement ($F-\Delta$) curve of the panels is described by Eq. (6.26) which represents the upper limit of the cyclic response as measured by the CASHEW model (the so-called backbone curve of Figure 6.15(a)).

$$F_b(\delta) = \begin{cases} \left[1 - e^{-\frac{k_0}{F_0}\delta} \right] (r_1 k_0 \delta + F_0) & \text{for } \delta \leq \delta_u \\ F_u + r_2 k_0 (\delta - \delta_u) & \text{for } \delta > \delta_u \end{cases} \quad (6.26)$$

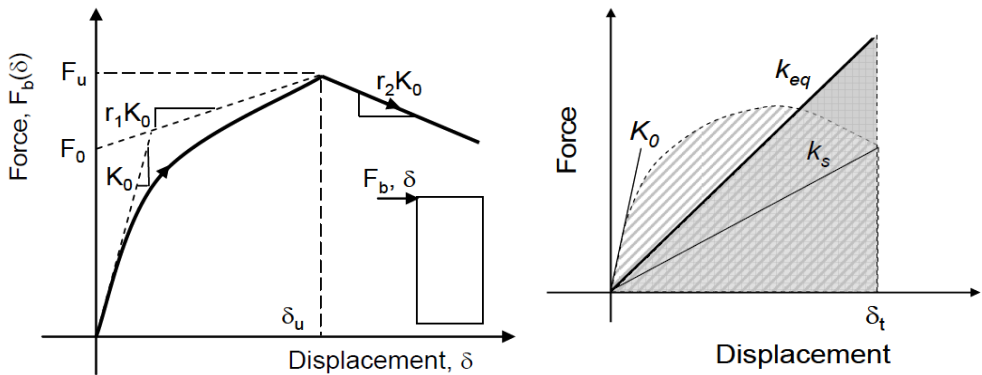


Figure 6.15 (a) Shearwall backbone curve parameters; (b) Equivalent linearization of non-linear backbone curve (modified from Pang and Rosowsky 2007)

The comparison parameters for testing the analytical model proposed in Chapter 4 are the ultimate displacement and, for consistency, the strength capacity in each *shear wall*. The displacement and load-bearing capacity of each *shear wall* are calculated using hypothetical mean values for the mechanical properties.

The properties of the timber elements, wood-based panels and connections are expressed by probability density functions, in accordance with the “Probabilistic Model Code” proposed by the Joint Committee on Structural Safety (JCSS 2007).

The density of the timber elements of the frame and wood-based sheathing panels are expressed by a normal curve and a coefficient of variation (COV) equal to 10%, while the tensile strength of the steel wire of the nails has a lognormal distribution with a coefficient of variation of 4%. The curves are anchored to the characteristic value of 380 kg/m³, 500 kg/m³ and 600 MPa, respectively, for the elements of timber frame, sheathing panels and tensile strength of steel wire (Figure 6.14(b)).

Table 6.1 Backbone numerical parameters for shear walls built with different configurations of connectors (selection from Pang and Rosowsky 2007)

Panel Width	Nail Spacing ext/int	Panel ID	k_0 , backbone	r_1 , backbone	r_2 , backbone	δ_u , backbone = Δ_d	F_0 , backbone	$F_{V,w}$, backbone
(m)	(mm)	(-)	(kN/mm)	(-)	(-)	(mm)	(kN)	(kN)
0.76	50/300	c1	1.34	0.04	-0.083	104	18.9	24.5
0.76	75/300	c2	1.12	0.038	-0.07	100	13	17.3
0.76	100/300	c3	0.95	0.037	-0.062	97	9.9	13.3
0.76	150/300	c4	0.73	0.035	-0.055	94	6.7	9.1
0.91	50/300	c5	1.73	0.042	-0.096	91	24.6	31.2
0.91	75/300	c6	1.43	0.042	-0.075	85	16.1	21.2
0.91	100/300	c7	1.21	0.041	-0.066	83	12.1	16.2
0.91	150/300	c8	0.94	0.039	-0.055	80	8.2	11.1
1.22	50/300	c9	2.51	0.037	-0.126	74	37.1	43.7
1.22	75/300	c10	2.18	0.042	-0.099	70	24.8	31.2
1.22	100/300	c11	1.91	0.043	-0.083	67	18.7	24.1
1.22	150/300	c12	1.55	0.042	-0.07	64	12.9	17.1

Table 6.2 shows the benchmarks expressed in terms of load-carrying capacity of each *shear wall* ($F_{V,w}$) and design displacement (Δ_d) (equal to ultimate displacement).

The error in the estimation of parameters is summarized in Table 6.3. The outcomes show good prediction of the design parameters, based on the average value of the mechanical properties of the elements.

EXTENSION OF DIRECT-DBD METHOD TO OTHER TIMBER BUILDINGS

Figure 6.16 shows the force-displacement curves for each *shear wall* and the analytical estimate of the design situation (ultimate state of *shear walls*) expressed by the coordinate points $(\Delta_d, F_{V,w})$ for each geometric configuration of the *shear walls*.

Table 6.2 Comparison between backbone parameters and estimated parameters for the selected shear walls

Panel Width	Nail Spacing ext/int	Panel ID	Design displacement			Load-carrying capacity		
			¹ Δ_d , NZS 3603 &	³ Δ_d ,	⁴ Δ_d ,	⁵	⁶ $F_{V,w}$,	⁷ $F_{V,w}$,
			² Δ_d , JUDD & FONSECA	YASUMURA	TESTS	$F_{V,w}$, EC5	PROPOSAL	TESTS
(m)	(mm)	(-)	(mm)	(mm)	(mm)	(kN)	(kN)	(kN)
0.76	50/300	c1	99.48	102.15	104	28.52	21.32	24.5
0.76	75/300	c2	95.78	100.46	100	19.01	14.21	17.3
0.76	100/300	c3	93.72	99.51	97	14.26	10.66	13.3
0.76	150/300	c4	91.56	98.51	94	9.51	7.11	9.1
0.91	50/300	c5	88.17	88.30	91	34.15	30.56	31.2
0.91	75/300	c6	84.25	86.33	85	22.76	20.38	21.2
0.91	100/300	c7	82.30	85.35	83	17.07	15.28	16.2
0.91	150/300	c8	80.30	84.34	80	11.38	10.19	11.1
1.22	50/300	c9	73.04	70.94	74	45.78	54.93	43.7
1.22	75/300	c10	69.85	69.11	70	30.52	36.62	31.2
1.22	100/300	c11	68.04	68.07	67	22.89	27.47	24.1
1.22	150/300	c12	66.26	67.04	64	15.26	18.31	17.1

LEGEND:

¹ Design displacement estimated with modified New Zealand timber-strand NZS 3603 (New Zealand Standard 1993) model.

² Design displacement estimated with modified Judd and Fonseca (2006) model.

³ Design displacement estimated with modified Yasumura (2000) model.

⁴ Design displacement calibrated using CASHEW program with shear wall test data.

⁵ Load-carrying capacity estimated with Eurocode 5 and 8 final version EN (CEN 2004a, 2004b).

⁶ Load-carrying capacity estimated with proposed formula.

⁷ Load-carrying capacity calibrated using CASHEW program with shear wall test data.

Table 6.3 Error in evaluation of shear wall design parameters

Panel Width	Nail Spacing ext/int	Panel ID	Error in design displacement			Error in load-carrying capacity	
			$E\Delta_d$	$E\Delta_{d,JUDD \& FONSECA}$	$E\Delta_d$	$E_{FV,w,EC5}$	${}^5E_{FV,w, PROPOSAL}$
			YASUMURA	FONSECA	NZS 3603	(%)	(%)
(m)	(mm)	(-)	(%)	(%)	(%)	(%)	(%)
0.76	50/300	c1	1.78%	4.34%	4.34%	-16.40%	12.99%
0.76	75/300	c2	-0.46%	4.22%	4.22%	-9.89%	17.85%
0.76	100/300	c3	-2.59%	3.38%	3.38%	-7.21%	19.86%
0.76	150/300	c4	-4.80%	2.60%	2.60%	-4.46%	21.91%
0.91	50/300	c5	2.97%	3.11%	3.11%	-9.44%	2.04%
0.91	75/300	c6	-1.57%	0.88%	0.88%	-7.38%	3.89%
0.91	100/300	c7	-2.83%	0.85%	0.85%	-5.39%	5.67%
0.91	150/300	c8	-5.42%	-0.38%	-0.38%	-2.54%	8.22%
1.22	50/300	c9	4.13%	1.30%	1.30%	-4.76%	-25.71%
1.22	75/300	c10	1.27%	0.21%	0.21%	2.18%	-17.38%
1.22	100/300	c11	-1.60%	-1.56%	-1.56%	5.02%	-13.97%
1.22	150/300	c12	-4.75%	-3.53%	-3.53%	10.76%	-7.08%

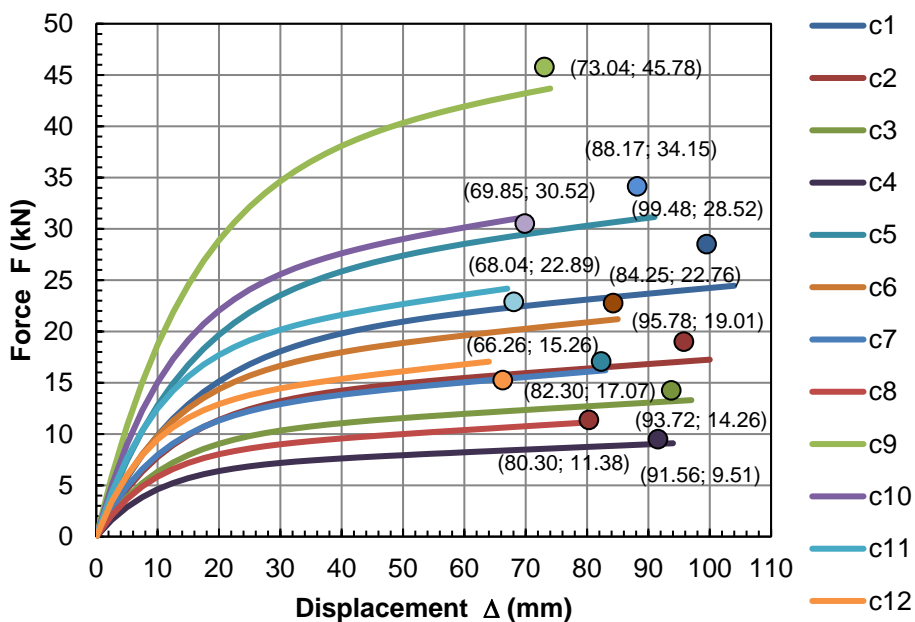


Figure 6.16 Backbone curve for a set of shear walls and in dots the corresponding design force/displacement analytical evaluation (adopted Judd & Fonseca modified model)

From the experimental values reported in Table 6.4 it is not possible to directly obtain the equivalent viscous damping for both load conditions, *Protocol II* and *Protocol III*, since they were tailored according to the envelope load-displacement curve of the panels. Thus, hereinafter we refer to the results obtained by Filiatrault *et al.* (2003, 2004) for the whole behaviour of *wood frame* buildings.

Table 6.4 Equivalent stiffness, k_{eq} (kN/mm) at target drift (% of wall height) for shear walls built with different configurations of connectors (selection from Pang and Rosowsky 2007)

Panel Width	Nail Spacing ext/int	Panel ID	0.5	1.0	1.5	2.0	2.5	3.0
(m)	(mm)	(-)	(%)	(%)	(%)	(%)	(%)	(%)
0.76	50/300	c1	1.05	0.85	0.71	0.6	0.53	0.47
0.76	75/300	c2	0.83	0.65	0.53	0.45	0.39	0.34
0.76	100/300	c3	0.69	0.53	0.42	0.35	0.3	0.27
0.76	150/300	c4	0.51	0.38	0.3	0.25	0.21	0.19
0.91	50/300	c5	1.36	1.1	0.92	0.79	0.69	0.61
0.91	75/300	c6	1.06	0.83	0.67	0.57	0.49	0.43
0.91	100/300	c7	0.87	0.66	0.53	0.44	0.38	0.33
0.91	150/300	c8	0.64	0.48	0.38	0.31	0.27	0.23
1.22	50/300	c9	1.98	1.61	1.35	1.16	1.01	0.9
1.22	75/300	c10	1.62	1.26	1.03	0.87	0.75	0.66
1.22	100/300	c11	1.36	1.03	0.83	0.69	0.59	0.52
1.22	150/300	c12	1.04	0.77	0.61	0.5	0.43	0.37

In the analytical model formulated, the evaluation of the Equivalent Viscous Damping is independent of the geometric configuration of the connections. Thus, for the ensemble of *shear walls* selected an equivalent viscous damping value, function of the connector used, is estimated from the properties of materials and the level of slip ductility reached on the nails.

For nails with a diameter d equal to 3.3 mm and wood-based panels made of OSB, the dimensionless ratio σ_F is of 0.3536. The parameter σ_F is evaluated by solving Eq. (6.23) with the values of $f_{h,t}=35.82$ MPa, $t_t=11$ mm, $\beta=0.72$, $x_t=5.975$ mm and $M_{y,R}=4295.06$ kNm, estimated with the average values of the mechanical properties of wood and steel.

The final value of σ_F is equal to 0.3062 and discounts the effect of the correction factors 1.05 and 1.1, respectively for consistency with the EYM model (CEN 2004a) and according to the instantaneous effects that change the strength properties of wood. The other parameters are numerically estimated at $\beta_k=2$, $\mu_\delta=8$ and $\Delta\delta/\delta=0.5$. The parameter $\Delta\delta/\delta$ assumes the compatibility of the analytical model to the loading protocol provided by Krawinkler *et al.* (2000) for *shear wall* tests, and used by Filiatrault *et al.* (2004). With the numerical values above the Equivalent Viscous Damping that matches the design displacement is estimated equal to 18.01% and 29.05%, respectively for *Protocol II* and *Protocol III*.

In the work by Filiatrault *et al.* (2003, 2004), after a significant number of analyses, two analytical expressions were proposed for estimating the Equivalent Viscous Damping, ξ_{eq} , in function of inter-storey drift of the inter-building.

For values of inter-storey drift higher than 0.35%, the model of Filiatrault *et al.* (2004) assumes the damping, ξ_{eq} , to be a constant value, equal to 28% for the first cycle of loading and 18% in subsequent cycles of loading. For the sample of selected *shear walls* the values of inter-storey drift are in the range 2.6÷4.26% (Table 6.2).

For direct comparison we estimate an error in the Equivalent Viscous Damping less than 3.6% in the situation of *Protocol III* and almost nothing for the situation of *Protocol II*. The estimated numerical values agree with the results obtained from Filiatrault *et al.* (2003, 2004) for American *wood frame* buildings. It is clear that the direct comparison implicitly assumes that the damping of the whole building is identifiable with that of a *shear wall* panel. The hypothesis is true within a certain regularity of the horizontal resisting system and assuming infinitely rigid storeys (e.g. the structures studied by Filiatrault *et al.* 2003, 2004). In particular the hypothesis requires the use of *shear walls* with the same length and same mechanical and geometrical configuration.

6.5 Conclusions

The numerical values of the design parameters (in the ULS condition) for the sample of selected *shear walls* are consistent with experimental results and validate the analytical model, presented in Chapter 4 and extended in this Section, to *shear walls* elements used in a timber frame building system.

The analytical model is also suitable for the design of *shear walls* that differ from the standardized elements and is useful for estimating the expected results from experimental tests.

The model is very sensitive to the load-slip curve of the metal connector; therefore, particular attention should be given to the evaluation of the F - δ parameters.

This Chapter has shown how the method proposed in Chapter 4 can be extended to other types of structural systems.

7 SUMMARY, CONCLUSIONS AND RECOMMENDATIONS

7.1 Summary and conclusions

The Direct Displacement-Based Design method (Direct-DBD), encoded by Priestley in 2003 (2003), requires an *a priori* estimate of the displacement and of the Equivalent Viscous Damping in the design process. These two structure design parameters were evaluated for a given level of performance required under seismic conditions, in function of the seismic risk in a given area. The design procedure can be applied to wooden building types with one degree of freedom, SDOF, and can be directly extended to MDOF systems as shown in this work. The performance level to which we refer is the Life Safety Level, known in Eurocode 8 as the ultimate limit state (ULS). In the ultimate condition of the structure, design parameters can be evaluated with the solution of the equilibrium problem related to an inelastic configuration.

Practical analytical expressions to estimate design parameters were given, for the case of the *single-storey portal frame* with different geometric configurations of the beam-to-column joint, and the *wood frame* panel, often used in multi-storey buildings for residential use. The algorithm was defined starting from the mechanical model assumed for the connections.

The connections are designed to reach the maximum dissipation and ductility capacity on the connectors (DCH, Eurocode 8, CEN 2004b) and ensuring the expected failure modes. The mechanical model chosen to describe the behaviour of the connector in the inelastic range is elastic-perfectly plastic. The state-of-the-art of dowel-type connectors supports the model and demonstrates the veracity of the initial assumptions. The analytical model formulated for the single connector is accompanied by auxiliary equations for calculating the design parameters of connectors.

The classic Direct-DBD approach encoded by Priestley (2003) estimates the dissipative capacity of the structure starting from the ductility level that matches the given design displacement (Δ_d). For wooden structures the uncertainty in the definition of the yield point plays a negative role in the estimation of the Equivalent Viscous Damping (EVD, ξ_{eq}). In this work, the hysteretic model used to assess EVD has been formulated in high ductility, and therefore, is less affected by the uncertainty of the yield point defined on the connection.

The proposed analytical model to calculate Δ_d and ξ_{eq} was verified using nonlinear static and dynamic analyses on a set of characteristic cases that cover the geometric variability of the structure. In addition, a refined model, calibrated with the results of numerical nonlinear analyses, was proposed to evaluate the design displacement and the EVD for the case of the *single-storey portal frame*.

We present guidelines for extending the analytical model to other geometric configurations or types of wooden structures with dowelled connections. The wood frame building with platform frame technology was presented as a *multiple degrees of freedom* (MDOF) case study. The correspondence between the experimental data collected and the numerical prediction by the proposed model, for a series of typical configurations, testified the model validity.

This work is based on the results of experiments showing that the plastic resources and dissipative capabilities of wooden structures exposed to earthquakes are ensured by the connections between the members. Therefore the inelastic deformation of the structure is assumed to be concentrated at the joints and is calculated according to the mechanical model (load-slip curve) of the connectors and the arrangement of the connectors within the joints. The expected non-linear response of the connection is either ductile or brittle as a function of the geometry and the strength characteristics of the materials. However, in the design process we can impose and control the mechanical behaviour expected of the joint.

This research extends the application of Direct Displacement-Based Design to wooden structures. Part of the research presented in this thesis was developed to support research line IV of the **RELUIS** project (**RE**te dei **L**aboratori **U**niversitari di **I**ngegneria **S**ismica), funded with the contribution of the Italian National Civil Protection Department. The final result of Line IV of the **RELUIS** project was the draft model code (DBD09) for the design of structures based on criteria expressed in terms of displacement and presented by the authors Calvi and Sullivan (2009). The part of DBD09 regarding wooden structures is based on early results of this research. A workbook containing design case studies resolved by the Direct-DBD approach is in press with expected publication in 2011.

In the future version of the code DBD09, the section dedicated to wooden structures will be improved with all the results of this research.

7.2 Future work

The formulation of the Direct-DBD method is consistent with the state-of-the-art of wooden structures and in particular of the connections. The possibility of immediate extension of the design algorithm to other kinds of structure, differing from that reported here, is an attractive aspect of the formulated method.

The extension process has some aspects which require further consideration. The design algorithm, though supported by numerical validation, needs further investigation in order to refine the reliability of results. Future amendment of the calibration coefficients for the cases studied cannot be excluded.

The positive results presented in this study should not lead to unconditional application of the method, without some precautionary measures. In particular, the deformed configuration of equilibrium from which we start to estimate the design parameters must be ensured. To achieve this objective, a series of design recommendations according to the principle of Capacity Design should be drawn up, similar to those available for other structural materials.

In addition, a detailed analysis of the dissipative capacity evaluation method for connections with dowel-type metal fasteners, may help to increase the reliability of the numerical and analytical model. In the literature there are several numerical models, some complex, generally developed for a given structure or wooden connection. The author is convinced that the commitment of the scientific community to drafting guidelines or protocols, to be followed during development of numerical models, can help us share results efficiently, as is already the case for tests.

Finally, we consider that full use of the scientific method with monitoring of prediction efficiency can help in achieving a calculation model for use as a rational design tool.

BIBLIOGRAPHY

Allotey, N. K. 1999. "A model for the response of single timber fasteners and piles under cyclic and dynamic loading." PhD Thesis, University of British Columbia, Vancouver, Canada.

American Forest and Paper Association. 2001. *Details For Conventional Woodframe Construction*. Washington: American Wood Council, 55pp.

APA. 2007. *Engineered Wood construction guide*. Washington: APA – The Engineered Wood Association, 80pp.

Ashraf, A. 2007. "Seismic analysis of wood building structures." *Engineering Structures* 29(2): 213-223.

ASTM. 2006. *D1761: Standard Test Methods for Mechanical Fasteners in Wood*. West Conshohocken. PA, USA: American Society for Testing and Materials International (ASTM).

Augustin, M. 2008a. "Wood Based Panels." In *Handbook 1 Timber Structures*. Ostrava: Leonardo da Vinci Pilot Project (TEMTIS Project).

Augustin, M. 2008b. "Ultimate Limit State - Joints." In *Handbook 1 Timber Structures*. Ostrava: Leonardo da Vinci Pilot Project (TEMTIS Project).

Australian Standard. 2001. *AS1649: Timber—Methods of test for mechanical fasteners and connectors—Basic working loads and characteristic*. Sydney, Australia: Standards Australia International.

Binderholz. 2010. "Cross laminated timber BBS." Accessed June 2010. <http://www.binderholz.com/>.

Blandon, A. C., and Priestley, M. J. N. 2005. "Equivalent viscous damping equations for direct displacement based design." *Journal of Earthquake Engineering* 9(si2): 257-278.

BIBLIOGRAPHY

Blass, H. J. 1994. "Characteristic strength of nailed joints." *Forest Products Journal* 44(4): 33-39.

Blass, H. J., Bienhaus, A., and Kramer, V. 2000. "Effective bending capacity of dowel-type fasteners." Paper presented at the 33th Meeting, International Council for Research and Innovation in Building and Construction, Working Commission W18 - Timber Structures, Delft, The Netherlands, August 28-30.

Buchanan, A., Deam, B., Fragiacomio, M., Pampanin, S., and Palermo, A. 2008. "Multi-Storey Prestressed Timber Buildings in New Zealand." *Structural Engineering International* 18(2): 166-173.

Calvi, G. M., and Sullivan, T.J. 2009. *A Model Code for the Displacement-Based Seismic Design of Structures*. Pavia, Italy: IUSS Press, 70pp.

Calvi, G. M. editor. 2003. *Displacement-Based Seismic Design of Reinforced Concrete Buildings*. Lausanne, Switzerland: fib Bulletin 25, 192pp.

Ceccotti, A. 1995. "Conessioni nelle strutture di legno soggette ad azioni sismiche." In *Manuale del legno strutturale*, edited by Uzielli L. Italy: Mancosu Editore Press.

Ceccotti, A., and Touliaatos., P. 1995. "Progettazione delle strutture di legno in zona sismica." In *Manuale del legno strutturale*, edited by Uzielli L. Italy: Mancosu Editore Press.

Ceccotti, A., and Vignoli, A. 1989. "A hysteretic behaviour model for semi-rigid joints." *European Earthquake Engineering Journal* 3: 3-9.

Ceccotti, A., and Vignoli, A. 1990. "Engineered Timber Structures. An Evaluation of their seismic behaviour." Paper presented at the International Timber Engineering Conference, Tokyo, Japan, October.

CEN. 1991. *EN 26891: Timber structures - Joints made with mechanical fasteners - General principles for the determination of strength and deformation characteristics (ISO 6891:1983)*. Belgium, Bruxelles: European Committee for Standardization.

CEN. 1993. *EN 20898-2: Mechanical properties of fasteners - Part 2: Nuts with specified proof load values - Coarse thread (ISO 898-2:1992)*. Belgium, Bruxelles: European Committee for Standardization.

CEN. 2000. *EN 14080: Timber structures. Glued laminated timber. Requirements*. Belgium, Bruxelles: European Committee for Standardization.

- CEN. 2001. *EN 12512: Timber Structures-Test methods-Cyclic testing of joints made with mechanical fasteners*. Belgium, Bruxelles: European Committee for Standardization.
- CEN. 2004a. *Eurocode 5: Design of timber structures. Part 1-1: General -Common rules and rules for buildings*. Belgium, Bruxelles: European Committee for Standardization.
- CEN. 2004b. *Eurocode 8: Design of structures for earthquake resistance. Part 1-1: General rules, seismic actions and rules for buildings*. Belgium, Bruxelles: European Committee for Standardization.
- CEN. 2004c. *EN 10025: Hot rolled products of structural steels-Part 1: General technical delivery conditions*. Belgium, Bruxelles: European Committee for Standardization.
- CEN. 2007. *EN 383: Timber Structures-Test methods-Determination of embedment strength and foundation values for dowel type fasteners*. Belgium, Bruxelles: European Committee for Standardization.
- Cheung, Kevin C. K. 2008. "Case Studies of Multi-Storey Wood-Frame Construction in USA." *Structural Engineering International* 18(2): 118-121.
- Chopra, A. K. 1995. *Dynamics of Structures: Theory and Applications to Earthquake Engineering*. New Jersey: Prentice-Hall, Inc.
- Chui, Y. H, and Yantao, L. 2005. "Modelling Timber Moment Connection under Reversed Cyclic Loading." *Journal of Structural Engineering* 131(11): 1757-1763.
- Chui, Y. H., and Smith, I. 1990. "Quantifying damping in structural timber components." Paper presented at the 2th Pacific Timber Engineering Conference Auckland, New Zealand, August 28-31.
- COST. 2004. "Proposal for the PROBABILISTIC MODEL CODE FOR DESIGN OF TIMBER STRUCTURES." E24-Reliability analysis of timber structures Web-publication, draft proposal by Köhler, J., and Faber, M. H. <http://www.km.fgg.uni-lj.si/coste24/coste24.htm>.
- Cramer, C. O. 1968. "Load distribution in multiple-bolt tension joints." *Journal of the Structural Division (ASCE)* 94(5): 1101-1117.
- CS.LL.PP. 2008. *DM 14 Gennaio, Norme tecniche per le costruzioni*. Italy: Gazzetta Ufficiale della Repubblica Italiana 29 (Italian version).

BIBLIOGRAPHY

CS.LL.PP. 2009. *Istruzioni per l'applicazione delle norme tecniche delle costruzioni*. Italy: Gazzetta Ufficiale della Repubblica Italiana 29 (Italian version).

Curee. 2008. "Consortium of Universities for Research in Earthquake Engineering: Caltech Woodframe Project." last updated 2004. <http://www.curee.org/projects/woodframe/>.

Dolan, J. D. 1989. "The dynamic response of timber shear walls." PhD Thesis, Department of Civil Engineering, University of British Columbia, Vancouver, BC, Canada.

Dolan, J. D. 1994. "Timber structures in seismic regions RILEM State-of-the-art Report." *Materials and Structures* 27: 157-184.

Dolan, J. D. 1995. "Cyclic lateral dowel connection tests for seismic and wind evaluation." Paper presented at the 28th Meeting, International Council for Research and Innovation in Building and Construction, Working Commission W18 - Timber Structures, Copenhagen, Denmark, April.

Dowell, R. K., Seible, F., and Wilson, E. L. 1998. "Pivot hysteresis model for reinforced concrete Members." *Structural Journal(ACI)* 95(5): 607-617.

Elishakoff, I. 2003. "Notes on Philosophy of the Monte Carlo Method." *International Applied Mechanics* 39(7): 753-762.

FEMA. 2000. *Prestandard and Commentary for the Seismic Rehabilitation of Buildings, FEMA 356*. Washington, DC: Federal Emergency Management Agency.

FEMA. 2010. "Federal Emergency Management Agency." Last modified August 2010. <http://www.photolibrary.fema.gov/photolibrary/index.jsp>.

Filiatrault, A., and Folz, B. 2002. "Performance-Based Seismic Design of Wood Framed Buildings." *Journal of Structural Engineering* 128(1): 39-47.

Filiatrault, A., and Folz, B. 2006. "Displacement-Based Seismic Design of Light-Frame Wood Buildings." Paper presented at the 9th World Conference on Timber Engineering, Portland, Oregon, USA, August 6-10.

Filiatrault, A., Epperson, M., and Folz, B. 2004. "Equivalent Elastic Modeling for the Direct-Displacement-Based Seismic Design of Wood Structures." *Journal of Earthquake Technology (ISET)* 41: 75-99.

Filiatrault, A., Isoda, H., and Folz, B. 2003. "Hysteretic damping of wood framed buildings." *Engineering Structures* 25: 461-471.

- Finnforest. 2009. "Kerto portal frames." Last modified February 2009. www.finnforest.co.uk.
- Foliente, G. C. 1993. "Stochastic Dynamic Response of Wood Structural Systems." PhD Thesis, Virginia Polytechnic Institute and state University, Blacksburg.
- Foliente, G. C. 1995. "Hysteresis modeling of wood joints and structural system." *Journal of Structural Engineer (ASCE)* 121(6): 1013-1022.
- Foliente, G. C. 1997. "Modeling and Analysis of Timber Structures Under Seismic Loads: State-of-the-Art." In *Earthquake Performance and Safety of Timber Structures*, edited by Greg C. Foliente. USA: Forest Products Society.
- Folz, B., and Filiatrault, A. 2001a. "Cyclic analysis of wood shear walls." *Journal of Structural Engineering (ASCE)* 127(4): 433-441.
- Folz, B., and Filiatrault, A. 2001b. *CASHEW-Version 1.1-A computer program for the cyclic analysis of wood SHEarWalls*. California: CUREE Publication No. W-08.
- Folz, B., and Filiatrault, A. 2003. *SAWS-Version 1.0- A computer program for the Seismic Analysis of Woodframe Shearwalls*. California: CUREE Publication No. W-21.
- Folz, B., and Filiatrault, A. 2004a. "Seismic Analysis of Woodframe Structures I: Model Formulation." *Journal of Structural Engineering (ASCE)* 130(8): 1353-1360.
- Folz, B., and Filiatrault, A. 2004b. "Seismic Analysis of Woodframe Structures II: Model Implementation and Verification." *Journal of Structural Engineering (ASCE)* 130(8): 1361-1370.
- Foschi, R. O. 1977. "Analysis of wood diaphragms and trusses. Part I: Diaphragms." *Canadian Journal of Civil Engineering* 4(3): 345-352.
- Foschi, R. O., and Bonac, T. 1977. "Load-Slip Characteristics for Connections with common nails." *Wood Science* 9(3): 118-128.
- Fragiacomo, M. 2009. "Edifici multipiano in legno a telaio leggero e a struttura mista." CISM Course, International Centre for Mechanical Science.
- Gojkovic, M., & Stojic, D. 1996. *Drvene Konstrukcije*. Beograd: Faculty of civil engineering.
- Gulkan, P., and Sozen, M. A. 1974. "Inelastic Response of Reinforced Concrete Structures to Earthquake Motions." *Structural Journal (ACI)* 71(12): 604-610.

BIBLIOGRAPHY

- Heiduschke, A., Kasal, B., and Haller, P. 2008. "Performance and Drift Levels of Tall Timber Frame Buildings under Seismic and Wind Loads." *Structural Engineering International* 18(2): 186-191.
- Hilson, B. O. 1995. "Unioni con mezzi del tipo a spinotto." In *Manuale del legno strutturale*, edited by Uzielli L. Italy: Mancosu Editore Press.
- Isoda, H., Folz, B., and Filiatrault, A. 2002. *Seismic Modelling of Index Woodframe buildings*. California: CUREE Publication No. W-12.
- Jacobsen, L. S. 1930. "Steady Forced Vibrations as Influenced by Damping." *Transactions ASME* 52(1): 169-181.
- JCSS. 2007. *Probabilistic Model Code*. JCSS Web-publication, ISBN 978-3-909386-79-6. <http://www.jcss.ethz.ch>.
- Johansen, K. W. 1949. "Theory of Timber Connections." *International Association of Bridge and Structural Engineering* 9: 249-262.
- Jorissen, A., and Leijten, A. 2008. "Tall Timber Buildings in The Netherlands." *Structural Engineering International* 18(2): 133-136.
- Judd, J. P., and Fonseca, F. S. 2006. "Equivalent Single degree of freedom model for wood shearwalls and diaphragms." Paper presented at the 9th World Conference on Timber Engineering, Portland, Oregon, USA, August 6-10.
- Kam, W. Y., Pampanin, A., Palermo, A., and Carr, A. 2008. "Implementation of advanced flag-shape (AFS) systems for moment-resisting frame structures." Paper presented at the 14th World Conference on Earthquake Engineering, Beijing, China, October 12-17.
- Karacabeyli, E., and Popovski, M. 2003. "Design for earthquake Resistance." In *Timber Engineering*, edited by Thelandersson, S., and Larsen, H. J. 267-299. England: John Wiley & Sons Ltd.
- Karacebeyli, E., and Ceccotti, A. 1996. "Quasi-static reversed-cyclic testing of nailed joints." Paper presented at the 29th Meeting, International Council for Research and Innovation in Building and Construction, Working Commission W18 - Timber Structures, Bordeaux, France, August.
- Kitagawa, Y., and Hiraishi, H. 2004. "Overview of the 1995 hyogo-ken nanbu earthquake and proposals for earthquake mitigation measures." *Journal of Japan Association for Earthquake Engineering* 4(3): 1-28.

- Kivell, B. T., Moss, P. J., and Carr, A. J. 1981. "Hysteretic modelling of moment resisting nailed timber joints." *Bull. New Zeal. Nat. Soc. Earthquake Engineering* 14(4): 233-245.
- Krawinkler, H., Parisi, F., Ibarra, L., Ayoub, A., and Medina, R. 2000. *Development of a testing protocol for wood frame structures*. California: CUREE Publication No. W-02.
- Lam, F., He, M., and Yao, C. 2008. "Example of Traditional Tall Timber Buildings in China - the Yingxian Pagoda." *Structural Engineering International* 18(2): 126-129.
- Langenbach, R. 2008a. "Building Tall with Timber: A Paeen to Wood Construction." *Structural Engineering International* 18(2): 130-132.
- Langenbach, R. 2008b. "Resisting Earth's Forces: Typologies of Timber Buildings in History." *Structural Engineering International* 18(2): 137-140.
- Lantos, G. 1969. "Load Distribution in a Row of Fasteners Subjected to Lateral Load." *Wood Science* 1(3): 129-136.
- Leijten, A. 2008. "Connections - Lateral load capacity - Withdrawal capacity – dowels." Paper presented at the workshop on Dissemination of information for training: Eurocodes Background and applications, Brussels, Belgium, February 18-20.
- LO, Y. P. Y. 2002. "A comparison of two hysteretic models in predicting the response of a connector under cyclic loading." PhD Thesis, University of British Columbia, Vancouver, BC, Canada.
- MCEER. 2010. "Earthquake Engineering to Extreme Events." Accessed June 2010. <http://mceer.buffalo.edu/publications/>.
- Microsoft Excel®. 2007. "Microsoft Office Excel." Redmond, Washington, USA: Microsoft Corporation. Accessed June 2010. <http://office.microsoft.com>.
- Möller, T. 1951. *En ny metod för beräkning av spikförband*. Sweden: Chalmers University of Technology.
- New Zealand Standard. 1993. *NZS3603: TIMBER STRUCTURES STANDARD*. New Zealand.
- Newcombe, M., Pampanin, S., Buchanan, A. And Palermo, A. 2008. "Section Analysis and Cyclic Behaviour of Post-Tensioned Jointed Ductile Connections for Multi-Storey Timber Buildings." *Journal of Earthquake Engineering* 12: 83-110.

BIBLIOGRAPHY

Palermo, A., Pampanin, S., and Fragiaco, M., 2006. "EXPERIMENTAL INVESTIGATIONS ON LVL SEISMIC RESISTANT WALL AND FRAME SUBASSEMBLIES." Paper presented at the First European Conference on Earthquake Engineering and Seismology, Geneva, Switzerland, September 3-8.

Palermo, A., Pampanin, S., Fragiaco, M., Buchanan, B., and Deam, B. 2006a. "Innovative Seismic Solutions for Multi-Storey LVL Timber Buildings." Paper presented at the 9th World Conference on Timber Engineering, Portland, Oregon, USA, August 6-10.

Palermo, A., Pampanin, S., Fragiaco, M., Buchanan, B., and Deam, B. 2006b. "CODE PROVISIONS FOR SEISMIC DESIGN OF MULTI-STOREY POST-TENSIONED TIMBER BUILDINGS." Paper presented at the 39th Meeting, International Council for Research and Innovation in Building and Construction, Working Commission W18 - Timber Structures, Florence, Italy, August.

Pang, W. C., Rosowsky, D. V., Pei, S., and van de Lindt, J. W. 2006. "Evolutionary Parameter Hysteretic Model for Wood Shear Walls." *Journal of Structural Engineering (ASCE)* 133(8): 1118:1130.

Pang, W., and Rosowsky, D. V. 2008. "Performance-Based Seismic Design of Six-Story Woodframe Structure." *Structural Engineering International* 18(2): 179-185.

Pang, W., and Rosowsky, D. V. 2007. *Direct Displacement Procedure for Performance-Based Seismic Design of Multistory Woodframe buildings*. Texas: Zachry Department of Civil Engineering, 42pp.

Pang, W., and Rosowsky, D.V. 2009. "Direct Displacement Procedure for Performance-based Seismic Design of Mid-rise Woodframe Structures." *Earthquake Spectra* 25(3): 583-605.

Pang, W., Rosowsky, D. V., Pei, S., and Van de Lindt, J. W. 2010. "Simplified Direct Displacement Design of Six-Story Woodframe Building and Pretest Seismic Performance Assessment." *Journal of Structural Engineering (ASCE)* 136(7): 813-825.

Pei, S., and van de Lindt, J. W. 2007. *User's manual for SAPWood for Windows, version 1.0*. Colorado. USA: Colorado State University, 75pp.

Piazza, M., Tomasi, R. and Crosatti, A. 2009. *Indagine sperimentale su sistemi di connessione legno-legno con elementi a gambo cilindrico ed elementi di superficie*. Trento: Università degli studi di Trento, 261pp.

- Piazza, M., Tomasi, R., and Modena, R. 2005. *Strutture in legno. Materiale, calcolo e progetto secondo le nuove normative europee*. Milan, Italy: Hoepli.
- Polastri, A., Tomasi, R., Piazza, M., and Smith, I. 2008. "Ductility of Moment Resisting Dowelled Connections in Heavy Timber Structures." Paper presented at the 41th Meeting, International Council for Research and Innovation in Building and Construction, Working Commission W18 - Timber Structures, St. Andrews, Canada, August.
- Polensek, A., and Bastendorff, K. M. 1987. "Damping in Nailed Joints of Light-Frame Wood Buildings." *Wood and Fiber Science* 19(2): 110-125.
- Premrov, M. 2008. "Timber Frame Houses." In *Handbook 1 Timber Structures*. Ostrava: Leonardo da Vinci Pilot Project (TEMTIS Project).
- Premrov, M., and Tajnik, M. 2008. "Planar Timber Structures." In *Handbook 1 Timber Structures*. Ostrava: Leonardo da Vinci Pilot Project (TEMTIS Project).
- Priestley, M. J. N. 1993. *Myths and Fallacies in Earthquake Engineering - Conflicts Between Design and Reality*. New Zealand: National Society for Earthquake Engineering 26(3), 329-341.
- Priestley, M. J. N. 1998. "Displacement-based approaches to rational limit states design of new." Paper presented at the 11th European Conference on Earthquake Engineering, Paris, France, September 6-11.
- Priestley, M. J. N. 2000. "Performance based seismic design." Paper presented at the 12th World Conferences on Earthquake Engineering, Auckland, New Zealand, January 30-February 4.
- Priestley, M. J. N. 2003. *Myths and Fallacies in Earthquake Engineering, Revisited*. Pavia, Italy: IUSS Press, 118pp.
- Priestley, M. J. N., Calvi, G. M., and Kowalsky, M. J. 2007. *Direct Displacement-Based Seismic Design*. Pavia, Italy: IUSS Press, 721pp.
- Prion, Helmut G.L. 2003. "Shear Walls and Diaphragms." In *Timber Engineering*, edited by Thelandersson, S., and Larsen, H. J. 383-408. England: John Wiley & Sons Ltd.
- Racher, P. 1995a. "Unioni meccaniche - principi generali." In *Manuale del legno strutturale*, edited by Uzielli L. Italy: Mancosu Editore Press.
- Racher, P. 1995b. "Connessioni resistenti a momento." In *Manuale del legno strutturale*, edited by Uzielli L. Italy: Mancosu Editore Press.

BIBLIOGRAPHY

Racher, P. 1995c. "Angoli dei telai." In *Manuale del legno strutturale*, edited by Uzielli L. Italy: Mancosu Editore Press.

Reluis. 2009. "Rete dei Laboratori Universitari di Ingegneria Sismica." Accessed June 2010. <http://www.reluis.it/>.

Robert, C. P., and Casella, G. 2004. *Monte Carlo Statistical Methods*. NJ, USA: Springer-Verlag New York, Inc.

Sakamoto, I., Kawai, N., Okada, H., and Yusa, S. 2004. "Final report of a research and development project on timber-based hybrid building structures." Paper presented at the 8th World Conferences on Timber Engineering, Lahti, Finland, June 14-17.

SAP 2000®. 2004. *Database Documentation*. Berkeley, California, USA: Computer and Structures, Inc.

SAP 2000®. 2006. *Linear and Nonlinear Static and Dynamic Analysis and Design of Three-Dimensional Structures, BASIC ANALYSIS REFERENCE MANUAL*. Berkeley, California, USA: Computer and Structures, Inc.

Sawata, K., and Yasumura, M. 2002. "Determination of embedment strength of wood for dowel-type-fasteners." *Journal of Wood Science* 48(2): 138-146.

Seesl. 2006. "Structural Engineering and Earthquake Simulation Laboratory: NEESWood Project." Last update September 2004. <http://nees.buffalo.edu/projects/NEESWood/>.

Shibata, A., and Sozen, M. 1976. "Substitute Structure Method for Seismic Design in Reinforced Concrete." *Journal Structural Division (ASCE)* 102(12): 3548-3566.

Smith, I., and Frangi, A. 2008. "Overview of Design Issues for Tall Timber Buildings." *Structural Engineering International* 18(2): 141-147.

Smith, I., Daneff, G., Ni, C., and Chui, Y. H. 1998. "Performance of Bolted and Nailed Timber Connections Subjected to Seismic Loading." *Forest Products Society* 7275 (Special Publication): 6-17.

Stewart, W. G. 1987. "The seismic design of plywood sheathed shear walls." PhD thesis, University of Canterbury, Christchurch, New Zealand.

Sullivan, T. J., Priestley, M.J.N., and Calvi, G.M. 2009. "Introduction to a Model Code for Displacement-Based Seismic Design." Paper presented at the ACES Workshop on Advances in Performance-Based Earthquake Engineering, Corfu, Greece, July 4-7.

- Teibinger, M. 2008. "Tall Timber Buildings: Introduction." *Structural Engineering International* 18(2): 114-117.
- Tomasi, R., Zandonini, R., Piazza, M., and Andreolli, M. (2008). "Ductile End Connections for Glulam Beams." *Structural Engineering International* 18(3): 290-296.
- Toratti, T. 2006. "Design guidance on Eurocode 8 for practicing engineers for timber structures." Paper presented at the International Workshop on Earthquake Engineering on Timber Structures, Coimbra, Portugal, November 9-10.
- Vanmarcke, E. H., Fenton, G. A., and Heredia-Zavoni, E. 1997. *SIMQKE-II: Simulation of Earthquake Ground Motions*. N. J., Princeton: Princeton University.
- Yasumura, M. 1996. "Evaluation of seismic performance of timber structures." Paper presented at the International Wood Engineering Conference IVEC, New Orleans, Louisiana, USA, October 28-31.
- Yasumura, M. 2000. "Dynamic analysis of wood-framed shear walls." Paper presented at World Conference on Timber Engineering, Whistler Resort, British Columbia, Canada, July 31-August 3.
- Yeh, T. C., Hartz, B. J., and Brown, C. B. 1971. "Damping sources in wood structures." *Journal of Sound and Vibration* 19(4): 411-419.

APPENDIX A

MONTE CARLO SOFTWARE FOR SIMULATIONS

This appendix presents specific information on the Monte Carlo simulation (MC).

The MC simulation was performed with a specific software tool created to manage in automatic manner the structural analysis program SAP 2000® (2006) and the spreadsheet Microsoft Excel® (2007) for data processing. The following pages outline the structure of the software, its syntax and the compilation of the program.

The software to perform the MC simulation, called "Wood Seismic Control Software" (WSSC) has been written with *Visual Basic for Applications* (VBA) language, within Microsoft Excel® environment. The WSSC software is controlled through a *user-friendly* graphical interface (Figure A.I). WSSC is structured on three sequential levels, defined as pre-processing, solving and post-processing. Each level has a different save location and is indexed, so as to facilitate the verification phase of the results and to prevent any faults, whether errors due to inconsistencies of code or execution crash.

The compiled code of WSSC was developed with the division into groups of the command lines, which are contained within sheets that form the structure of the software. Each subroutine is recalled by the user through dialog boxes (*inputbox*) and then controlled through message windows (*msgbox*). The internal variables are declared by specifying the data type (e.g. *Integer*, *Long*, *String*), to minimize the time of execution and the physical memory required by the hardware. The methods *Do while/loop*, *For/to/Step/Next* and instructions *If/then /Else/End if* have been used to perform the iterative cycles required by the MC simulation.

WSSC interacts with the user via the *Form* (Figure A.I), which contains all the graphic objects necessary for the generation of events and the running of procedures during the MC simulation. WSSC has been designed to simplify the testing and any code changes.

The screenshot displays the WSSC software interface, organized into three main stages: **PREPROCESSING**, **SOLVING**, and **POSTPROCESSING**.

- PREPROCESSING** is divided into two options:
 - GENERAZIONE DEL SINGOLO MODELLO** (Selected): Includes buttons for **IMPLEMENTAZIONE SINGOLA DEI MODELLI** (with sub-buttons: SET LIMITI CAMPIONI, SET COEF. di VARIAZIONE, GENERA VARIABILI, IMPLEMENTA GEOMETRIA, ESPORTA FILE, SALVA GENERAZIONE).
 - GENERAZIONE DI UN INSIEME DI MODELLI**: Includes buttons for **IMPLEMENTAZIONE MULTIPLA DEI MODELLI** (with sub-elements: Scelta del numero dei modelli da generare, N° MODELLI GENERATI, AVVIO SIMULAZIONE, GENERA APPLICATIVO SAP).
- SOLVING** includes:
 - ANALISI AL SAP 2000**: Buttons for **IMPLEMENTAZIONE SAP**, **PROCESSING SAP**, and **RUN PUSHOVER**.
 - PERCORSO DI RIFERIMENTO**: A text field containing the path `D:\Facoltà di Ingegneria\TESI\MIO NUOVO \SIMULAZIONE MONTE CARLO`.
 - PARAMETRI COSTANTI DURANTE L'ANALISI**: Four input fields for:
 - Diametro dello spinotto [mm]
 - Classe del legno [GL]
 - Classe dell'acciaio [S]
 - Duttilità dello spinotto [μ]
- POSTPROCESSING** includes:
 - ELABORAZIONE DEI RISULTATI**: A button labeled **ELABORA**.
 - A large green button labeled **USCITA** (Exit).

Figure A.I Screenshot of the “Wood Seismic Software Control” (WSSC) Form

In the next sections the three fundamental levels implemented within the WSSC software: *pre-processing*, *solving* e *post-processing* are analyzed in detail.

7.3 Pre-processing

Each geometrical and mechanical configuration of the portal frame structure requires a finite element model implemented to perform non-linear static analyses. The WSSC software allows a database of models of size equal to N to be autonomously generated. The database contains a number N of excel files (.xls), each defined by the compilation of 35 worksheets, based on the geometry and mechanical properties of materials. All worksheets are named in accordance with the protocol of recognition of SAP 2000® (2004) and enable the creation of a specific Finite Element Model (FEM Model). Table A.I gives a brief description of all worksheets (Microsoft Excel® 2007) generated by WSSC.

Table A.I Meaning of each Worksheet used to generate the i^{th} FEM Model according to the recognition protocol of SAP 2000®

ID	Name of sheet	Brief Description
1	<i>Active Degrees of Freedom</i>	Definition of the Available Degrees of Freedom
2	<i>Analysis Case Definitions</i>	Definition of loading conditions
3	<i>Case - Static 1 - Load Assigns</i>	Assignment of general loading conditions
4	<i>Case - Static 2 - NL Load App</i>	Definition of static and non-linear loading conditions
5	<i>Case - Static 4 - NL Parameters</i>	Definition of control parameters that manage the non-linear numerical solution of the problem
6	<i>Connectivity - Frame</i>	Identification of initial (i -end) and final nodes (j -end) of the individual elements
7	<i>Constraint Definitions - Body</i>	Definition of internal constraints
8	<i>Coordinate Systems</i>	Introduction of system reference
9	<i>Database Format Types</i>	Defining units of measure and parameters for the import process
10	<i>Frame Loads - Gravity</i>	Application of gravity loads on the elements

APPENDIX A

11	<i>Frame Props 01 - General</i>	Definition of the section of elements
12	<i>Frame Releases 1 - General</i>	Assignment of end-releases on each element
13	<i>Frame Releases 2 - Part Fixity</i>	Assignment of the stiffness value for the end-releases of elements
14	<i>Frame Section Assignments</i>	Assignment of the section on each element
15	<i>Groups 1 - Definitions</i>	Creation of groups of elements.
16	<i>Groups 2 - Assignments</i>	Selection of elements (frame) and nodes that belong to each group
17	<i>Hinges Ass 02 - User Prop</i>	Assignment of plastic hinges on the elements
18	<i>Hinges Def 01 - Overview</i>	Assignment of the non-linear behaviour of plastic hinges
19	<i>Hinges Def 02 - Non - DC - Gen</i>	Definition of the general characteristics of the plastic hinge
20	<i>Hinges Def 03 - Non - DC - FD</i>	Assignment of the constitutive function of plastic hinges
21	<i>Joint Constraint Assignments</i>	Assignment of constraints on elements
22	<i>Joint Coordinates</i>	Assignment of the coordinate system to each node (cartesian, cylindrical or spherical).
23	<i>Joint Loads - Force</i>	Application of concentrated loads to individual nodes
24	<i>Joint Restraint Assignments</i>	Assignment of external constraints to the nodes
25	<i>Load Case Definitions</i>	Definition of load groups.
26	<i>Material Prop 01 - General</i>	Definition of the material basic properties
27	<i>Material Prop 02 - Advanced</i>	Definition of the material advanced properties
28	<i>Named Sets - DBTables 1 - Gen</i>	Definition of the output table format
29	<i>Named Sets - DBTables 2 - Sel</i>	Selection of groups of elements and the type of output required in the output table

30	<i>Named Sets - Pushover</i>	Definition of the "pushover" analyses
31	<i>Preferences - Dimensional</i>	Definition of accuracy in graphical model building
32	<i>Program Control</i>	Check of program version and license
33	<i>Pushover Params - Axis Data</i>	Formatting the chart of the "pushover curve"
34	<i>Pushover Params - Force Displ</i>	Control of the "pushover curve"
35	<i>Tables AutoSaved After Analysis</i>	Set of parameters to automatically save output tables

The preprocessing phase ends with the conversion of any text file (extension in excel format) into a finite element model and the running of the internal compiler of Sap 2000®. The final result is a new database file with an extension conforming to the SAP2000® software, available to perform the successive stages of analysis.

7.4 Solving

In the phases successive to the generation of the FEM models, the WSSC software performs all analyses with a sequential process in order to minimize the time in the opening and closing of each file. The WSSC software manages SAP2000® (2006) via the function *Batch File Control*, which allows the opening of the i^{th} -model, analysis and monitoring of results.

For each FEM model, SAP 2000® runs the solver, which assembles and solves the matrix system generated from data entered in the previous phase. The analysis process is monitored by WSSC that queries the SAP 2000® software on the outcome of the numerical solution through the dialog box that appears after each analysis. When the analysis is complete, WSSC shows a *Summary* which lists the time of analysis of individual models and the grand total, as well as information on the successful analyses and those with anomalies. The analysis phase ends with

the saving of data and preparation of the sample of FEM models for the phase of final processing.

7.5 Post-processing

The WSSC software opens the sample of FEM models (of size N), extracts some of the numerical results from all the non-linear analyses and organizes the data in preparation for subsequent comparisons. To limit the memory required, WSSC saves only the data strictly necessary for the comparison.

In the post-processing phase WSSC performs the statistical analysis aimed at validating the analytical model presented in Chapter 4. The calibration phase is also managed in an automated manner. The WSSC software compiles a report, which summarizes all the parameters and indices measured on the representative sample of N FEM models. The post-processing phase concludes the Monte Carlo simulation.

The Monte Carlo simulation is fully managed by the WSSC software, designed ad hoc for the structure presented in Chapter 4 of this research (the prototype portal frame). The WSSC software is open source and can be easily extended to other types of wooden structures and geometric configurations.

Additional information may be requested by contacting the author of this research, at: cristiano.loss@ing.unitn.it.

APPENDIX B

ADDITIONAL DETAILS OF GLULAM PORTAL FRAME SYSTEMS AND OF WOODFRAME SYSTEMS

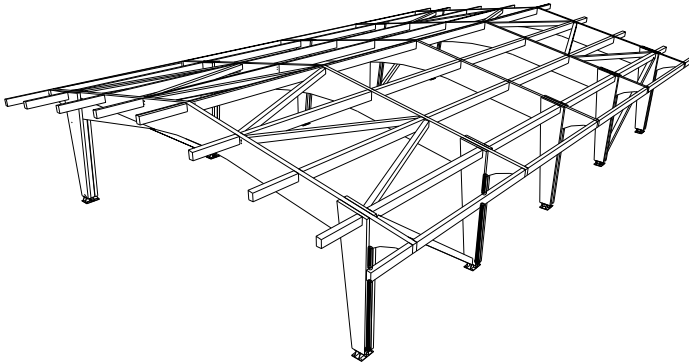
This Appendix provides additional information on the timber structures examined within this research. There are in detail the design drawings of an industrial building built in Trentino (Italy).

GLULAM PORTAL FRAME SYSTEM

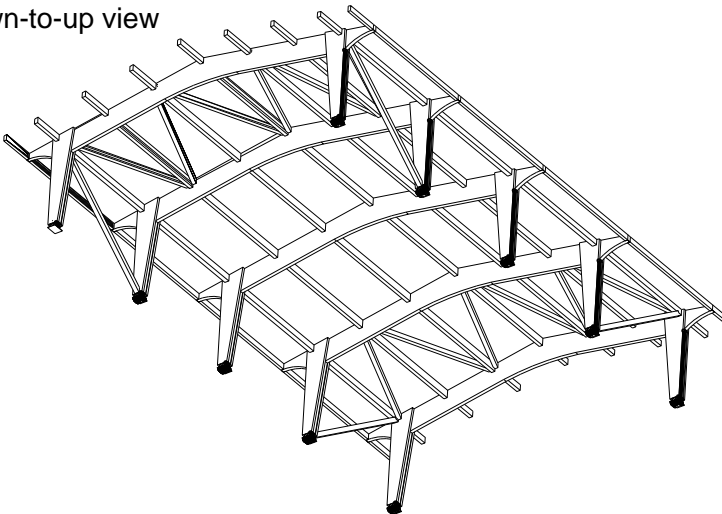
DESIGN PARAMETERS

FIRE RESISTANCE: R60
LIVE LOAD (SNOW): 2 kN/m^2
PERMANENT LOAD: 0.1 kN/m^2
DEAD LOAD: 0.5 kN/m^3

3D view

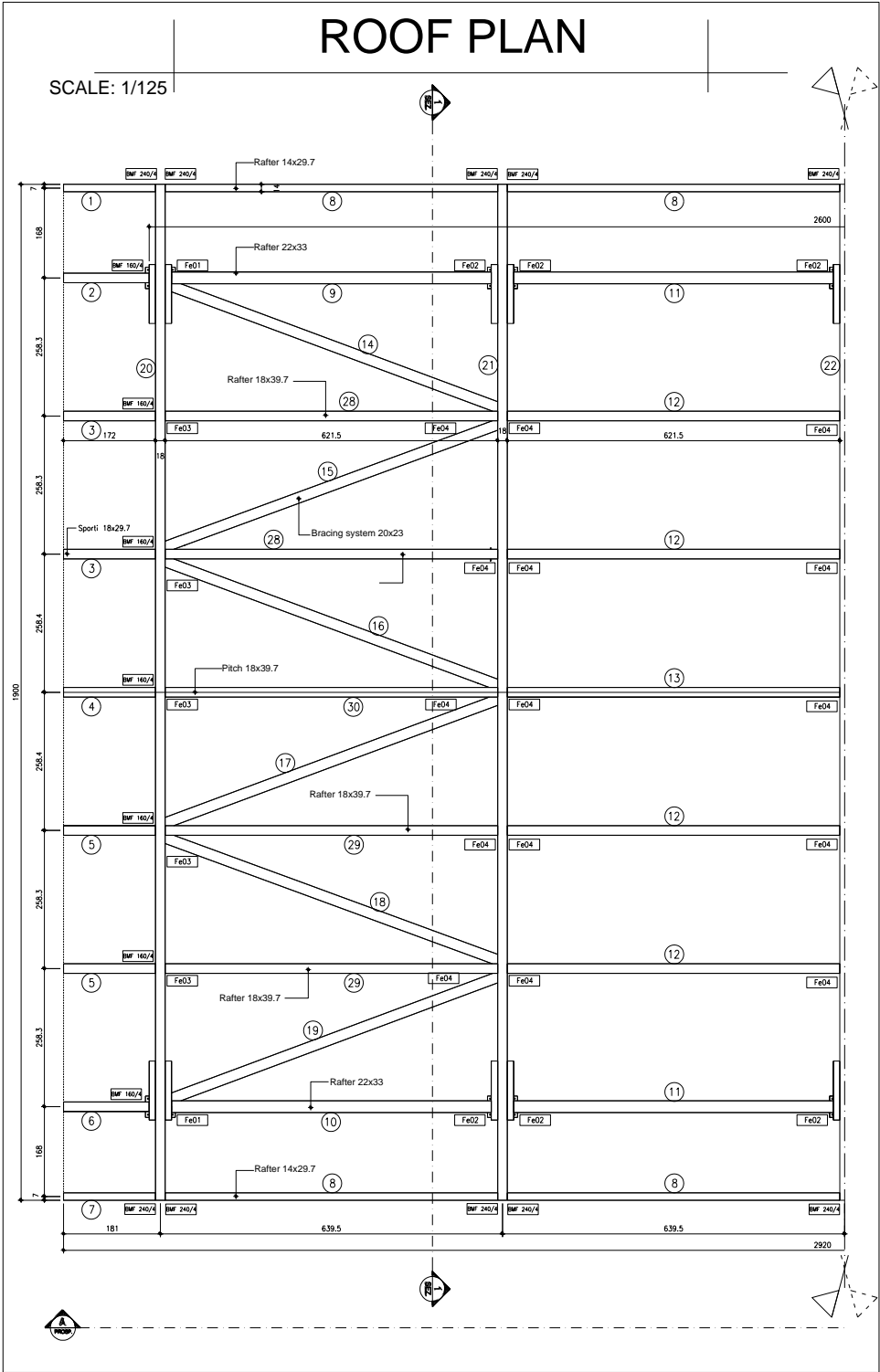


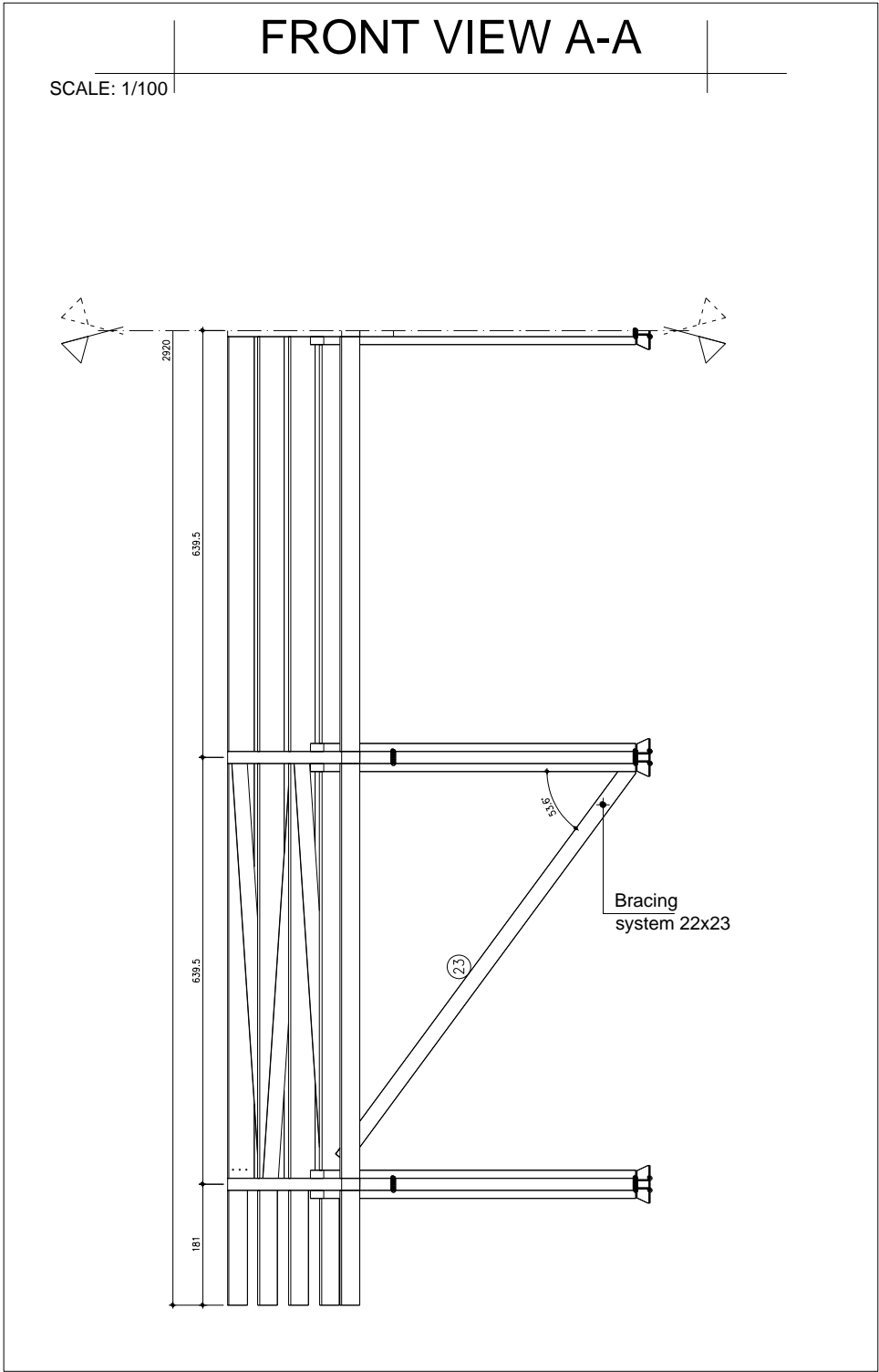
Down-to-up view



ROOF PLAN

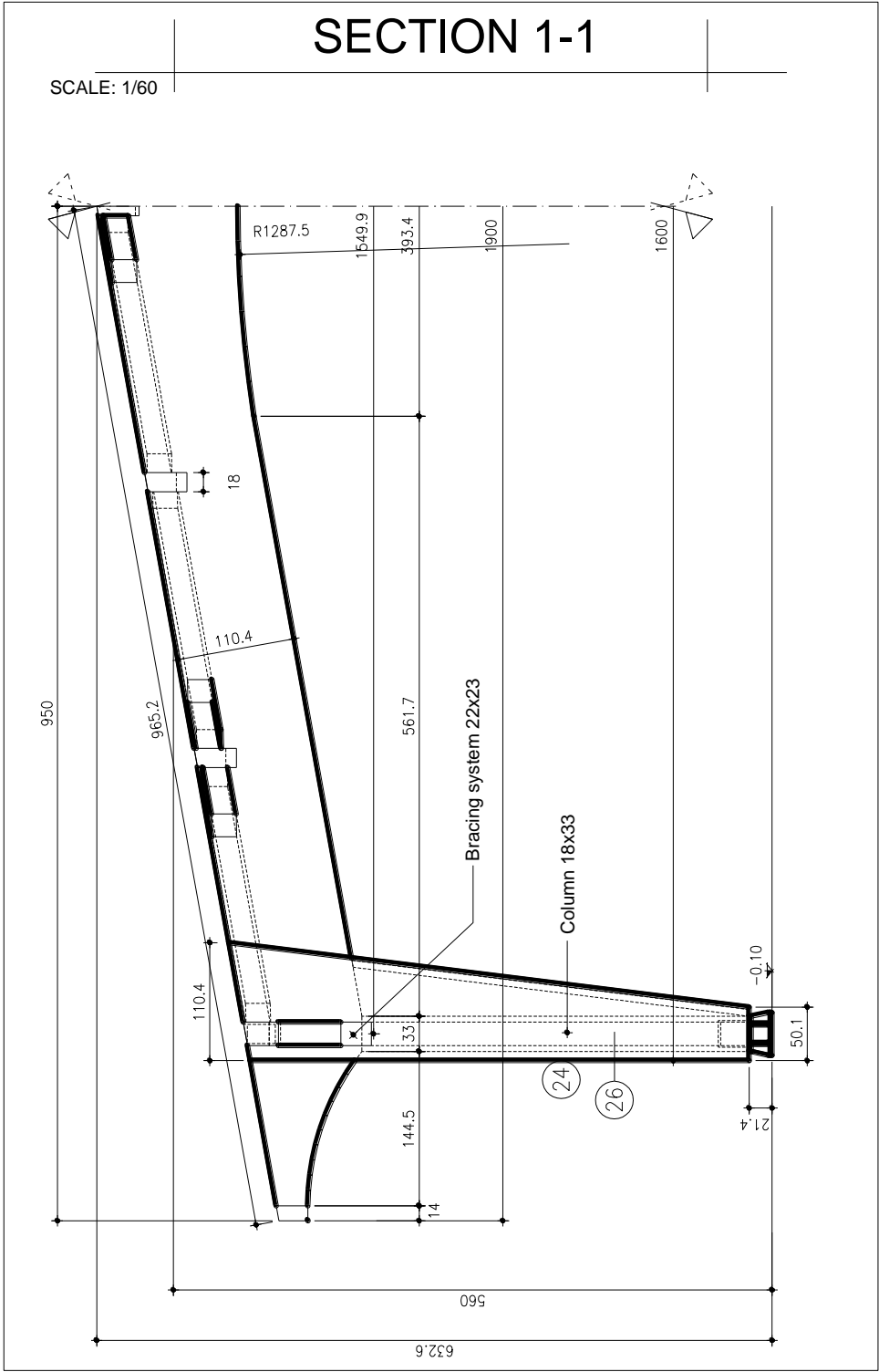
SCALE: 1/125

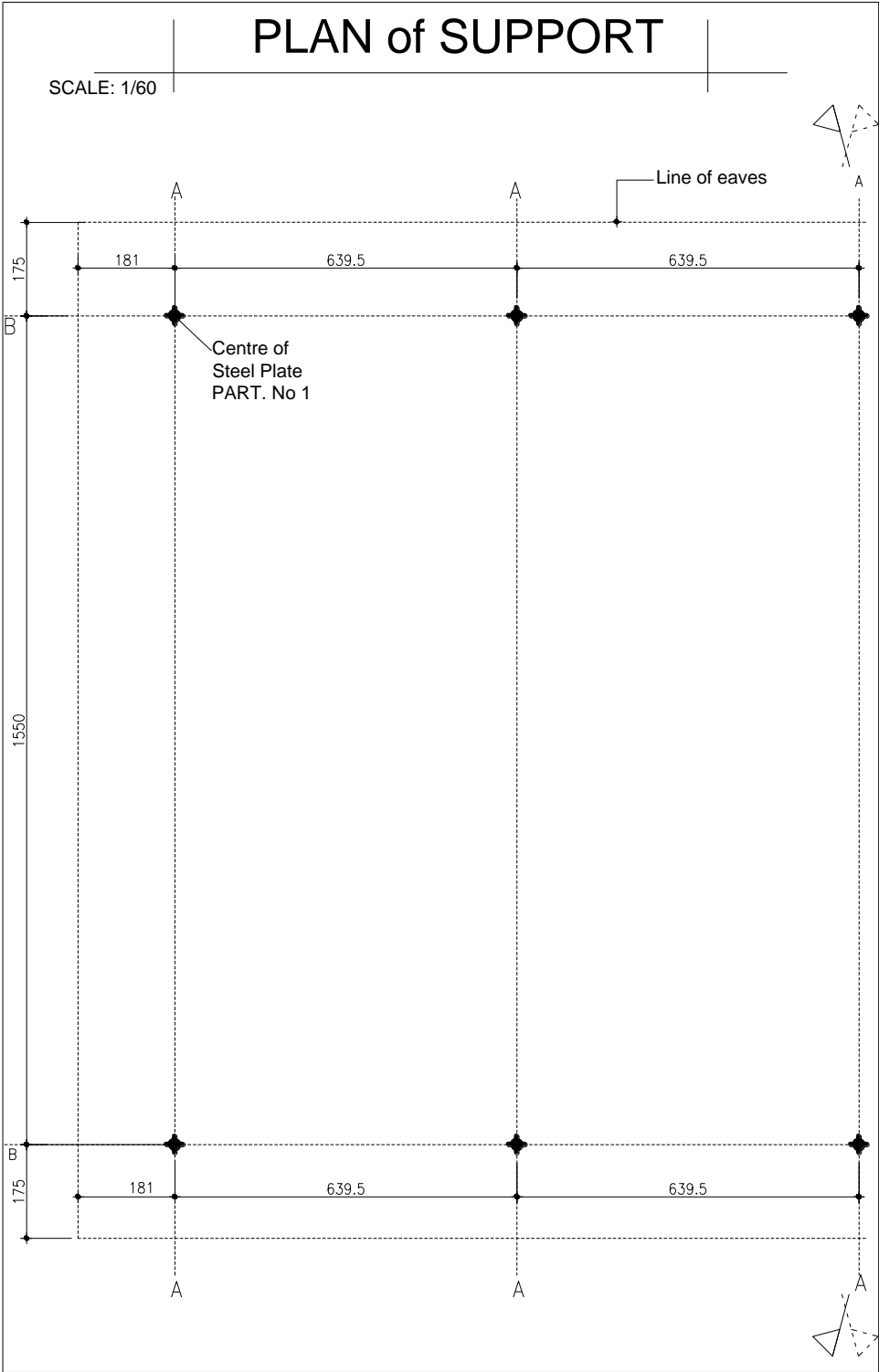




SECTION 1-1

SCALE: 1/60

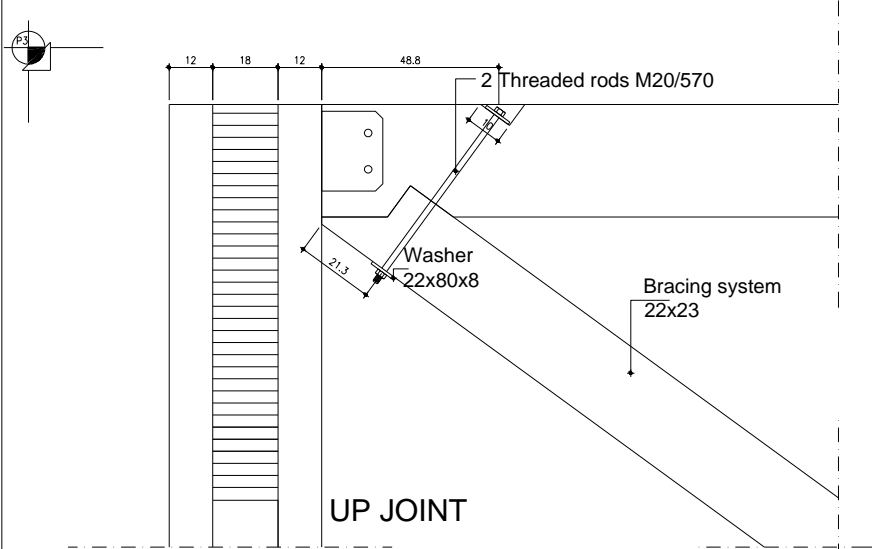




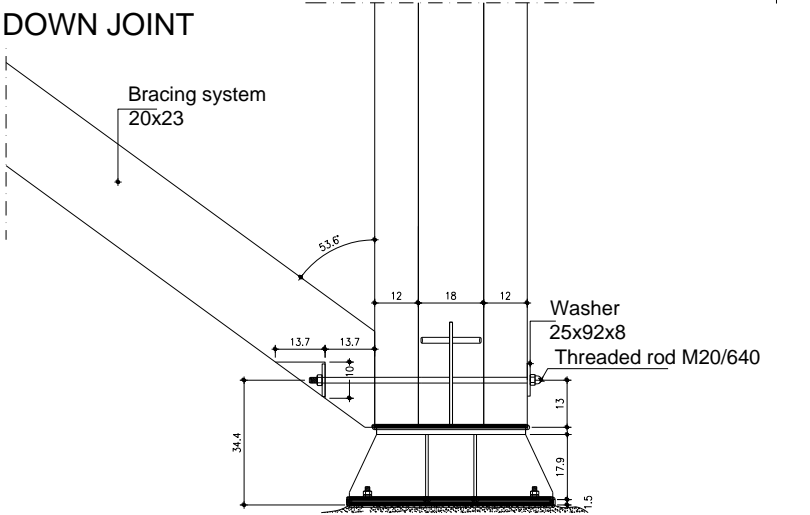
PARTICULAR No 3

SCALE: 1/20

BRACING SYSTEM JOINT



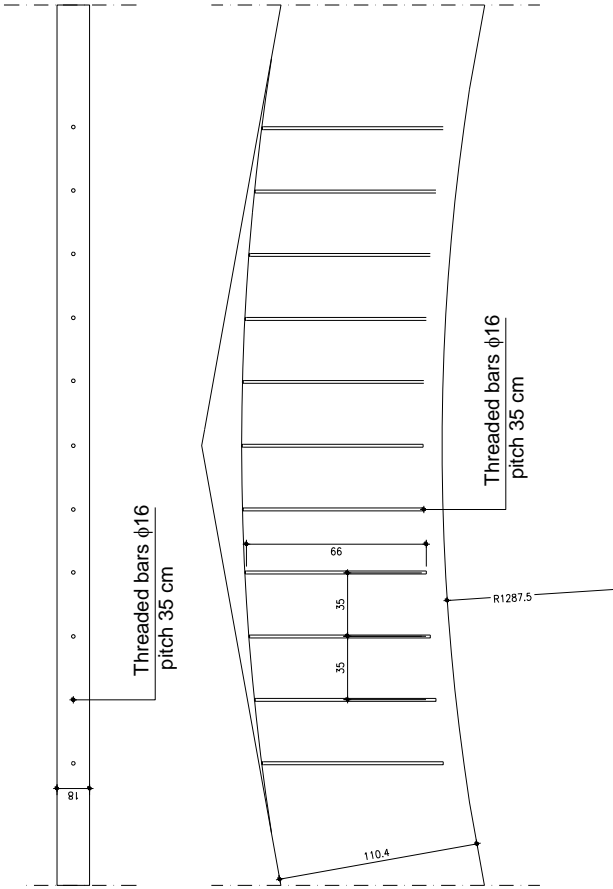
DOWN JOINT



PARTICULAR No 4

SCALE: 1/20

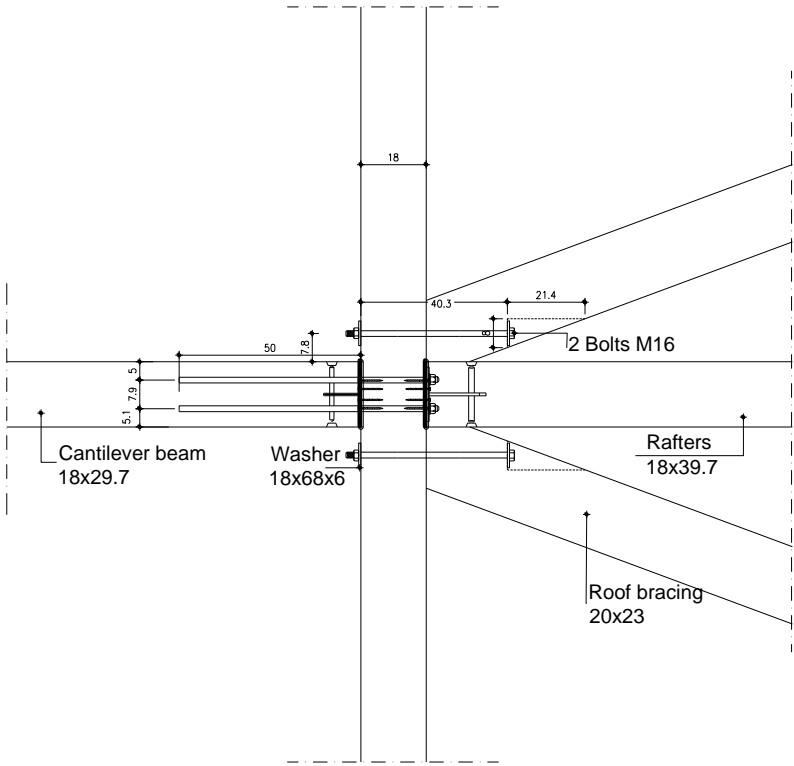
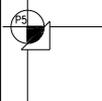
REINFORCEMENT OF THE CURVED BEAM



PARTICULAR No 5

SCALE: 1/20

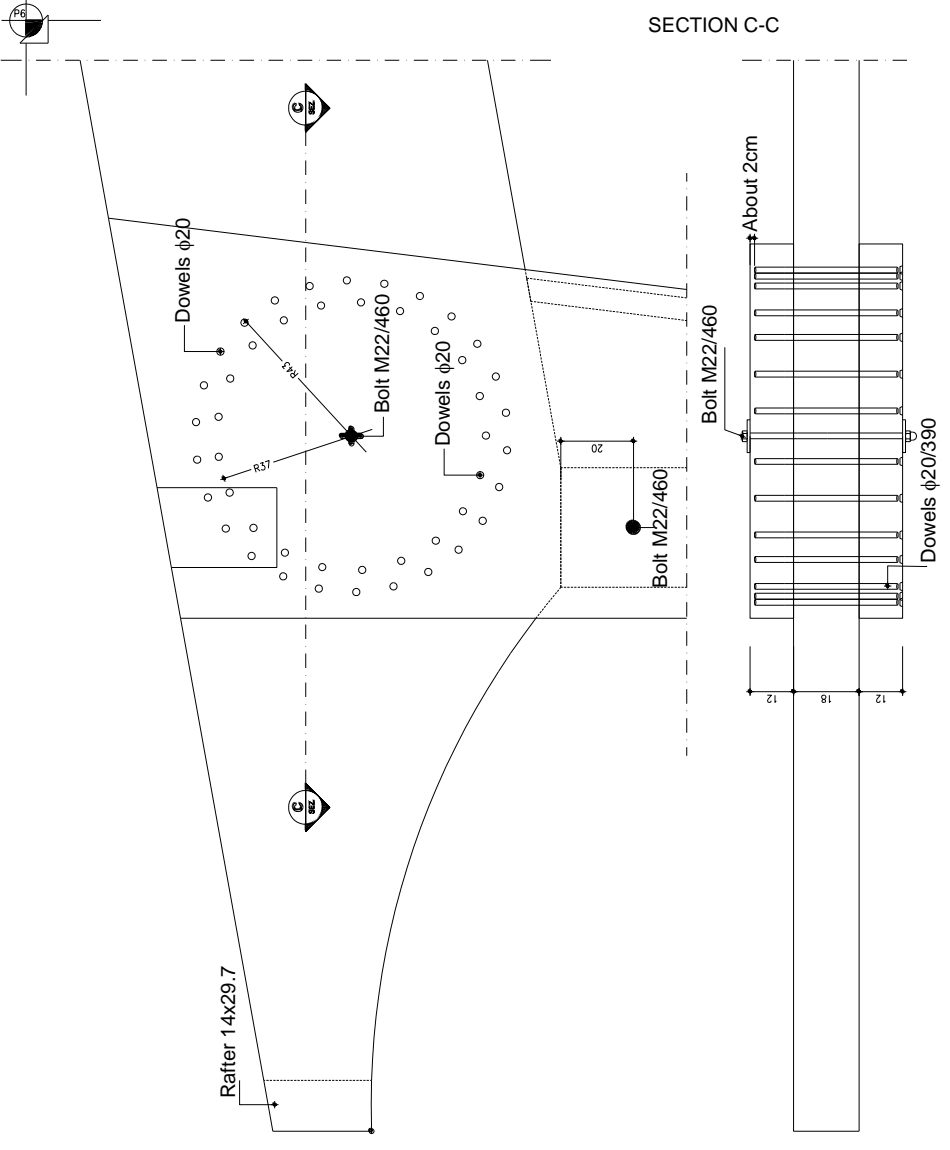
ROOF BRACING-TO-BEAM JOINTS



PARTICULAR No 6

SCALE: 1/20

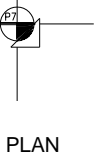
COLUMNS-TO-BEAM JOINT



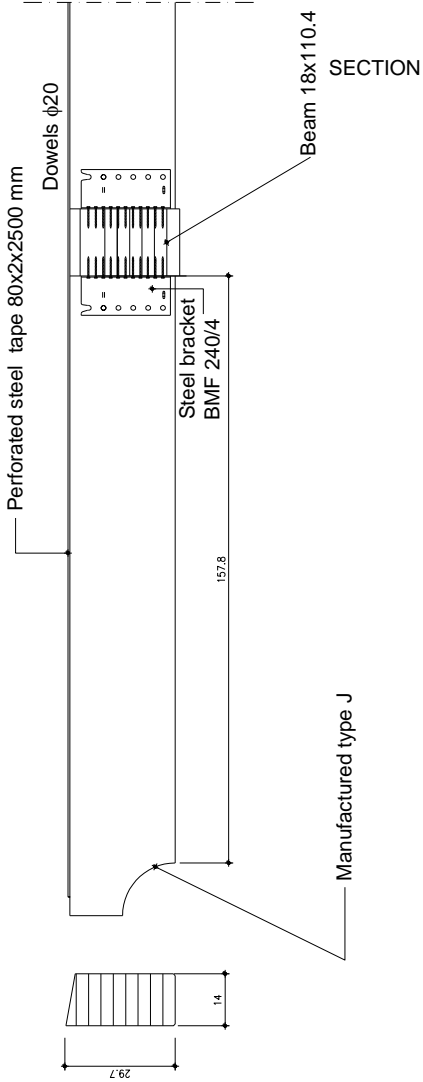
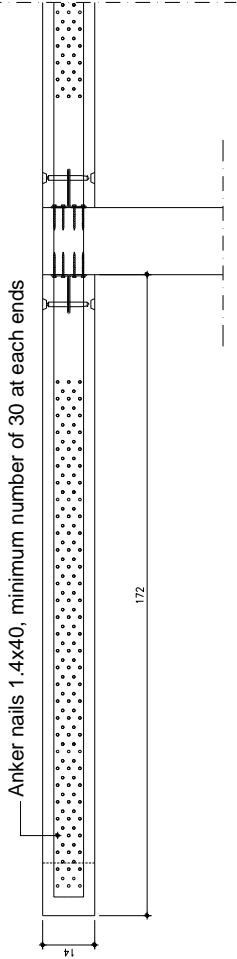
PARTICULAR No 7

SCALE: 1/20

CANTILEVER RAFTER END-JOINT



PLAN



APPENDIX C

EQUIVALENT VISCOUS DAMPING ANALYTICAL MODEL FOR CONNECTIONS WITH METAL DOWEL-TYPE FASTENERS

The extension of the analytical model to calculate the equivalent viscous damping ($\xi_{eq,dowel}$), described in Chapter 4, is proposed in this Appendix for dowel-type metal connectors, in which an elastic-plastic hardening load-slip curve ($F-\delta$) of dowels is assumed.

The elastic-plastic hardening relationship requires, in addition to the five parameters of the elastic-perfectly plastic curve, the post-yield strain hardening of the connector described by the dimensionless parameter α_{sh} . For the three reference situations *Protocol I*, *Protocol II* and *Protocol III*, defined in Chapter 4, the analytical expressions of $\xi_{eq,dowel}$ are formulated based on the same assumptions regarding materials and the geometry of the connection.

With the help of Figure D.1 we can derive analytical expressions for the calculation of $\xi_{eq,dowel}$ of the single connector, for a given value of ultimate slip of the dowel (δ_u).

The three analytical expressions for the reference situations are presented below:

Protocol I

$$\begin{aligned} \xi_{eq,dowel} &= E_p + E_f = \\ &= \frac{1}{2\pi} \left(\frac{(1 - \alpha_{sh}^2)}{\alpha_{sh} \mu_\delta} \right) + \frac{1}{2\pi} \left(1 + \frac{1}{\alpha_{sh}} \right) \left(1 - \frac{1}{\mu_\delta} \right) + \frac{\sigma_F}{\alpha_{sh} \pi} \left(1 - \frac{\alpha_{sh}}{\mu_\delta} - \frac{\sigma_F}{2\mu_\delta} \right) \end{aligned} \quad (D. 1)$$

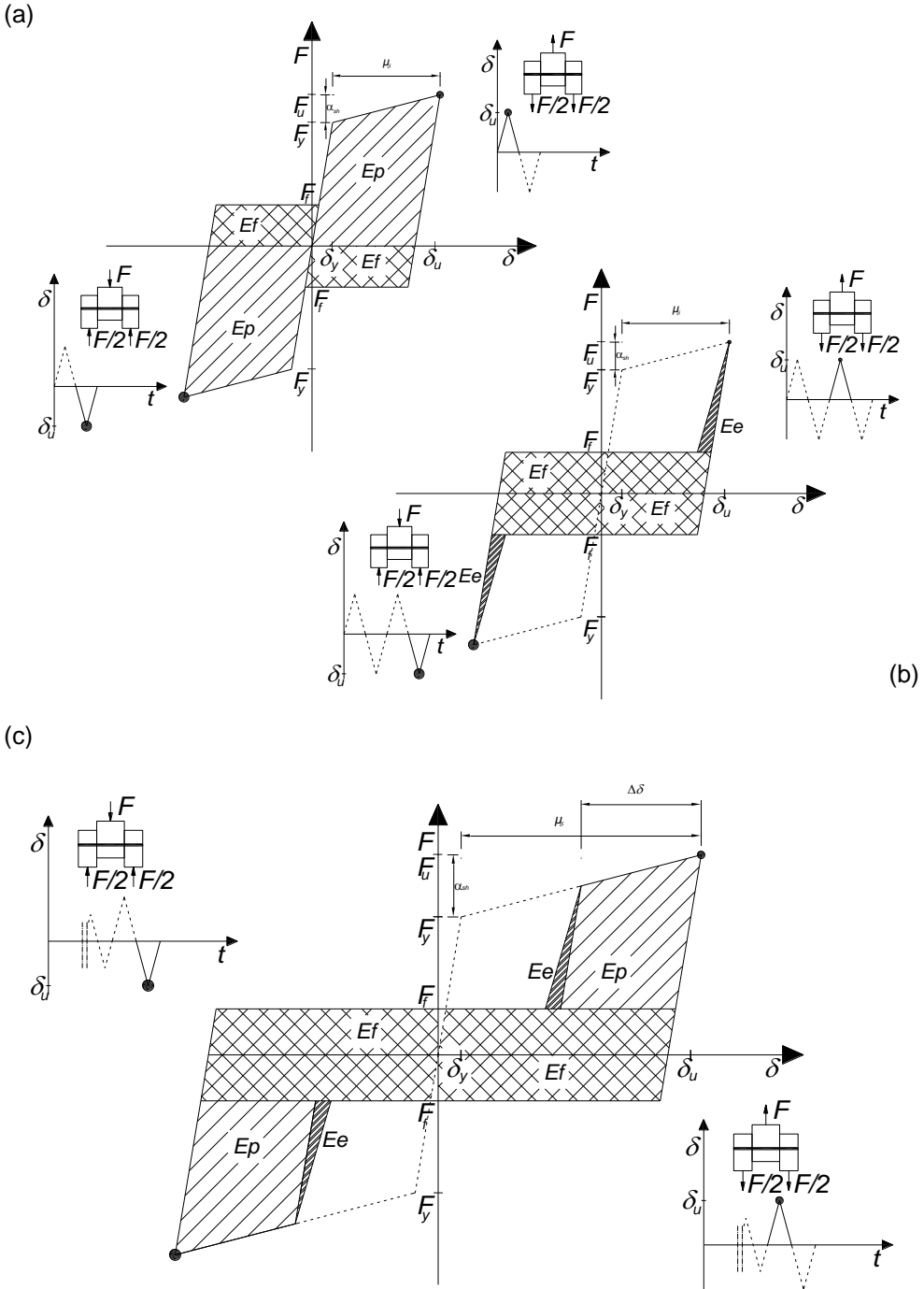


Figure D.1 Three typical force-slip hysteretic cycles of dowel connections with the elastic-plastic hardening law; (a) Protocol I; (b) Protocol II; (c) Protocol III

Protocol II

$$\begin{aligned}\xi_{eq,dowel} &= E_f + E_e = \\ &= \frac{(\alpha_{sh} - \sigma_F)^2 (\beta_k - 1)}{2\pi\alpha_{sh}\mu_\delta} + \frac{2\sigma_F}{\alpha_{sh}\pi} \left(1 - \frac{\alpha_{sh}}{\mu_\delta}\right)\end{aligned}\quad (D. II)$$

Protocol III

$$\begin{aligned}\xi_{eq,dowel} &= E_p + E_f + E_e = \\ &= \frac{\Delta\delta}{\delta} \frac{1}{\pi} \left[1 - \frac{\sigma_F}{\alpha_{sh}} - \left(\frac{\alpha_{sh} - 1}{\alpha_{sh}}\right) \frac{\Delta\delta}{\delta} \frac{1}{2} \frac{1}{(1 - 1/\mu_\delta)}\right] - \frac{\alpha_{sh}}{2\pi\mu_\delta} \left(1 - \frac{\sigma_F}{\alpha_{sh}}\right)^2 + \\ &\frac{2\sigma_F}{\alpha_{sh}\pi} \left(1 - \frac{\alpha_{sh}}{\mu_\delta}\right) + \frac{\alpha_{sh}\beta_k}{2\pi\mu_\delta} \left[1 - \frac{\sigma_F}{\alpha_{sh}} - \left(\frac{\alpha_{sh} - 1}{\alpha_{sh}}\right) \frac{\Delta\delta}{\delta} \frac{1}{(1 - 1/\mu_\delta)}\right]^2\end{aligned}\quad (D. III)$$

From Eqs. (D. I), (D. II) and (D. III) it is possible to estimate the equivalent viscous damping by assigning numerical values to the parameters σ_F , α_{sh} , μ_δ , β_k and $\Delta\delta/\delta$. Remember here that $\sigma_F = F_y/F_y$, μ_δ is the slip ductility of the dowel, β_k is the ratio of stiffness during reloading and the initial stiffness, α_{sh} is the hardening coefficient and, finally, $\Delta\delta/\delta$ is the ratio between the change in slip during loading and the maximum load reached in the previous cycle.

APPENDIX D

Appended papers

In this Appendix have been reported the following papers written during my Ph.D. research (chronological order):

- 1) Zonta, D., Piazza, M., Zanon, P., Loss, C., and Sartori, T. 2008. "DIRECT DISPLACEMENT-BASED DESIGN OF GLULAM TIMBER FRAME BUILDINGS." Paper presented at the 14th World Conference on Earthquake Engineering, Beijing, China, October 12-17.
- 2) Loss, C., Piazza, M., Zonta, D., and Zanon, P. 2009. "Direct Displacement Based Design applicato alle strutture in legno lamellare: calibrazione dello spostamento di progetto." Paper presented at the XIII Convegno Nazionale: L'Ingegneria Sismica in Italia, ANIDIS 2009, Bologna, Italy, June 28-July 2.
- 3) Zanon, P., Piazza, M., Zonta, D., and Loss, C. 2009. "Timber Structures." In *A Model Code for the Displacement-Based Seismic Design of Structures*, edited by Calvi, G.M. and Sullivan, T.J., 17-19 and 35-36. Pavia, Italy: IUSS Press. (ISBN: 978-88-6198-038-9).
- 4) Zanon, P., Piazza, M., Zonta, D., and Loss, C. 2009. "Timber Structures." In *The state of Earthquake Engineering Research in Italy: the ReLUIS-DPC 2005-2008 Project*, edited by Manfredi, G. and Dolce, M., 155-157. Napoli, Italy: Doppiavoce.

- 5) Zonta, D., Loss, C., Piazza, M., and Zanon, P. 2011. "Direct Displacement Based Design of glulam timber frame buildings." *Journal of Earthquake Engineering* 15:491-510.

- 6) Loss, C., Zonta, D., Piazza, M., and Zanon, P. 2011. "Direct Displacement Based Design: Design Displacement calibration." *Earthquake Engineering Structural Dynamics*, (Paper in proceeding).

- 7) Loss, C. 2011. "Design of a glulam timber portal frame." In *Case Study examples of displacement- based seismic design* edited by Calvi, G.M., Sullivan, T.J. and Lago, A., 85-96. Pavia, Italy: IUSS Press. (Book in publishing).